Experimental and Simulation Approaches for Optimizing the Thermal Performance of Building Enclosures Containing Phase Change Materials

By

Kyoung Ok Lee

M.S., The University of Kansas, Lawrence, Kansas, 2013
M.Eng., Chung-Ang University, Korea, Rep. of, 2003
B.Eng., Chung-Ang University, Korea, Rep. of, 2001

Submitted to the graduate degree program in the Department of Civil, Environmental, and Architectural Engineering and the Graduate Faculty of the University of Kansas in partial fulfillment of the requirements for the degree of Doctor of Philosophy in Civil Engineering.

_____
Mario A. Medina, Ph.D., P.E., Chairperson

_____
Hongyi Cai, Ph.D., Member

_____
Jae D. Chang, Ph.D., Member

_____
Steve Padget, AIA, LEED AP, Member

_____
C. Bryan Young, Ph.D., P.E., Member

Date Defended: _____

The Dissertation Committee for Kyoung Ok Lee
certifies that this is the approved version of the following dissertation:

Experimental and Simulation Approaches for Optimizing the Thermal Performance of Building Enclosures Containing Phase Change Materials

_____

Mario A. Medina, Ph.D., P.E., Chairperson

Date approved: _____

ABSTRACT

It has been proven that the integration of phase change materials (PCM) into building enclosures helps with wall thermal management as well as in reducing building energy consumption. Most older and some current PCM integration methods for building enclosures are impractical and create problems such as PCM leakage and evaporation, PCM water absorption, moisture transfer problems leading to building materials degradation, and problems related to the improper mixing of PCMs with insulation products (e.g., cellulose insulation). The use of thin PCM layers assembled and contained in blanket-like or board products would be practical to install and would eliminate or ameliorate these problems.

In this dissertation, the integration of thin PCM layers into building enclosure components, such as walls and ceilings, was accomplished via the use of thin PCM thermal shields (PCM shields) and via thin PCM boards. The thermal performance of building enclosures integrated with PCM shields and PCM boards was studied using experimental and simulation methods. The performance of PCM shields was evaluated experimentally using two identical, fully-instrumented test houses built with typical residential construction features and geometry. The performance of PCM boards was also evaluated experimentally using fully-instrumented wall panels that made up the walls of an institutional building with commercial construction features and geometry. For the modeling and simulations, a public-domain building energy simulation software, known as EnergyPlus, that included a new open-source

algorithm, known as CondFD, was used. CondFD was developed specifically for handling the transient heat transfer with phase transition which is characteristic of PCM-outfitted enclosures. EnergyPlus was also used for energy simulations of buildings with and without PCM-enhanced enclosures located in several climate zones across the United States. Specific inputs related to the phase transition process of PCMs were required by CondFD. These were determined via differential scanning calorimeter (DSC) tests using the PCMs contained in the shields and the PCM composites in the boards.

From the experimental evaluation of the PCM shields, it was observed that their thermal performance depended on their installation location within the cavities of the walls and ceilings. Therefore, a critical part of this research was to discover which installation location would produce the optimal performance of an enclosure outfitted with PCM shields. For this, several locations, measured from the interior surface of the wallboard which was in contact with the conditioned space, were specified as locations 1, 2, 3, 4, and 5. The location number increased with distance from the surface indicated in the preceding sentence. It was discovered that in terms of peak heat fluxes, the integration of PCM shields in enclosure components produced the maximum percent reductions of 57.4% when installed in location 3 (i.e., in the middle of the wall cavity) in a south-facing wall, 37.3% when installed in location 2 in a west-facing wall, and 41.1% when installed in location 4 in a ceiling. In terms of daytime total heat transfer, the integration of PCM shields produced the

maximum percent reductions of 47.9% for location 3 for a south wall, 34.1% for location 3 for a west wall, and 27.5% for location 4 for a ceiling.

The PCM boards were installed in a single location over the internal surface of the indoor surface that bound the walls of the institutional building. From experimental evaluations, the results indicated that wall panels outfitted with PCM boards would produce percent reductions in peak heat fluxes of 67.0% when installed in a south-facing wall and 80.2% when installed in a west-facing wall. In terms of total heat transfer, the integration of the PCM boards produced average daily percent reductions of 27.4% when installed in a south wall and 10.5% when installed in a west wall.

For model calibration purposes, the model predictions were compared against experimental data. The accuracy of the model predictions (i.e., surface temperatures and heat fluxes) related to the walls and ceilings of the test houses was higher than the accuracy of the model predictions related to the institutional building wall panels when the walls and panels had not yet been outfitted with the PCM shields and PCM boards, respectively. The accuracy of the model predictions once the PCM shields and the PCM boards were integrated into the modeling was relatively lower than those for the pre-retrofit cases. This happened because, as it was eventually determined, the CondFD algorithm was not able to model phase transition processes of PCMs as accurately as had been expected. Similar to the former case, in the latter case, the model predictions were also more accurate for the house enclosure

components than for the institutional wall panels. As a result, only the integration of PCM shields in residential enclosure components was evaluated via the simulations.

For evaluating overall energy savings produced by the integration of PCM shields into building walls and ceilings, simulations of a typical residential building with and without PCM shields were carried out for a building located in four cities, which were selected according to the DOE Climate Zone Map and included climate zones 1 - 4. The simulations predicted that the optimal installation location of the PCM shield would be location 2 for both the walls and ceilings of the residential building regardless of city location. Furthermore, it was discovered that PCM installation at location 1 in any enclosure component should be avoided because the heat transfer, and thus the energy consumption, in the cooling and heating seasons would both increase. The average reduction in total heat transfer into the conditioned space increased as the location of the house moved from a hot and humid to a mixed humid climate during the cooling season. The average reduction in total heat transfer out of the conditioned space increased as the location of the house moved from a mixed humid to a hot and humid climate during the heating season. The simulation results indicated that the PCM shields would produce a maximum space cooling energy percent reduction of 2.7% in Kansas City, MO (Zone 4). A maximum space cooling energy demand percent reduction of 7.9% was predicted for a house located in Miami, FL (Zone 1). A maximum space heating energy percent reduction of 33.1% was predicted also for a house located in Miami, FL (Zone 1).

ACKNOWLEDGEMENTS

It is an honor for me to thank those who made this dissertation possible.

Foremost, I would like to express my deepest gratitude to my advisor, Prof. Mario A. Medina for his patience, motivation, and guidance to this research. His kindness and benignity as well as his academic support helped me to overcome difficulties and complete my Ph.D. degree.

I would like to show my sincere gratitude to Prof. Hongyi Cai, Prof. Jae D. Chang, Prof. Steve Padget, and Prof. C. Bryan Young for their participation on my committee. Their encouragement and insightful comments helped me to accomplish this dissertation.

I would also like to thank my co-researchers, Erik Raith, Xiaoqin Sun, and Joseph Rendall for their assistance with this research. I am grateful to Mr. Matt Maksimowicz, Electronics Technologist, Mr. Craig Calixte, Building Complex Manager, and Mr. Jim Weaver, Laboratories Manager for their expertise and assistance.

Finally, I would like to thank my parents, Hong-Hwa Lee and Han-Ja Park, for their full support for my study. I am particularly thankful to my sisters and brother, Ju-Uk, Jun-Sung, and Su-Gwang, for being always with my parents instead of me.

Kyoung Ok Lee

TABLE OF CONTENTS

Abstract iii
Acknowledgements vii
Table of Contents viii
List of Figures xii
List of Tables xx
Nomenclature xxii
CHAPTER I: INTRODUCTION 1
1.1 Thermal Energy Storage in Building Enclosures 1
1.2 Phase Change Materials (PCMs) 3
1.2.1 Inorganic PCMs 7
1.2.2 Organic PCMs 8
1.3 PCM Incorporation Methods 9
1.3.1 Imbibing 9
1.3.2 Direct Incorporation 9
1.3.3 Macroencapsulation 10
1.3.4 Microencapsulation 10
1.3.5 Shape-stabilized PCMs 11
1.4 PCM Numerical Models 12
1.4.1 Enthalpy Method 12
1.4.2 Effective (Apparent) Heat Capacity Method 14
1.4.3 Heat Source Method 16
1.5 Building Energy Simulation Programs Including PCM Models 18
1.5.1 EnergyPlus 18
1.5.2 Transient System Simulation Tool (TRNSYS) 18
1.5.3 Energy Systems Research Unit (ESP-r) 19
CHAPTER II: LITERATURE REVIEW 20

CHAPTER III: RESEARCH FRAMEWORK 28
3.1 Current State of the Problem 28
3.2 Proposed Solution 29
3.3 Research Objectives 30
3.4 Research Approach 30
CHAPTER IV: EXPERIMENTAL SET-UPS 33
4.1 Experimental Set-up for Field-testing of PCM Shields 33
4.1.1 Test Houses 33
4.1.2 Space Cooling System 35
4.1.3 Data Acquisition System 36
4.1.3.1 Temperature Measurements 37
4.1.3.2 Heat Flux Measurements 37
4.1.3.3 Water Flow Rate Measurements 38
4.1.4 Weather Data 39
4.1.5 PCM Shields 40
4.1.5.1 Properties of the PCM Contained in the Shields 41
4.1.5.2 Installation of the PCM Shields 42
4.2 Experimental Set-up for Field-testing of PCM Boards 43
4.2.1 Measurement, Materials, and Sustainable Environment Center (M2SEC) 44
4.2.2 Space Cooling System 46
4.2.3 Data Acquisition System 47
4.2.3.1 Temperature Measurements 48
4.2.3.2 Heat Flux Measurements 50
4.2.4 PCM Boards 51
4.2.4.1 Properties of the PCM Boards 52
4.2.4.2 Installation of the PCM Boards 52
CHAPTER V: EXPERIMENTAL RESULTS AND DISCUSSION 54
5.1 Thermal Performance of the PCM Shields 54
5.1.1 Pre-retrofit Thermal Performance Verification of the Test Houses 54

5.1.1.1 Air and Surface Temperatures 54
5.1.1.2 Heat Fluxes 60
5.1.2 Retrofit Thermal Performance of the Test House 63
5.1.2.1 Heat Fluxes Across the South Wall 63
5.1.2.2 Heat Fluxes Across the West Wall 80
5.1.2.3 Heat Fluxes Across the Ceiling 96
5.2 Thermal Performance of the PCM Boards 104
5.2.1 Pre-retrofit Thermal Performance Verification of the Wall Panels in M2SEC 104
5.2.1.1 Surface Temperatures 105
5.2.1.2 Heat Fluxes 109
5.2.2 Retrofit Thermal Performance of the Wall Panels in M2SEC 111
5.2.2.1 Heat Fluxes Across the Wall Panels in the South Wall 111
5.2.2.2 Heat Fluxes Across the Wall Panels in the West Wall 116
CHAPTER VI: DIFFERENTIAL SCANNING CALORIMETER (DSC) ANALYSIS 120
6.1 Differential Scanning Calorimeter (DSC) 120
6.2 Thermal Properties of the PCMs 122
6.2.1 PCM Contained in the PCM Shield 122
6.2.2 PCM Composite Contained in the PCM Board 128
CHAPTER VII: MODEL DEVELOPMENT AND VERIFICATION 133
7.1 EnergyPlus 133
7.1.1 PCM Model in EnergyPlus 134
7.1.2 Inputs for PCM in EnergyPlus 137
7.1.2.1 Enthalpy of PCM as a Function of Temperature 137
7.1.2.2 Thermal Conductivity of PCM as a Function of Temperature 140
7.2 Model Verification for the Control Case 143
7.2.1 Test House Model 143
7.2.2 M2SEC Wall Panel Model 149
7.3 Model Verification for the Retrofit Case 153

7.3.1 Test House Model with the PCM Shields 153
7.3.2 M2SEC Wall Panel Model with the PCM Boards 160
CHAPTER VIII: COMPUTER SIMULATIONS 164
8.1 Representative Cities 164
8.2 Model House 165
8.3 EnergyPlus Simulations by Climate Type 169
8.3.1 Climate Zone 1 - Miami, FL 169
8.3.1.1 Climate Conditions for Miami, FL 169
8.3.1.2 Simulation Results for Miami, FL 170
8.3.2 Climate Zone 2 - Phoenix, AZ 175
8.3.2.1 Climate Conditions for Phoenix, AZ 175
8.3.2.2 Simulation Results for Phoenix, AZ 176
8.3.3 Climate Zone 3 - Las Vegas, NV 179
8.3.3.1 Climate Conditions for Las Vegas, NV 179
8.3.3.2 Simulation Results for Las Vegas, NV 180
8.4.4 Climate Zone 4 - Kansas City, MO 184
8.4.4.1 Climate Conditions for Kansas City, MO 184
8.4.4.2 Simulation Results for Kansas City, MO 185
8.4 Computer Simulation Discussion 188
8.5 Overall Space Cooling and Space Heating Energy Reductions 189
CHAPTER IX: CONCLUSIONS AND RECOMMENDATIONS 194
9.1 Summary of Research Work 194
9.2 Conclusions 197
9.3 Recommendations for Future Research 200
REFERENCES 202

LIST OF FIGURES

Figure 1.1.1. Heat Storage Capacity of PCM Compared to Conventional Building Materials 2

Figure 1.2.1. Example of a Paraffin-based PCM's Specific Heat Changes During a Melting Process 4

Figure 1.2.2. Example of a Paraffin-based PCM's Temperature Changes During a Melting Process 5

Figure 1.3.1. Example of Improper Mixing 11

Figure 1.3.2. Timeline of Research and Development of PCM Incorporation Methods Used in Building Enclosures 12

Figure 3.1.1. Research Framework 32

Figure 4.1.1. Test Houses 33

Figure 4.1.2. Test House Schematic 34

Figure 4.1.4. Cooling System 36

Figure 4.1.5. T/C Grids on West Wall 37

Figure 4.1.6. HFMs Attached on South and West Walls and Ceiling 38

Figure 4.1.7. Flow Sensor 39

Figure 4.1.8. Weather Station 40

Figure 4.1.9. PCM Shield 40

Figure 4.1.10. Differential Scanning Calorimeter (DSC) 41

Figure 4.1.11. Sample DSC Test Results of the PCM Contained in the PCM Shields 42

Figure 4.1.12. PCM Shields Attached to Insulation Boards Inside the Cavities of the South and West Walls 43

Figure 4.1.13. PCM Shields Attached to Insulation Boards Inside the Ceiling Cavities 43

Figure 4.2.1. Measurement, Materials, and Sustainable Environment Center (M2SEC) Building 44

Figure 4.2.2. Interchangeable Wall Panels 45

Figure 4.2.3. Interchangeable Wall Panel Fastenings 46

Figure 4.2.4. Chiller and Water Tank 47
Figure 4.2.5. Schematic of the Wall Panel and the PCM Board Including Surface Temperature and Heat Flux Measuring Points 48
Figure 4.2.6. T/C Grids on the Interior Surfaces of the Panels..... 49
Figure 4.2.7. T/C Grids on the Exterior Surfaces of the Panels..... 49
Figure 4.2.8. Indoor Air Temperature Measurements 50
Figure 4.2.9. Outdoor Air Temperature Measurements..... 50
Figure 4.2.10. PCM Board..... 51
Figure 4.2.11. Section View of the PCM Board 51
Figure 4.2.12. Installed PCM Boards..... 53
Figure 5.1.1. Indoor Air Temperatures During Pre-retrofit Tests..... 57
Figure 5.1.2 (a). Exterior Surface Temperatures of the South Walls During Pre-retrofit Tests 57
Figure 5.1.2 (b). Interior Surface Temperatures of the South Walls During Pre-retrofit Tests..... 58
Figure 5.1.3 (a). Exterior Surface Temperatures of the West Walls During Pre-retrofit Tests..... 58
Figure 5.1.3 (b). Interior Surface Temperatures of the West Walls During Pre-retrofit Tests..... 59
Figure 5.1.4 (a). Attic Air Temperatures During Pre-retrofit Tests..... 59
Figure 5.1.4 (b). Interior Surface Temperatures of the Ceiling During Pre-retrofit Tests 60
Figure 5.1.5 (a). Heat Fluxes Across the South Walls During Pre-retrofit Tests 62
Figure 5.1.5 (b). Heat Fluxes Across the West Walls During Pre-retrofit Tests 62
Figure 5.1.5 (c). Heat Fluxes Across the Ceilings During Pre-retrofit Tests..... 63
Figure 5.1.6. Schematic of Wall Section Showing the Locations of the PCM Shield 64
Figure 5.1.7. Temperature Measurement Locations on the PCM Shields in the South Wall..... 65
Figure 5.1.8. Wall Heat Fluxes (Top), Temperatures (Middle), and Solar Irradiation (Bottom) for the Case of PCM Shields Installed at Location 1 in the South Wall 67

Figure 5.1.9. Total Heat Storage Capacity of the PCM During Phase Transition and Actual Heat Stored by the PCM Contained in the PCM shield at Location 1 in the South Wall 68

Figure 5.1.10. Wall Heat Fluxes (Top), Temperatures (Middle), and Solar Irradiation (Bottom) for the Case of PCM Shields Installed at Location 2 in the South Wall 70

Figure 5.1.11. Total Heat Storage Capacity of the PCM During Phase Transition and Actual Heat Stored by the PCM Contained in the PCM shield at Location 2 in the South Wall 71

Figure 5.1.12. Wall Heat Fluxes (Top), Temperatures (Middle), and Solar Irradiation (Bottom) for the Case of PCM Shields Installed at Location 3 in the South Wall 73

Figure 5.1.13. Total Heat Storage Capacity of the PCM During Phase Transition and Actual Heat Stored by the PCM Contained in the PCM shield at Location 3 in the South Wall 74

Figure 5.1.14. Wall Heat Fluxes (Top), Temperatures (Middle), and Solar Irradiation (Bottom) for the Case of PCM Shields Installed at Location 4 in the South Wall 75

Figure 5.1.15. Total Heat Storage Capacity of the PCM During Phase Transition and Actual Heat Stored by the PCM Contained in the PCM shield at Location 4 in the South Wall 76

Figure 5.1.16. Wall Heat Fluxes (Top), Temperatures (Middle), and Solar Irradiation (Bottom) for the Case of PCM Shields Installed at Location 5 in the South Wall 78

Figure 5.1.17. Total Heat Storage Capacity of the PCM During Phase Transition and Actual Heat Stored by the PCM Contained in the PCM shield at Location 5 in the South Wall 79

Figure 5.1.18. Wall Heat Fluxes (Top), Temperatures (Middle), and Solar Irradiation (Bottom) for the Case of a PCM Shield Installed at Location 1 in the West Wall..... 82

Figure 5.1.19. Total Heat Storage Capacity of the PCM During Phase Transition and Actual Heat Stored by the PCM Contained in the PCM shield at Location 1 in the West Wall 84

Figure 5.1.20. Wall Heat Fluxes (Top), Temperatures (Middle), and Solar Irradiation (Bottom) for the Case of a PCM Shield Installed at Location 2 in the West Wall..... 86

Figure 5.1.21. Total Heat Storage Capacity of the PCM During Phase Transition and Actual Heat Stored by the PCM Contained in the PCM shield at Location 2 in the West Wall 87

Figure 5.1.22. Wall Heat Fluxes (Top), Temperatures (Middle), and Solar Irradiation (Bottom) for the Case of a PCM Shield Installed at Location 3 in the West Wall..... 88

Figure 5.1.23. Total Heat Storage Capacity of the PCM During Phase Transition and Actual Heat Stored by the PCM Contained in the PCM shield at Location 3 in the West Wall 90

Figure 5.1.24. Wall Heat Fluxes (Top), Temperatures (Middle), and Solar Irradiation (Bottom) for the Case of a PCM Shield Installed at Location 4 in the West Wall..... 91

Figure 5.1.25. Total Heat Storage Capacity of the PCM During Phase Transition and Actual Heat Stored by the PCM Contained in the PCM shield at Location 4 in the West Wall 92

Figure 5.1.26. Wall Heat Fluxes (Top), Temperatures (Middle), and Solar Irradiation (Bottom) for the Case of a PCM Shield Installed at Location 5 in the West Wall..... 94

Figure 5.1.27. Total Heat Storage Capacity of the PCM During Phase Transition and Actual Heat Stored by the PCM Contained in the PCM shield at Location 5 in the West Wall 95

Figure 5.1.28. Schematic of Ceiling Section Showing the Locations of the PCM Shield..... 96

Figure 5.1.29. Ceiling Heat Fluxes (Top), Temperatures (Middle), and Solar Irradiation (Bottom) for the Case of a PCM Shield Installed at Location 2 in the Ceiling..... 98

Figure 5.1.30. Ceiling Heat Fluxes (Top), Temperatures (Middle), and Solar Irradiation (Bottom) for the Case of a PCM Shield Installed at Location 3 in the Ceiling..... 100

Figure 5.1.31. Total Heat Storage Capacity of the PCM During Phase Transition and Actual Heat Stored by the PCM Contained in the PCM shield at Location 3 in the Ceiling..... 101

Figure 5.1.32. Ceiling Heat Fluxes (Top), Temperatures (Middle), and Solar Irradiation (Bottom) for the Case of a PCM Shield Installed at Location 4 in the Ceiling..... 102

Figure 5.1.33. Total Heat Storage Capacity of the PCM During Phase Transition and Actual Heat Stored by the PCM Contained in the PCM shield at Location 4 in the Ceiling..... 103

Figure 5.2.1. Southwest View of M2SEC Showing the Locations of Control and Pre-retrofit Wall Panels in the South and West Walls 104

Figure 5.2.2 (a). Exterior Surface Temperatures of the Wall Panels in the South Wall During Pre-retrofit Testing..... 107

Figure 5.2.2 (b). Interior Surface Temperatures of the Wall Panels in the South Wall During Pre-retrofit Testing..... 107

Figure 5.2.3 (a). Exterior Surface Temperatures of the Wall Panels in the West Wall During Pre-retrofit Testing..... 108

Figure 5.2.3 (b). Interior Surface Temperatures of the Wall Panels in the West Wall During Pre-retrofit Testing..... 108

Figure 5.2.4 Heat Fluxes Across the Wall Panels in the South Wall During Pre-retrofit Testing..... 110

Figure 5.2.5. Heat Fluxes Across the Wall Panels in the West Wall During Pre-retrofit Testing 110

Figure 5.2.6. Wall Heat Fluxes (Top) and Temperatures (Middle and Bottom) for the PCM Board Installed in the South Wall 114

Figure 5.2.7. Wall Heat Fluxes (Top) and Temperatures (Middle and Bottom) for the PCM Board Installed in the West Wall 118

Figure 6.1.1. Sample of a DSC Curve 121

Figure 6.2.1 Specific Heat Curves of Sample A at Various Heating Rates (a) 0.5 °C/min, (b) 1 °C/min, and (c) 2 °C/min..... 123

Figure 6.2.2 Specific Heat Curves of Sample B at Various Heating Rates (a) 0.5 °C/min, (b) 1 °C/min, and (c) 2 °C/min..... 125

Figure 6.2.3. Enthalpy Curve of Sample A at Heating Rate of 0.5 °C/min As a Function of Temperature 128

Figure 6.2.4 Specific Heat Curves of Sample C at Various Heating Rates (a) 0.5 °C/min, (b) 1 °C/min, and (c) 2 °C/min..... 129

Figure 6.2.5 Specific Heat Curves of Sample D at Various Heating Rates (a) 0.5 °C/min, (b) 1 °C/min, and (c) 2 °C/min 130

Figure 6.2.6. Enthalpy Curve of Sample C at Heating Rate of 0.5 °C/min As a Function of Temperature 132

Figure 7.1.1. Node Types for CondFD Model in EnergyPlus 136

Figure 7.1.2. Calculated Input of Enthalpy as a Function of Temperature ..... 138 for the PCM Contained in the PCM Shield and Used by CondFD from Table 7.1.1 138

Figure 7.1.3. Calculated Input of Enthalpy as a Function of Temperature for the PCM Composite Contained in the PCM Board and Used by CondFD from Table 7.1.2 139

Figure 7.1.4. Calculated Input of Conductivity as a Function of Temperature for the PCM Contained in the PCM Shield and Used by CondFD from Table 7.1.3 142

Figure 7.1.5. Calculated Input of Conductivity as a Function of Temperature for the PCM Composite Contained in the PCM Board and Used by CondFD from Table 7.1.4 142

Figure 7.2.1. Modeling Schematic of the Test House 143

Figure 7.2.2. Model Prediction and Experimental Heat Fluxes Across the South Wall (Top) and Temperatures (Bottom) 145

Figure 7.2.3. Model Prediction and Experimental Heat Fluxes Across the West Wall (Top) and Temperatures (Bottom) 146

Figure 7.2.4. Model Prediction and Experimental Heat Fluxes Across the Ceiling (Top) and Temperatures (Bottom) 148

Figure 7.2.5. Modeling Schematic of the Wall Panels in the South and West Walls of M2SEC 150

Figure 7.2.6. Model Prediction and Experimental Heat Fluxes Across the South Wall Panel (Top) and Temperatures (Bottom) 151

Figure 7.2.7. Model Prediction and Experimental Heat Fluxes Across the West Wall Panel (Top) and Temperatures (Bottom) 152

Figure 7.3.1. Predicted Heat Fluxes Across the Retrofit South Wall Compared with the Experimental Data 155

Figure 7.3.2. Heat Flux Comparisons for the South Wall (a) Experiment and (b) Model Prediction 156

Figure 7.3.3. Predicted Heat Fluxes Across the Retrofit West Wall Compared with the Experimental Data 157

Figure 7.3.4. Heat Flux Comparisons for the West Wall (a) Experiment and (b) Model Prediction 158

Figure 7.3.5. Predicted Heat Fluxes Across the Retrofit Ceiling Compared with the Experimental Data 159

Figure 7.3.6. Predicted Heat Fluxes Across the Retrofit South Wall Panel in M2SEC Compared with the Experimental Data 161

Figure 7.3.7. Predicted Heat Fluxes Across the Retrofit West Wall Panel in M2SEC Compared with the Experimental Data 162

Figure 8.1.1. DOE Climate Zone Map Showing the Cities Included in the Simulation 164

Figure 8.2.1. Schematic of the Model House Used in the Simulation 166

Figure 8.3.1. Reductions in Total Heat Transfer at Various Locations of the PCM Shield in the South Wall for Miami, FL 173

Figure 8.3.2. Reductions in Total Heat Transfer at Various Locations of the PCM Shield in the West Wall for Miami, FL 173

Figure 8.3.3. Reductions in Total Heat Transfer at Various Locations of the PCM Shield in the Ceiling for Miami, FL 174

Figure 8.3.4. Total Heat Transfer Reduction at Combined Optimum Locations of the PCM Shield in the South Wall, West Wall and Ceiling for Miami, FL 174

Figure 8.3.5. Reductions of Total Heat Transfer at Various Locations of the PCM Shield in the South Wall for Phoenix, AZ 177

Figure 8.3.6. Reductions of Total Heat Transfer at Various Locations of the PCM Shield in the West Wall for Phoenix, AZ 178

Figure 8.3.7. Reductions of Total Heat Transfer at Various Locations of the PCM Shield in the Ceiling for Phoenix, AZ 178

Figure 8.3.8. Total Heat Transfer Reduction at Combined Optimum Locations of the PCM Shield in the South Wall, West Wall and Ceiling for Phoenix, AZ 179

Figure 8.3.9. Reductions of Total Heat Transfer at Various Locations of the PCM Shield in the South Wall for Las Vegas, NV 182

Figure 8.3.10. Reductions of Total Heat Transfer at Various Locations of the PCM Shield in the West Wall for Las Vegas, NV 182

Figure 8.3.11. Reductions of Total Heat Transfer at Various Locations of the PCM Shield in the Ceiling for Las Vegas, NV 183

Figure 8.3.12. Total Heat Transfer Reduction at Combined Optimum Locations of the PCM Shield in the South Wall, West Wall and Ceiling for Las Vegas, NV 183

Figure 8.3.13. Reductions of Total Heat Transfer at Various Locations of the PCM Shield in the South Wall for Kansas City, MO 186

Figure 8.3.14. Reductions of Total Heat Transfer at Various Locations of the PCM Shield in the West Wall for Kansas City, MO 187

Figure 8.3.15. Reductions of Total Heat Transfer at Various Locations of the PCM Shield in the Ceiling for Kansas City, MO 187

Figure 8.3.16. Total Heat Transfer Reduction at Combined Optimum Locations of the PCM Shield in the South Wall, West Wall and Ceiling for Kansas City, MO 188

Figure 8.4.1. Comparison of Total Heat Transfer Reductions at Combined Optimal Locations of the PCM Shield in the South Wall, West Wall, and Ceiling for the Various Cities 189

Figure 8.5.1. Reductions of Space Cooling Energy, Space Cooling Energy Demand, and Space Heating Energy at Combined Optimal Locations of the PCM Shield in the South Wall, West Wall, and Ceiling for the Various Cities 190

LIST OF TABLES

Table 1.2.1. Examples of Hydrated Salt PCMs 8

Table 1.2.2. Examples of Organic PCMs 9

Table 4.2.1. Properties of the PCM Boards 52

Table 5.1.1. Temperature Comparisons Between Control and Soon-to-be Retrofit Houses 56

Table 5.1.2. Peak Heat Flux Reductions Across the South Wall and Peak Heat Flux Time Lags Produced by the PCM Shield..... 80

Table 5.1.3. Peak Heat Flux Reductions Across the West Wall and Peak Heat Flux Time Lags Produced by the PCM Shield..... 95

Table 5.1.4. Peak Heat Flux Reductions Across the Ceiling and Peak Heat Flux Time Lags Produced by the PCM Shield 103

Table 5.2.1. Temperature Comparisons Between Control and Soon-to-be Retrofit Wall Panels..... 106

Table 5.2.2. Interior Surface Temperatures Comparisons of the South Wall Panels 115

Table 5.2.3. Heat Flux Reduction Comparisons Between the South and West Wall Panels Produced by the PCM Board..... 119

Table 6.2.1. DSC Test Results Comparisons of the PCM Contained in the PCM Shield..... 126

Table 6.2.2. DSC Test Results Comparisons of the PCM Composite Contained in the PCM Board 131

Table 7.1.1. Experimental Temperature and Corresponding Enthalpy for the PCM Contained in the PCM Shield..... 138

Table 7.1.2. Experimental Temperature and Corresponding Enthalpy for the PCM Compositein the PCM Board 139

Table 7.1.3. Conductivity of the PCM Contained in the PCM Shield..... 141

Table 7.1.4. Conductivity of the PCM Composite Contained in the PCM Board.... 142

Table 7.3.1. Additional Inputs for the PCM Contained in the PCM Shield 153

Table 7.3.2. Additional Inputs for the PCM Composite Contained in the PCM Board 160

Table 8.2.1. Model House Basic Information 166

Table 8.3.1. Climate Summary for the City of Miami, FL 170

Table 8.3.2. Annual Total Heat Transfer Reductions per Unit Area for Various Locations of the PCM Shield for Miami, FL 172

Table 8.3.3. Climate Summary for the City of Phoenix, AZ 175

Table 8.3.4. Annual Total Heat Transfer Reductions per Unit Area for Various Locations of the PCM Shield for Phoenix, AZ 177

Table 8.3.5. Climate Summary for the City of Las Vegas, NV 180

Table 8.3.6. Annual Total Heat Transfer Reductions per Unit Area for Various Locations of the PCM Shield for Las Vegas, NV 181

Table 8.3.7. Climate Summary for the City of Kansas City, MO 184

Table 8.3.8. Annual Total Heat Transfer Reductions per Unit Area for Various Locations of the PCM Shield for Kansas City, MO 186

NOMENCLATURE

c_{avg}	average specific heat of the solid and liquid phases, kJ/kg°C (Btu/lb_m°F)
c_{eff}	effective heat capacity, kJ/kg°C (Btu/lb_m°F)
c_l	specific heat of the liquid phase, kJ/kg°C (Btu/lb_m°F)
c_p	specific heat, kJ/kg°C (Btu/lb_m°F)
c_s	specific heat of the solid phase, kJ/kg°C (Btu/lb_m°F)
$C_p(T)$	specific heat as a function of temperature, kJ/kg°C (Btu/lb_m°F)
ρ	density, kg/m^3 (lb_m/ft^3)
ϵ	melting temperature range, °C (K) (°F (°R))
f_l	liquid fraction
h	enthalpy, kJ/kg (Btu/lb_m)
h(T)	enthalpy as a function of temperature, kJ/kg (Btu/lb_m)
k	thermal conductivity, W/m°C (Btu/hr·ft°F, Btu·in/hr·ft^2°F)
L	latent heat of fusion, kJ/kg (Btu/lb_m)
Q	heat storage capacity, kJ/m^3 (Btu/ft^3)
T	temperature, °C (K) (°F (°R))
ΔT	temperature interval, °C (K) (°F (°R))
T_l	highest temperature in the melting temperature range, °C (K) (°F (°R))
T_m	melting temperature, °C (K) (°F (°R))
T_s	lowest temperature in the melting temperature range, °C (K) (°F (°R))
t	time, seconds

Δt	calculation time step, seconds
x	space distance, m (ft)
Δx	finite difference layer thickness, m (ft)

CHAPTER I

INTRODUCTION

In recent years, climate change, which in part is the result of increased energy-related CO_2 emissions, mostly from fossil fuels, has become a major environmental issue worldwide (IEA, 2012). As part of a global action, 191 countries have put forth various efforts to reduce greenhouse gas emissions. Such efforts include, but are not limited to, developing renewable energy technologies and energy efficiency strategies, including those for buildings (EIA, 2013).

In the U.S., buildings consume about 40% of total energy used in the country (EIA, 2012) and about 40% of greenhouse gas emissions are attributed to building energy consumption (EIA, 2011). Space cooling and heating energy usage tops the list of energy consumption in buildings at roughly 50% (EIA, 2012). For this reason, energy savings in building space cooling and heating would produce a significant reduction in total energy consumption, which in turn would reduce greenhouse gas emissions.

1.1 Thermal Energy Storage in Building Enclosures

In buildings, enclosure thermal storage, which is related to building thermal mass, has gained importance in energy management and energy conservation (Mirzaei and Haghighat, 2012; and Zhou et al., 2012). In general, thermal mass is achieved by constructing massive structures, which is expensive and old-fashioned.

The principle of thermal mass can be significantly assisted by the incorporation of latent heat storage technologies. This can be achieved by the use of phase change materials (PCMs), which absorb and release heat in greater amounts than conventional building materials. This is the case because conventional building materials store heat energy in a sensible rather than a latent manner. For example, PCMs store 44 times more heat than concrete by using their latent heat storage capacity during phase transition. This is shown in Figure 1.1.1, which also include sandstone and brick. In other words, much less volume is required to achieve high thermal mass in building enclosures when PCMs are used instead of conventional building materials.

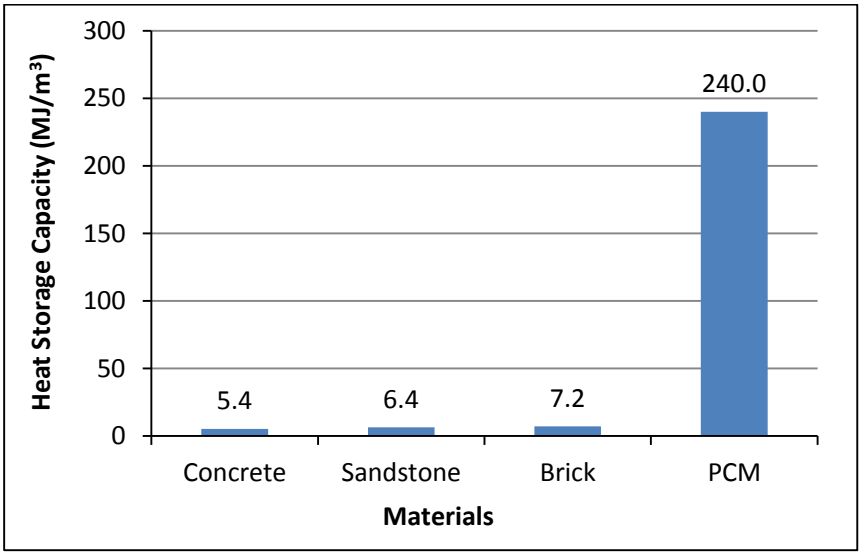

Figure 1.1.1. Heat Storage Capacity of PCM Compared to Conventional Building Materials (Source: Mehling and Cabeza, 2008)

The heat storage capacity can be estimated by Equation (1-1) below, which is

$$Q = c_p \times \rho \times \Delta T \quad (1\text{-}1)$$

where:

Q = heat storage capacity, kJ/m^3 (Btu/ft^3)

c_p = specific heat, kJ/kg°C (Btu/lb_m°F)

ρ = density, kg/m^3 (lb_m/ft^3)

ΔT = temperature interval, °C (K) (°F (°R)), 4 °C (K) (7.2 °F (°R)) was used because this was the melting temperature range of the PCM.

1.2 Phase Change Materials (PCMs)

All materials transform from solid-to-liquid and from liquid-to-gas as their temperatures are progressively increased from absolute zero. Energy, in the form of heat, is absorbed as PCMs transition from solid-to-liquid. Conversely, heat is released during their transition from liquid-to-solid. The energy that is stored and released during the changes of state is called latent heat, and for some substances, including PCMs, it occurs over a range of temperatures. Figure 1.2.1 shows an example of a paraffin-based PCM's melting temperature range of about 15.0 °C (59.0 °F) from 23 to 38 °C (73.4 to 100.4 °F), as recorded by a differential scanning calorimeter (DSC). The specific heat of the PCM is nearly constant when the PCM is all in the solid phase. While the PCM melts, the specific heat increases significantly and then decreases back when it completes its phase transition. The temperature range during

this process represents the melting temperature range of the PCM. When the PCM is all liquid after completing its phase transition, the specific heat of the PCM remains nearly constant. From Figure 1.2.1, one can see how the specific heat values differ when the PCM is in the solid and liquid phases.

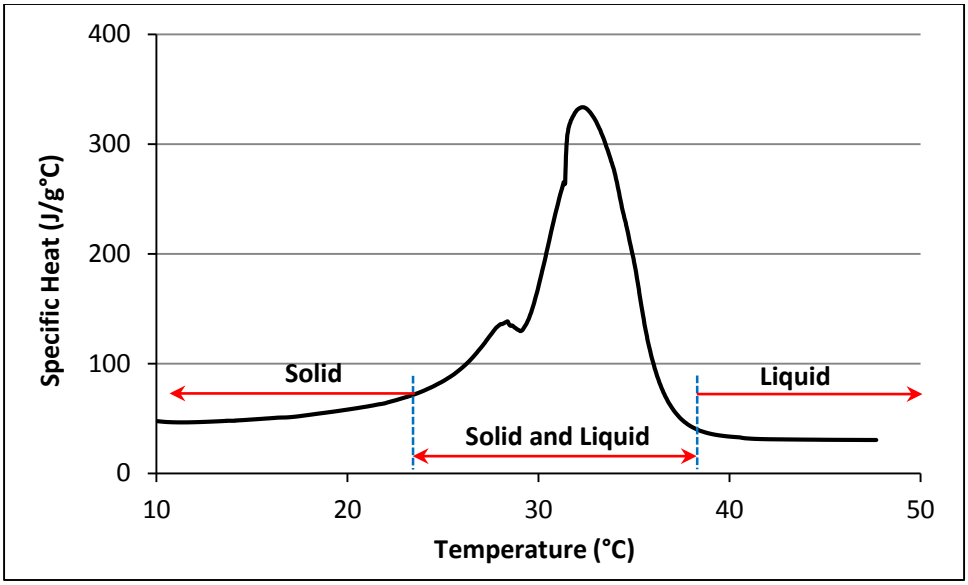

Figure 1.2.1. Example of a Paraffin-based PCM's Specific Heat Changes During a Melting Process

For other substances (e.g., water), during the substances' transition from solid-to-liquid and from liquid-to-gas and their reversed transitions, the substances remain at nearly constant temperatures until the phase transition process is complete.

PCMs are ordinary substances, usually waxes, oils, and hydrated salts, that have been *engineered* to change phase in specific temperature ranges depending on the intended application. In addition, PCMs have noticeably higher latent heats of

fusion. Their phase change in specific temperature ranges and their relatively large latent heats of fusion make PCMs attractive for thermal storage systems.

The PCM's phase transition process from solid to liquid is shown in Figure 1.2.2. While the PCM is in the solid phase, its temperature increases almost linearly as its enthalpy increases. This happens because the PCM is storing sensible heat. During melting, the temperature of the PCM increases, but at a lower rate as more energy is being absorbed. This is the case because the PCM is storing latent heat. Once the PCM is completely melted, its temperature increases significantly when more heat is added. This heat is stored as sensible heat.

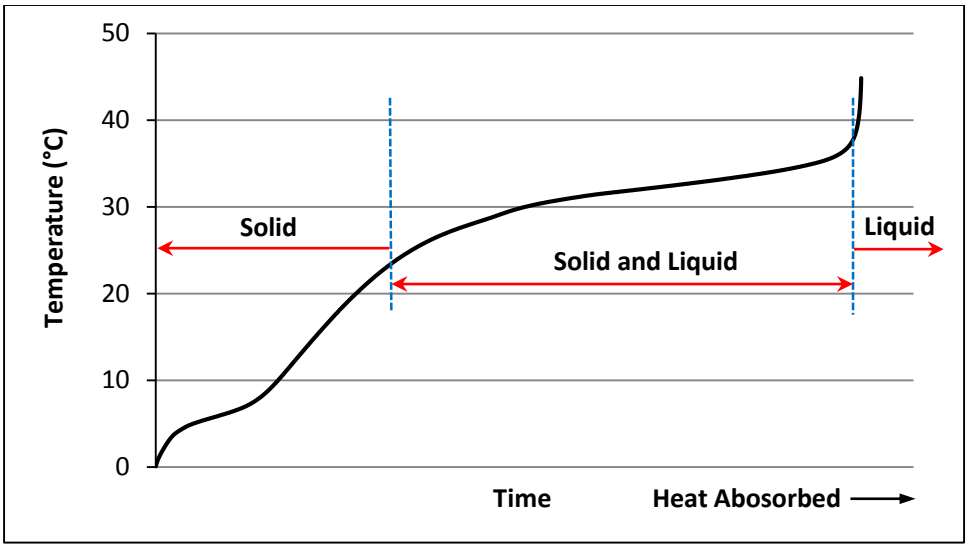

Figure 1.2.2. Example of a Paraffin-based PCM's Temperature Changes During a Melting Process

In buildings, the integration of PCMs with appropriate melting and solidification temperature ranges and sufficiently high latent heats of fusion results in a means of converting regular building enclosures, such as walls, ceilings, roofs, and

foundations into high thermal mass components. In buildings, high thermal mass creates inertia against indoor and wall temperature fluctuations and reduces the amount of heat transfer during daily peak times. This may help in decreasing electricity usage during peak times by time-shifting the peak heat fluxes to later times of the day (Lee, 2013).

In general, the candidate PCMs must have the following characteristics to make them attractive for building thermal storage. They must have (1) high latent heat of fusion, (2) phase change transition temperatures in the desirable range, (3) high thermal conductivity (to minimize thermal gradients), (4) high specific heat and density (for high thermal inertia), (5) long term reliability during repeated cycling, (6) low volume change during phase transition, (7) low vapor pressure (for mass conservation), (8) be nontoxic, and (9) exhibit little or no supercooling (Ghoneim et al., 1991). Supercooling is the process experienced by some substances when their molecules tend to not solidify (crystallize) even when its solidification temperature has been reached and surpassed in a cooling process. This creates an incongruent solidification process that leads to inefficiencies.

The PCMs used in building applications can be both inorganic and organic materials. For building applications, the phase changes are predominantly of the solid-liquid transitions type, although solid-solid types are also used at higher operating temperatures in other applications (e.g., metallurgical and ceramic) (Hawes et al., 1993). Upon heating, however, some paraffins also exhibit solid-to-solid phase

transition at temperatures below their melting range. These transitions are the result of distortions of their crystal structures (Chazhengina et al., 2003).

PCMs are classified as inorganic and organic.

1.2.1 Inorganic PCMs

Inorganic PCMs include hydrated salts, molten salts, and metals. In buildings, hydrated salts, of which some are shown in Table 1.2.1, are among those that offer the potential for enhancing building thermal mass. These PCMs have some attractive properties such as high latent heat values, non-flammability, relatively low cost and their availability. On the other hand, hydrated salt PCMs also have some unwanted characteristics. They are corrosive, and therefore, are incompatible with several materials used in buildings, especially metals. For this reason, hydrated salts must be encapsulated using special containment methods that require support and space. They also have the tendency to supercool. Supercooling in hydrated salts leads to an incongruent solidification with internal molecular segregation. This affects the PCM cycle by not allowing all the stored heat to be released, which leads to subsequent poor melting-solidification cycling. Proprietary chemicals, known as nucleating agents, are added to prevent supercooling. For example, a common nucleating agent used with calcium chloride hexahydrate is strontium chloride hexahydrate because of its low price and because it meets other technological requirements, like desired melting temperature range (Feilchenfeld et al., 1985).

Table 1.2.1. Examples of Hydrated Salt PCMs (typical values)
(Source: Hawes et al., 1993)

PCM	Melting point °C (°F)	Heat of fusion J/g (Btu/lb_m)
$KF \cdot 4H_2O$ Potassium fluoride tetrahydrate	18.5 (65.3)	231 (99.3)
$CaCl_2 \cdot 6H_2O$ Calcium chloride hexahydrate	29.7 (85.5)	171 (73.5)
$Na_2SO_4 \cdot 10H_2O$ Sodium sulphate decahydrate	32.4 (90.3)	254 (109.2)
$Na_2HPO_4 \cdot 12H_2O$ Sodium orthophosphate dodecahydrate	35.0 (95.0)	281 (107.9)
$Zn(NO_3)_2 \cdot 6H_2$ Zinc nitrate hexahydrate	36.4 (97.5)	147 (63.2)

Recommended for building applications.

1.2.2 Organic PCMs

Organic PCMs, some of which are shown in Table 1.2.2, have a number of characteristics that make them useful for building applications. These characteristics include their non-toxicity, high latent heat of fusion, availability, and the fact that they melt congruently, where supercooling is not a significant problem. In addition, they are chemically stable and they comprise a broad choice of substances. They are compatible with various building materials. However, organic PCMs also have some drawbacks. The most significant is their flammability. A few have odors, which may make them objectionable, and for some, the volume change during phase transition can be appreciable (Hawes et al., 1993).

Table 1.2.2. Examples of Organic PCMs (typical values) (Source: Hawes et al., 1993)

PCM	Melting point °C (°F)	Heat of fusion J/g (Btu/lb_m)
$CH_3(CH_2)_{16}COO(CH_2)_3CH_3$ butyl stearate	19 (66.2)	140 (60.2)
$CH_3(CH_2)_{11}OH$ 1-dodecanol	26 (78.8)	200 (86.0)
$CH_3(CH_2)_{12}OH$ 1-tetradecanol	38 (100.4)	205 (88.1)
$CH_3(CH_2)_nCH_3$ paraffin	20 - 60 (68.0 - 140.0)	~200 (~86.0)
45% $CH_3(CH_2)_8COOH$ 55% $CH_3(CH_2)_{10}COOH$ 45/55 capric-lauric acid	21 (69.8)	143 (61.5)
$CH_3(CH_2)_{12}COOC_3H_7$ propyl palmitate	19 (66.2)	186 (80.0)

Recommended for building applications.

1.3 PCM Incorporation Methods

PCM incorporation methods into the building enclosures are described below.

1.3.1 Imbibing

Imbibing is a technology in which a building enclosure material, such as gypsum, brick or concrete, is dipped into a melted PCM and then absorbs the PCM into its internal pores. This method, however, produces PCM leakages and creates humidity transfer problems within the building enclosure.

1.3.2 Direct Incorporation

Direct incorporation is a technology in which liquid or powdered PCMs are directly added to building materials such as gypsum, concrete, or plaster during

production or directly mixed with building insulation materials such as cellulose. This method is simple, but leakage, incompatibility with construction materials, and their degradation and eventual dematerialization may represent serious problems.

1.3.3 Macroencapsulation

Macroencapsulation is the technology when PCMs are encapsulated in containers, larger than 1 mm, to prevent some of the problems found with imbibing and direct incorporation. Examples of containers include tubes and spheres. With macroencapsulated PCMs, the structural components of the building enclosure become the restraining and holding elements of the containers. For example, the studs in residential wall frames would hold the PCM containers in place. However, the use of large containers may result in large temperature differentials between the walls of the containers and the PCM core (i.e., the geometric center of the PCM bulk), leading to uneven temperature distributions. For example, the PCM next to the container walls may remain solid while the core part of the PCM may still remain in the liquid form, thus preventing the effective transfer of heat or vice versa.

1.3.4 Microencapsulation

Microencapsulation is a technology in which PCM particles are enclosed in thin and sealed films of sizes up to 1000 μm (39.370×10^{-3} in.), which allows the PCMs to maintain their shape and prevent them from leaking during the phase change process. Microencapsulation results in higher heat transfer rates as compared to those

of macroencapsulation. Higher heat transfer rate results in rapid melting and solidification of the microencapsulated PCM. With microencapsulation, improper mixing of the PCMs with building materials may result in uneven PCM distribution, leading to partial melting and solidification of the PCMs. An example of improper mixing is shown in Figure 1.3.1.

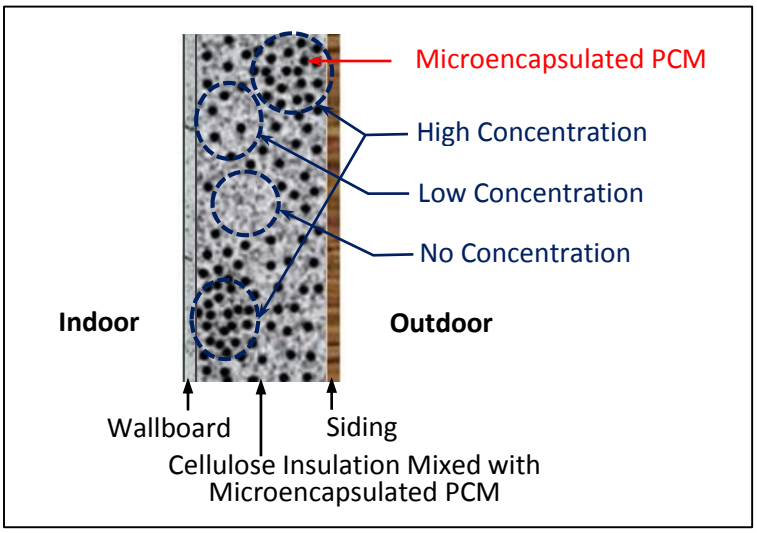

Figure 1.3.1. Example of Improper Mixing (Cellulose Insulation Mixed with Microencapsulated PCM) - Section View of Wall Cavity

1.3.5 Shape-stabilized PCMs

Shape-stabilized PCMs is a technology where the PCMs are dispersed in another phase of supporting materials (e.g., high density polyethylene) to form a stable composite material. These types of composites are generally heavy and have a fixed geometry, such as square floor tiles. Therefore, their applications in building enclosures are limited to floor systems.

Figure 1.3.2 shows the timeline of research and development of PCM incorporation methods used in building enclosures.

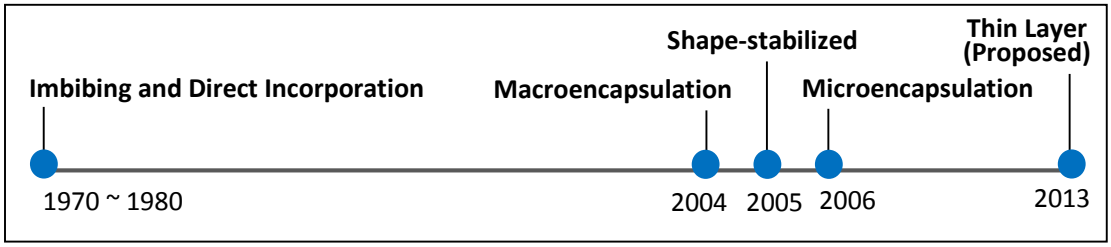

Figure 1.3.2. Timeline of Research and Development of PCM Incorporation Methods Used in Building Enclosures

1.4 PCM Numerical Models

Several numerical models have been developed to solve phase change problems. The most commonly used are described below. These include the enthalpy method, the effective (apparent) heat capacity method, and the heat source method (Al-Saadi and Zhai, 2013).

1.4.1 Enthalpy Method

Eyres et al. (1946) developed the enthalpy method to solve heat transfer problems involving variations of the media's thermal properties. These variations were with respect to temperature. In the enthalpy method, the latent and specific heat are combined into an enthalpy term. In equation form, the enthalpy method is described by:

$$\rho \frac{\partial h}{\partial t} = \frac{\partial}{\partial x}\left(k \frac{\partial T}{\partial x}\right) \tag{1-2}$$

where:

ρ = density, kg/m^3 (lb$_m$/ft^3)

h = enthalpy, kJ/kg (Btu/lb$_m$)

t = time, seconds

x = space distance, m (ft)

k = thermal conductivity, W/m°C (Btu/hr·ft°F)

T = temperature, °C (K) (°F (°R))

The enthalpy at a node is dependent on the temperature and a temperature-enthalpy function is established as follows:

$$T = \begin{cases} \frac{h}{c_s}, & h \le c_s \times (T_m - \epsilon) \\ \frac{h + \left(\frac{c_l - c_s}{2} + \frac{L}{2\times\epsilon}\right) \times (T_m - \epsilon)}{\left(\frac{c_l - c_s}{2} + \frac{L}{2\times\epsilon}\right)}, & c_l \times (T_m - \epsilon) < h < c_s \times (T_m + \epsilon) + L \\ \frac{h - (c_s - c_l) \times T_m - L}{c_l}, & h \ge c_l \times (T_m + \epsilon) + L \end{cases} \tag{1-3}$$

where:

T = temperature, °C (K) (°F (°R))

h = enthalpy, kJ/kg (Btu/lb$_m$)

c_s = specific heat of the solid phase, kJ/kg°C (Btu/lb$_m$°F)

c_l = specific heat of the liquid phase, kJ/kg°C (Btu/lb$_m$°F)

L = latent heat of fusion, kJ/kg (Btu/lb_m)

ϵ = half range of melting temperatures, °C (K) (°F (°R))

T_m = melting temperature, °C (K) (°F (°R))

1.4.2 Effective (Apparent) Heat Capacity Method

In the effective (apparent) heat capacity method, the heat capacity term imitates the effect of enthalpy by using various heat capacities during the phase change transitions. Hashemi and Sliepcevich (1967) developed the effective (apparent) heat capacity method to solve the one-dimensional heat conduction equation during phase change transitions. The equation using the effective (apparent) heat capacity method is shown below.

$$\rho \times c_{eff} \times \frac{\partial h}{\partial t} = \frac{\partial}{\partial x}\left(k \frac{\partial T}{\partial x}\right) \tag{1-4}$$

where:

ρ = density, kg/m^3 (lb_m/ft^3)

c_{eff} = effective heat capacity, kJ/kg°C (Btu/lb_m°F)

T = temperature, °C (K) (°F (°R))

h = enthalpy, kJ/kg (Btu/lb_m)

t = time, seconds

x = space distance, m (ft)

k = thermal conductivity, W/m°C (Btu/hr·ft°F)

To estimate the effective heat capacity, two methods are usually used: an analytical/empirical relationship and a numerical approximation. Analytical/empirical relationships are used when the properties of the PCMs are provided on a limited basis. For example, these relationships can be used when DSC data are not available, but limited manufacturer's or published data are available. The effective heat capacity of the PCM can be determined by using these limited PCM properties, such as it is shown in Equation (1-5) (Voller, 1997).

$$c_{eff} = \begin{cases} c_s, \ T \leq T_m - \epsilon \ \text{(solid state)} \\ \frac{c_s + c_l}{2} + \frac{L}{2\epsilon}, \ T_m - \epsilon < T < T_m + \epsilon \ \text{(phase transition state)} \\ c_l, \ T \geq T_m + \epsilon \ \text{(liquid state)} \end{cases} \quad (1\text{-}5)$$

where:

c_{eff} = effective heat capacity, kJ/kg°C (Btu/lb_m°F)

c_s = specific heat of the solid phase, kJ/kg°C (Btu/lb_m°F)

c_l = specific heat of the liquid phase, kJ/kg°C (Btu/lb_m°F)

L = latent heat of fusion, kJ/kg (Btu/lb_m)

ϵ = melting temperature range, °C (K) (°F (°R))

T_m = melting temperature, °C (K) (°F (°R))

The numerical approximation can be used when the detailed properties of the PCMs are obtained from differential scanning calorimeter (DSC) tests such as the various enthalpies at corresponding temperatures. The effective heat capacity is

determined by using the derivative of enthalpy with respect to temperature. This is shown in Equation (1-6) (Morgan, 1978).

$$c_{eff} = \frac{\Delta h}{\Delta T} = \frac{h^n - h^{n-1}}{T^n - T^{n-1}} \quad (1\text{-}6)$$

where:

c_{eff} = effective heat capacity, kJ/kg°C (Btu/lb_m°F)

h = enthalpy, kJ/kg (Btu/lb_m)

T = temperature, °C (K) (°F (°R))

n = new time step, seconds

n-1 = previous time step, seconds

1.4.3 Heat Source Method

In the heat source method, the enthalpy is separated into the specific heat and the latent heat, where the latent heat is considered as a heat source term. This is shown in Equation (1-7) (Eyres, 1946).

$$\rho \times c_{avg} \times \frac{\partial T}{\partial t} = \frac{\partial}{\partial x}\left(k \frac{\partial T}{\partial x}\right) - \rho \times L \times \frac{\partial f_l}{\partial t} \quad (1\text{-}7)$$

where:

ρ = density, kg/m^3 (lb_m/ft^3)

c_{avg} = average specific heat of the solid and liquid phases,

kJ/kg°C (Btu/lb_m°F)

T = temperature, °C (K) (°F (°R))

t = time, seconds

x = space distance, m (ft)

k = thermal conductivity, W/m°C (Btu/hr·ft°F)

L = latent heat of fusion, kJ/kg (Btu/lb_m)

f_l = liquid fraction

The liquid fraction is determined by Equation (1-8) (Swaminathan and Voller, 1997).

$$f_l = \begin{cases} 0, \ T \leq T_m - \epsilon \text{ (solid state)} \\ \frac{(T-T_s)}{(T_l-T_s)} + \frac{L}{2\epsilon}, \ T_m - \epsilon < T < T_m + \epsilon \text{ (phase transition state)} \\ 1, \ T \geq T_m + \epsilon \text{ (liquid state)} \end{cases} \quad (1\text{-}8)$$

where:

T = temperature, °C (K) (°F (°R))

T_s = lowest temperature in the melting temperature range, °C (K) (°F (°R))

T_l = highest temperature in the melting temperature range, °C (K) (°F (°R))

L = latent heat of fusion, kJ/kg (Btu/lb_m)

ϵ = melting temperature range, °C (K) (°F (°R))

T_m = melting temperature, °C (K) (°F (°R))

1.5 Building Energy Simulation Programs Including PCM Models

There are a few whole-building energy simulation programs that include PCM models. Some of them are EnergyPlus, TRNSYS, and ESP-r (Al-Saadi and Zhai, 2013).

1.5.1 EnergyPlus

EnergyPlus is a building energy analysis and thermal load simulation program. PCMs can be simulated using EnergyPlus with a conduction finite difference (CondFD) solution algorithm. The PCM model within EnergyPlus was validated by comparing its results with experimental data and other models such as Heating 7.3 (Tabares-Velasco et al., 2012).

1.5.2 Transient System Simulation Tool (TRNSYS)

TRNSYS is a transient systems simulation program with a modular structure. Several modules for PCM modeling have been developed (Ahmad et al., 2006; Ghoneim et al., 1991; Ibáñez et al., 2005; Kuznik et al., 2011; Schranzhofer et al., 2006; and Stritih and Novak, 1996). One such module is a simplified PCM module that was developed and added to its commercially-available version. The module simulates PCMs as an internal layer within an enclosure system. The model is currently limited to its assumptions that materials melt and solidify isothermally and have constant specific heats in both of the solid and liquid phases. In addition, in the

transition state, the temperature of the solid-liquid interface of the PCM is assumed constant.

1.5.3 Energy Systems Research Unit (ESP-r)

ESP-r is a dynamic energy simulation tool used for modeling thermal, visual, and acoustic performance of buildings. ESP-r has the capability to model PCMs using the effective heat capacity method and the heat source method (Heim and Clarke, 2004; and Schossig et al., 2005). While simulation results using ESP-r have been found in the literature, none have shown any substantial validations for these two algorithms.

CHAPTER II

LITERATURE REVIEW

Phase Change Material (PCM) incorporation in building enclosures helps with wall thermal management as well as in reducing building energy consumption (Kosny et al., 2012; Mazo et al., 2012; Qureshi et al., 2011; Zhu et al., 2011; Castell et al., 2010; Diaconu and Cruceru, 2010; and Kosny et al., 2010). Furthermore, it is required that PCM applications be practical, reliable, and cost effective. Therefore, it was necessary to study several approaches for the optimization of the thermal performance of building enclosures containing PCMs. Many studies on the application of PCMs in building components appear in the technical literature and the most relevant are summarized below.

Tomlinson and Heberle (1990) studied the thermal and economic performance of PCM-imbibed wallboards. Two houses were tested with and without PCM-imbibed wallboards. Then, a simulation program was modified based on the results from test houses. The simulation results using a Denver, CO weather data showed that PCM wallboards, for example, had a significant impact in reducing space heating energy consumption. The PCM wallboards retained 200% more heat when compared to conventional wallboards. The optimized PCM-wallboards produced a simple payback of less than five years.

Salyer and Sircar (1990 and 1997) developed a cost-effective, environmentally-acceptable PCM as well as several PCM incorporating methods for

buildings that used concrete and gypsum wallboards. Their research was developed around imbibing the PCM into porous materials (e.g., wallboard), permeating the PCM into polymeric carriers (e.g., cross-linked pellets of high-density polyethylene), and absorbing the PCM into finely divided special silicas to form soft free-flowing dry powders. However, it was later determined that PCM imbibing produced PCM leakage (e.g., "surface sweating") (Kosny et al., 2006).

Hawes et al. (1993) conducted a number of studies related to building energy-storage materials including imbibing PCMs into concrete blocks and gypsum wallboards. Their research showed the potential of producing functional and effective building elements that could significantly affect energy savings. Their research suggested that butyl stearate and paraffin appeared to be the most effective PCMs. Paraffin-based PCMs, however, had incompatible characteristics with building materials and occupants' comfort. These included flammability and fume generation, odors, reactions with the products of hydration in building materials (e.g., concrete), and volume changes at phase transition.

Kissock et al. (1998) and Kissock (2000) carried out experimental and simulation studies of the thermal performance of phase-change wallboards in simple structures. Two test cells were built for the experiments which were carried out in Dayton, OH; one with PCM imbibed wallboards and the other with conventional wallboards. Annual space heating and cooling loads were simulated through wallboards, concrete sandwich walls, and steel roofs with and without the PCM. The simulations showed that the addition of PCM to wallboards, concrete sandwich walls,

and steel roofs reduced the peak space cooling loads by 16, 19, and 30%, respectively. Their research, however, indicated that moisture transfer problems in PCM imbibed wallboards created condensation that was observed on interior surfaces of glazing in the test cell with PCM wallboards. It was explained that possibly "PCM wallboard was effectively waterproof and therefore water vapor would not be able to diffuse through the PCM wallboard."

Lin et al. (2005) developed shape-stabilized PCM plates in which paraffin PCM was mixed with polyethylene that was also used as a supporting material. These plates were tested on residential floors using an under-floor electric heating system during the heating season. It was observed that the PCM plates stored heat during electricity off peak periods and released the heat during periods of peak demand. The results showed that more than half of the electricity used for the space heating shifted from peak to off peak periods. Zhang et al. (2006) continued the study by modeling the shape-stabilized PCM plates based on the previous experimental results. The new results indicated that a PCM optimum melting temperature of 2.0 °C (3.6 °F) higher than the indoor air temperature existed for space heating.

Ahmad et al. (2006) tested PCM wallboards with PVC panels containing a polyethylene glycol PCM. The melting temperature range of the PCM used was between 21.0 and 25.0 °C (69.8 and 77.0 °F). A vacuum insulation panel (VIP) technology was used to develop a lightweight building structure, as well as to increase a thermal resistance of the walls. The VIP was a thermal insulation, which was sealed in a barrier film creating a vacuum. Two identical test-cells were built;

one with and one without PCM wallboards. The simulations were conducted using TRNSYS. The model showed a good agreement with the experimental results. In summer, the indoor air temperature fluctuations of the cell with PCM decreased by 20.0 °C (36.0 °F) when compared to the cell without PCM. In winter, the indoor air temperature of the cell with PCM wallboards was kept above 0 °C (32.0 °F) while the indoor air temperature of the cell without PCM was -9.0 °C (15.8 °F). Their study presented that PCM wallboards were useful for space cooling and space heating comfort management.

Kuznik and Virgone (2009a and 2009b) conducted experimental and numerical studies of the thermal performance of PCM copolymer composite wallboards. Two identical test cells were used to conduct experiments to evaluate the performance of the wallboards with and without PCMs in a climate-controlled laboratory. The results indicated that indoor air temperature and wall surface temperature fluctuations were reduced by 4.7 and 3.5 °C (8.5 and 6.3 °F), respectively, in the test cell with PCM wallboards. A numerical model was developed and validated against experimental data. The results from the model showed good agreement with the data, but only when the specific heat curves of melting or solidification for the PCM being used were integrated into the model. Specific heat curves of PCMs' melting processes were different from their solidification processes. For this reason, specific heat curves of melting were not applicable to predict cooling processes of PCMs, or specific heat curves of solidification were not applicable to predict the PCM heating processes correctly. This was the result of the hysteresis

phenomenon, which occurred when the melting process of the PCM started at higher temperatures than the temperature of solidification. This suggested that the hysteresis phenomenon should be considered when modeling PCMs.

Qureshi et al. (2011) studied the application of PCM wallboards on walls and ceilings. PCM wallboards used in their research were gypsum boards containing microencapsulated PCMs whose melting temperature range was 18.0 to 20.0 °C (64.4 to 68.0 °F). Two identical test offices were constructed; one finished with PCM wallboards on walls and ceilings and the other finished with conventional wallboards. Both test offices were equipped with electric heaters. The electricity consumption for space heating was measured during the heating season. Indoor air temperatures were set to the range of 18.0 to 22.0 °C (64.4 to 71.6 °F) in both test offices, while outdoor air temperatures were around 10.0 °C (50.0 °F) in early morning and night to 20.0 °C (68.0 °F) during the day. The results showed that the electricity consumption was reduced by about 30% for space heating when the PCM wallboards were used.

Since 2000, research at the University of Kansas has been conducted to evaluate the thermal performance of building walls enhanced with PCMs (King, 2004; Zhang, 2004; Zhang et al., 2005; Zhu, 2005; Evers, 2008; Medina et al., 2008; Medina and Zhu, 2008; Fang, 2009; Fang and Medina, 2009; Reshmeen, 2009; Evers et al., 2010; and Lee, 2013). The purpose of these investigations was to produce a thermally enhanced wall that would reduce heat transfer to and from the building interior, and therefore, produce peak air conditioning demand reductions, thermal load shifting, and energy savings. Their research included experimental studies using

two identical test houses under full weather conditions, a dynamic wall simulator, and modeling and simulation studies. Different PCM application methods, such as pipe encapsulation methods, PCM mixed with cellulose insulation, and PCM shields were tested, as well as different types of PCMs such as n-paraffin based PCMs and hydrated salt based PCMs with various melting temperatures. Differential scanning calorimeter (DSC) tests were also conducted to study the thermal properties of the PCMs.

Two identical test houses, with identical thermal performance before any retrofit, were used. The thermal performance of the retrofit house using n-paraffin based PCM (Zhang et al., 2005) and hydrated salt based PCM (Lee, 2013) showed that the average peak heat flux across the walls decreased by 21.0 and 27.3%, respectively. The thermal performance of the retrofit house using Phase Change Material - Structural Insulated Panel (PCM-SIP) with n-paraffin based PCM (Medina et al., 2008) showed that the average peak heat flux across the walls decreased by 62%. In all cases, the PCM concentration was 20%. PCM concentration was given by weight of the internal siding (e.g., wallboard). In addition, it was found that the average interior surface temperatures were more steady than those of the control house during the cooling seasons.

Experiments using a dynamic wall simulator, which was built to perform controlled laboratory experiments, also showed reductions in peak heat transfer rate when paraffin-based PCM mixed with cellulose insulation (Evers et al., 2010) and a prototype of the proposed PCM shield (Reshmeen, 2009) were tested. PCM modeling

(Fang, 2009) and building energy simulations (Lee, 2013) were conducted to extrapolate the experimental results to other locations under different weather conditions.

Incorporating PCMs into walls and ceilings of building enclosures offers energy, environmental, and economic benefits. Some of the benefits are listed below.

1. Energy savings in space cooling/heating could be produced by the reduction of heat transfer across walls and ceilings.
2. Peak electricity demand could be shaved off by shifting electricity demand for space cooling from on-peak to off-peak times. The electricity usage for building space cooling/heating causes the electric demand to peak in the early to mid afternoon in most of the country. Shifting peak demand for building space cooling could reduce peak electricity demand, thus allowing power producers to keep lower operating costs, and subsequently, consumer electricity bills low.
3. The mechanical systems used for space cooling/heating (i.e., chillers, fan-coil units, pumps, ducts, fans, etc.) could be downsized by the reduction of peak heat transfer across the walls and ceilings.
4. The efficiency of space cooling/heating systems could increase by decreasing equipment on/off cycles. Space cooling/heating devices run at optimum conditions when operating at longer on-times. This could also increase the equipment's operating life.

5. Occupants' comfort could increase by decreasing the amplitude of wall or ceiling surface temperature fluctuations.
6. The need for space cooling/heating systems could be eliminated in parts of the country during some times of the year.
7. Greenhouse gas emissions could be reduced from lower energy use for space cooling.

CHAPTER III

RESEARCH FRAMEWORK

3.1 Current State of the Problem

The study of PCM integration methods in building materials started from direct incorporation methods, such as imbibing (Tomlinson and Heberle, 1990; Salyer and Sircar, 1990 and 1997; Hawes et al., 1993; and Kissock et al., 1998). The imbibing technique consisted of the immersion of the construction materials, such as gypsum boards, bricks, or concrete blocks into PCM baths where the PCM was absorbed into their pores. Direct incorporation was practical; however, in this method the PCM-filled materials suffered from leakage and created moisture transfer problems (Zhou et al., 2012; and Kissock et al., 1998).

Then, macroencapsulation methods were suggested, which entailed encapsulating PCMs in tubes or other containers where leakage and moisture problems would be eliminated (Zhang et al., 2005). These methods, however, proved not practical for the incorporation of PCMs into building walls because these containers had to be fastened to a part of the wall cavity and there was/is no building trade in charge of such task.

Later, another approach of direct incorporation of PCM in building walls was investigated in which direct mixing of PCM with blown-in insulation, such as cellulose, was used (Fang and Medina, 2009; and Evers et al., 2010). Unless the PCMs were micro-encapsulated, direct mixing of PCM with insulation presented

problems dealing with PCM water absorption, in the case of inorganic PCMs, and PCM evaporation, degradation, and eventual dematerialization, in the case of organic PCMs. With micro-encapsulation, improper mixing of the PCM with the insulation was a potential problem. Improper mixing included volumes of heavier concentrations of PCM, volumes containing no PCM at all, and volumes containing evenly distributed PCM; all of which were shown in Figure 1.3.1. In the case of evenly distributed PCM there existed the potential of partial melting and solidification of the PCM, mainly because of the location of part of the PCM. That is, PCMs located further away from the heat source would tend to not melt or PCMs located towards the middle of the wall cavity would tend to not solidify (Fang, 2009).

3.2 Proposed Solution

To fully melt and solidify over daily cycles, PCMs must be incorporated as thin layers placed longitudinally within the walls and horizontally within the ceilings (Jin et al., 2013). Two methods were proposed in this research. One method was via thermal shields, where the PCM was contained in thin sealed polymer pouches, arranged in sheets laminated with aluminum foil on both sides. The second method was via thin boards of polymeric compounds saturated with PCMs and laminated with aluminum foil on both sides.

These proposed PCM shields and boards would eliminate leakage of PCM, moisture transfer related problems, evaporation, degradation, water absorption, improper mixing, and the issue of impracticality presented by the previous methods.

The use of shields and boards would make it easier to integrate PCMs within the inside cavities of building walls and ceilings. However, the optimal location of the shields or boards within the wall and ceiling cavities must still be found. This represented a major part of the proposed research.

3.3 Research Objectives

The main objectives of this research were:

1. To propose and evaluate practical methods of PCMs integration for the inside cavities of building walls and ceilings.
2. To find the location of the thin PCM layer within the wall and ceiling cavities for optimum thermal performance; where optimum performance was based on reducing peak demand and energy consumption in building space cooling and heating.
3. To extend the PCM work from residential to non-residential buildings, such as institutional and commercial.

3.4 Research Approach

In this research, two thin layer approaches of incorporating PCM into building enclosures were proposed: PCM shields containing hydrated salt-based PCM and PCM boards containing paraffin-based PCM.

The PCM shields were evaluated in wood framed test houses with typical residential construction and the PCM boards were evaluated on a steel framed

institutional building. In both cases, the buildings were exposed to full weather conditions. The experimental results were used to study the effects of PCMs in building enclosures. Wall and ceiling surface temperatures and heat flux reductions were used as the criteria for evaluating the proposed thermally-enhanced enclosures.

In-house differential scanning calorimeter (DSC) experiments were conducted to obtain additional PCM properties. These included specific heats, latent and total heat storage capacities, latent heat of fusions, enthalpy, melting temperatures, and onset of melting temperatures. This information was used to analyze the experimental data in which PCMs were involved and to select the most appropriate input PCM data for the modeling and simulations.

Phase change materials were simulated in EnergyPlus using a conduction finite difference (CondFD) solution algorithm, which included data from the in-house DSC experiments. EnergyPlus was used to simulate the energy dynamics across the walls and ceilings of the test houses with and without PCM, including overall house energy consumption and energy reduction produced by the PCM. EnergyPlus was also used to simulate the thermal performance of the panels in the M2SEC building walls with and without PCM. Before the simulations, the results from EnergyPlus, integrated with CondFD, were validated against experimental data.

EnergyPlus simulations were carried out for four major cities, which were Miami, FL, Phoenix, AZ, Las Vegas, NV, and Kansas City, MO. These cities, which by their locations facilitated the inclusion of DOE Climate Zones 1 - 4, were selected because their locations enabled a wide range of climatic conditions to be simulated,

including climates such as hot and humid (Zone 1 - Miami), hot and dry (Zone 2 - Phoenix), mixed dry (Zone 3 - Las Vegas), and mixed humid (Zone 4 - Kansas City) (DOE, 2010). Once the cities had been selected, TMY3 weather files for each of the cities were downloaded and linked to EnergyPlus.

A schematic of the research framework is shown in Figure 3.1.1.

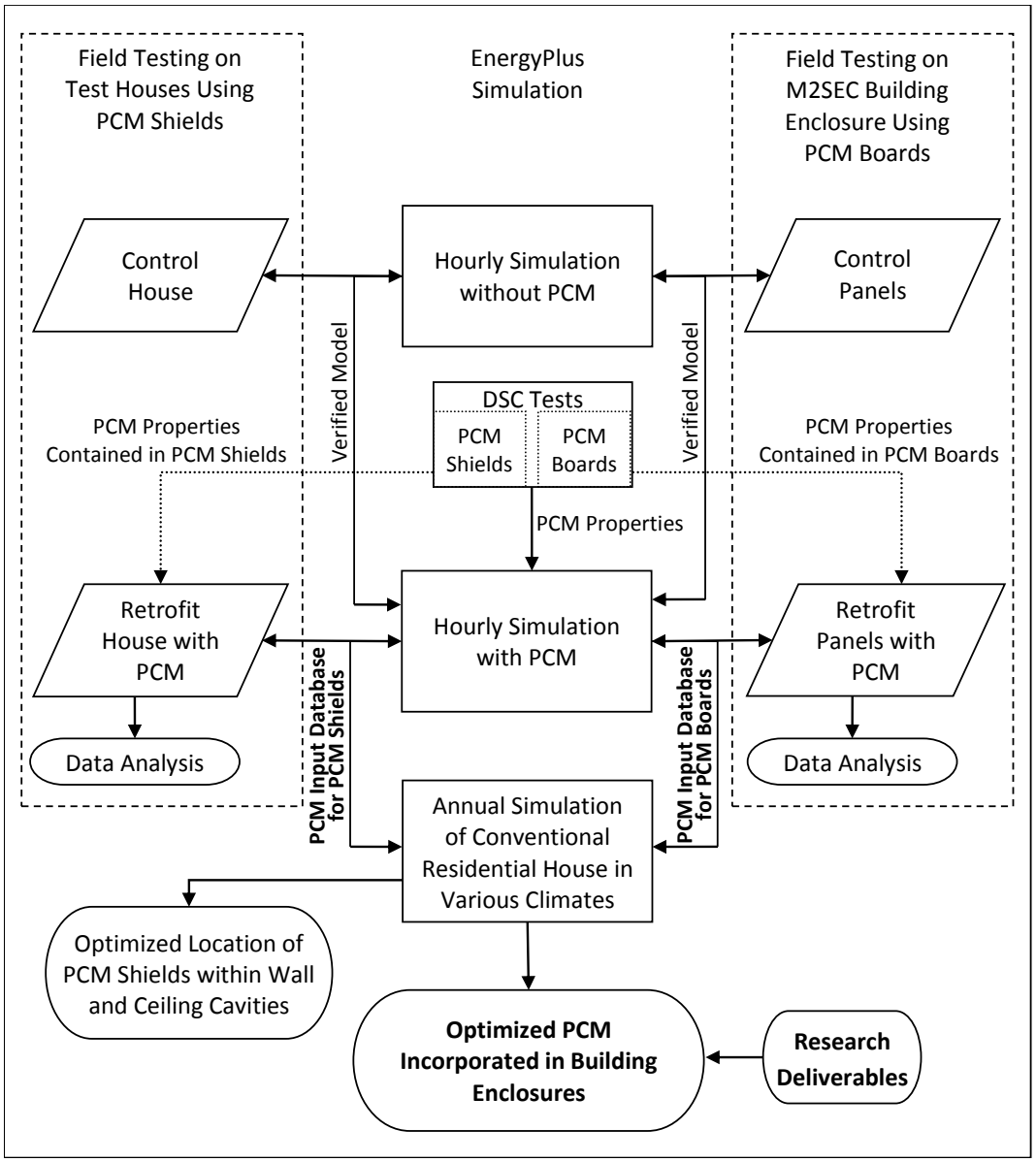

Figure 3.1.1. Research Framework

CHAPTER IV

EXPERIMENTAL SET-UPS

4.1 Experimental Set-up for Field-testing of PCM Shields

4.1.1 Test Houses

The field tests were performed using two 1.83 m × 1.83 m × 1.22 m (6 ft × 6 ft × 4 ft) identical test houses located in Lawrence, KS. The houses featured conventional residential construction and were air conditioned using scaled down cooling and heating systems. The test houses are shown in Figure 4.1.1. One house was used as the control and the other house was used as the retrofit house. In other words, the south and west walls and ceiling of the retrofit house were outfitted with the PCM shields.

Figure 4.1.1. Test Houses (Southeast View)

The roofs were a built-up roofs with gray asphalt shingles, 6.8 kg (15 lb_m) felt, and 1.27 cm (1/2 in.) plywood sheathing. The wall assemblies were made of 0.95 cm

(3/8 in.) plywood siding, 5.08 cm × 10.16 cm (2 in. × 4 in.) studs, and 0.95 cm (3/8 in.) wallboards. Five layers of rigid foam board insulation, with thermal resistance of 0.53 m^2·K/W (R-3) and thickness of 1.27 cm (1/2 in.), were installed in the cavities of the walls and ceilings. In each test house, a window with an area of 0.32 m^2 (3.4 ft^2) was placed in the south-facing wall. Fan coil units (FCUs) were installed inside each house next to the east-facing wall. The construction details of the test house are shown in Figure 4.1.2 and Figure 4.1.3.

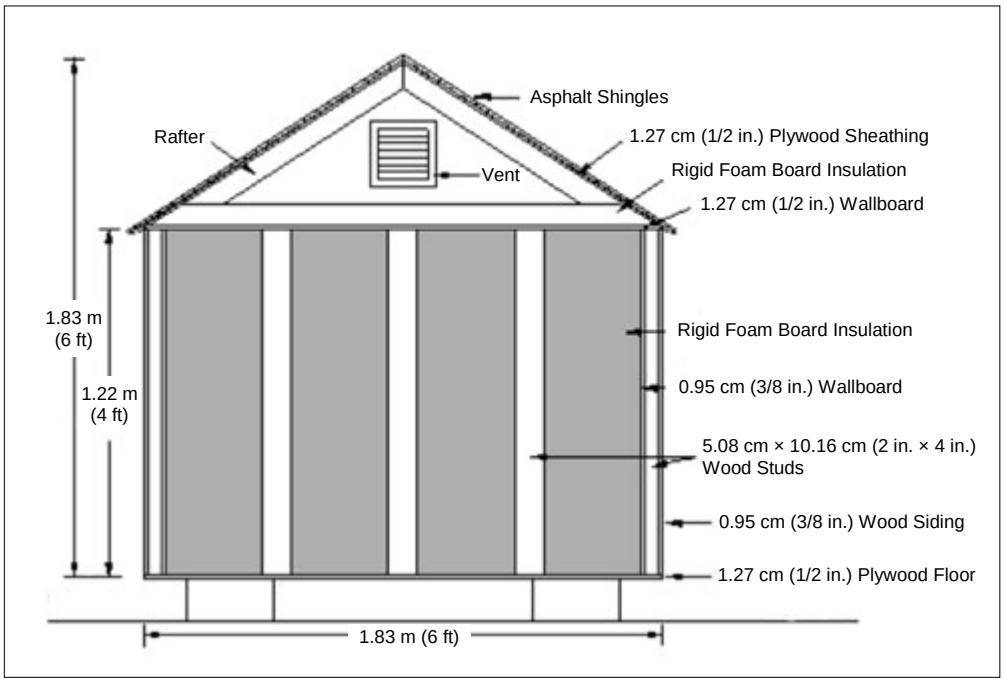

Figure 4.1.2. Test House Schematic

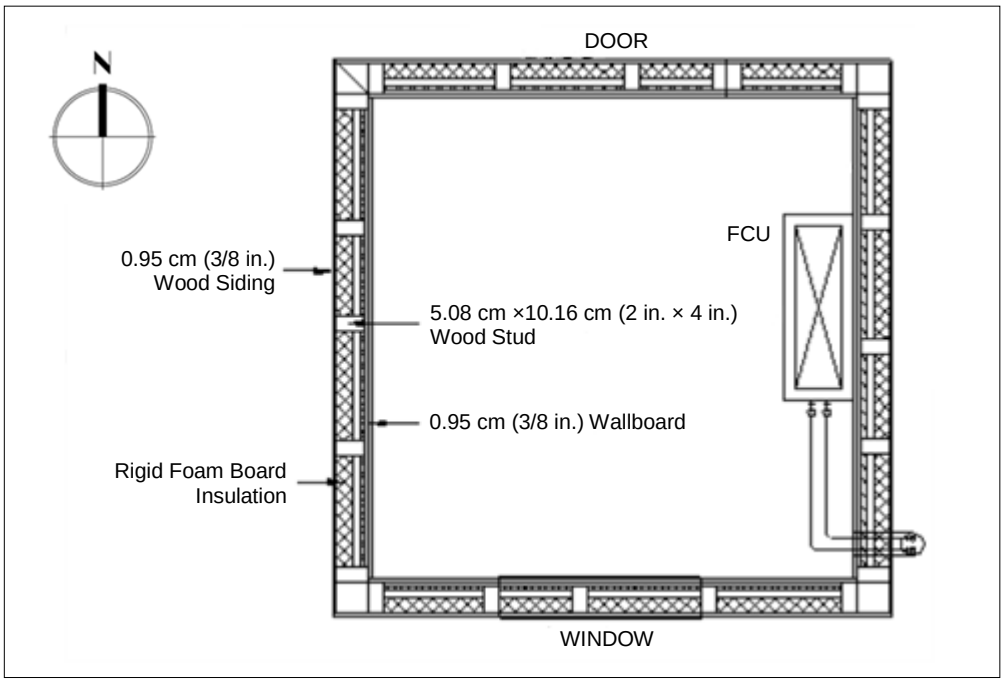

Figure 4.1.3. Test House - Top Section

4.1.2 Space Cooling System

The test houses were air conditioned using a chilled water system and fan-coil-units (FCUs) as shown in Figure 4.1.4. The chilled water produced by the chilled water system was stored in a water tank and kept at 7.2 °C (45.0 °F). The chilled water was circulated by pumps from the water tank to FCUs, which were placed inside the houses. Indoor air temperatures were controlled by thermostats set at the same temperatures in both test houses. By following this test protocol, the thermal parameters of the retrofit house were compared to those of the control house while the outdoor conditions were the same for both houses and the indoor air temperatures were also the same in both test houses.

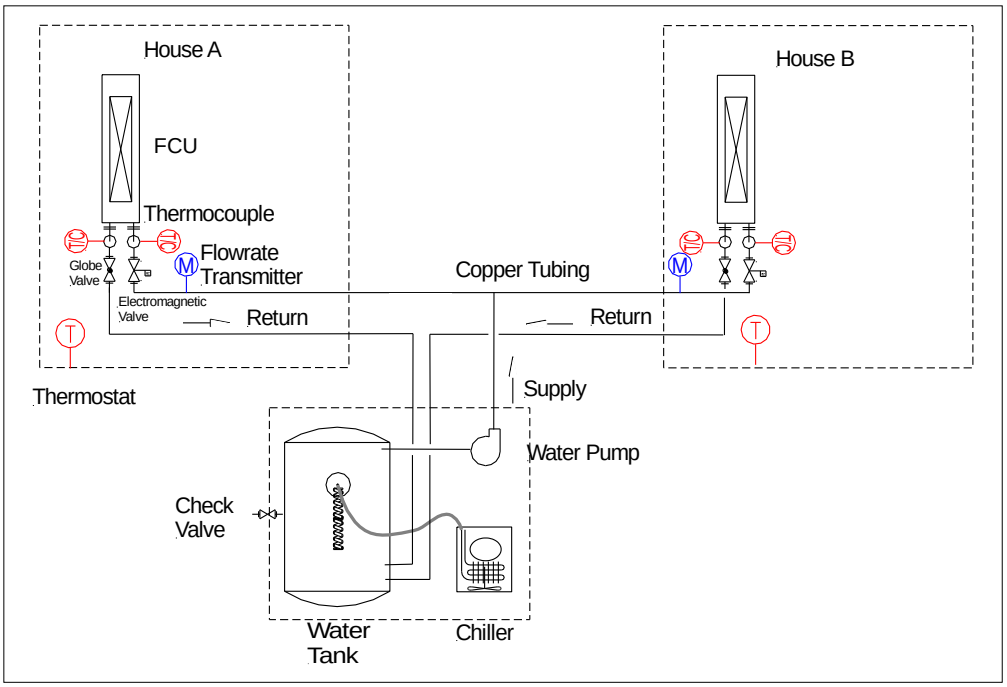

Figure 4.1.4. Cooling System (Source: Zhang, 2004)

4.1.3 Data Acquisition System

An Agilent 34970A Data Acquisition Unit (DAU) with 66 channels was used to collect data from thermocouples, heat flux sensors, water flow sensors, and relative humidity transducers. The data were transferred to a computer for analysis and archiving. All monitored data were collected every 10 seconds by the DAU; however, they were averaged hourly, which minimized the effects caused by sudden changes in outdoor and/or indoor conditions such as wind speed, passing clouds, and indoor air temperature changes produced by the cooling system's "on/off" cycles.

4.1.3.1 Temperature Measurements

Type T thermocouples (T/C) were used to measure temperatures. All surface and air temperatures were measured using T/C grids connected in parallel, where the measured temperatures represented the average temperature of the T/Cs in the grids. The T/Cs were attached at the same locations in both houses and were shielded with aluminum tape to minimize radiation effects. The error of the T/C was ± 0.6 °C (± 1.1 °F). An example of a T/C grid is shown in Figure 4.1.5. The south walls, west walls, and ceilings were instrumented with 12 T/Cs (6 on the interior surface and 6 on the exterior surface), 18 T/Cs (9 on the interior surface and 9 on the exterior surface), and 21 T/Cs (9 on the interior surface and 12 on the exterior surface), respectively.

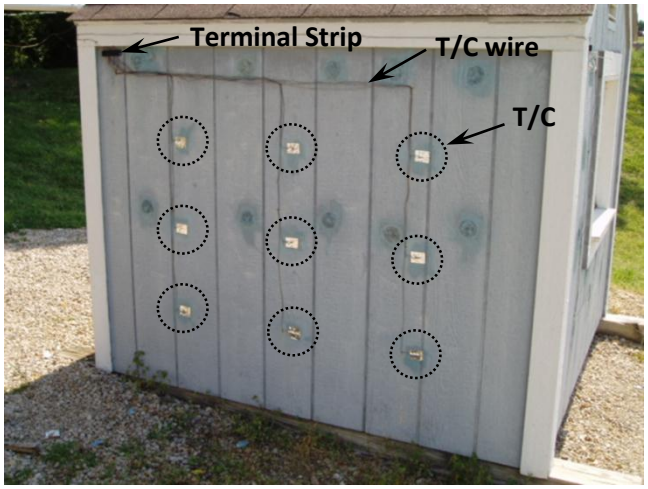

Figure 4.1.5. T/C Grids on West Wall

4.1.3.2 Heat Flux Measurements

Heat flux meters (HFMs) with dimension of 5.08 cm × 5.08 cm × 0.48 cm (2 in. × 2 in. × 3/16 in.) were installed on the interior wall and ceiling surfaces to

measure heat fluxes across the south walls, west walls, and ceilings. The error of these sensors was ± 2%. An example of installed HFMs is shown in Figure 4.1.6. The south walls, west walls, and ceilings were instrumented with 4 HFMs, 6 HFMs, and 4 HFMs, respectively.

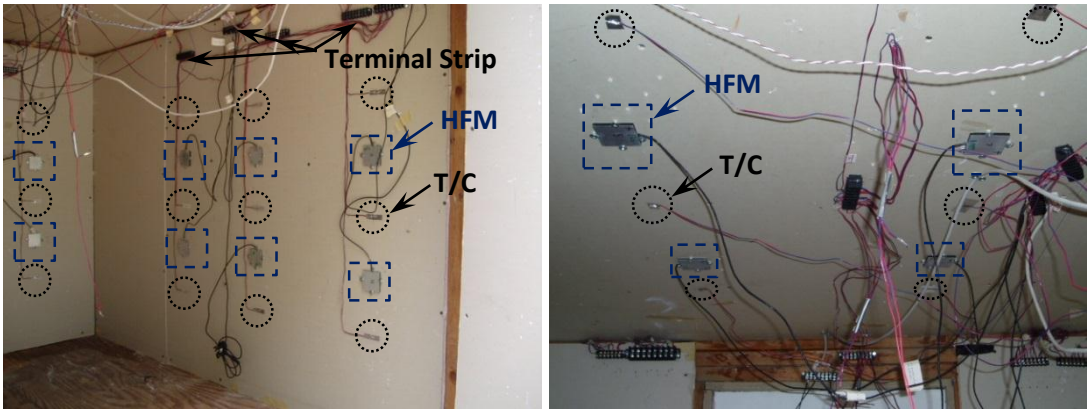

Figure 4.1.6. HFMs Attached on South and West Walls and Ceiling

4.1.3.3 Water Flow Rate Measurements

Water flow rates were measured with water flow sensors to calculate space cooling loads. These sensors were installed at the chilled water inlet of the FCUs, as shown in Figure 4.1.7. Output signals of 0 - 5 VDC were linearly proportional to a flow range of 20 - 100 ml/min (0.68 - 3.38 fl oz/min) with an error of ± 1%. The space cooling loads were determined by:

$$Q_{cooling} = \int_{on-time\ of\ FCU} \dot{m} C_p (T_{out} - T_{in})\, dt \qquad (4\text{-}1)$$

where:

$\dot{m}$ = Mass flow rate of the chilled water, kg/sec (lb_m/sec)

C_p = Specific heat of water, kJ/kg°C (Btu/lb_m°F)

T_{out} = Water Outlet temperature of FCU, °C (K) (°F (°R))

T_{in} = Water Inlet temperature of FCU, °C (K) (°F (°R))

dt = Integration variable (10 seconds intervals)

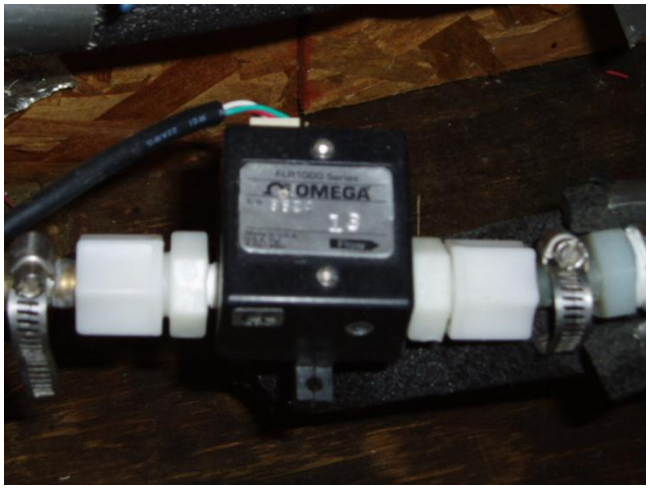

Figure 4.1.7. Flow Sensor

4.1.4 Weather Data

A weather station was used to collect weather data such as outdoor air temperature, outdoor air relative humidity, wind speed and direction, rainfall, and solar irradiation. The weather station is shown in Figure 4.1.8.

Figure 4.1.8. Weather Station

4.1.5 PCM Shields

The PCM shields were thin sheets containing polymer pouches laminated with aluminum foil on both sides. The PCM was contained in the sealed polymer pouches. An example of a PCM shield is shown in Figure 4.1.9.

Figure 4.1.9. PCM Shield

4.1.5.1 Properties of the PCM Contained in the Shields

The type of PCM contained in the PCM shields was a hydrated salt-based PCM. The PCM properties were obtained using a differential scanning calorimeter (DSC). A picture of the DSC is shown in Figure 4.1.10.

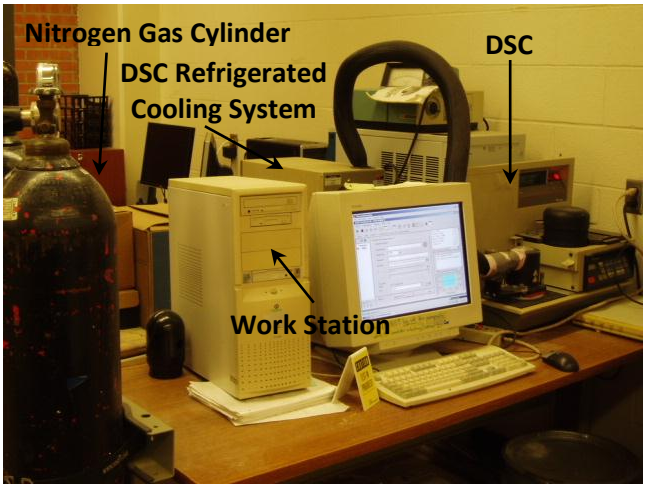

Figure 4.1.10. Differential Scanning Calorimeter (DSC)

A sample of the results of such tests is shown in Figure 4.1.11. The melting temperature was 31.36 °C (88.4 °F), the onset of melting temperature was 24.79 °C (76.6 °F), and the latent heat of fusion was 149.9 J/g (64.4 Btu/lb_m). The onset of melting temperature of the PCM, as given by the DSC, was located by drawing a tangent line from the peak of the melting curve along the melting line. The latent heat of fusion was calculated based on two selected points, namely the start of melting and the end of melting. The melting temperature range was around 18.0 - 38.0 °C (64.4 - 100.4 °F). The solidification temperature was 16.01 °C (60.8 °F), the onset of solidification temperature was 17.61 °C (63.7 °F) and the latent heat of solidification

was 152.3 J/g (65.5 Btu/lb_m). The onset of solidification temperature of the PCM was located by drawing a tangent line from the lowest point in the solidification curve along the solidification line. The latent heat of solidification was calculated based on two selected points, namely the start of solidification and the end of solidification. The solidification temperature range was around 20.0 - 9.0 °C (68.0 - 48.2 °F).

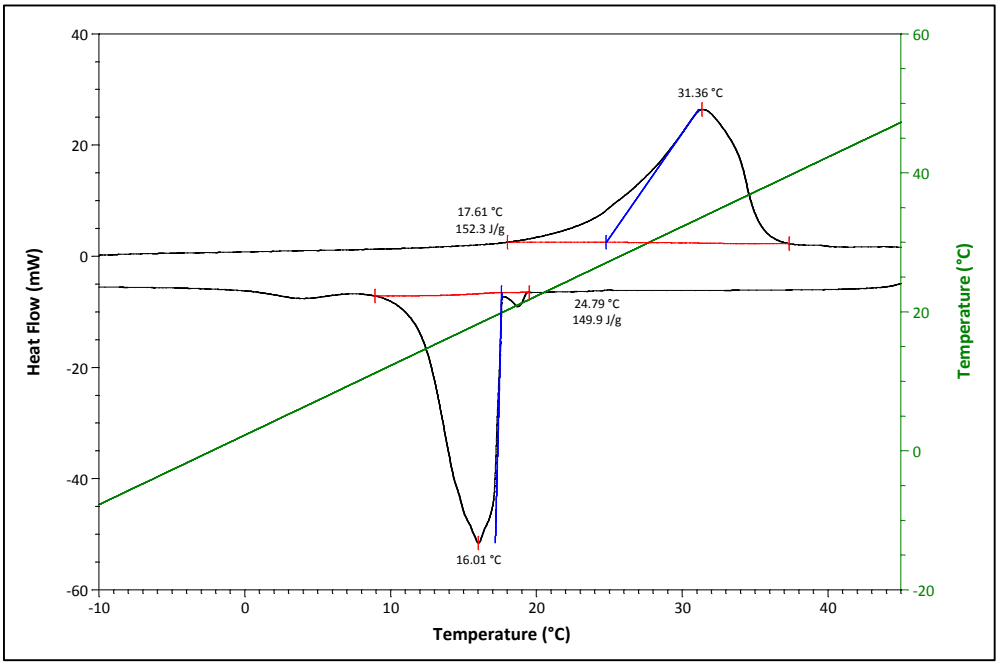

Figure 4.1.11. Sample DSC Test Results of the PCM Contained in the PCM Shields

4.1.5.2 Installation of the PCM Shields

The PCM shields were installed in the retrofit house as shown in Figure 4.1.12 and Figure 4.1.13. That is, the PCM shields were attached to the insulation boards and placed at several depths inside the cavities of the south and west walls and ceiling.

Figure 4.1.12. PCM Shields Attached to Insulation Boards Inside the Cavities of the South and West Walls

Figure 4.1.13. PCM Shields Attached to Insulation Boards Inside the Ceiling Cavities (For clarity, the insulation boards were lifted up during photographing)

4.2 Experimental Set-up for Field-testing of PCM Boards

The field tests for the performance evaluation of the PCM boards were carried out in the south and west external walls of the Measurement, Materials and Sustainable Environment Center (M2SEC) building, located in Lawrence, KS.

4.2.1 Measurement, Materials, and Sustainable Environment Center (M2SEC) Building

The M2SEC building is shown in Figure 4.2.1. This building was inaugurated in the fall of 2012. The building was constructed so that its enclosure could be used to perform heat and mass transfer experiments across the components of its enclosure.

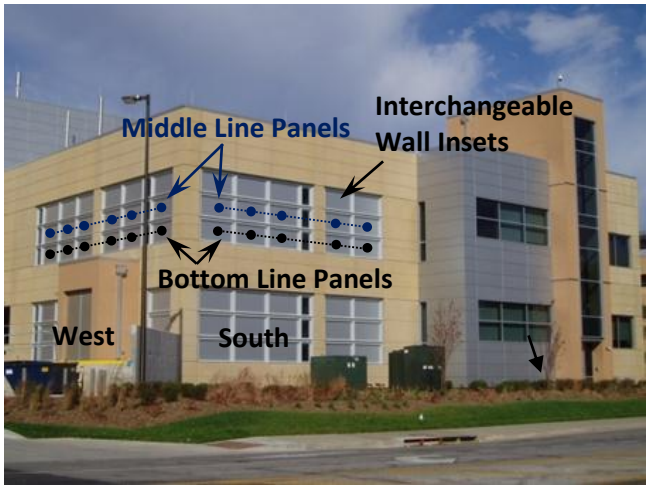

Figure 4.2.1. Measurement, Materials, and Sustainable Environment Center (M2SEC) Building (Southwest View)

Sixty interchangeable panels in the south and west walls (27 panels in the ground floor and 33 panels in the 1st floor) allowed testing of different wall constructions. In this research, a total of 22 panels located along the middle and bottom lines (10 panels in the south wall and 12 panels in the west wall) in the 1st floor were tested and evaluated to assess the performance of the PCM boards. A set of interchangeable wall panels, as viewed from the interior of the building, are shown in Figure 4.2.2.

Figure 4.2.2. Interchangeable Wall Panels

The original panels were constructed of metallic-coated steel sheets as an exterior finish, a foamed insulation core, and a siliconized polyester as an interior finish. Each panel had a size of 1.62 m x 0.88 m (5.3 ft x 2.8 ft), a thickness of 76 mm (3.0 in.), and a nominal minimum total thermal resistance of 2.82 $m^2 \cdot K/W$ (R-16). These panels were fastened using sets of clamps and metal frames as shown in Figure 4.2.3. The clamps had self-tapping screws with rubber tips, which fastened the metal frames to the wall panels. The depths of the screws were adjustable to fit various wall thicknesses. The metal frames were made of cold-rolled channels for the purpose of providing more stiffened fastenings.

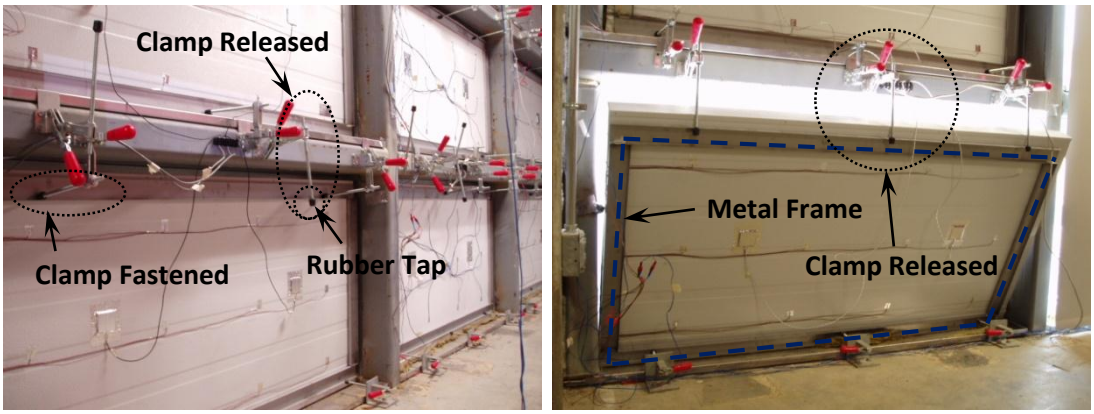

Figure 4.2.3. Interchangeable Wall Panel Fastenings
(For demonstration, the panel on the right is open)

4.2.2 Space Cooling System

The interior space next to the panels (see Figure 4.2.2) was air conditioned by a central air conditioning system. The thermostat for this area was set at 24.4 °C (76.0 °F). The air conditioning system used a chilled water loop and air handling units (AHUs). One chiller and a water tank are shown in Figure 4.2.4. The chiller capacity was 994.9 kW (282.9 tons, 3.4 MMBtu/hr) and the water tank volume was 3,937 L (1,040 gal.).

Figure 4.2.4. Chiller and Water Tank

4.2.3 Data Acquisition System

An Agilent 34972A Data Acquisition Unit (DAU) with 66 channels was used. All monitored data were collected every 10 seconds; however, these values were averaged on an hourly basis.

The older versions of DAUs used at the University of Kansas were hard-wired to the workstations. In this research, however, the DAUs were connected to the workstations via Internet network. This allowed for the monitoring of far away points without the extra expense and logistics incurred when cables were used. In this experimental set-up, the panels were located in a long and narrow corridor which was occasionally opened to visitors as per grantor's request (see Figure 4.2.2). By locating the workstation in the adjacent room (not in the corridor), the instruments would not block the corridor space and the data collection would not be interrupted by the visitors.

Temperatures and heat fluxes across the walls were measured in the location shown in the schematic of Figure 4.2.5.

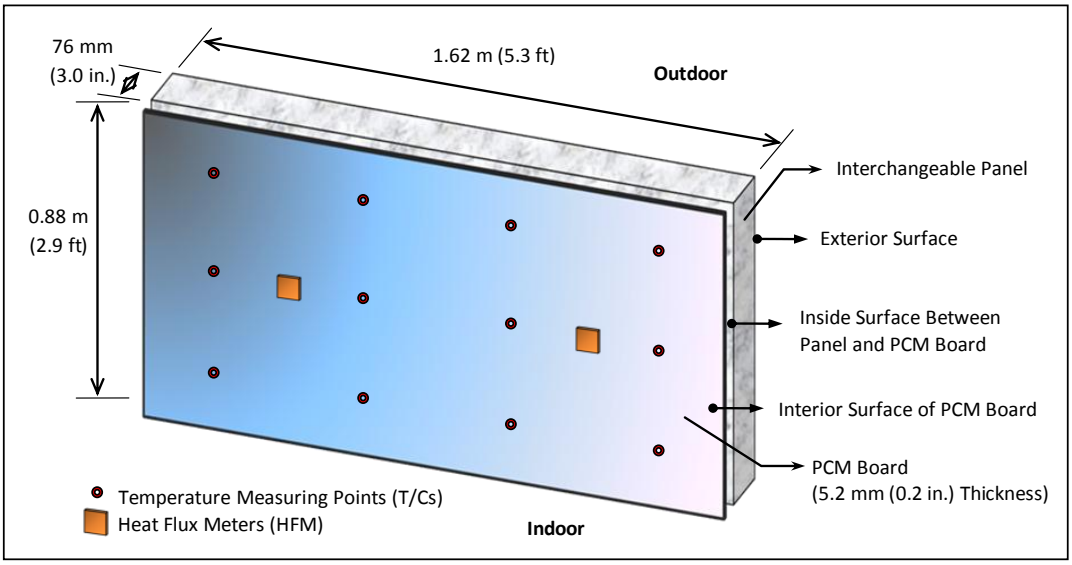

Figure 4.2.5. Schematic of the Wall Panel and the PCM Board Including Surface Temperature and Heat Flux Measuring Points

4.2.3.1 Temperature Measurements

Type T thermocouples (T/C) were used to measure all surface and air temperatures. Each panel was instrumented with T/C grids using 12 T/Cs connected in parallel to measure average temperature of the surfaces. The T/Cs were attached at the same locations on all panels and were shielded with aluminum tape to minimize radiation effects. The T/C error was ± 0.6 °C (± 1.1 °F). The interchangeable panel surfaces in which T/Cs were installed included their interior and exterior surfaces. These are shown in Figure 4.2.6 and Figure 4.2.7. In addition, average interface temperatures between the panels and PCM boards were measured.

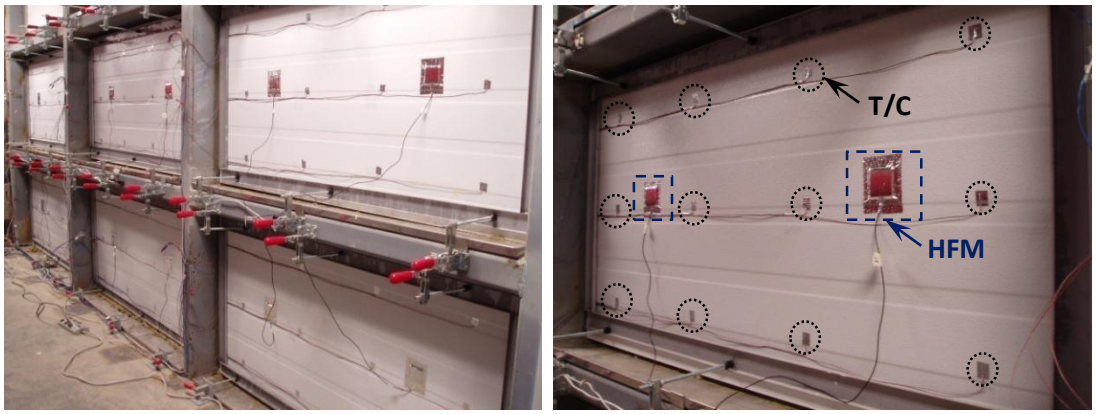

Figure 4.2.6. T/C Grids on the Interior Surfaces of the Panels

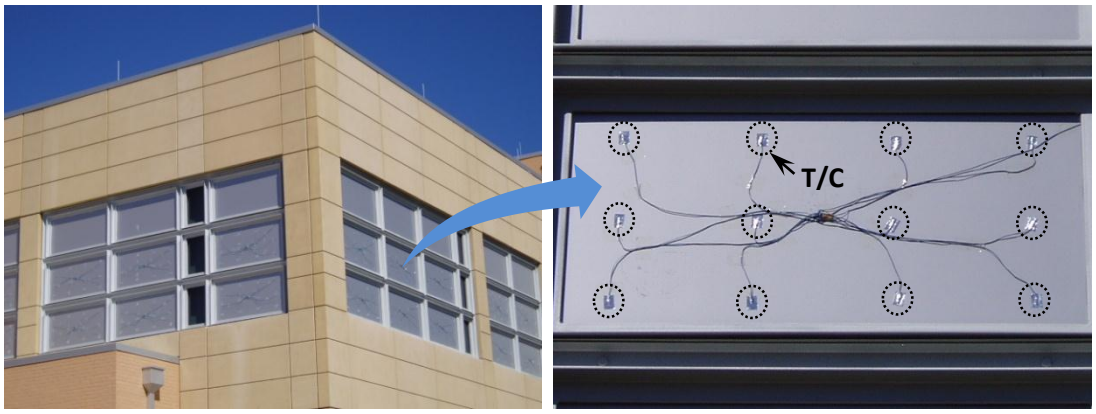

Figure 4.2.7. T/C Grids on the Exterior Surfaces of the Panels

The indoor air temperatures were measured at three locations 0.44 m (17.5 in.) above the floor and at three locations 1.47 m (58.0 in.) above the floor as shown in Figure 4.2.8 on both the south and west corridors. Outdoor air temperatures were measured at two locations on both the south and west facing sides. These T/Cs were placed at a distance of 0.41 m (16.0 in.) from the external surface of the panels as shown in Figure 4.2.9.

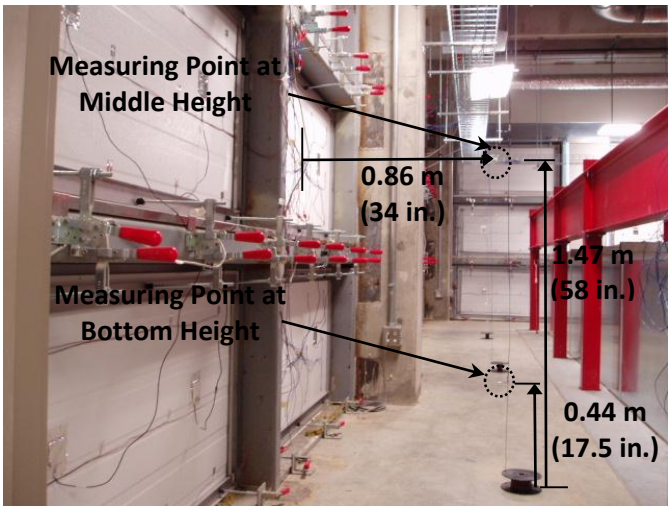

Figure 4.2.8. Indoor Air Temperature Measurements

Figure 4.2.9. Outdoor Air Temperature Measurements
(Left: South Facing Wall, Right: West Facing Wall)

4.2.3.2 Heat Flux Measurements

Two heat flux meters (HFMs) with dimension of 5.08 cm × 5.08 cm × 0.48 cm (2 in. × 2 in. × 3/16 in.) were installed on the interior surfaces of each panel. Their error was ± 2%.

4.2.4 PCM Boards

The PCM boards were thin boards of polymeric compounds saturated with PCMs and laminated with aluminum foil on both sides and around the edges. An example of a PCM board is shown in Figure 4.2.10. Figure 4.2.11 shows a section of the PCM board and a microscopic image magnified 50 times. This shows PCM particles within the copolymer matrix.

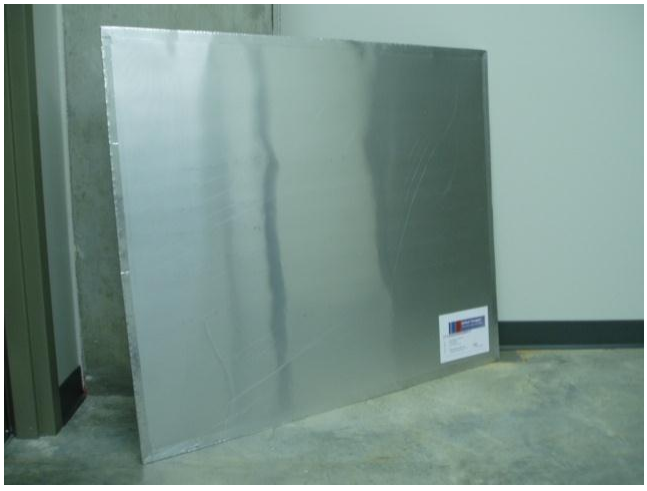

Figure 4.2.10. PCM Board

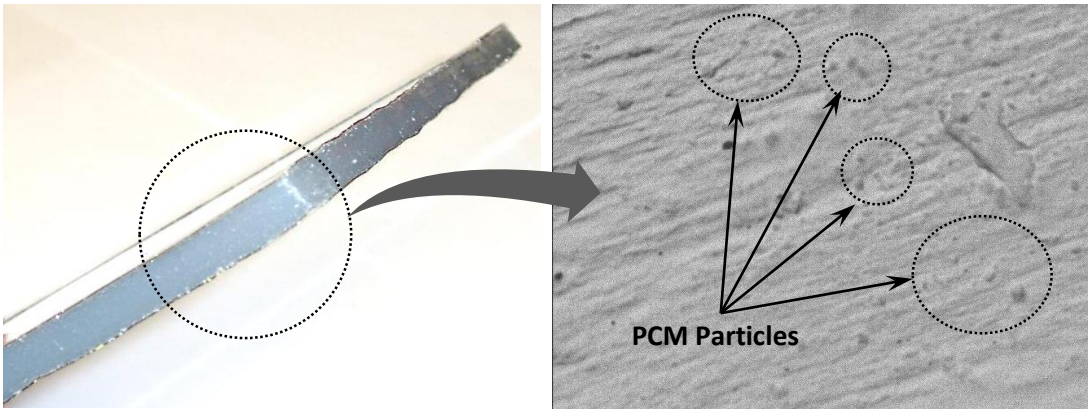

Figure 4.2.11. Section View of the PCM Board
(Left: Section Surface, Right: Microscopic Image, 50X)

4.2.4.1 Properties of the PCM Boards

The type of PCM contained in the PCM boards was a paraffin-based PCM. The properties of the PCM boards are shown in Table 4.2.1.

Table 4.2.1. Properties of the PCM Boards (Source: DuPont™ Energain® Datasheet)

Property	Value
Thickness	5.2 mm (0.2 in.)
Width	1,000 mm (3.3 ft)
Length	1,198 mm (3.9 ft)
Area weight	4.5 kg/m^2 (0.9 lb_m/ft^2)
Aluminum thickness (sheet)	100 µm (3.94×10^{-3} in.)
Aluminum thickness (edges)	75 µm (2.95×10^{-3} in.)
Paraffin loading	60%
Melting point (paraffin)	21.7 °C (71.1 °F)
Latent heat storage capacity (0 °C - 30 °C (32 °F - 86 °F))	> 70 kJ/kg (30.1 Btu/lb_m)
Total heat storage capacity (Temperature range 0 °C to 30 °C (32 °F to 86 °F))	~ 140 kJ/kg (60.2 Btu/lb_m)
Conductivity solid	0.18 W/m°C (0.104 Btu/hr·ft°F)
Conductivity liquid	0.14 W/m°C (0.081 Btu/hr·ft°F)

4.2.4.2 Installation of the PCM Boards

The PCM boards were installed on the interchangeable panels' interior surfaces. Two panels located 1.03 m (40.5 in.) above the floor and two panels located at the bottom of the floor on both the south and west walls were retrofitted with the PCM boards. The aluminum surfaces of PCM boards were covered with a finish material that had the same color as the interior finish of the panels. This matched the

interior surfaces of the control panels in relation to radiation properties, such as reflectivity and emissivity. The PCM boards were held in place with sets of metal frames and clamps as discussed in Section 4.2.1 and as shown in Figure 4.2.12.

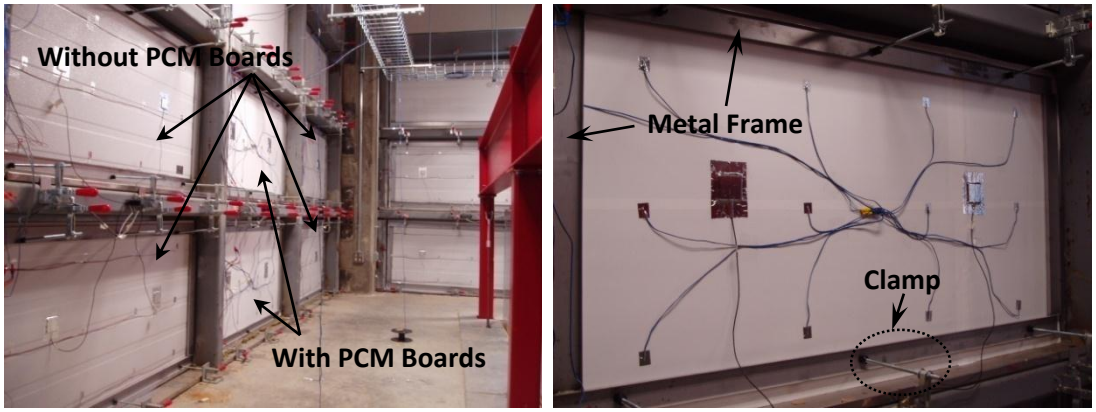

Figure 4.2.12. Installed PCM Boards

CHAPTER V

EXPERIMENTAL RESULTS AND DISCUSSION

5.1 Thermal Performance of the PCM Shields

5.1.1 Pre-retrofit Thermal Performance Verification of the Test Houses

It was necessary to perform calibration tests before any retrofit. For this, the thermal performance of the two houses were compared and recorded as reference. Average indoor air temperatures, average exterior and interior wall surface temperatures, average attic air temperatures, average interior ceiling surface temperatures, and average wall and ceiling heat fluxes were measured and compared to verify their similarity.

5.1.1.1 Air and Surface Temperatures

During the calibration period, the average indoor air temperatures of the test houses were controlled to 0.34 °C (0.6 °F) difference between both test houses. That is, the control house was kept at an average indoor air temperature of 21.52 °C (70.7 °F), while the soon-to-be-retrofit house was kept at an average temperature of 21.18 °C (70.1 °F).

The exterior surface of the south wall in the control house had an average temperature of 35.69 °C (96.2 °F). The exterior surface of the south wall in the soon-to-be retrofit house had an average temperature of 35.44 °C (95.8 °F). That is, an average temperature difference of 0.25 °C (0.4 °F) between both exterior surfaces

was recorded. The interior surface temperature of the south wall in the control house was kept at an average of 22.16 °C (71.9 °F). The interior surface temperature of the south wall in the soon-to-be retrofit house was kept at an average of 21.33 °C (70.4 °F). That is, an average temperature difference of 0.83 °C (1.5 °F) between both interior surfaces was achieved.

The exterior surface of the west wall in the control house had an average temperature of 36.15 °C (97.1 °F). The exterior surface temperature of the west wall in the soon-to-be retrofit house had an average temperature of 36.31 °C (97.4 °F). That is, an average temperature difference of 0.16 °C (0.3 °F) between both exterior surfaces was recorded. The interior surface temperature of the west wall in the control house was kept at an average of 22.78 °C (73.0 °F). The interior surface temperature of the west wall in the soon-to-be retrofit house was kept at an average of 22.70 °C (72.9 °F). That is, an average temperature difference of 0.08 °C (0.1 °F) between both interior surfaces was achieved.

The attic air in the control house had an average temperature of 31.56 °C (88.8 °F). The attic air in the soon-to-be retrofit house had an average temperature of 31.42 °C (88.6 °F). That is, an average air temperature difference of 0.14 °C (0.2 °F) between both attics was recorded. The interior surface temperature of the ceiling in the control house was kept at an average of 21.48 °C (70.7 °F). The interior surface temperature of the ceiling in the soon-to-be retrofit house was kept at an average of 21.84 °C (71.3 °F). That is, an average temperature difference of 0.36 °C (0.6 °F) between both interior surfaces was achieved.

Table 5.1.1 summarizes the temperatures between both test houses.

Table 5.1.1. Temperature Comparisons Between Control and Soon-to-be Retrofit Houses

		Control (°C (°F))	Soon-to-be Retrofit (°C (°F))	Difference (°C (°F))
Indoor Air		21.52 (70.7)	21.18 (70.1)	0.34 (0.6)
South Wall	Average Exterior Surface	35.69 (96.2)	35.44 (95.8)	0.25 (0.4)
	Average Interior Surface	22.16 (71.9)	21.33 (70.4)	0.83 (1.5)
West Wall	Average Exterior Surface	36.15 (97.1)	36.31 (97.4)	0.16 (0.3)
	Average Interior Surface	22.78 (73.0)	22.70 (72.9)	0.08 (0.1)
Ceiling	Average Attic Air	31.56 (88.8)	31.42 (88.6)	0.14 (0.2)
	Average Interior Surface	21.48 (70.7)	21.84 (71.3)	0.36 (0.6)

Figure 5.1.1, Figures 5.1.2 (a), (b), Figures 5.1.3 (a), (b), and Figures 5.1.4 (a), (b) show the level of similarity between the average indoor air temperatures, average exterior and interior surface temperatures and average attic air temperatures were controlled. In Figure 5.1.1 and all subsequent figures used for comparison purposes, the solid lines represent data from the test house that was always kept as the control house. The dashed lines with the symbols (dots) represent the data of the house that was always used as the retrofit house.

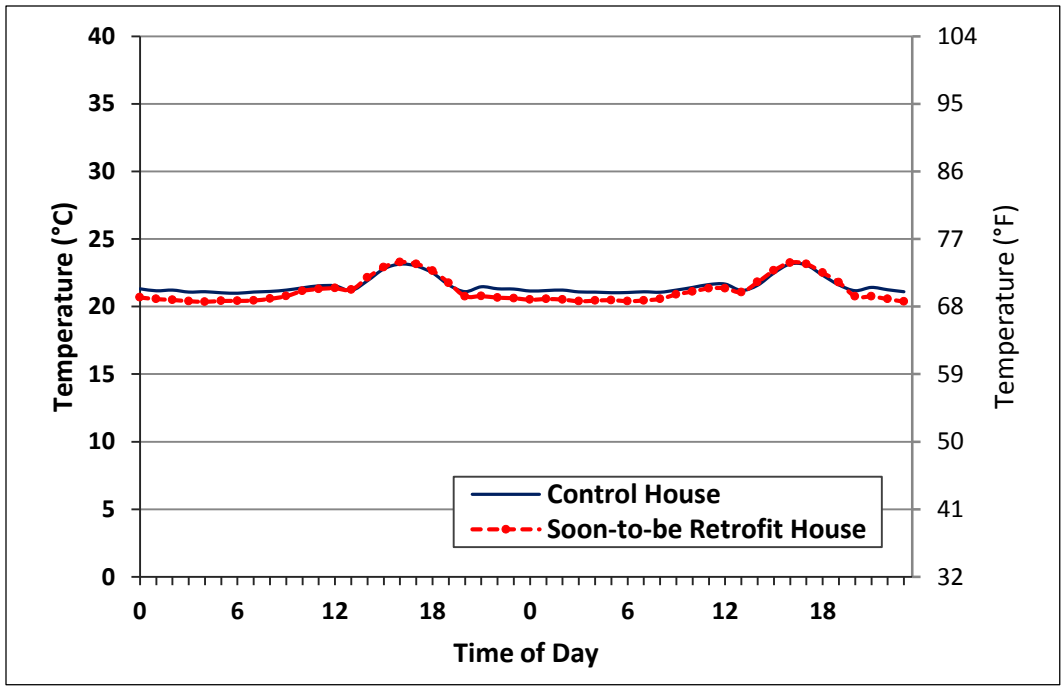

Figure 5.1.1. Indoor Air Temperatures During Pre-retrofit Tests

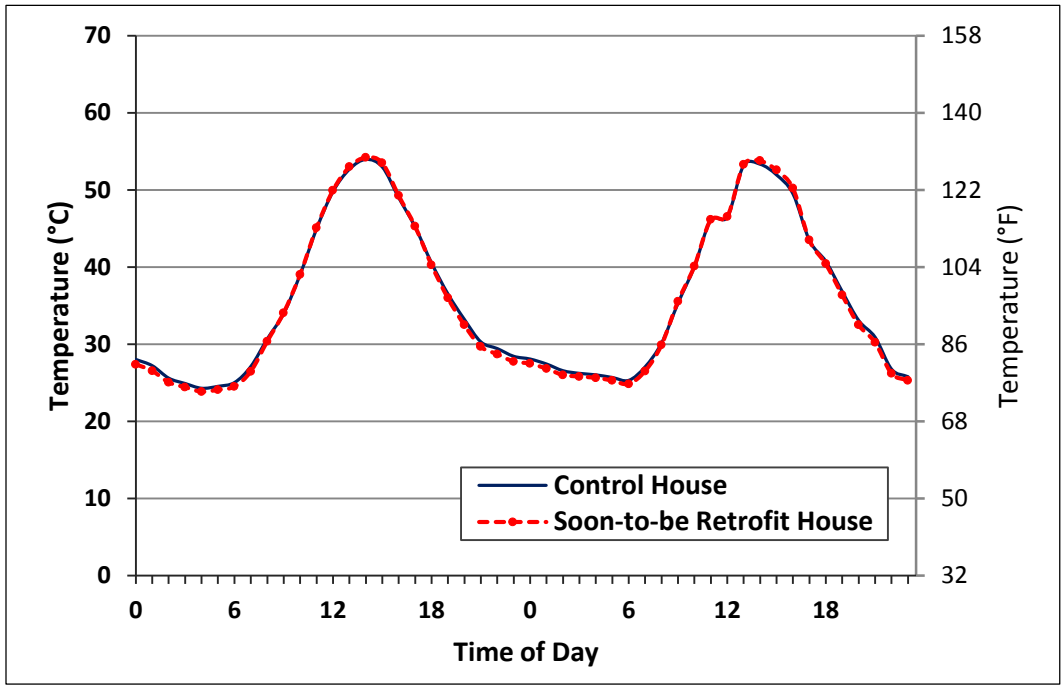

Figure 5.1.2 (a). Exterior Surface Temperatures of the South Walls During Pre-retrofit Tests

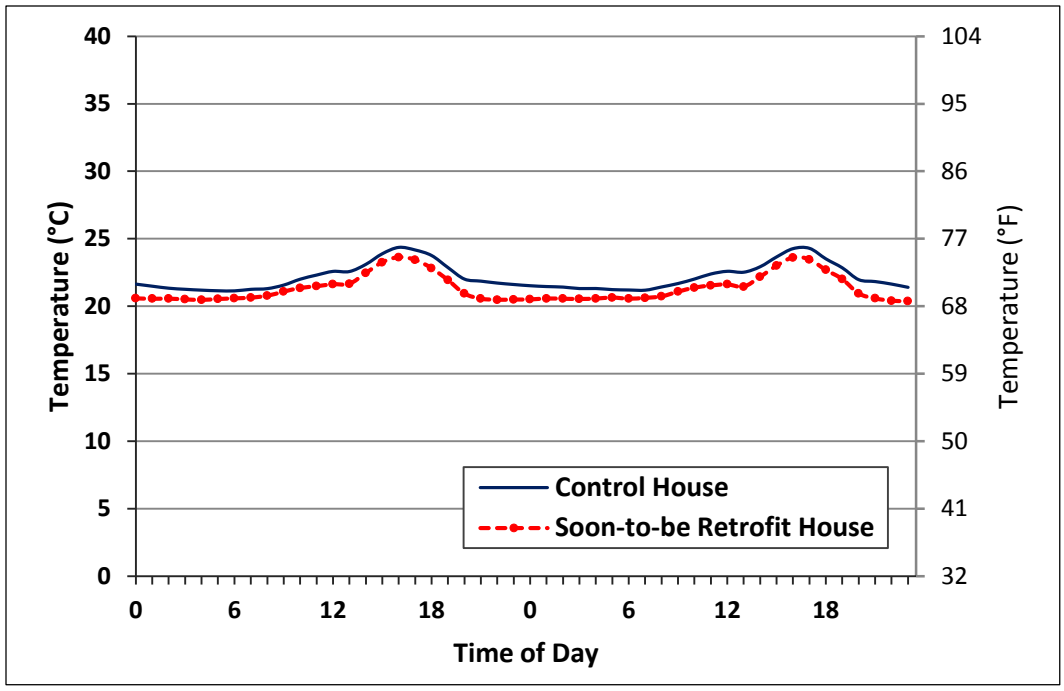

Figure 5.1.2 (b). Interior Surface Temperatures of the South Walls During Pre-retrofit Tests

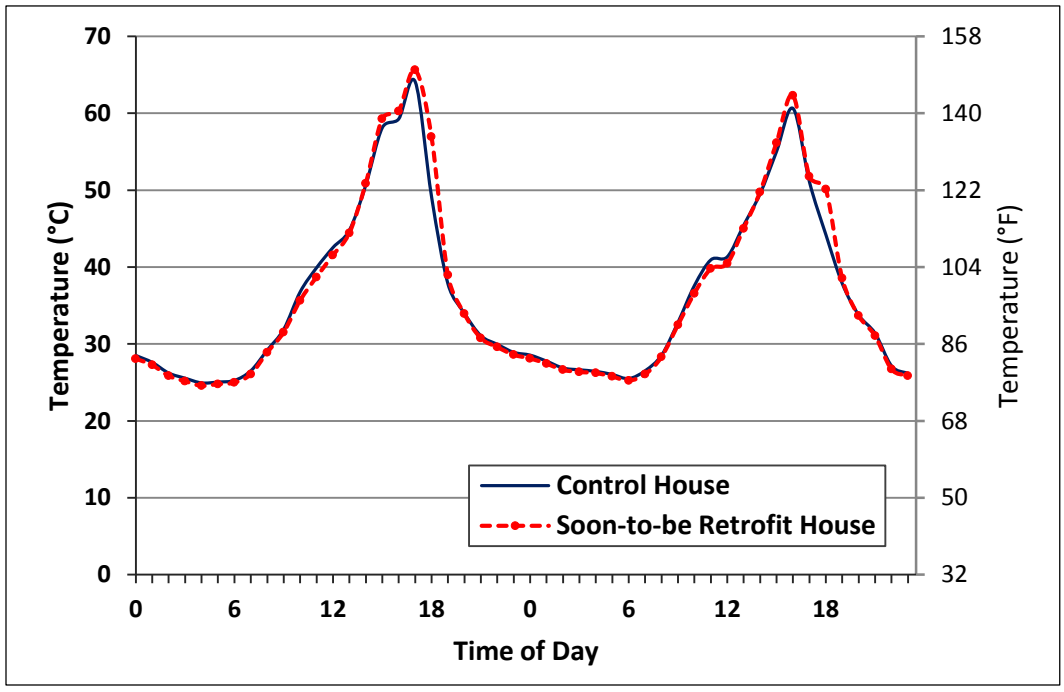

Figure 5.1.3 (a). Exterior Surface Temperatures of the West Walls During Pre-retrofit Tests

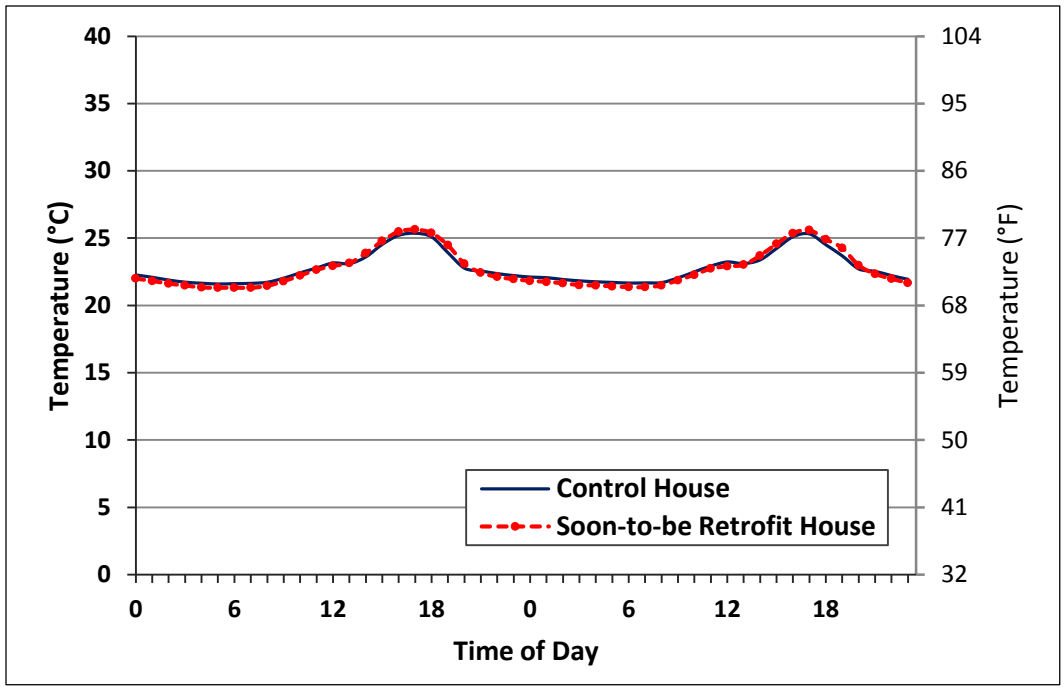

Figure 5.1.3 (b). Interior Surface Temperatures of the West Walls During Pre-retrofit Tests

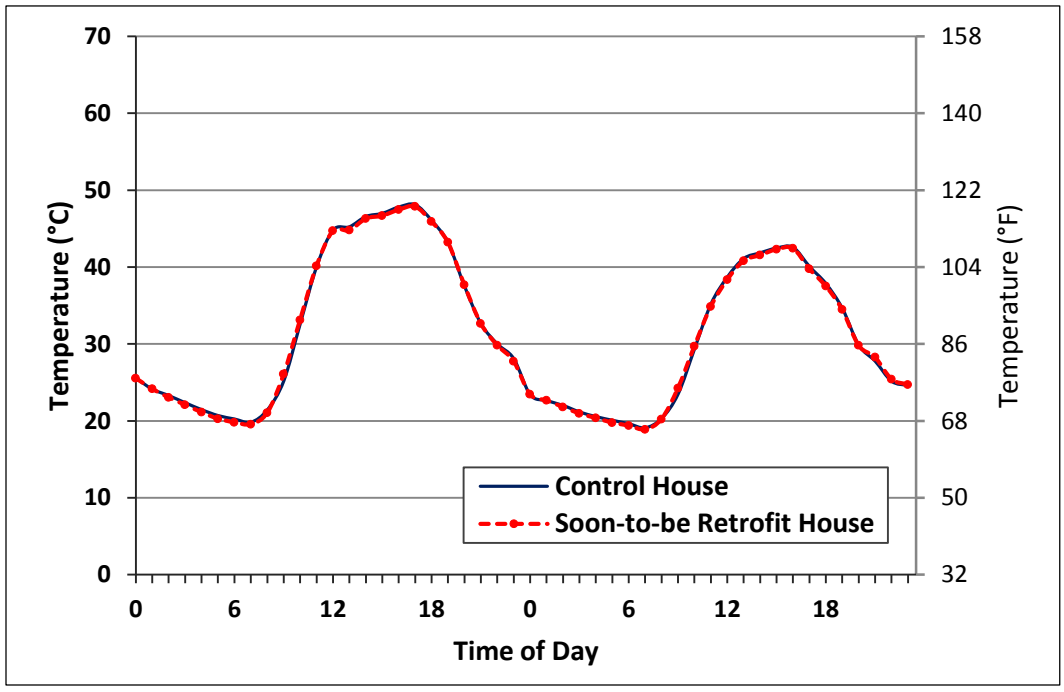

Figure 5.1.4 (a). Attic Air Temperatures During Pre-retrofit Tests

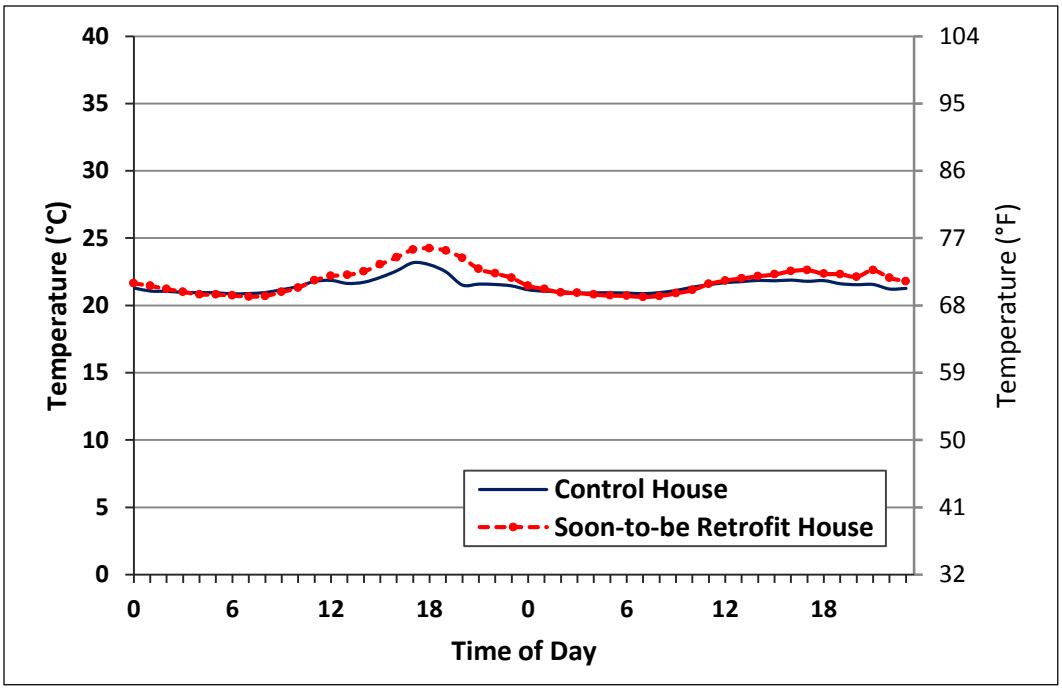

Figure 5.1.4 (b). Interior Surface Temperatures of the Ceiling During Pre-retrofit Tests

Figures 5.1.1, 5.1.2 (b), 5.1.3 (b), and 5.1.4 (b) demonstrate the level of control that was achieved in terms of keeping indoor air and indoor surface temperatures as similar in both test houses as possible.

5.1.1.2 Heat Fluxes

Figures 5.1.5 (a), (b), and (c) show the heat flux comparisons for the south and west walls and ceiling, respectively. From the trend shown in these figures, it was concluded that the thermal responses of south and west walls were nearly identical. The average differences in peak heat flux for the south and west walls and ceiling were approximately 3.4, 2.1, and 8.3%, respectively.

Although the heat fluxes between control and soon-to-be retrofit panels did not appear to be as similar as was the case for the temperatures, it is important to mention that it was believed that heat fluxes were very similar at any instant of time. With heat flux sensing technology, percent differences of the level reported above are considered acceptable and are the result of careful instrumentation and control. Heat flux sensors are inherently less accurate than temperature sensors. In addition to other experimental errors (e.g., surface emissivity and view factors), thermal contact conductance between the sensor and the testing surface varies between sensor-surface combinations. Thermal contact conductance is the heat conduction between solid bodies in thermal contact (Cooper et al., 1969). Factors influencing thermal contact conductance include interstitial materials (i.e., microscopically not smooth), surface roughness, surface cleanliness, and other factors. That is, when two bodies are in contact, this contact is not along a full surface, but instead in a finite number of points. This happens because there are no truly smooth surfaces in actual cases. Surface characteristics such as roughness and cleanliness vary because of their finishes and particulate accumulation (Fletcher, 1972; and Madhusudana and Ling, 1995).

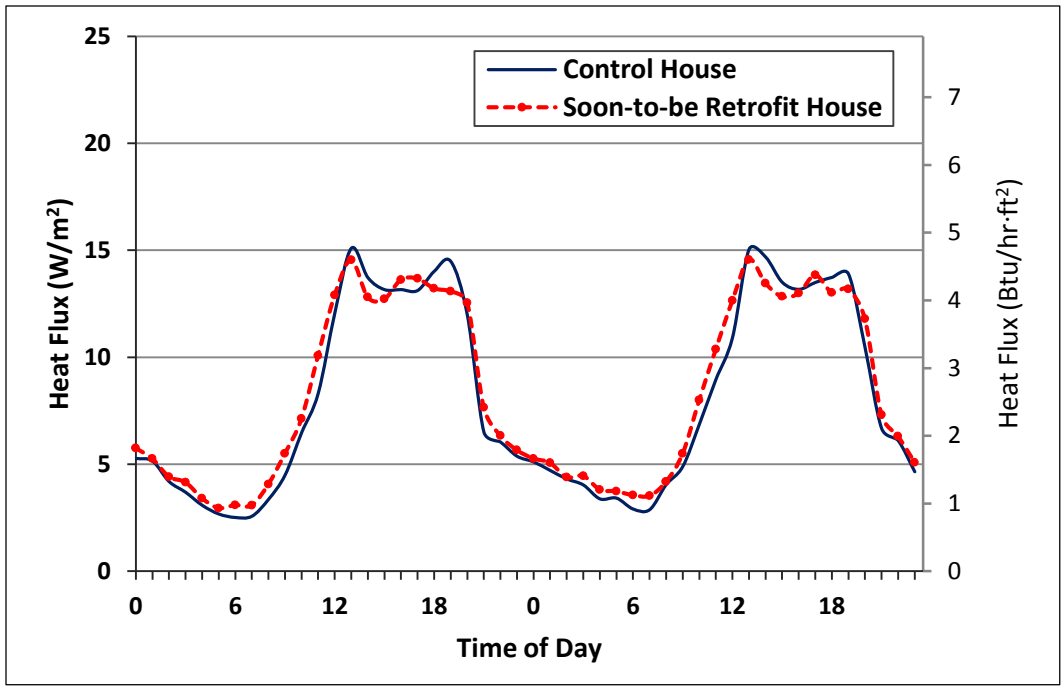

Figure 5.1.5 (a). Heat Fluxes Across the South Walls During Pre-retrofit Tests

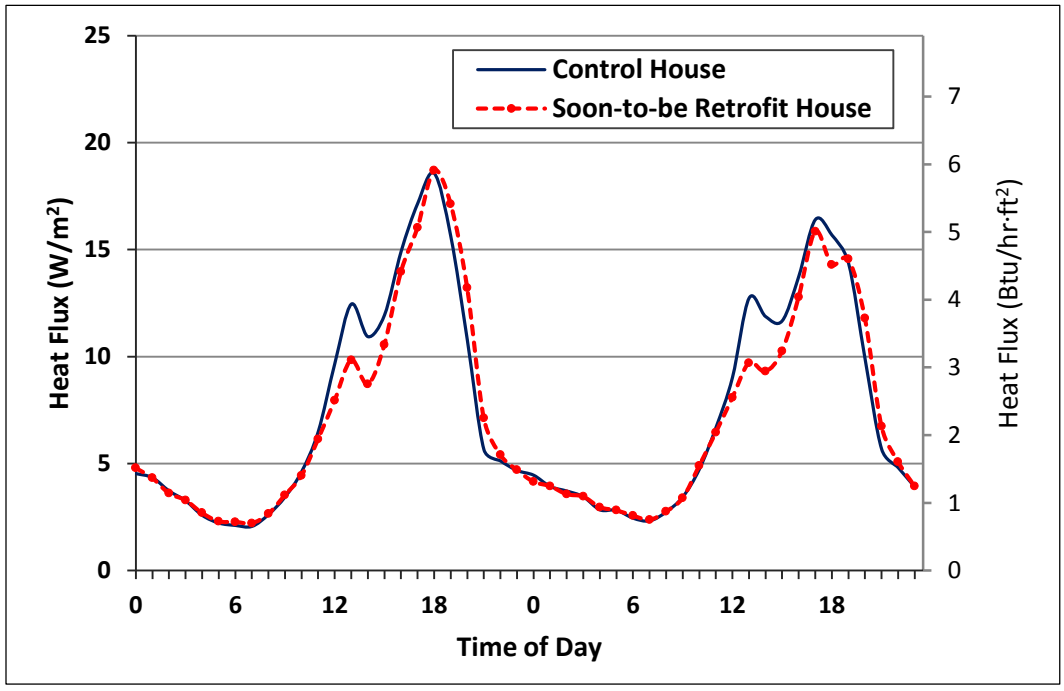

Figure 5.1.5 (b). Heat Fluxes Across the West Walls During Pre-retrofit Tests

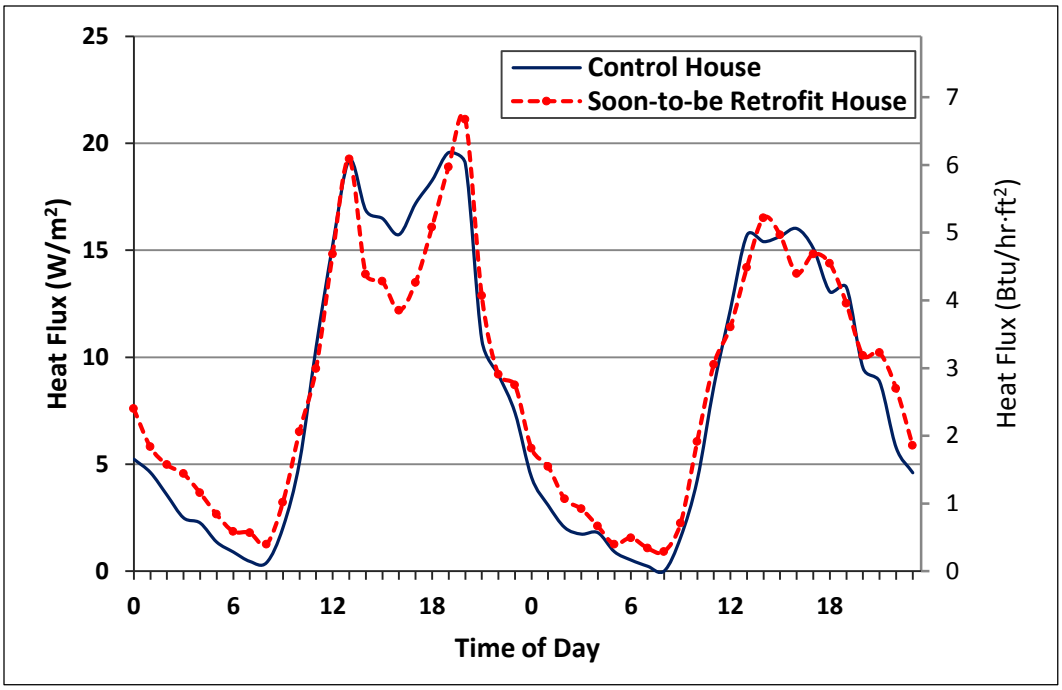

Figure 5.1.5 (c). Heat Fluxes Across the Ceilings During Pre-retrofit Tests

5.1.2 Retrofit Thermal Performance of the Test House

The performance of PCM shields was evaluated by measuring and analyzing the heat fluxes across the south and west walls and ceilings.

5.1.2.1 Heat Fluxes Across the South Wall

For the retrofit tests, the PCM shields were installed between the layers of rigid foam board insulation ("board insulation") inside the cavities of the south wall. A number order of the locations of the PCM shields started from the interior side and proceeded to the exterior side of the wall. For example, the first location of the PCM shield ("Location 1") was between the wallboard and the first insulation board. The PCM shields were tested at this location first. In the following experiments, the PCM

shields were installed at locations 2, 3, 4 and 5. The schematic of the PCM shield locations is shown in Figure 5.1.6.

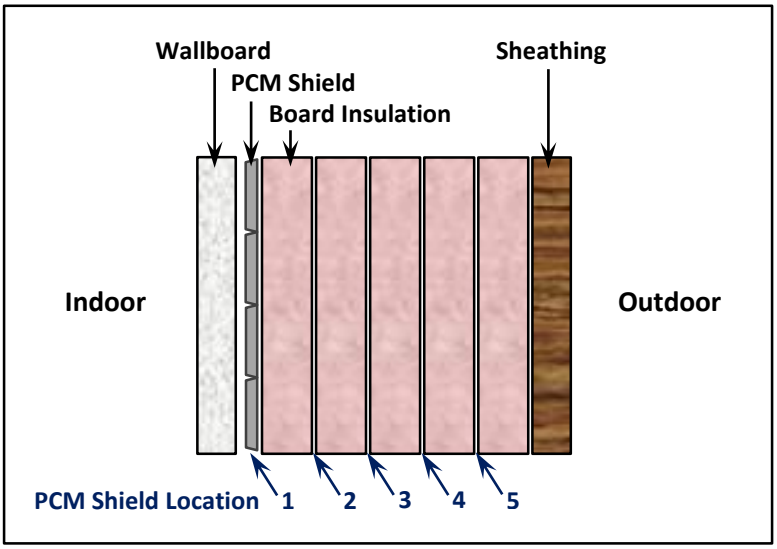

Figure 5.1.6. Schematic of Wall Section Showing the Locations of the PCM Shield

Average temperatures of the PCM shield at each location were measured using six T/Cs connected in parallel. The locations of T/Cs are shown in Figure 5.1.7. These temperatures were used for detailed explanations of the experimental observations.

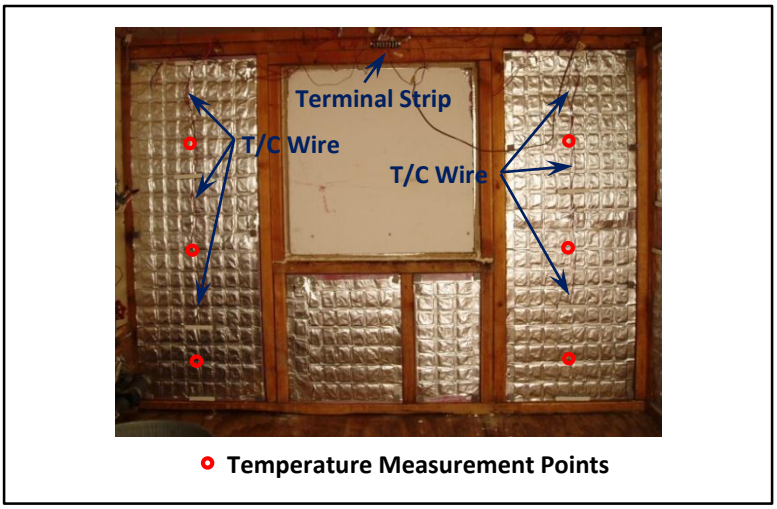

Figure 5.1.7. Temperature Measurement Locations on the PCM Shields in the South Wall

The average reductions in peak heat fluxes when using the PCM shields in the south wall were 28.9, 34.2, 57.4, 49.4, and 25.9%, for locations 1, 2, 3, 4, and 5, respectively. The average time lags of the peak heat fluxes were 6.3, 5, 5, 2.3, and 3 hours, for locations 1, 2, 3, 4, and 5, respectively. The average peak heat flux reduction was maximum when the PCM shield was installed at location 3. The average peak time lag, however, was longer when the PCM shield was installed at location 1.

Percent reductions of peak heat fluxes were calculated as follows:

$$Percent\ Reduction\ (\%) = \frac{(PHF\ for\ Control\ Wall - HF\ for\ Retrofit\ Wall\ at\ Cotrol\ Wall\ Peak\ Time)}{PHF\ for\ Control\ Wall} \times 100 \qquad (5\text{-}1)$$

where:

PHF and HF were the peak heat fluxes and heat fluxes, respectively.

Explanations for these observations were put forth in the following sections. Figures 5.1.8, 5.1.10, 5.1.12, 5.1.14, and 5.1.16 show the heat flux comparisons for the south walls between retrofit and control cases. Each of these figures also depicts relevant temperatures and solar data.

Location 1

In Figure 5.1.8, it appeared that the PCM started to melt at about one hour after sunrise as indicated by the solar irradiation data collected by the weather station and shown at the bottom section of the figure. Also, from this figure, it was apparent that the degree of PCM melting was low. In other words, according to temperature data, which monitored PCM shield temperature, the PCM shield only got as hot as 25.86 °C (78.6 °F), while the PCM melting temperature was 31.36 °C (88.4 °F) and the start of melting temperature for this PCM was around 18.00 °C (64.4 °F) (see Figure 6.2.1 (a)).

The dips that are observed after the peaks in the heat flux graph were the result of increased indoor air temperature in both houses. That is, the summer when the experiments carried out was unusually hot, and therefore, air conditioners did not keep up with the space cooling loads. This was also the case for the experimental set-up. After 5 PM, it was observed that the PCM started to release whatever small amount of heat it had absorbed during the daytime.

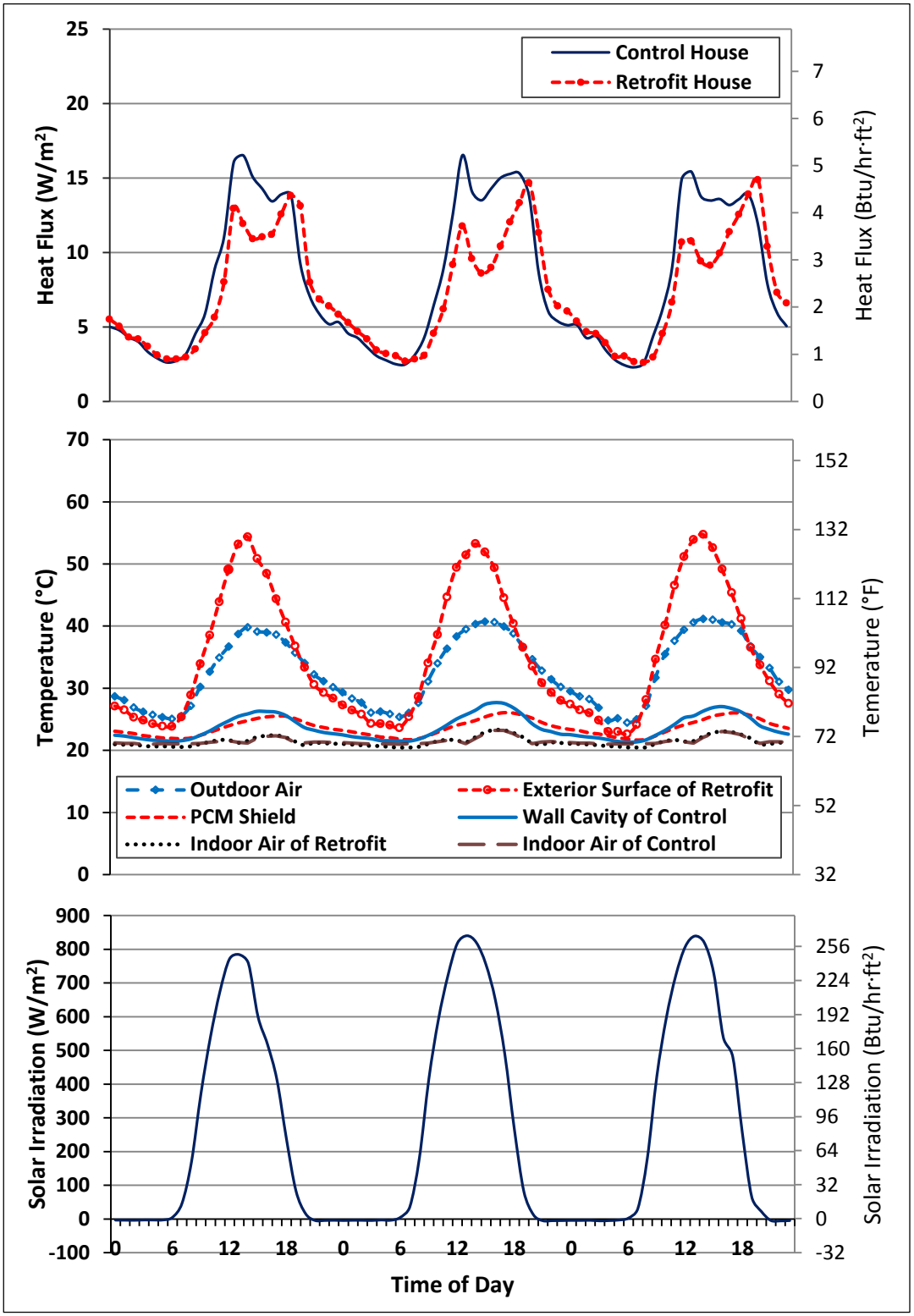

Figure 5.1.8. Wall Heat Fluxes (Top), Temperatures (Middle), and Solar Irradiation (Bottom) for the Case of PCM Shields Installed at Location 1 in the South Wall

For a PCM shield installed at location 1, the average heat transfer reduction was 23.5% during the daytime, while the daily average heat transfer reduction was 11.1% for the retrofit wall. This value is the difference in the areas under the control and retrofit curves. The difference between the terms “daytime” and “daily” as used in this research was related to the exclusion or inclusion of nighttime hours. In other words, the term “daytime” excluded nighttime hours, while “daily” included this time period. The temperature range and the duration of the PCM melting process were from 21.74 and 25.86 °C (71.1 and 78.6 °F) for 9 hours, respectively. This temperature range was superimposed in the curve of specific heat vs. temperature of the PCM, which is shown in Figure 5.1.9.

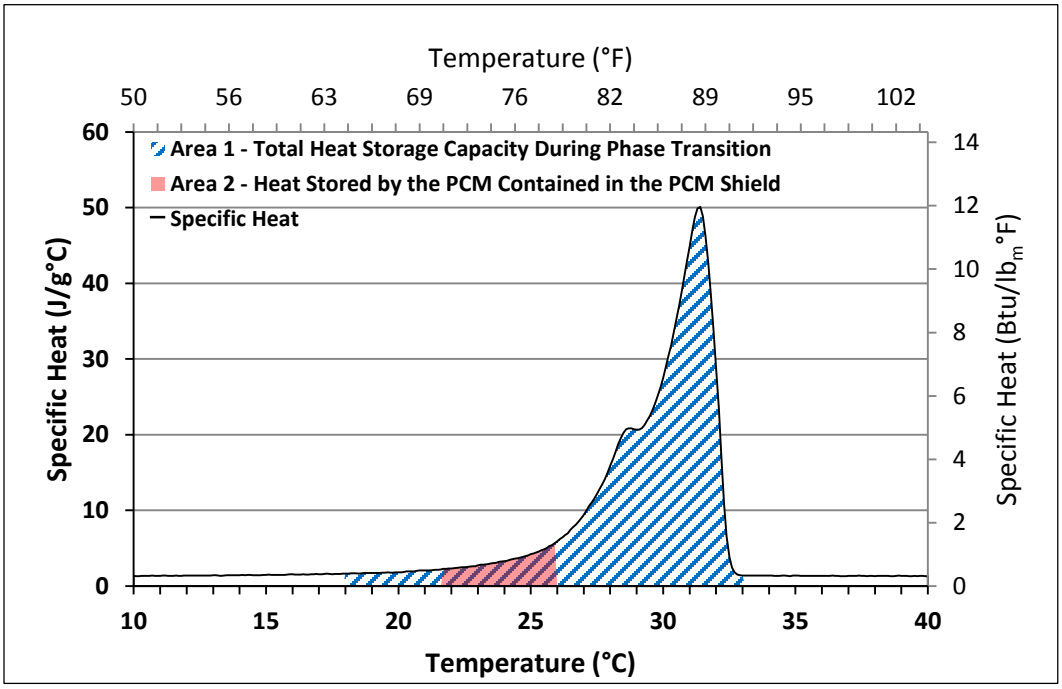

Figure 5.1.9. Total Heat Storage Capacity of the PCM During Phase Transition and Actual Heat Stored by the PCM Contained in the PCM shield at Location 1 in the South Wall

The specific heat curve of Figure 5.1.9 was obtained from DSC experiments. The total heat storage capacity for this PCM was calculated by integrating the area under the specific heat curve (Area 1) from the start of melting temperature to the end of melting temperature. The amount of heat absorbed by the PCM when the shield was placed at location 1 is labeled within figure as Area 2. Based on these areas, the PCM within the shield absorbed an average of 8.1% of the total available heat storage capacity during phase transition.

Location 2

In Figure 5.1.10, it is already apparent that the PCM was melting at a higher degree than in the case shown in Figure 5.1.8. This is more easily perceived during the heat release period, which is when the retrofit house's heat fluxes were above the control house's heat fluxes. For the case when the PCM shield was installed at location 2, the temperature of the PCM shield reached 27.08 °C (80.7 °F) which was closer to the melting temperature of the PCM. This indicated that the PCM had a higher degree of melting, but still did not completely melt. This is shown in Figure 5.1.11. Also, from the solar data it appears that the PCM started the melting process at about 3 hours after sunrise. For a PCM shield installed at location 2, the average heat transfer reduction was 35.7% during the daytime, while the daily average heat transfer reduction was 5.9% for the retrofit wall. Note that according to the heat transfer and temperature data, the days in which the shield was installed at locations 1 and 2 were similar.

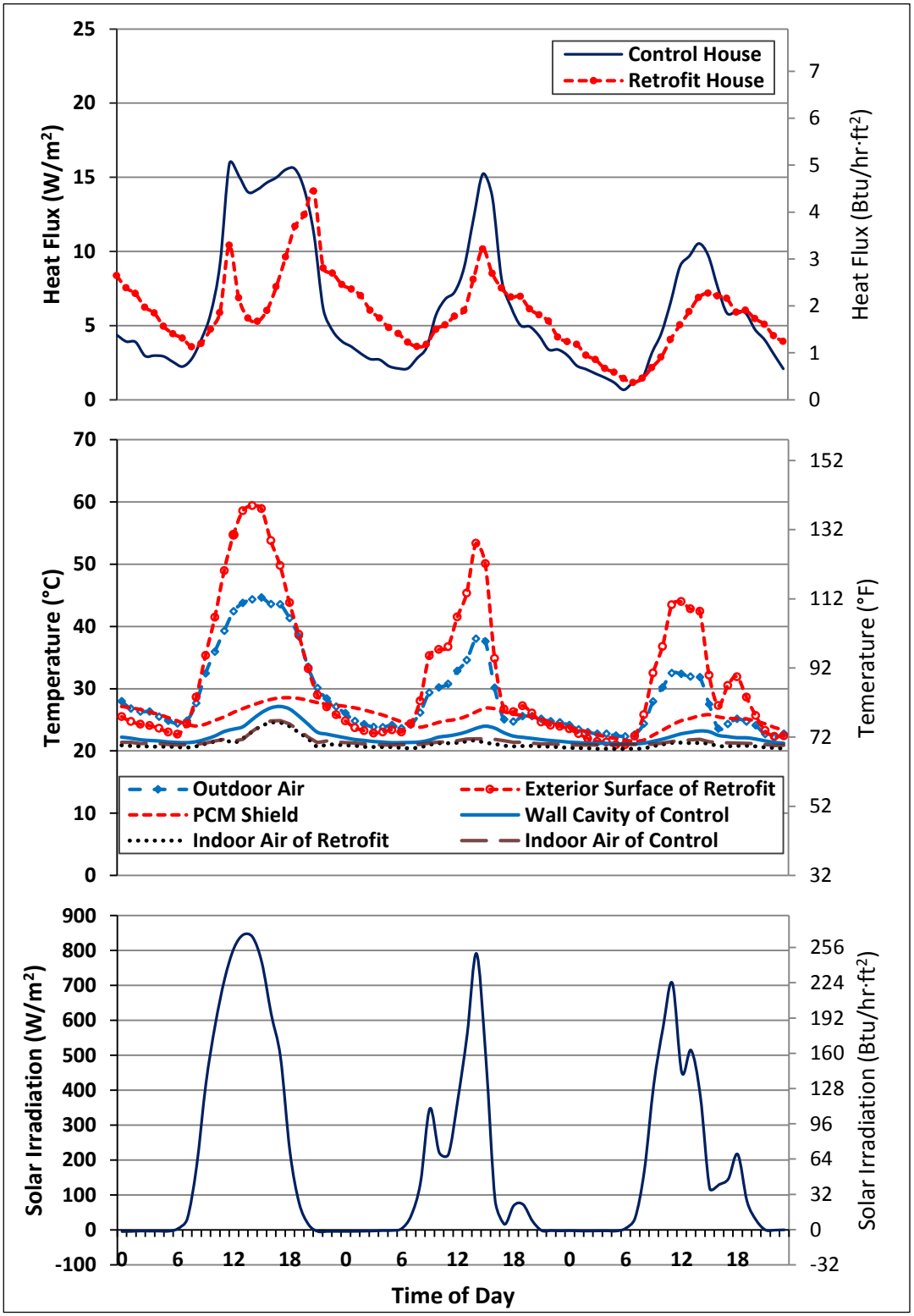

Figure 5.1.10. Wall Heat Fluxes (Top), Temperatures (Middle), and Solar Irradiation (Bottom) for the Case of PCM Shields Installed at Location 2 in the South Wall

The temperature range and the duration of the PCM melting process were from 23.12 to 27.08 °C (73.6 to 80.7 °F) and 7 hours, respectively. At this location, the PCM within the shield absorbed an average of 11.3% of the total available heat storage capacity during phase transition.

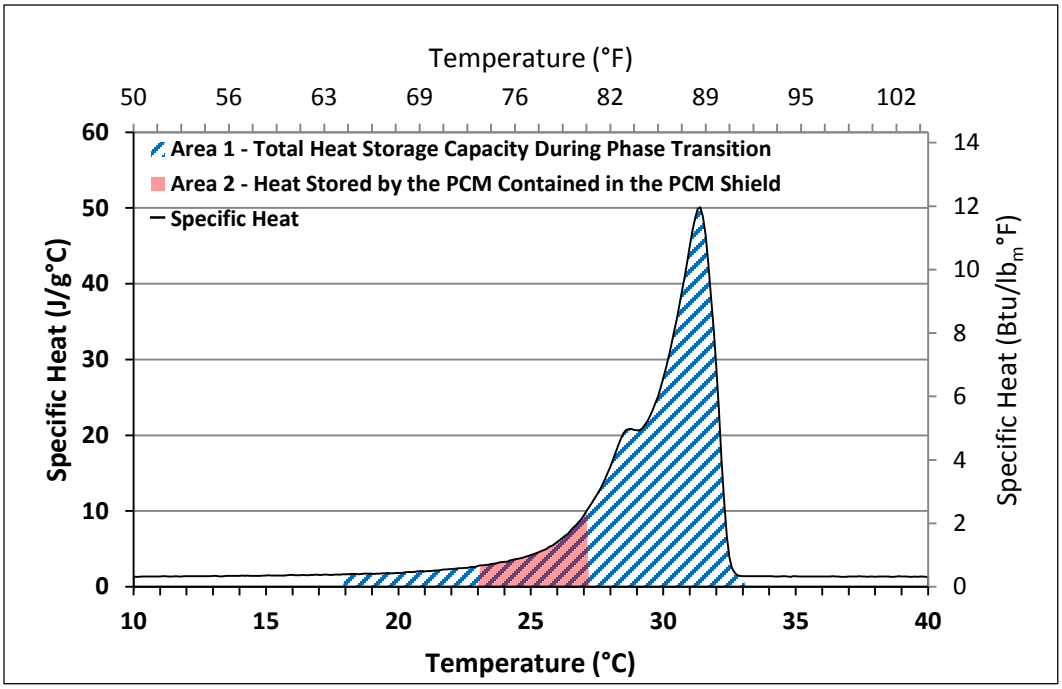

Figure 5.1.11. Total Heat Storage Capacity of the PCM During Phase Transition and Actual Heat Stored by the PCM Contained in the PCM shield at Location 2 in the South Wall

Location 3

In Figure 5.1.12, it is evident that the PCM melted at an even higher degree than in the previous two cases. This is shown in Figure 5.1.13. This is also seen during the heat release period, which in this case started at around 6 PM each evening. For the case when the PCM shield was installed at location 3, the temperature of the

PCM shield reached 30.24 °C (86.4 °F), which indicated that the PCM had a higher degree of melting than when the shield was at locations 1 and 2. The maximum temperature of the PCM shield was close to the melting temperature of this PCM. In addition, the heat fluxes remained more constant, which means that the heat flux fluctuations were smaller during this period.

Also, from solar data it appears that the PCM started the melting process at about 2 hours after sunrise. For a PCM shield installed at location 3, the average heat transfer reduction was 47.9%, while the daily heat transfer reduction was 27.1% for the retrofit wall. The temperature range and duration of PCM melting process were from 24.95 to 30.24 °C (76.6 to 86.4 °F) and 9 hours, respectively. The PCM shield absorbed an average of 44.5% of the total available heat storage capacity during phase transition.

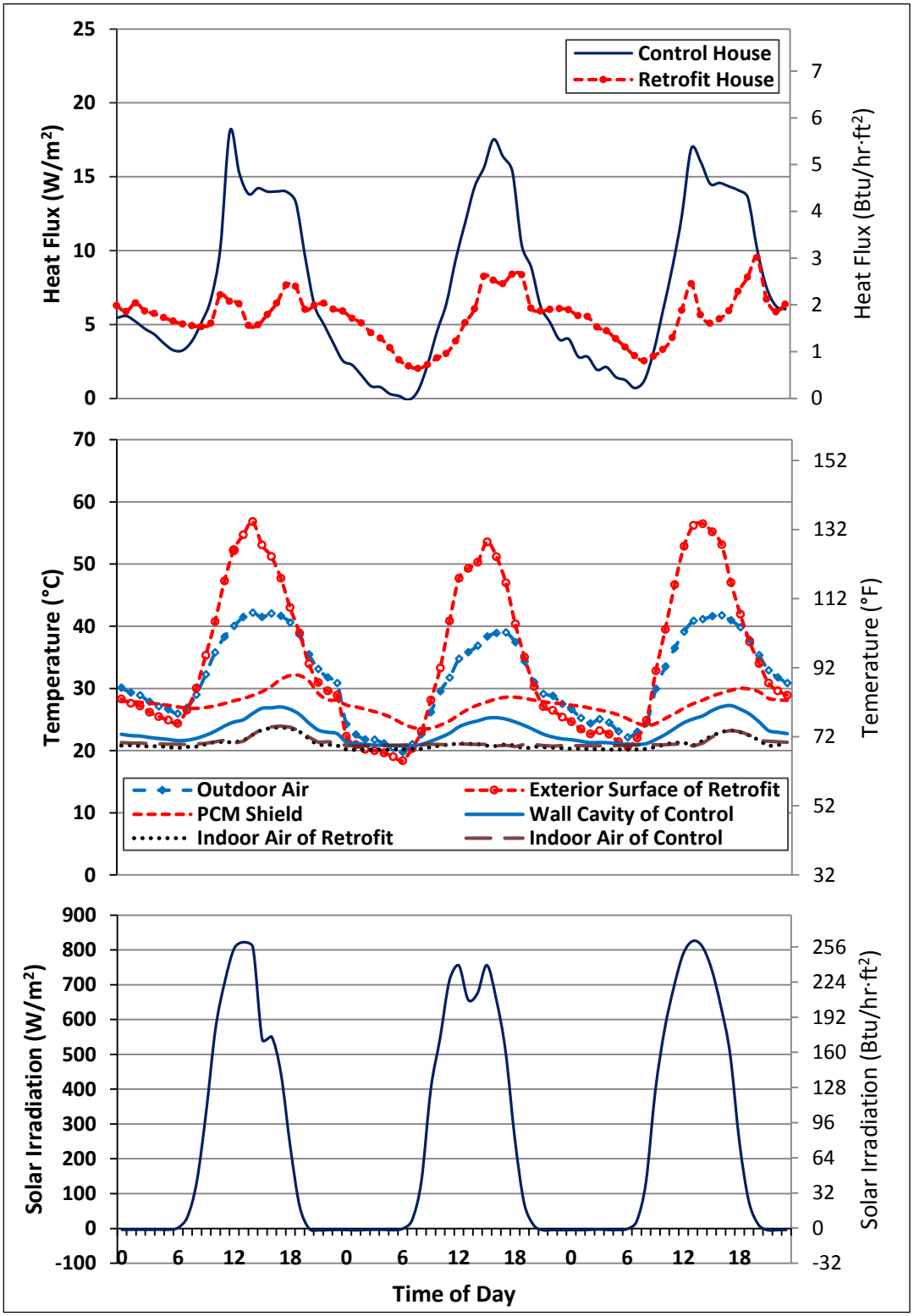

Figure 5.1.12. Wall Heat Fluxes (Top), Temperatures (Middle), and Solar Irradiation (Bottom) for the Case of PCM Shields Installed at Location 3 in the South Wall

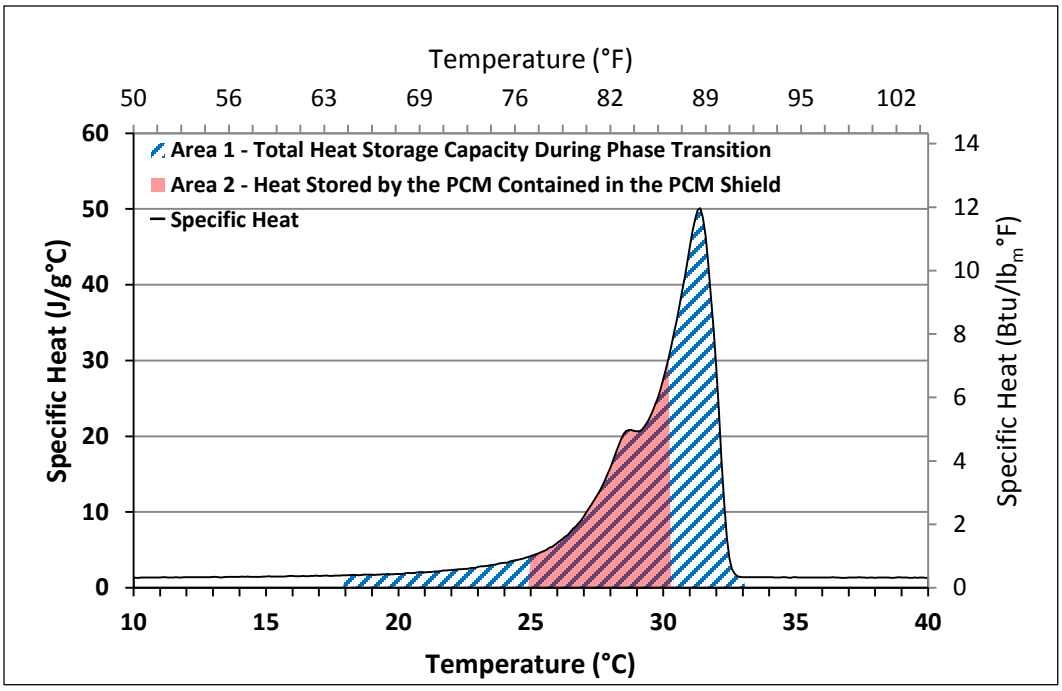

Figure 5.1.13. Total Heat Storage Capacity of the PCM During Phase Transition and Actual Heat Stored by the PCM Contained in the PCM shield at Location 3 in the South Wall

Location 4

In Figure 5.1.14, for the case when the PCM shield was installed at location 4, it was shown that heat flux reductions were similar with Figure 5.1.12. The heat release period started at around 5 PM each evening. For this case, the temperature of the PCM shield reached 37.2 °C (99.0 °F) which was 5.84 °C (10.5 °F) higher than the melting temperature of the PCM. This indicated that the PCM had a higher degree of melting. From solar data it appears that the PCM started the melting process at about 3 hours after sunrise. For a PCM shield installed at location 4, the average heat transfer reduction was 39.9% during the daytime, while the daily average heat transfer reduction was 15.6% for the retrofit wall.

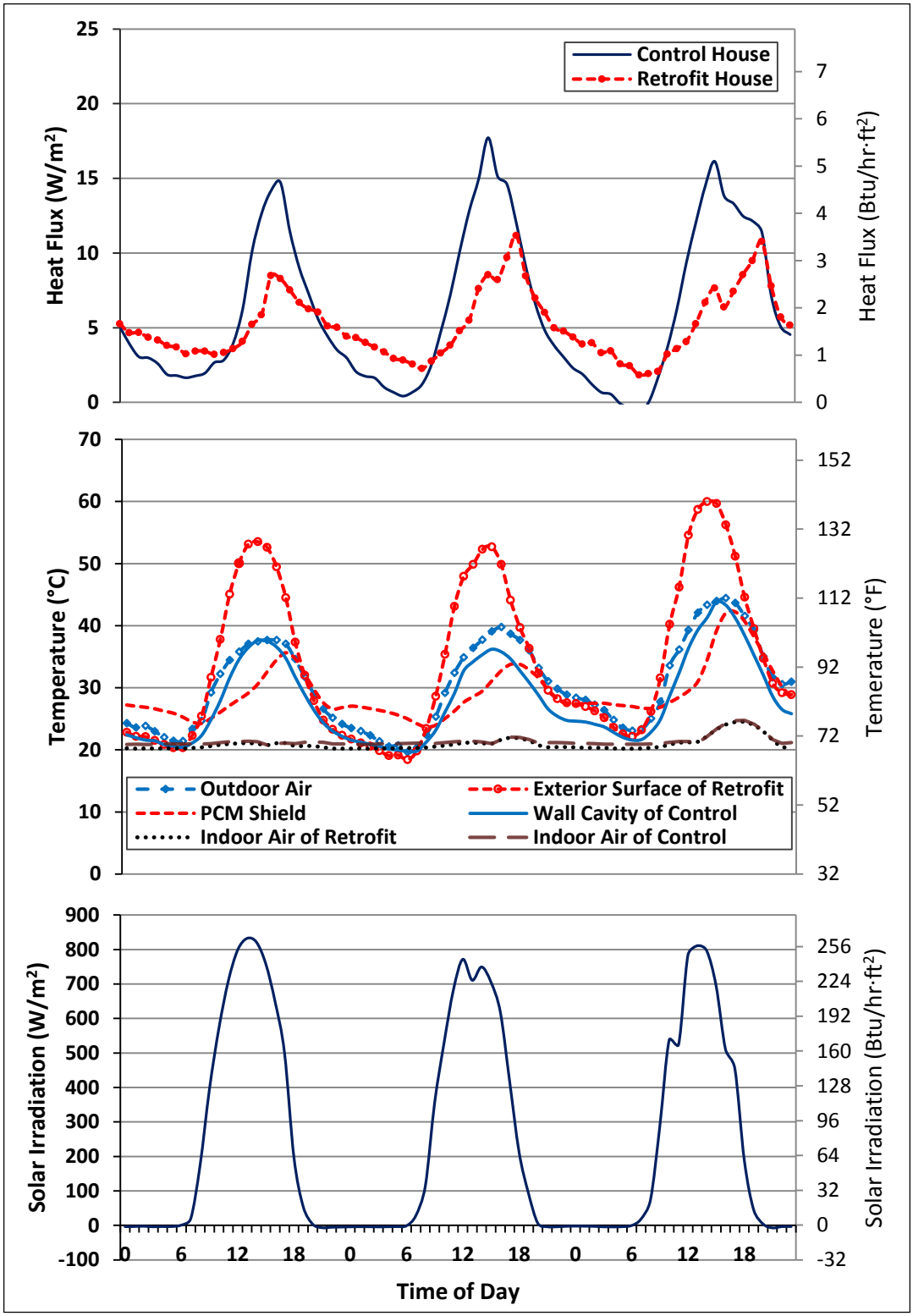

Figure 5.1.14. Wall Heat Fluxes (Top), Temperatures (Middle), and Solar Irradiation (Bottom) for the Case of PCM Shields Installed at Location 4 in the South Wall

The temperature range and duration of PCM melting process were from 24.84 to 37.2 °C (76.7 to 99.0 °F) and 8 hours, respectively. The PCM shield absorbed an average of 90.6% of the total available heat storage capacity during phase transition, which was double of the heat absorbed in the previous case when the PCM shield was installed at location 3. However, the average heat transfer reduction was almost the same as in the previous case. This temperature range was superimposed in the curve of specific heat vs. temperature of the PCM, which is shown in Figure 5.1.15.

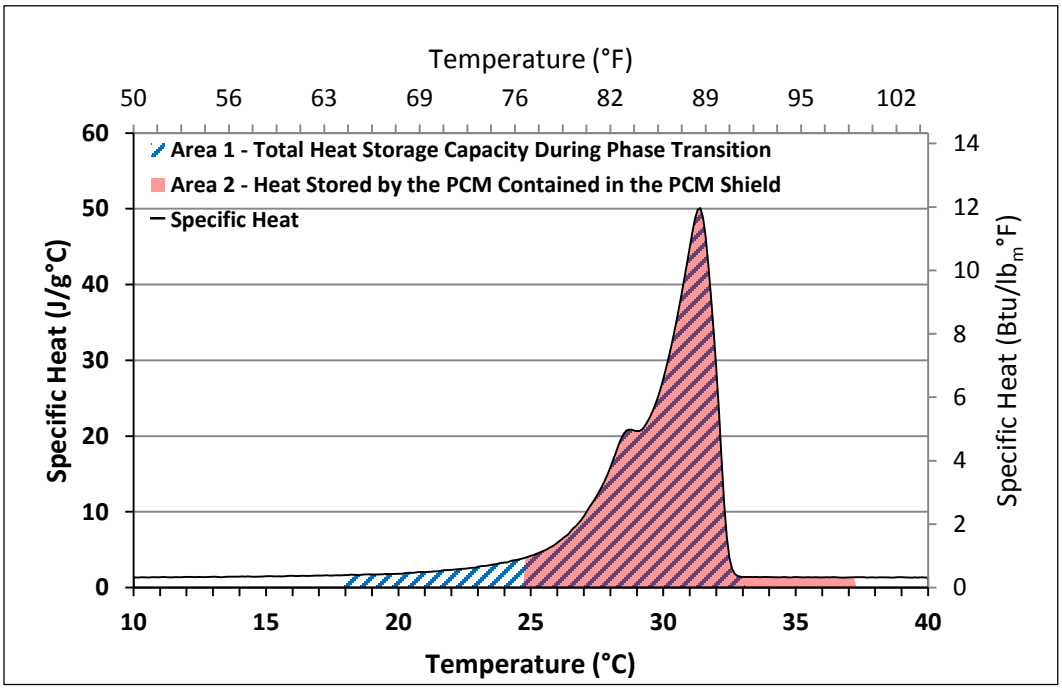

Figure 5.1.15. Total Heat Storage Capacity of the PCM During Phase Transition and Actual Heat Stored by the PCM Contained in the PCM shield at Location 4 in the South Wall

Location 5

In Figure 5.1.16, for the case when the PCM shield was installed at location 5, the heat release period started at around 4 PM each afternoon. In this case, the temperature of the PCM shield reached 41.11 °C (106.0 °F), which was the highest of all five cases. From solar data it appears that the PCM started the melting process at about 2 hours after sunrise.

For a PCM shield installed at location 5, the average heat transfer reduction was 27.3% during the daytime, while the daily average heat transfer reduction was 14.7% for the retrofit wall. The temperature range and duration of PCM melting process were from 25.26 to 41.11 °C (77.5 to 106.0 °F) and 8 hours, respectively. The PCM shield absorbed an average of 89.5% of the total available heat storage capacity during phase transition, which was also double of the heat absorbed in the case for location 3. This temperature range was superimposed in the curve of specific heat vs. temperature of the PCM, which is shown in Figure 5.1.17.

The average heat transfer reduction, however, was almost half of that case. This is because the temperature of the PCM reached a maximum at around 1 PM. This means that the PCM absorbed the majority of the latent heat before 1 PM. The peak heat flux, however, started to occur at around 2 PM. By this time, the PCM had already finished the phase transition process before the wall heat flux reached its highest value. Therefore, the PCM did not absorb any more heat after 1 PM.

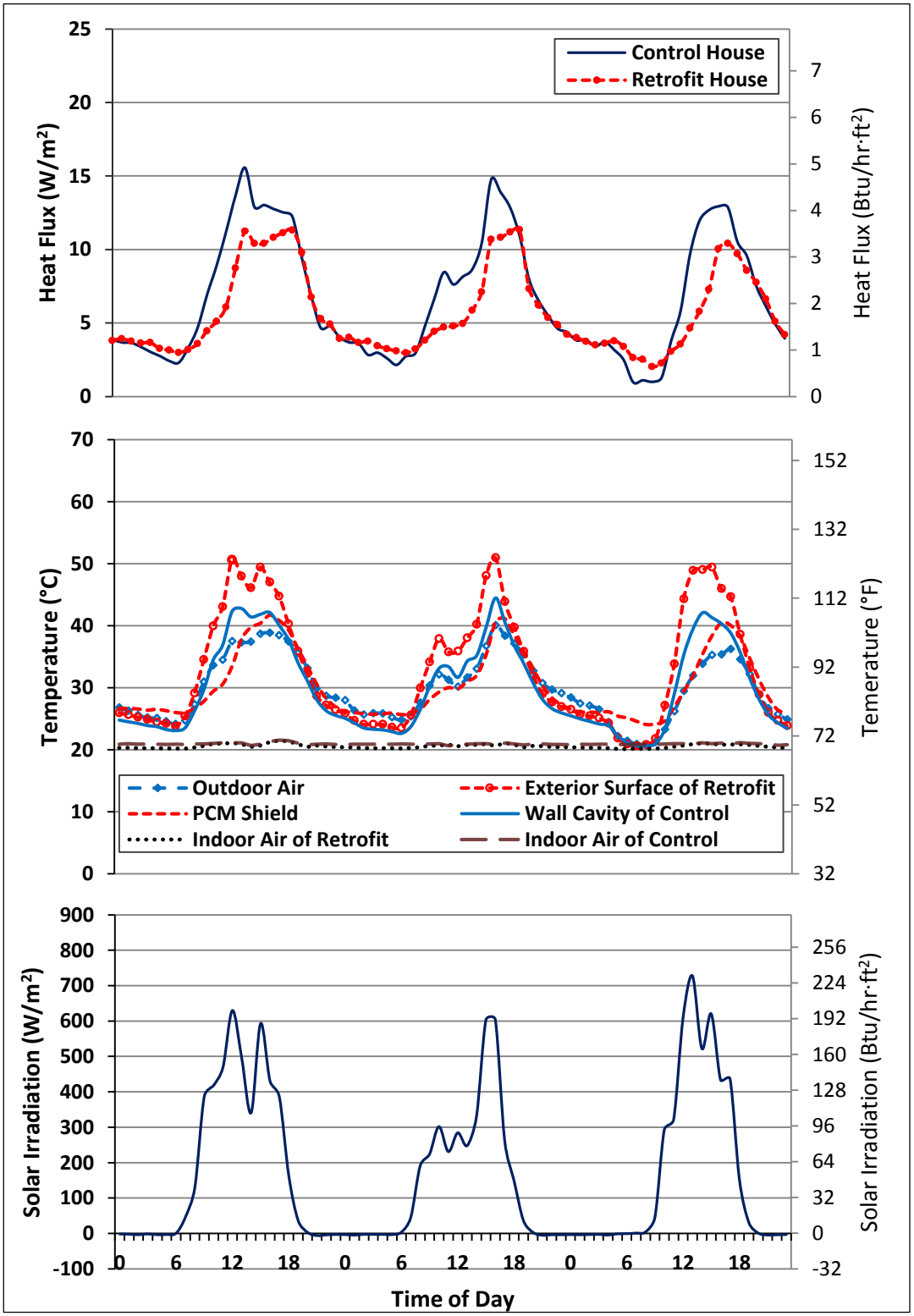

Figure 5.1.16. Wall Heat Fluxes (Top), Temperatures (Middle), and Solar Irradiation (Bottom) for the Case of PCM Shields Installed at Location 5 in the South Wall

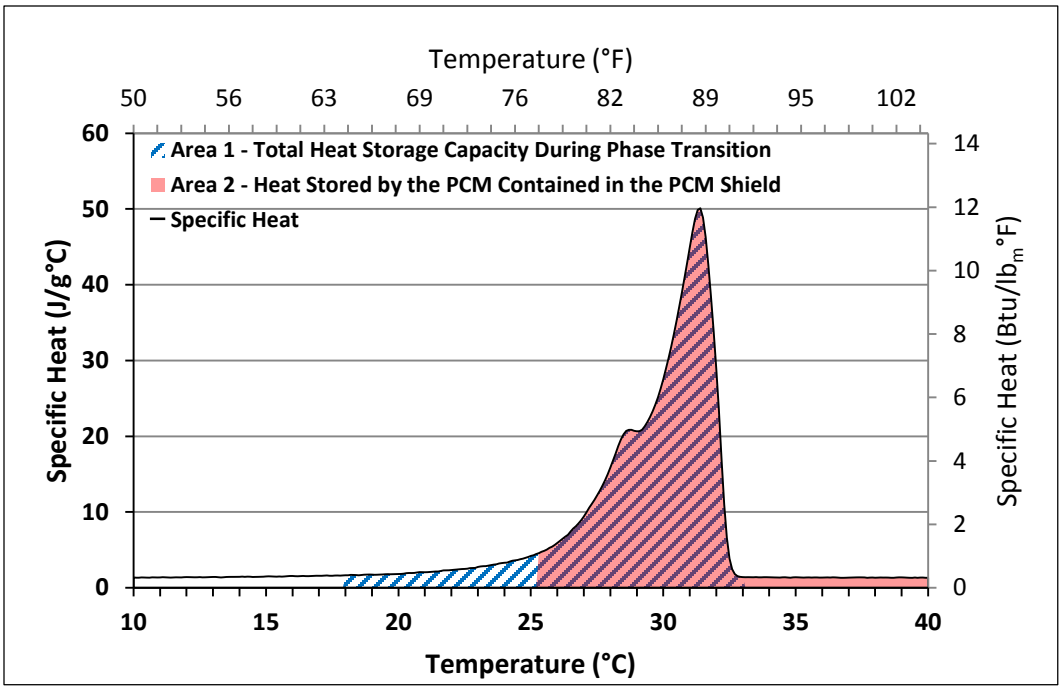

Figure 5.1.17. Total Heat Storage Capacity of the PCM During Phase Transition and Actual Heat Stored by the PCM Contained in the PCM shield at Location 5 in the South Wall

For all figures, the steeper increases in heat flux after the dips indicated the points when the PCM started to release the absorbed heat. When the PCM released the heat, the temperatures of the PCM shields were more constant while the temperatures of the wall cavity without a PCM shields decreased. This caused the higher rates of heat flux increase in the retrofit walls.

Table 5.1.2 summarizes the average peak heat flux reductions and the average peak heat flux time lags when using the PCM shields in the south wall.

Table 5.1.2. Peak Heat Flux Reductions Across the South Wall and Peak Heat Flux Time Lags Produced by the PCM Shield

PCM Shield Location	Peak Heat Flux Reduction (%)	Average Peak Heat Flux Time Lag (hrs)
1	28.9	6.3
2	34.2	5
3	57.4	5
4	49.4	2.3
5	25.9	3
Average	39.1	4.3

5.1.2.2 Heat Fluxes Across the West Wall

The number order of the locations of the PCM shield was the same as the order for the south wall (see Figure 5.1.6). It also started from the interior side and proceeded to the exterior side of the wall. Average temperatures of the PCM shield at these locations were also measured using nine T/Cs connected in parallel. These temperatures were also used to produce a detailed set of explanations of the observations seen during the experiments.

The average reductions in peak heat fluxes when using the PCM shield in the west wall were 26.1, 37.3, 36.3, 2.5, and 14.2%, for locations 1, 2, 3, 4, and 5, respectively. The average time lags of the peak heat fluxes were 2, 2.3, 1, 0.7, and 1 hours, for the same locations, respectively. When the PCM shield was installed at locations 2 and 3, both average peak heat flux reductions were similar and higher than in the rest of the locations. The average time lag, however, was longer when the PCM shield was installed at location 2. These observations are explained in later sections using Figures 5.1.19, 5.1.21, 5.1.23, 5.1.25, and 5.1.27. These figures show

comparisons of the heat fluxes and relevant temperatures between retrofit and control cases as well as solar data.

Location 1

In Figure 5.1.18, it appears that the PCM started to melt at about two hours after sunrise as indicated by the solar irradiation data collected by the weather station and shown at the bottom section of the figure. According to the PCM shield temperature data, the PCM reached 26.46 °C (79.6 °F), which was less than the melting temperature of the PCM. This indicated that the PCM inside the shield did not completely melt when the shield was placed at location 1.

As was the case for the south wall, the dips that are observed after the peaks in the heat flux graph were also the result of increased indoor air temperature in both houses as described in the previous section. The heat fluxes of the west retrofit wall had lower values than those of the control wall two hours after the temperature of the PCM started to increase. However, the heat fluxes of the south retrofit wall had lower values than those of the control wall one hour after the temperature of the PCM started to increase. The reason for this is that the temperature of the PCM in the south retrofit wall increased faster than those of the west retrofit wall. The PCM in the south wall absorbed more heat because of more solar exposure than the west wall. This resulted faster heat flux reductions in the south wall than the west wall.

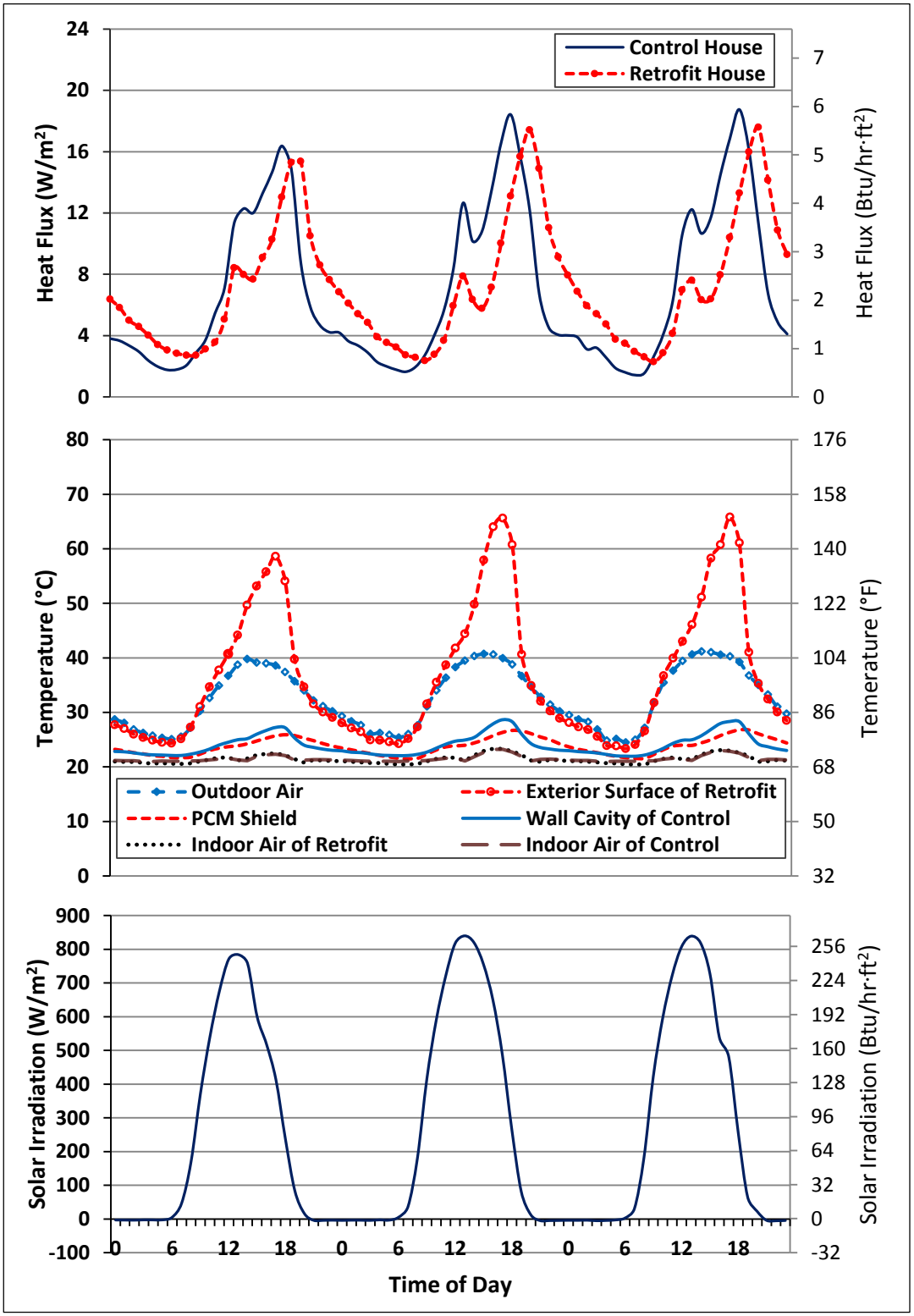

Figure 5.1.18. Wall Heat Fluxes (Top), Temperatures (Middle), and Solar Irradiation (Bottom) for the Case of a PCM Shield Installed at Location 1 in the West Wall

As the outdoor conditions became more favorable for heat transfer from the wall to the outside, the heat fluxes of the west retrofit wall had higher values than those of the control wall at the same time when the temperature of the PCM started to decrease. However, the heat fluxes of the south retrofit wall had higher values than those of the control wall two hours after than the temperature of the PCM started to decrease. The fact that the heat fluxes across the retrofit walls were higher than those of the control walls indicated that the PCM within the shields was solidifying; thus, releasing the heat that had been absorbed during melting. It appears that the PCM in the retrofit walls started the solidification process at the same time. The time of overlap between the heat fluxes in the retrofit and control walls was different for the west and south walls. This had to do with the time of solar exposure by each wall.

Similar to the south wall when the shield was at location 1, it was observed that the temperature of the PCM started to increase one hour after sunrise. The temperature of the PCM started to decrease at around 6 PM, which was one hour later than the temperature of the PCM started to decrease in the south wall. For a PCM shield installed at location 1, the average heat transfer reduction was 32.5% during the daytime. However, during the entire day, the average heat transfer was increased 2.6% for the retrofit wall. It is shown that the heat fluxes of the retrofit wall were higher than the control during the nighttime while the PCM was releasing the heat which was absorbed during the daytime. This value is the difference in the areas under the heat flux curves of the control and retrofit walls. This indicates that a shield at this

location in the west wall may even pose detrimental effects in energy conservation. This will not be the case for all locations as it will be explained later.

The temperature range and the duration of the PCM melting process were from 21.56 to 26.46 °C (70.8 to 79.6 °F) and 11 hours, respectively. This temperature range was superimposed in the curve of specific heat vs. temperature of the PCM, which is shown in Figure 5.1.19. The specific heat curve of Figure 5.1.19 was obtained from DSC experiments.

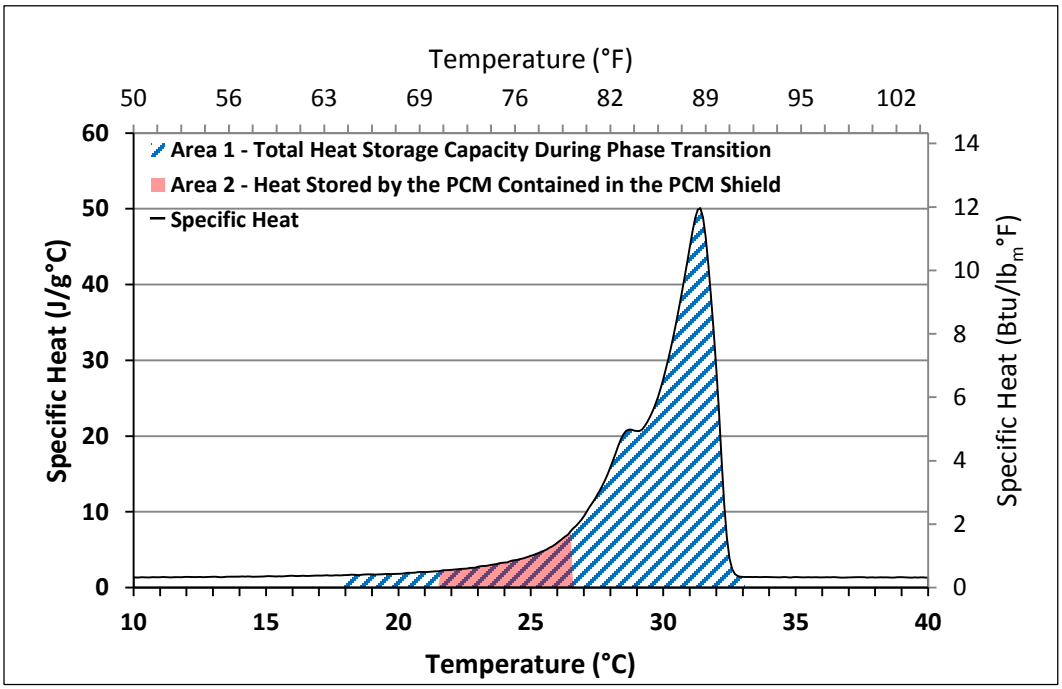

Figure 5.1.19. Total Heat Storage Capacity of the PCM During Phase Transition and Actual Heat Stored by the PCM Contained in the PCM shield at Location 1 in the West Wall

Location 2

Figure 5.1.20 shows data related to placing the PCM shield at location 2. In Figure 5.1.20, it is shown that the PCM also started to melt at about two hours after sunrise. For the case when the PCM shield was installed at location 2, the temperature of the PCM shield reached 26.98 °C (80.6 °F) which was still below the melting temperature of the PCM. This, just as before, indicated that the PCM did not completely melt. This is shown in Figure 5.1.21. For a PCM shield installed at location 2, the average heat transfer reduction was 32.4%, while the daily average heat transfer was increased 27.9% for the retrofit wall.

The temperature range and the duration of the PCM melting process were from 23.54 to 26.98 °C (74.4 to 80.6 °F) and 8 hours, respectively. The data of Figure 5.1.20 show that the first day was about 4.0 °C (7.2 °F) hotter than the one data in Figure 5.1.18. However, the second and third days were between 2.0 and 6.0 °C (3.6 and 10.8 °F) colder than those of Figure 5.1.18.

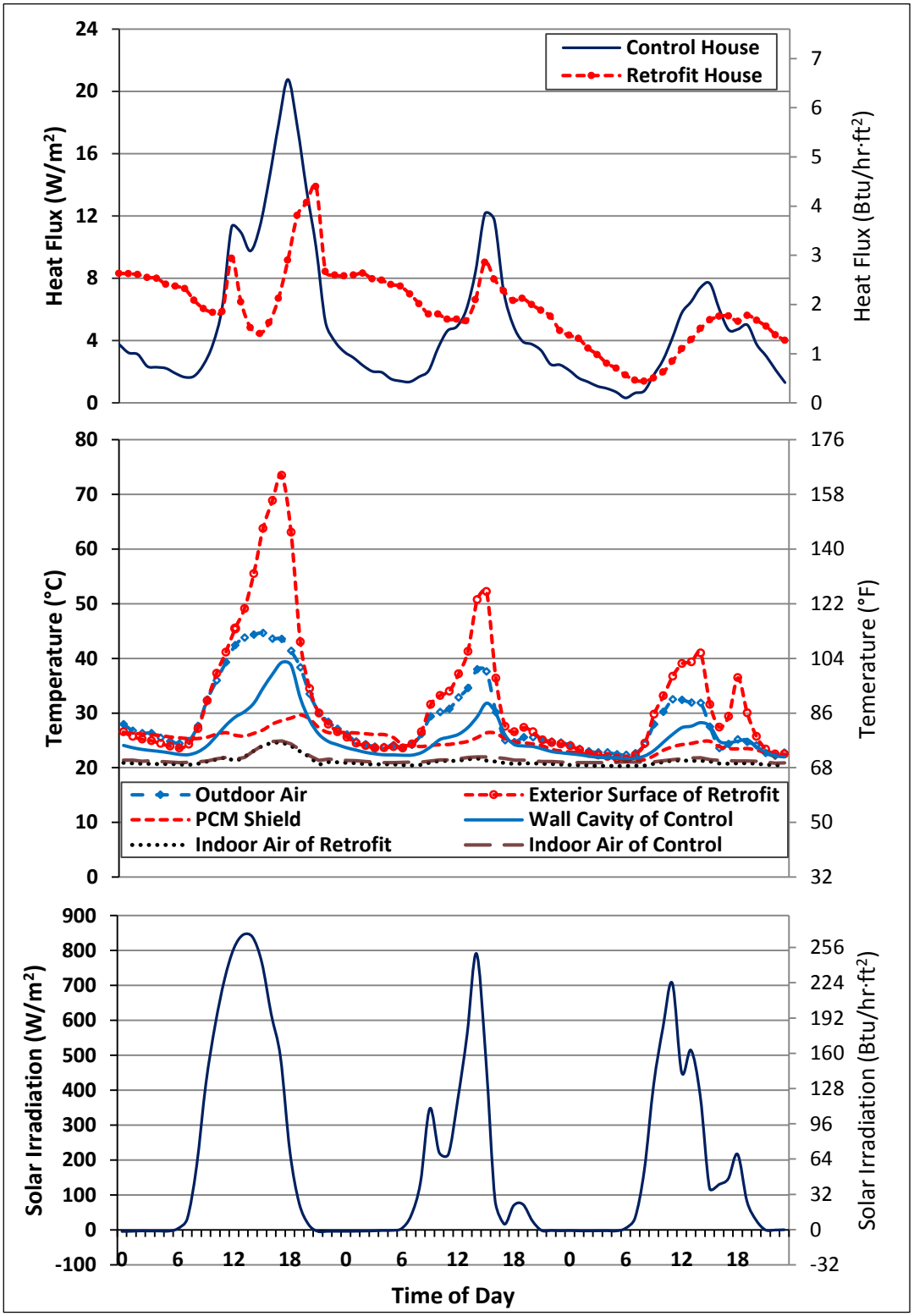

Figure 5.1.20. Wall Heat Fluxes (Top), Temperatures (Middle), and Solar Irradiation (Bottom) for the Case of a PCM Shield Installed at Location 2 in the West Wall

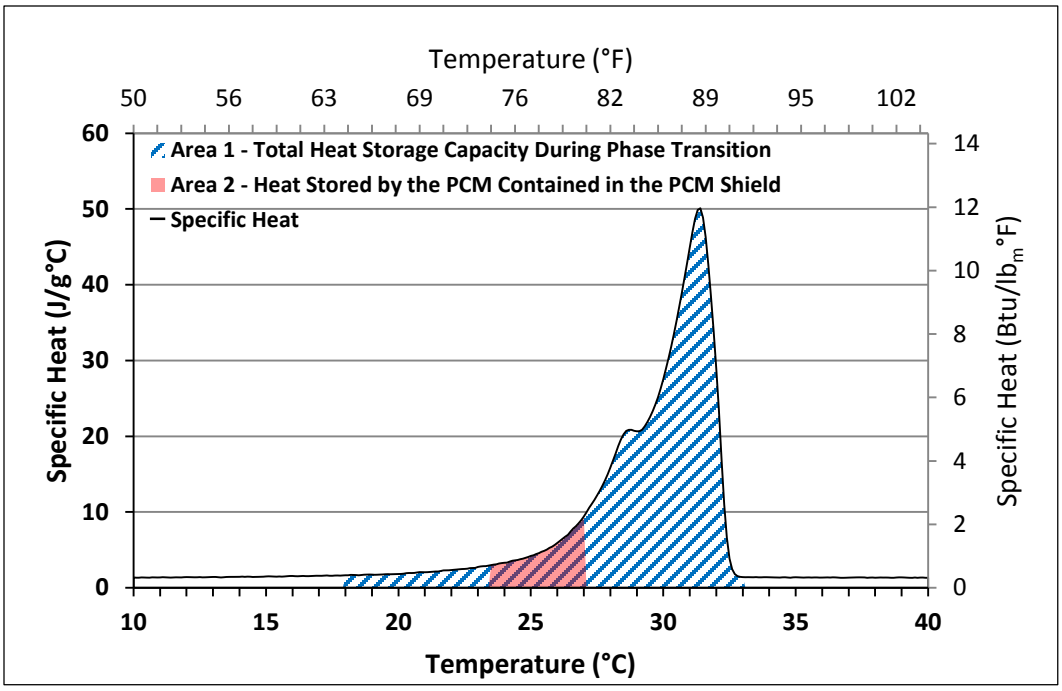

Figure 5.1.21. Total Heat Storage Capacity of the PCM During Phase Transition and Actual Heat Stored by the PCM Contained in the PCM shield at Location 2 in the West Wall

Location 3

Figure 5.1.22 presents data for the PCM shield placed at location 3. In Figure 5.1.22, it is shown that the PCM also melted partially, as was the case for when the shield in the other locations. The PCM also started to melt at about two hours after sunrise. It was observed that the PCM started to release heat after 7 PM.

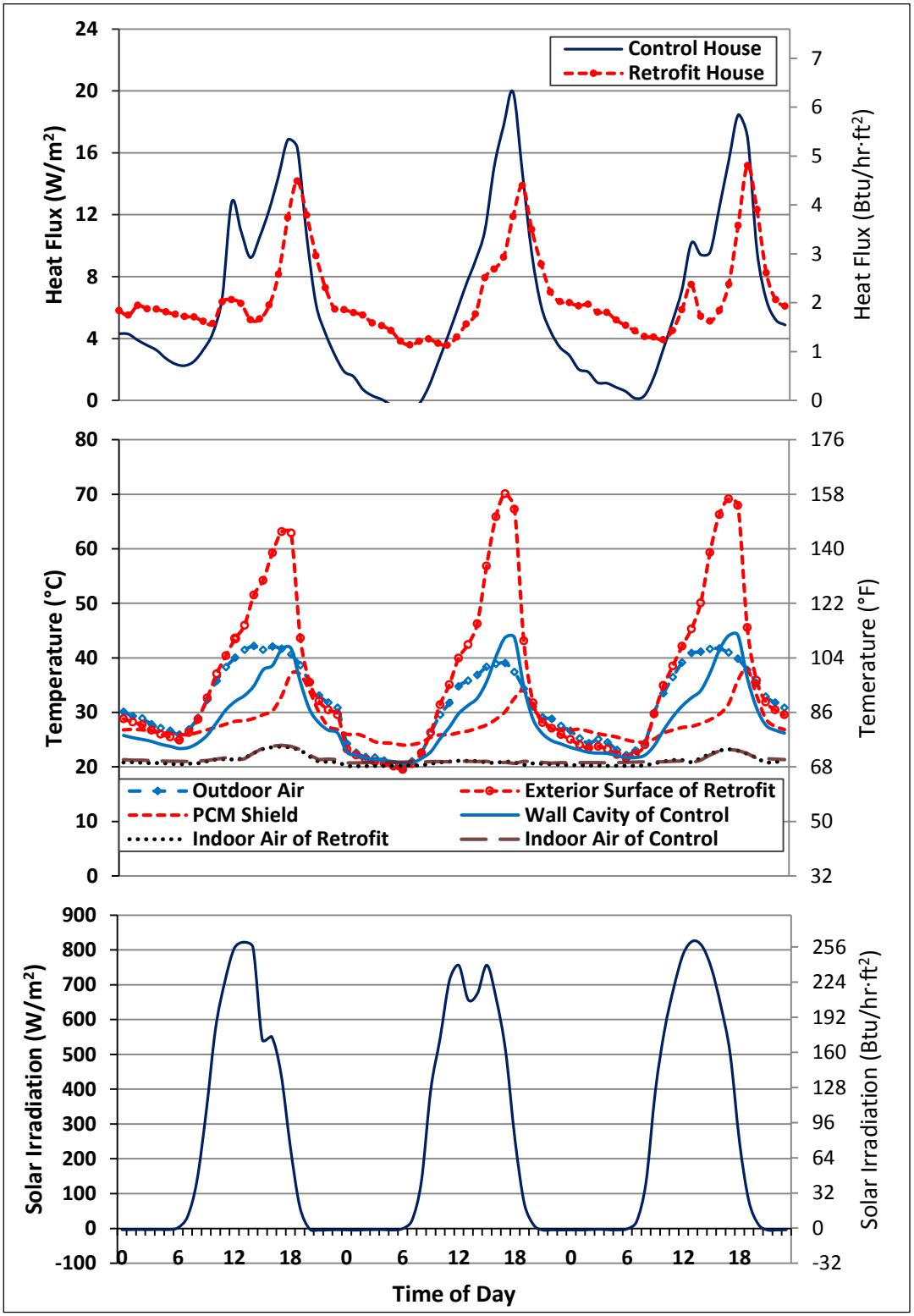

Figure 5.1.22. Wall Heat Fluxes (Top), Temperatures (Middle), and Solar Irradiation (Bottom) for the Case of a PCM Shield Installed at Location 3 in the West Wall

For the case when the PCM shield was installed at location 3, the temperature of the PCM shield reached 36.33 °C (97.4 °F), which was higher than the temperature of the shield when it was in locations 1 and 2. The maximum temperature of the PCM shield surpassed the end of melting temperature of the PCM. The average heat transfer reduction was 35.1% during the daytime, which was somewhat higher than in the previous cases. However, the daily average heat transfer was increased 6.0% for the retrofit wall.

The temperature range of the PCM melting process was from 24.82 to 36.33 °C (76.7 to 97.4 °F) as shown in Figure 5.1.23. The duration of the PCM melting process was 12 hours. The climate data indicated that the three days plotted in Figure 5.1.22 were similar, yet hotter, to the days plotted in Figure 5.1.18. This, together with the fact that the shield was closer to the external surface, may have contributed to the higher degree of melting of the PCM as it is shown in Figure 5.1.23.

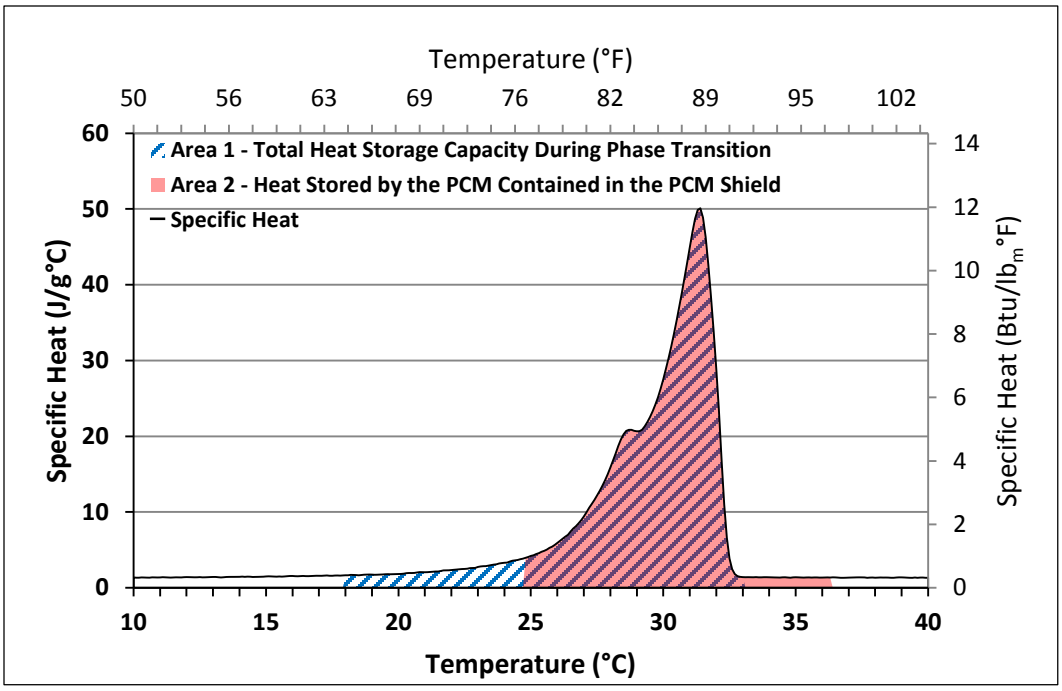

Figure 5.1.23. Total Heat Storage Capacity of the PCM During Phase Transition and Actual Heat Stored by the PCM Contained in the PCM shield at Location 3 in the West Wall

Location 4

In Figure 5.1.24, which is for the case when the PCM shield was installed at location 4, shows that heat fluxes were almost not reduced when compared to the control case. In fact, the peak heat fluxes for days 2 and 3 were larger than the peak heat fluxes of the control house. The reason for this is shown in Figure 5.1.25. That is, the temperature of the PCM shield reached 47.87 °C (118.2 °F), which was more than 16.51 °C (29.7 °F) higher than the melting temperature of the PCM.

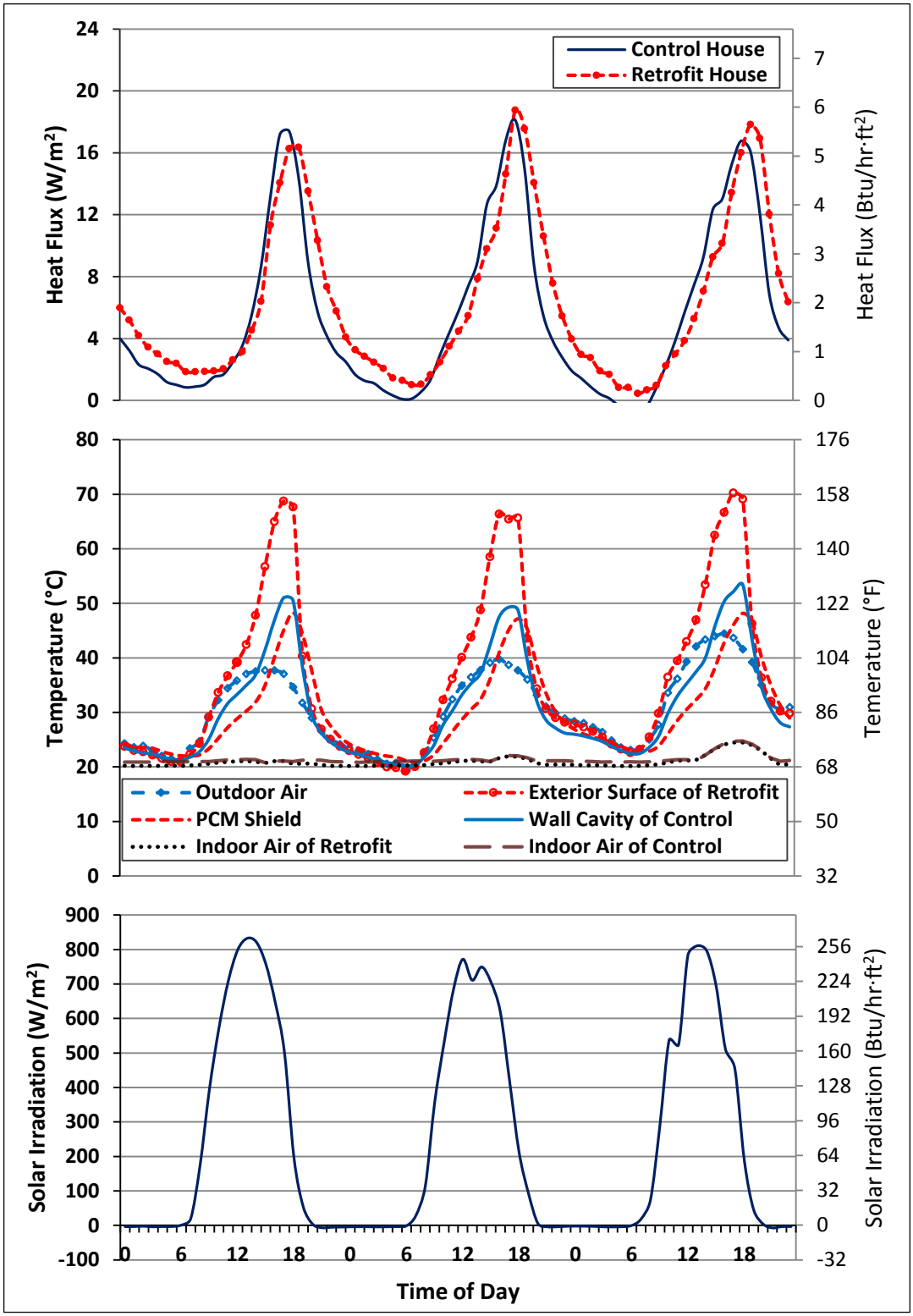

Figure 5.1.24. Wall Heat Fluxes (Top), Temperatures (Middle), and Solar Irradiation (Bottom) for the Case of a PCM Shield Installed at Location 4 in the West Wall

For a PCM shield installed at location 4, the average heat transfer reduction was 17.2% during the daytime, while the daily average heat transfer was increased 14.2% for the retrofit wall. The temperature range and duration of PCM melting process were from 21.87 to 47.87 °C (71.4 to 118.2 °F) and 13 hours, respectively. However, the average heat transfer reduction was smaller though the PCM temperature reached higher than previous case.

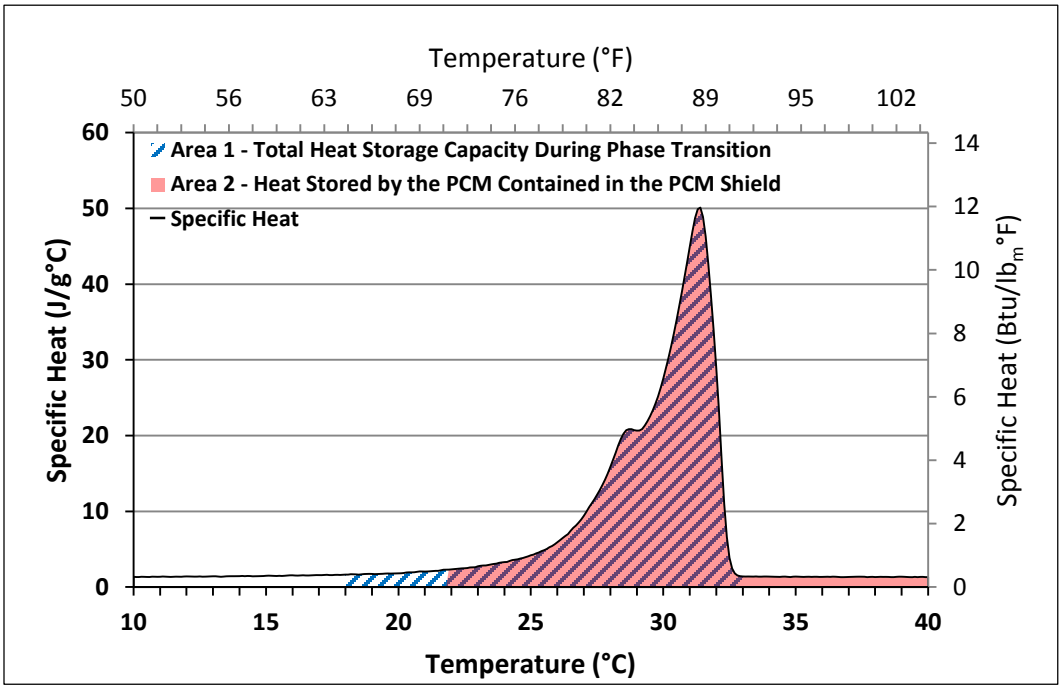

Figure 5.1.25. Total Heat Storage Capacity of the PCM During Phase Transition and Actual Heat Stored by the PCM Contained in the PCM shield at Location 4 in the West Wall

Location 5

In Figure 5.1.26, for the case when the PCM shield was installed at location 5, it appears that the PCM started the melting process at about two hours after sunrise.

The heat release period started at around 6 PM each evening. In this case, the temperature of the PCM shield reached 52.26 °C (126.1 °F) as shown in Figure 5.1.27, which was the highest of all five cases.

For a PCM shield installed at location 5, the average heat transfer reduction was 22.6% during the daytime. For this case only, the daily heat transfer was also reduced 3.6% for the retrofit wall. The temperature range and duration of PCM melting process were from 22.60 to 52.26 °C (72.7 to 126.1 °F) and 11 hours, respectively. The average heat transfer reduction, however, was smaller than when the PCM shield was installed at location 1, 2, and 3, even though the PCM reached its highest temperature of all five cases.

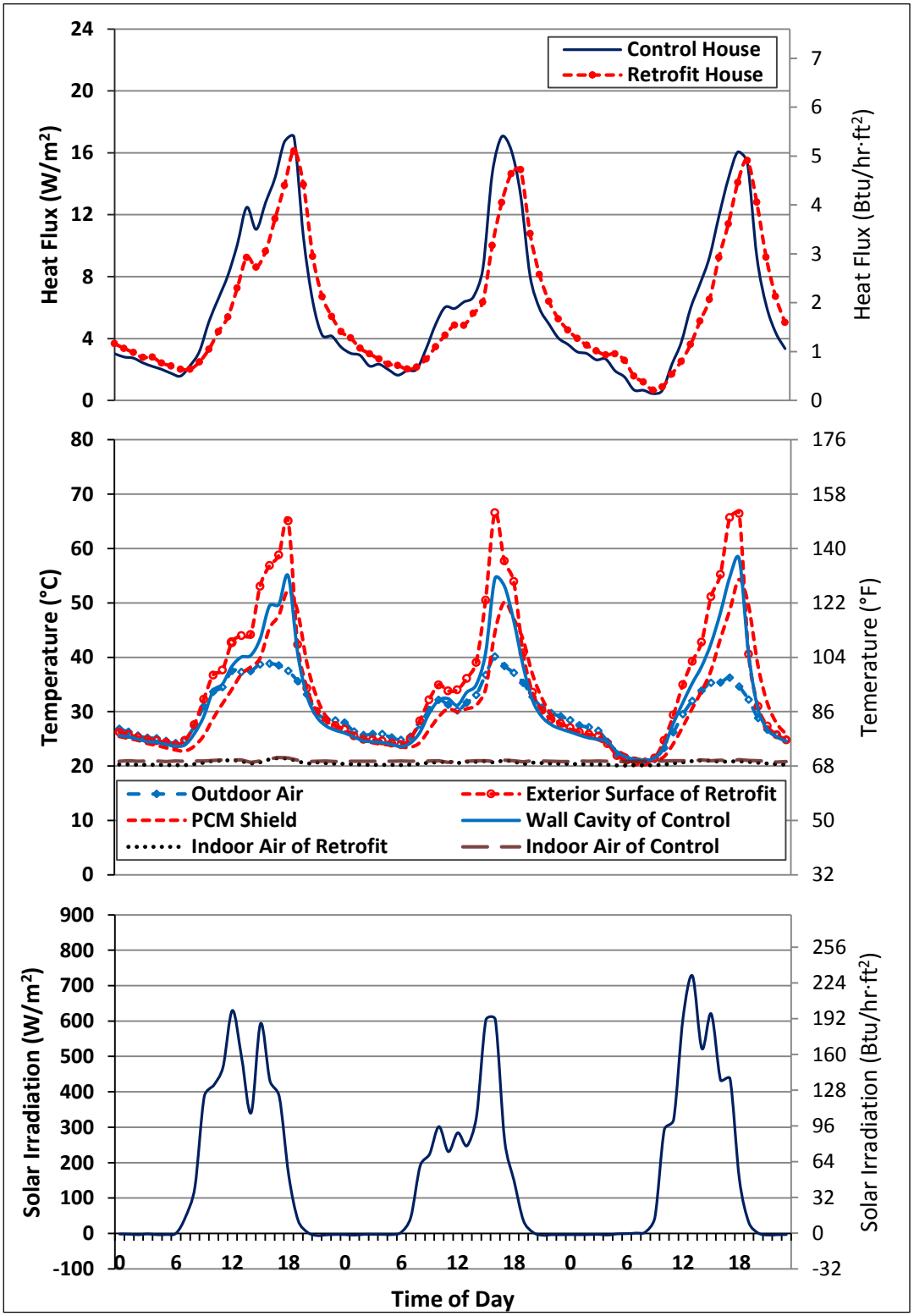

Figure 5.1.26. Wall Heat Fluxes (Top), Temperatures (Middle), and Solar Irradiation (Bottom) for the Case of a PCM Shield Installed at Location 5 in the West Wall

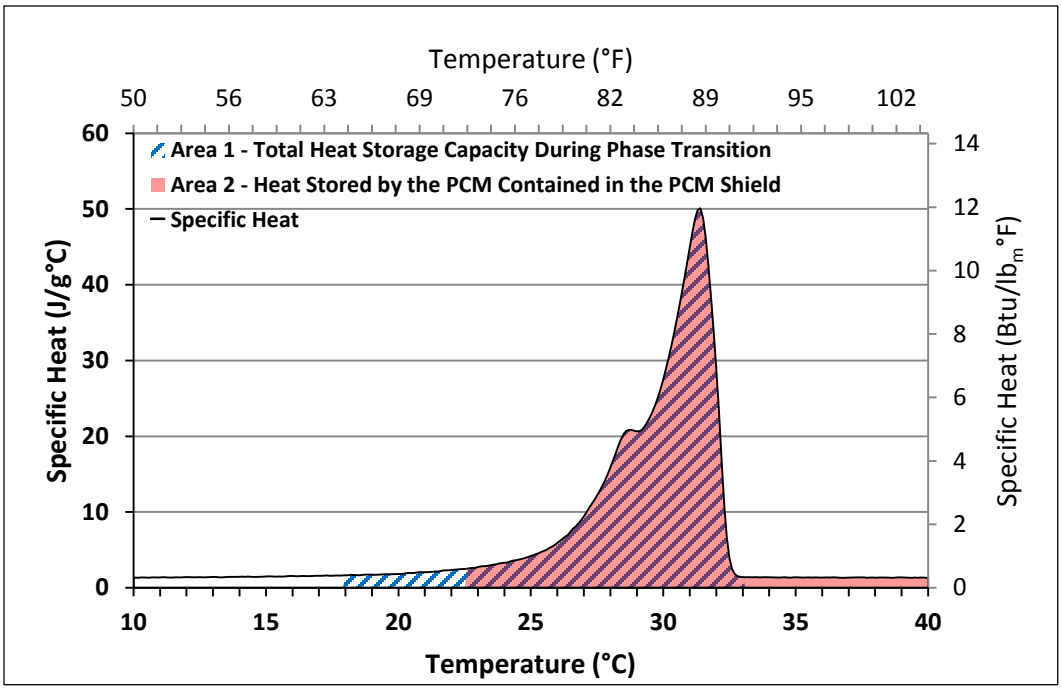

Figure 5.1.27. Total Heat Storage Capacity of the PCM During Phase Transition and Actual Heat Stored by the PCM Contained in the PCM shield at Location 5 in the West Wall

Table 5.1.3 summarizes the average peak heat flux reductions and the average heat flux time lags when using the PCM shield in the west wall.

Table 5.1.3. Peak Heat Flux Reductions Across the West Wall and Peak Heat Flux Time Lags Produced by the PCM Shield

PCM Shield Location	Peak Heat Flux Reduction (%)	Average Peak Heat Flux Time Lag (hrs)
1	26.1	2
2	37.3	2.3
3	36.3	1
4	2.5	0.7
5	14.2	1
Average	23.3	1.4

5.1.2.3 Heat Fluxes Across the Ceiling

The number order of the locations of the PCM shield was the same as the order for the south and west walls. It also started from the interior side and proceeded to the exterior side of the ceiling. In other words, it started from the bottom to the top as shown in Figure 5.1.28. However, the PCM shield was only tested for locations 2, 3, and 4 for the ceiling. Average temperatures of the PCM shield at each location were measured using 12 T/Cs connected in parallel. These temperatures were used for the detailed explanations of the observations as previous test cases.

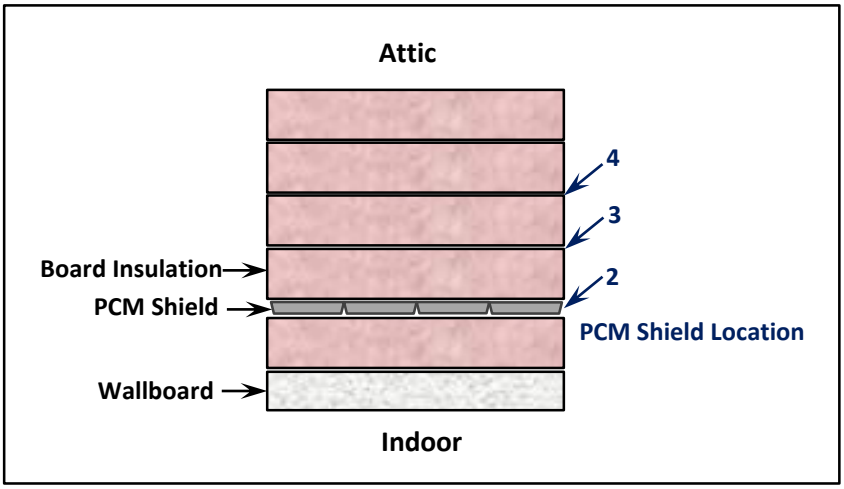

Figure 5.1.28. Schematic of Ceiling Section Showing the Locations of the PCM Shield

The average reductions in peak heat fluxes when using the PCM shield in the ceiling were 0, 25.0, and 41.1%, for locations 2, 3, and 4, respectively. The average time lags of the peak heat fluxes were 0, 1, and 2 hours, for locations 2, 3, and 4, respectively. The average peak heat flux reduction and the average peak time lags were maximum when the PCM shield was installed at location 4. Explanations for

these observations were put forth in the following sections using Figures 5.1.29, 5.1.30, and 5.1.32. These figures represent heat fluxes, relevant temperatures, and solar data.

Location 2

In Figure 5.1.29, the heat fluxes of the retrofit ceiling were larger than those of the control case. This is because the indoor air temperature of the retrofit house was about 1.00 °C (1.8 °F) lower than the control house. From the temperature graphs in Figure 5.1.29, the temperature of the PCM shield only reached 21.60 °C (70.9 °F) while the start of melting temperature of the PCM was 31.36 °C (88.4 °F). This indicates that the degree of the PCM melting was very low. During a test period for this case, the outdoor air temperatures and the solar irradiation were not as high as in previous days.

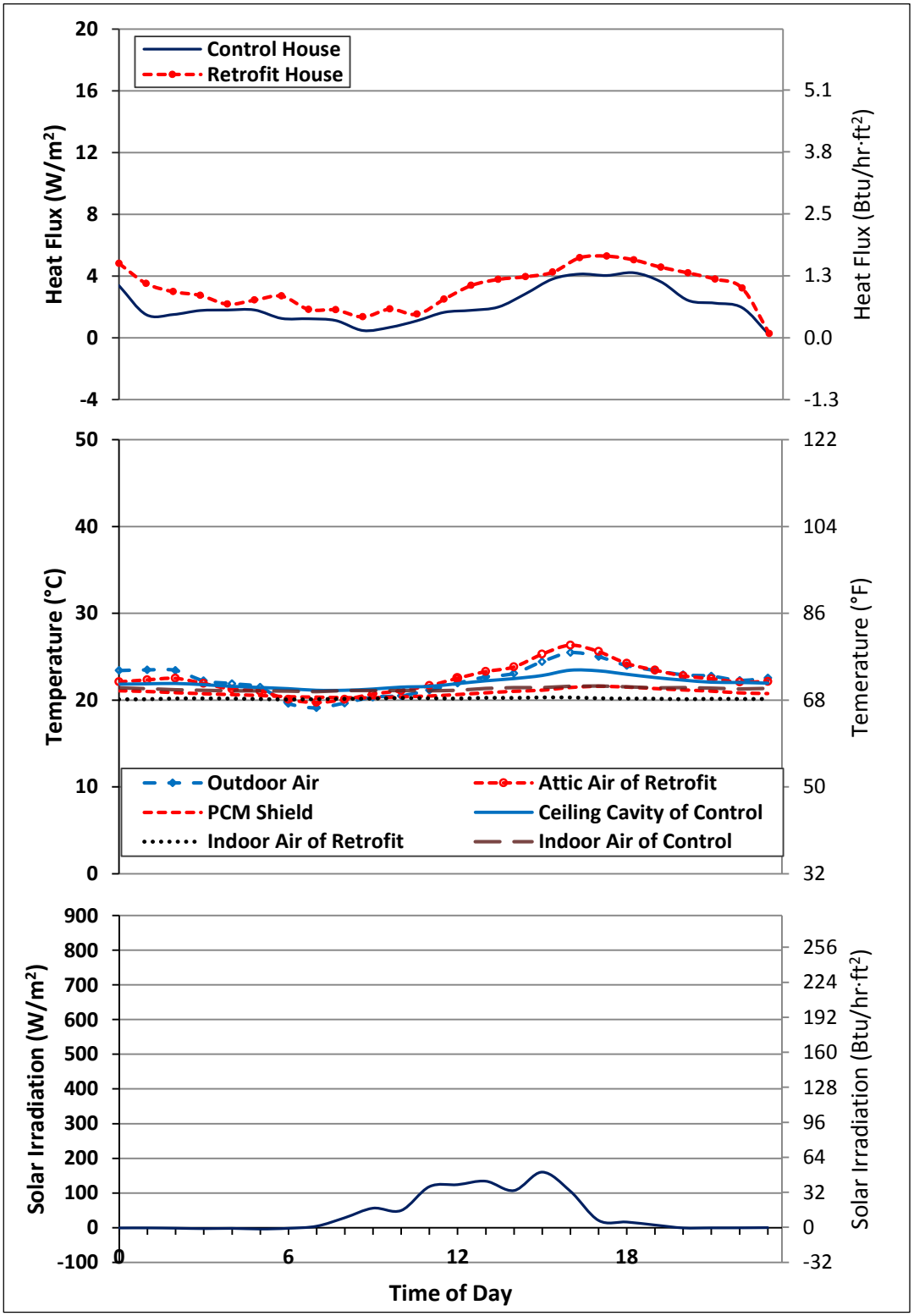

Figure 5.1.29. Ceiling Heat Fluxes (Top), Temperatures (Middle), and Solar Irradiation (Bottom) for the Case of a PCM Shield Installed at Location 2 in the Ceiling

Location 3

For a PCM shield installed at location 3 as shown in Figure 5.1.30, the average heat transfer reduction was 22.7% during the daytime. However, the average heat transfer was increased 6.8% for the retrofit ceiling during the entire day. As was the case for the west wall, the heat fluxes of the retrofit ceiling were higher than those the control case during the nighttime. The temperature of the PCM started to increase at about 2 hours after sunrise. From this time, the PCM was in the melting process. The PCM stopped the melting process at about 4 PM. The temperature range and the duration of the PCM melting process were from 19.84 to 26.08 °C (67.7 to 78.9 °F) and 8 hours, respectively. This temperature range is shown in Figure 5.1.31. For the first day, the heat flux of the control ceiling became negative at about 10 PM while the heat flux of the retrofit was still positive. The heat flux of the retrofit ceiling became negative 4 hours after the control. This indicates that the control ceiling required heating earlier than the retrofit attic when the outdoor air temperature dropped below the indoor air temperature.

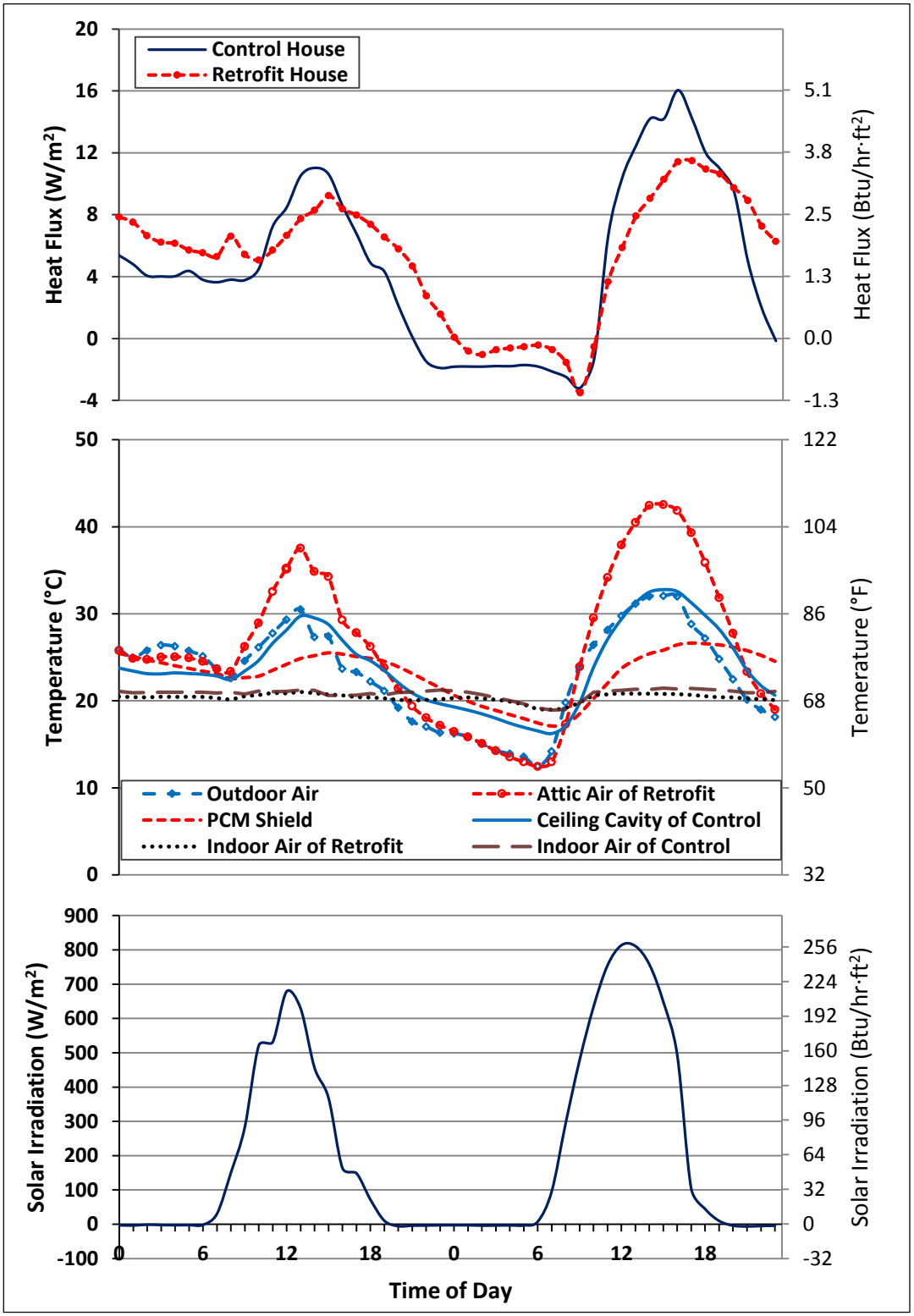

Figure 5.1.30. Ceiling Heat Fluxes (Top), Temperatures (Middle), and Solar Irradiation (Bottom) for the Case of a PCM Shield Installed at Location 3 in the Ceiling

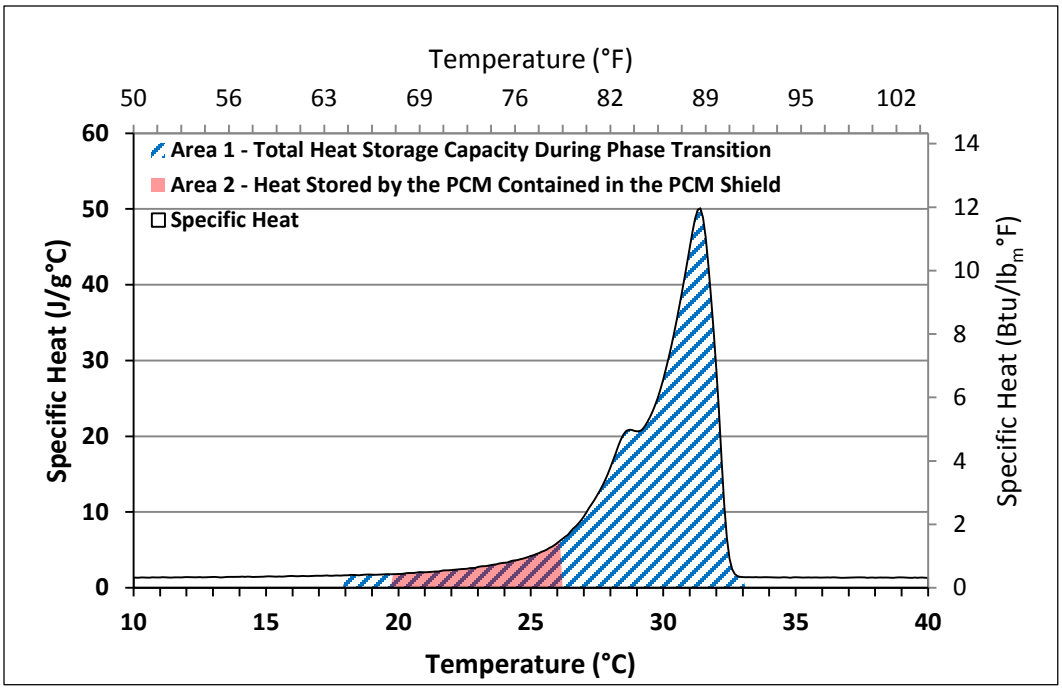

Figure 5.1.31. Total Heat Storage Capacity of the PCM During Phase Transition and Actual Heat Stored by the PCM Contained in the PCM shield at Location 3 in the Ceiling

Location 4

From the heat flux graph in Figure 5.1.32, the average heat transfer reduction was 27.5% during the daytime. However, the average heat transfer during the entire day was increased 6.6%. As in the previous case, the heat fluxes of the retrofit ceiling were higher than those of the control case during the nighttime. The temperature range of the PCM melting process was from 20.32 to 23.59 °C (68.6 to 74.5 °F) as shown in Figure 5.1.33. The duration of the PCM melting was 8 hours. The heat flux of the control ceiling became negative at 9 PM while the heat flux of the retrofit case was still positive as in the previous case.

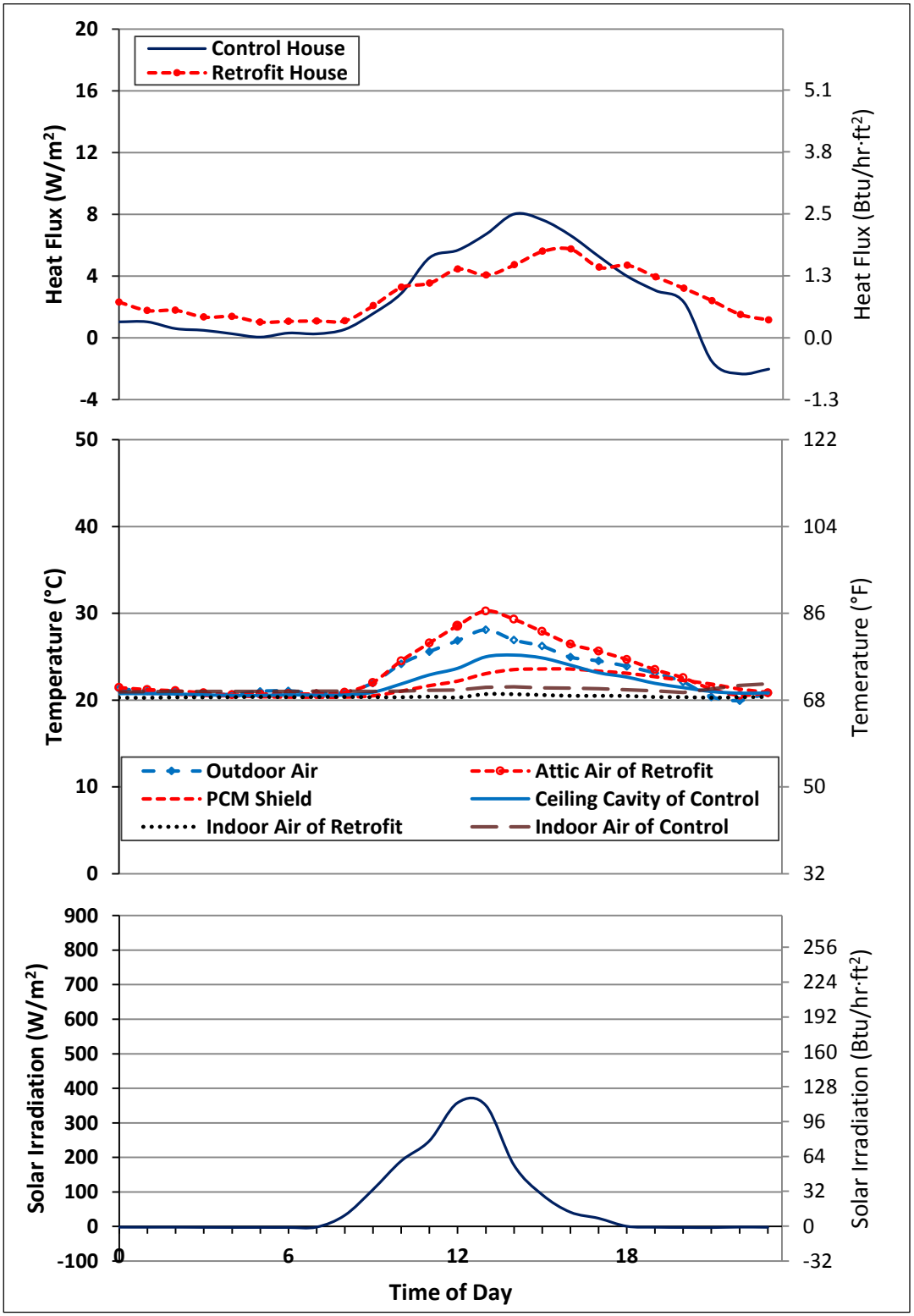

Figure 5.1.32. Ceiling Heat Fluxes (Top), Temperatures (Middle), and Solar Irradiation (Bottom) for the Case of a PCM Shield Installed at Location 4 in the Ceiling

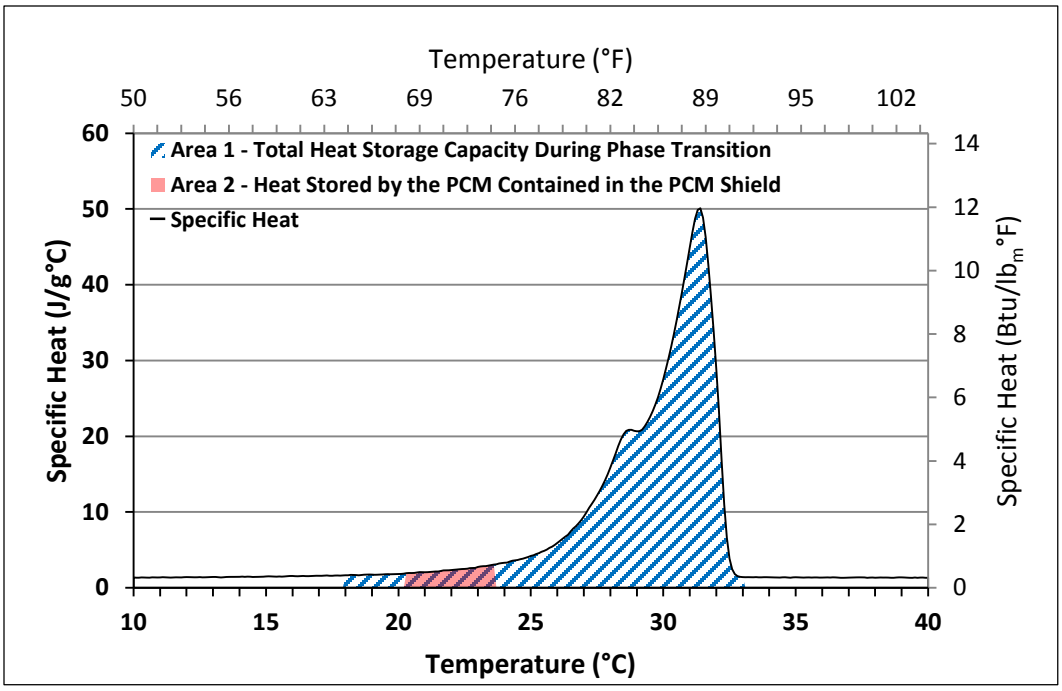

Figure 5.1.33. Total Heat Storage Capacity of the PCM During Phase Transition and Actual Heat Stored by the PCM Contained in the PCM shield at Location 4 in the Ceiling

Table 5.1.4 summarizes the average peak heat flux reductions and the average peak heat flux time lags when using the PCM shield in the ceiling.

Table 5.1.4. Peak Heat Flux Reductions Across the Ceiling and Peak Heat Flux Time Lags Produced by the PCM Shield

PCM Shield Location	Peak Heat Flux Reduction (%)	Average Peak Heat Flux Time Lag (hrs)
2	0	0
3	26.9	1
4	41.1	2
Average	22.7	1

5.2 Thermal Performance of the PCM Boards

5.2.1 Pre-retrofit Thermal Performance Verification of the Wall Panels in M2SEC

Calibration tests were performed to verify that the panels had similar thermal performance before any retrofit. Average exterior and interior surface temperatures and average heat fluxes of the wall panels were measured and compared to verify their thermal similarity. For this case, indoor air temperatures were not compared since all wall panels were under the same indoor conditions.

Ten wall panels in the south wall and 12 wall panels in the west wall were tested. However, only the results from 2 panels in the south wall and 2 panels in the west wall are presented here. The locations of these panels are shown in Figure 5.2.1. One set of panels was used as control panels and another set of panels was used as retrofit panels in both the south and west walls.

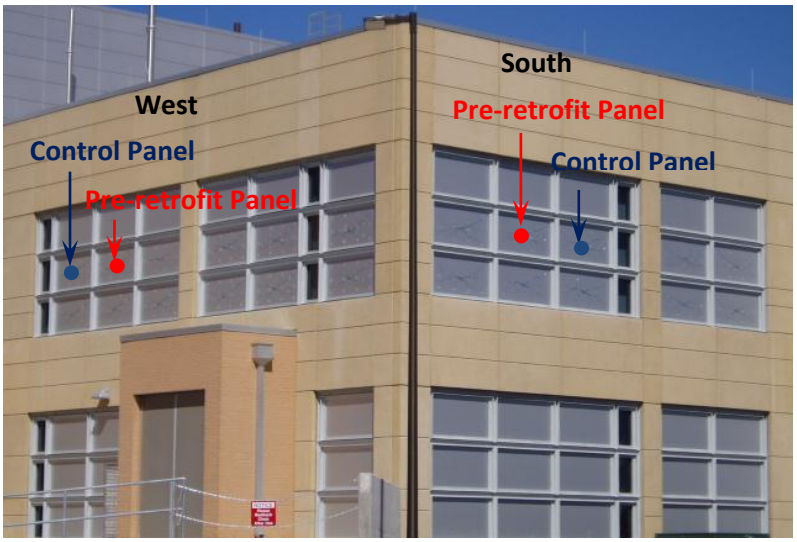

Figure 5.2.1. Southwest View of M2SEC Showing the Locations of Control and Pre-retrofit Wall Panels in the South and West Walls

5.2.1.1 Surface Temperatures

During the calibration period, the exterior surface temperature of the control panel in the south wall was at an average of 20.88 °C (69.6 °F). The exterior surface temperature of the soon-to-be retrofit panel in the same wall was at an average of 20.98 °C (69.8 °F). That is, an average temperature difference of 0.10 °C (0.18 °F) between both exterior surfaces existed. The interior surface temperature of the control panel in the south wall was kept at an average of 21.12 °C (70.0 °F), while the interior surface temperature of the soon-to-be retrofit was kept at an average of 21.20 °C (70.2 °F). That is, an average temperature difference of 0.08 °C (0.14 °F) between both interior surfaces was achieved. The fact that the average interior temperature was slightly higher than the average exterior surface temperature does not mean that the interior was hotter than the exterior. This only means that the amplitude of the temperature swings were smaller in the interior surfaces than in the exterior ones.

Similarly, the exterior surface temperature of the control panel in the west wall was at an average of 21.26 °C (70.3 °F), while the exterior surface temperature of the soon-to-be retrofit panel was at an average of 21.40 °C (70.5 °F), or an average temperature difference of 0.14 °C (0.25 °F) between both exterior surfaces. The interior surface temperature of the control panel in the west wall was kept at an average of 21.53 °C (70.8 °F), while the interior surface temperature of the soon-to-be retrofit panel was kept at an average of 21.71 °C (71.1 °F), or an average temperature difference of 0.18 °C (0.32 °F) between both interior surfaces.

Table 5.2.1 summarizes the temperatures between the wall panels.

Table 5.2.1. Temperature Comparisons Between Control and Soon-to-be Retrofit Wall Panels

		Control (°C (°F))	Soon-to-be Retrofit (°C (°F))	Difference (°C (°F))
South Wall	Average Exterior Surface	20.88 (69.58)	20.98 (69.77)	0.10 (0.18)
	Average Interior Surface	21.12 (70.02)	21.20 (70.16)	0.08 (0.14)
West Wall	Average Exterior Surface	21.26 (70.26)	21.40 (70.52)	0.14 (0.25)
	Average Interior Surface	21.53 (70.76)	21.71 (71.07)	0.18 (0.32)

From Table 5.2.1, it can be inferred that the level of temperature control was very high and further extrapolation would not be necessary based on the fact that the temperature difference of the exterior surfaces of the control panels facing south and west was 0.38 °C (0.68 °F), while the same temperature difference for the soon-to-be retrofit panels was 0.42 °C (0.75 °F). Similarly, the interior surface temperature difference of both the control panels facing south and west was 0.41 °C (0.74 °F), while the same temperature difference for the soon-to-be retrofit panels was 0.51 °C (0.91 °F).

Figures 5.2.2 (a), (b) and 5.2.3 (a), (b) also show the level of similarity between the average exterior and interior surface temperatures of the wall panels in the south and west walls of the M2SEC building were controlled at any time during the experiments.

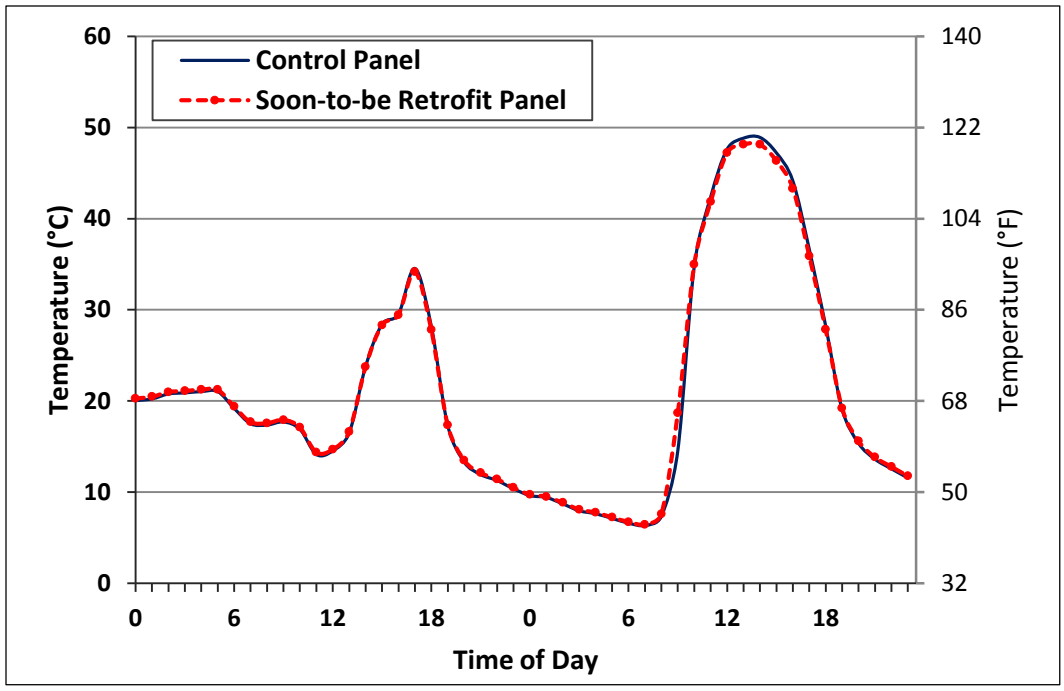

Figure 5.2.2 (a). Exterior Surface Temperatures of the Wall Panels in the South Wall During Pre-retrofit Testing

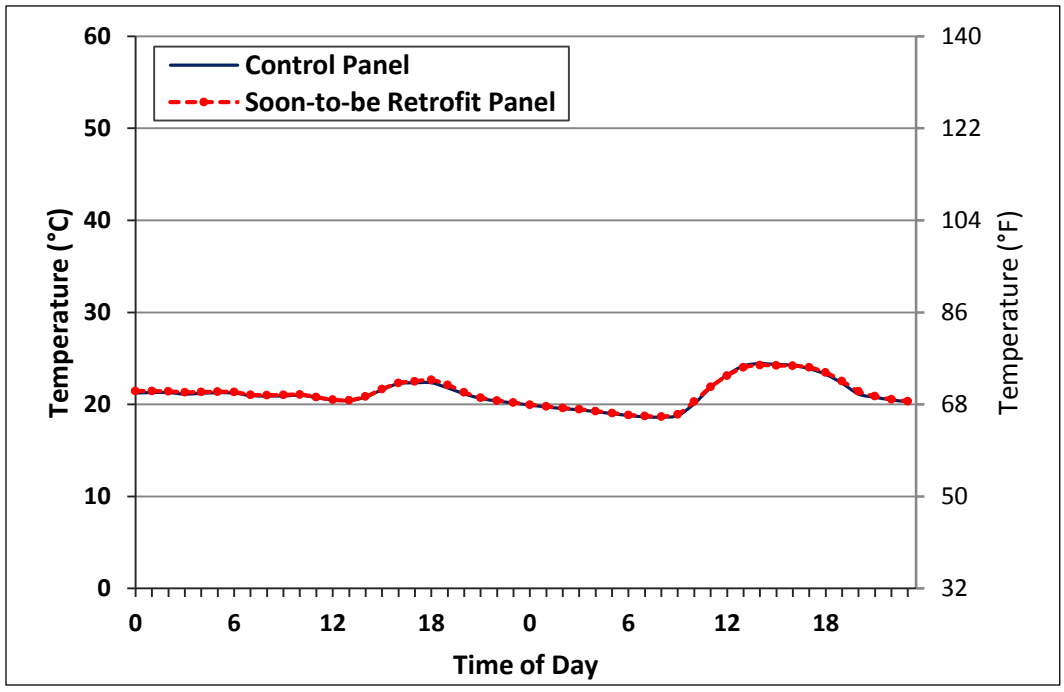

Figure 5.2.2 (b). Interior Surface Temperatures of the Wall Panels in the South Wall During Pre-retrofit Testing

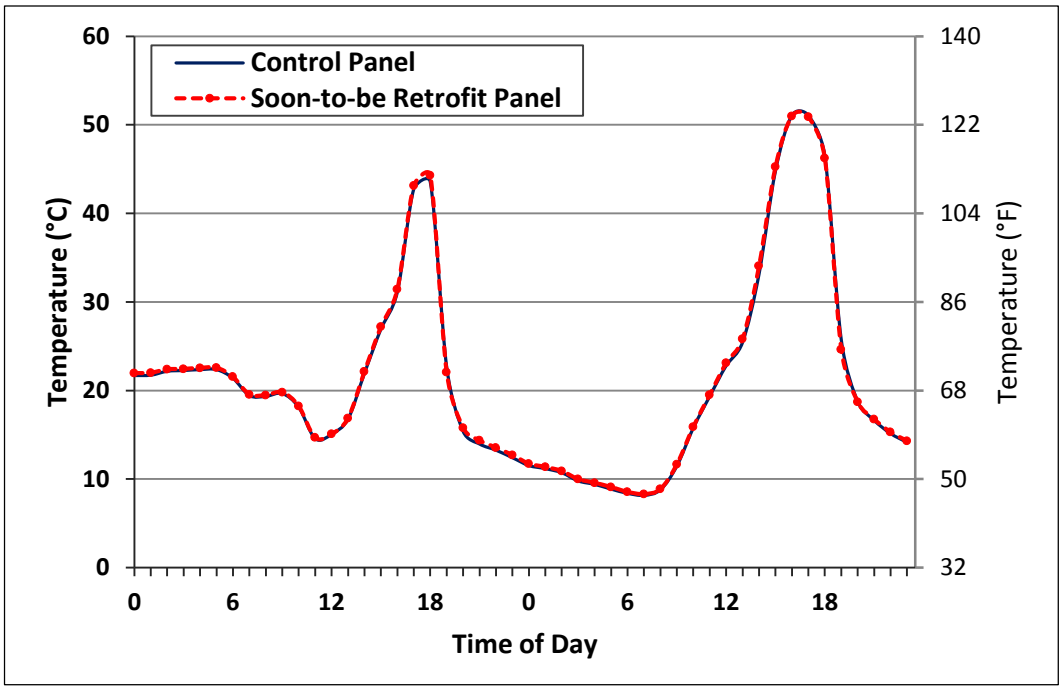

Figure 5.2.3 (a). Exterior Surface Temperatures of the Wall Panels in the West Wall During Pre-retrofit Testing

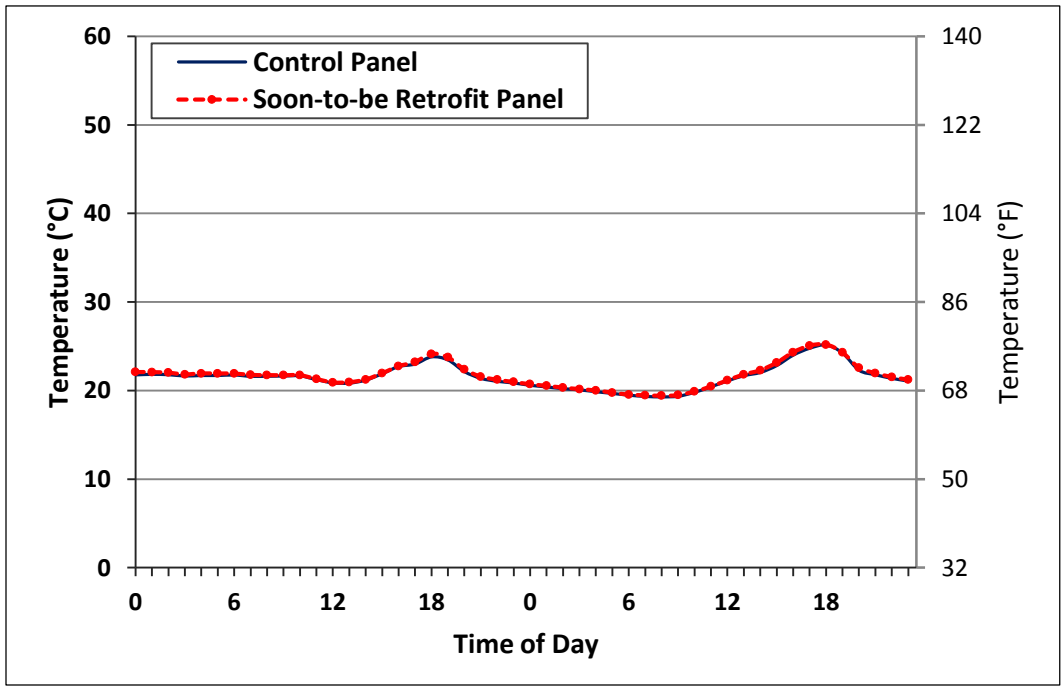

Figure 5.2.3 (b). Interior Surface Temperatures of the Wall Panels in the West Wall During Pre-retrofit Testing

Given that 12 T/Cs were used per surface to produce a single temperature every ten seconds, which were then averaged hourly, plus the level of control (i.e., temperature similarities) achieved in this phase of the research, was indicative of how careful and thorough the experiments were conducted, especially because these wall panels were undergoing transient energy transport.

5.2.1.2 Heat Fluxes

Figures 5.2.4 and 5.2.5 show the heat flux comparisons between the control and soon-to-be retrofit panels in both the south and west walls, respectively. From the trend shown in these figures, it was concluded that the thermal responses of the panels were similar. That is, the average differences in peak heat flux across the two panels in the south wall and the two panels in the west wall were approximately 3.0 and 3.8%, respectively.

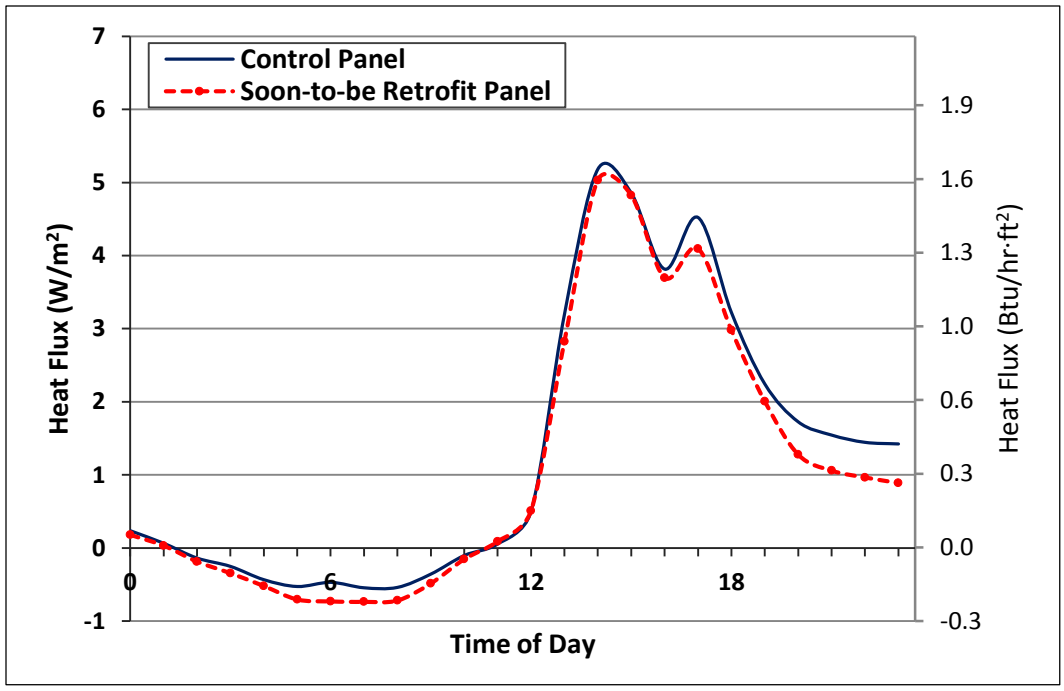

Figure 5.2.4 Heat Fluxes Across the Wall Panels in the South Wall During Pre-retrofit Testing

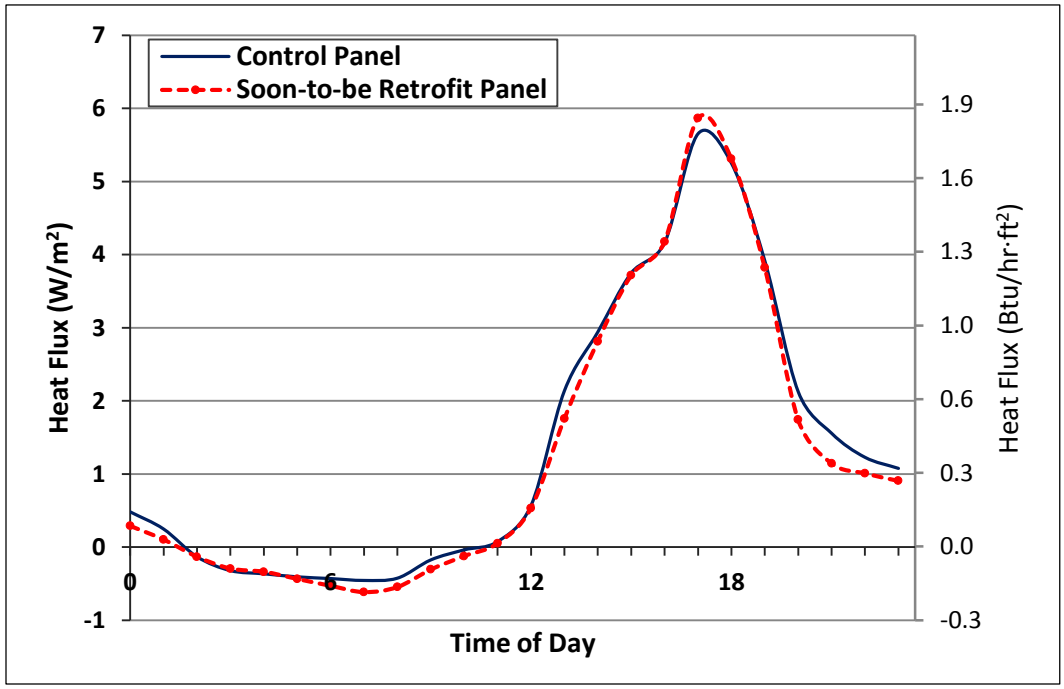

Figure 5.2.5. Heat Fluxes Across the Wall Panels in the West Wall During Pre-retrofit Testing

5.2.2 Retrofit Thermal Performance of the Wall Panels in M2SEC

The performance of PCM boards was evaluated by measuring and analyzing the temperatures and heat fluxes across the wall panels located in the south and west walls.

5.2.2.1 Heat Fluxes Across the Wall Panels in the South Wall

For the retrofit tests, the PCM boards were installed over the interior surfaces of the wall panels (see Figure 4.2.12). Temperatures between the interior surfaces of the panels and the PCM boards were measured using 12 T/Cs connected in parallel. These temperatures were assumed to be the temperatures of the PCM boards and subsequently were used for detailed explanations of the observed phenomena.

Figure 5.2.6 shows the heat flux comparisons between the control and retrofit panels in the south wall. This figure also depicts relevant temperature data. Because in Figures 5.2.2 and 5.2.3 it was shown that exterior surface temperatures of both the control and retrofit panels were almost identical, only the exterior surface temperature of the retrofit panel is shown in Figure 5.2.6.

When the PCM board was installed in this wall, the average daily heat transfer reduction was 27.4%. This value was the average of the differences between the curves of heat fluxes across the control wall panel and heat fluxes across the retrofit wall panel. The average heat flux reduction produced by the retrofit panel when the heat fluxes of the control panel were at their peaks (i.e., A_1, A_2, and A_3 in Figure 5.2.6), was 67.0%. The average peak heat flux reduction produced by the retrofit

panel when comparing the peaks of control and retrofit panels (i.e., the differences between A and C in Figure 5.2.6) was 10.7%. The percent reduction when the heat fluxes of the control panel were at their peaks is presented because this information is of importance to the electricity generation sector. For air conditioning size reductions, the peak to peak reduction should be the one to consider. For energy conservation, the area under the curves of the control and the retrofit heat fluxes (i.e., heat transfer reductions) should be considered.

The average time lag of the peak heat fluxes was three hours. A peak heat flux time lag implies that electricity generation utilities may be able to attend to this new peak without having to run extra electricity generating equipment. This may potentially reduce their operating costs and increase their load factors during the cooling season. A load factor is the ratio of the averaged load over a designated period of time to the peak load occurring during the same period (IEEE, 1990). Electricity generation utilities are required to meet their peak loads at all times. In the summer time, these peaks occur for only several hours in the afternoons and are mainly the result of increased air conditioning usage (Denholm, 2012). By shifting a portion of the peak demand from air conditioning usage to off-peak times, peak loads would be reduced. Thus, utility companies would run their power plants more efficiently and at higher load factors. Also, residents and businesses would save on their electricity bills by consuming some of the electricity for air conditioning during off-peak times rather than on-peak. This cost savings are produced because utility companies usually charge lower rates for electricity usage during off-peak times

(Lowell, 2006). From the temperature graphs of Figure 5.2.6, the PCM inside the PCM board started to melt at around 8 AM when the temperature of the PCM was 16.43 °C (61.6 °F). The PCM finished its melting process at around 4 PM when its temperature was 22.86 °C (73.1 °F). In other words, the duration of the PCM melting process was 8 hours.

In Figure 5.2.6, the top portion represents the instantaneous heat fluxes across both the control and retrofit panels. The area under these curves represents the total heat transferred over the testing periods. Generally, the parts of this graph when the retrofit panel heat fluxes were below the control panel heat fluxes mean that the PCM was melting. On the other hand, when these heat fluxes were reversed, it means that the PCM was solidifying. Furthermore, the amplitude of heat fluxes (i.e., the difference between peaks and valleys) across the retrofit panel was smaller than the amplitude of the heat fluxes across the control panel. This is relevant because a controlled and an attenuated amplitude may result in a more constant wall temperatures and longer equipment operating life.

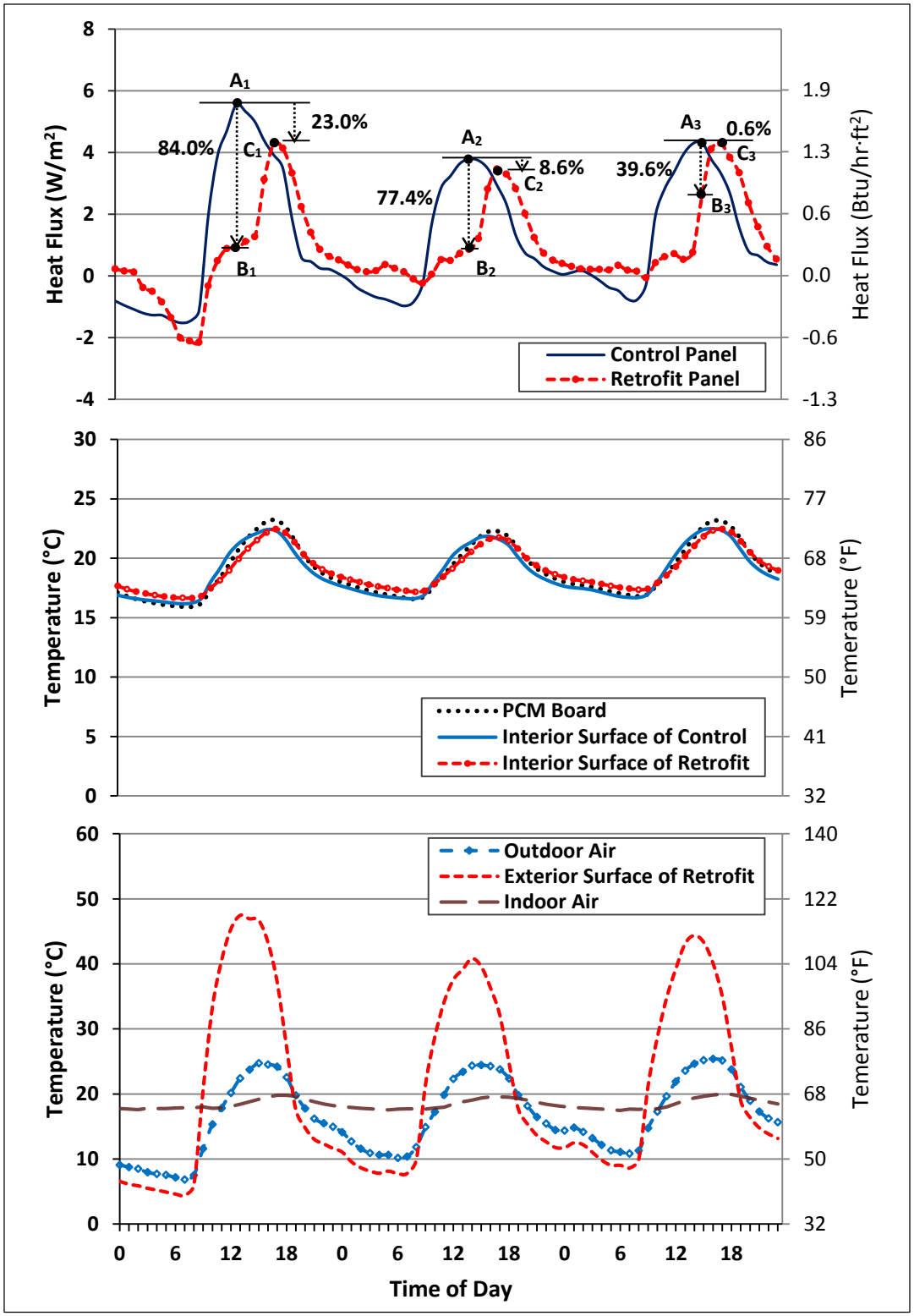

Figure 5.2.6. Wall Heat Fluxes (Top) and Temperatures (Middle and Bottom) for the PCM Board Installed in the South Wall

Table 5.2.2 shows comparisons of interior surface temperatures of the control and the retrofit wall panels in the south wall. The maximum interior surface temperatures of both the control and the retrofit panels were almost the same, while the minimum interior surface temperature of the retrofit panel was -0.57 °C (-1.03 °F) greater than the minimum interior surface temperature of the control panel. As the results show, the amplitude of the interior surface temperature swings of the retrofit panel was 0.58 °C (1.04 °F).

Table 5.2.2. Interior Surface Temperatures Comparisons of the South Wall Panels

	Control (°C (°F))	**Retrofit (°C (°F))**	**Difference (Control-Retrofit) (°C (°F))**
Average	18.83 (65.89)	19.07 (66.33)	-0.24 (-0.44)
Maximum	22.24 (72.03)	22.22 (72.00)	0.02 (0.03)
Minimum	16.50 (61.70)	17.07 (62.73)	-0.57 (-1.03)
Amplitude (Max. – Min.)	5.74 (10.33)	5.16 (9.29)	0.58 (1.04)

A more constant wall temperature translates to occupants' comfort (Stein, 1996). This happens because human comfort is related to wall temperature (Bauer et al., 2009). In other words, a wall with a significantly-varying surface temperature affects the mean radiant temperature (MRT), which is a measure of comfort (ASHRAE, 2010). Furthermore, a longer 'on' time by the air conditioners, helps in removing indoor air humidity, which is also a parameter that affects human comfort.

In addition, equipment's operating lifetime increases because the 'on-off' cycling is reduced. That is, comfort equipment runs longer, but stays off longer as well. This reduces mechanical fatigue, which is cited as one of the causes for equipment failure (Callister and Rethwisch, 2009).

5.2.2.2 Heat Fluxes Across the Wall Panels in the West Wall

Figure 5.2.7 shows the heat flux comparisons for the west wall panels between the control and retrofit cases. For a PCM board installed in the west wall, the daily average heat transfer reduction was 10.5%. The average heat flux reduction of the retrofit panel when the heat fluxes of the control panel were at their peaks was 80.2%. The average peak heat flux reduction of the retrofit panel when comparing the peaks was 8.5%. The average time lag of the peak heat fluxes was two hours. These results also imply the same effects on energy management as explained in the previous section.

The PCM started to melt at around 9 AM which was one hour later than the melting start time of the PCM installed in the south wall panel. The temperature of the PCM was 17.01 °C (62.6 °F) which was about 0.58 °C (1.0 °F) higher than the temperature of the PCM in the south wall panel. The PCM finished its melting process at around 6 PM, which was two hours later than the melting finish time of the PCM in the south wall panel. The temperature of the PCM was of 23.56 °C (74.4 °F) which was about 0.70 °C (1.3 °F) higher than the temperature of the PCM in the south wall panel. The duration of the PCM melting process was 9 hours.

The minimum temperature of the PCM placed in the west wall panel was slightly higher than the PCM temperature in the south wall panel, while the maximum temperature of the PCM in the west wall panel was slightly lower than the PCM temperature in the south wall panel. For further explanation of the case of the PCM board placed in the west wall panel, the temperature range of the PCM melting process was smaller, while the duration of the PCM melting process was shorter than the case of the PCM board in the south wall panel. This indicates that the PCM installed in the west wall panel was heated up slower than the PCM installed in the south wall panel.

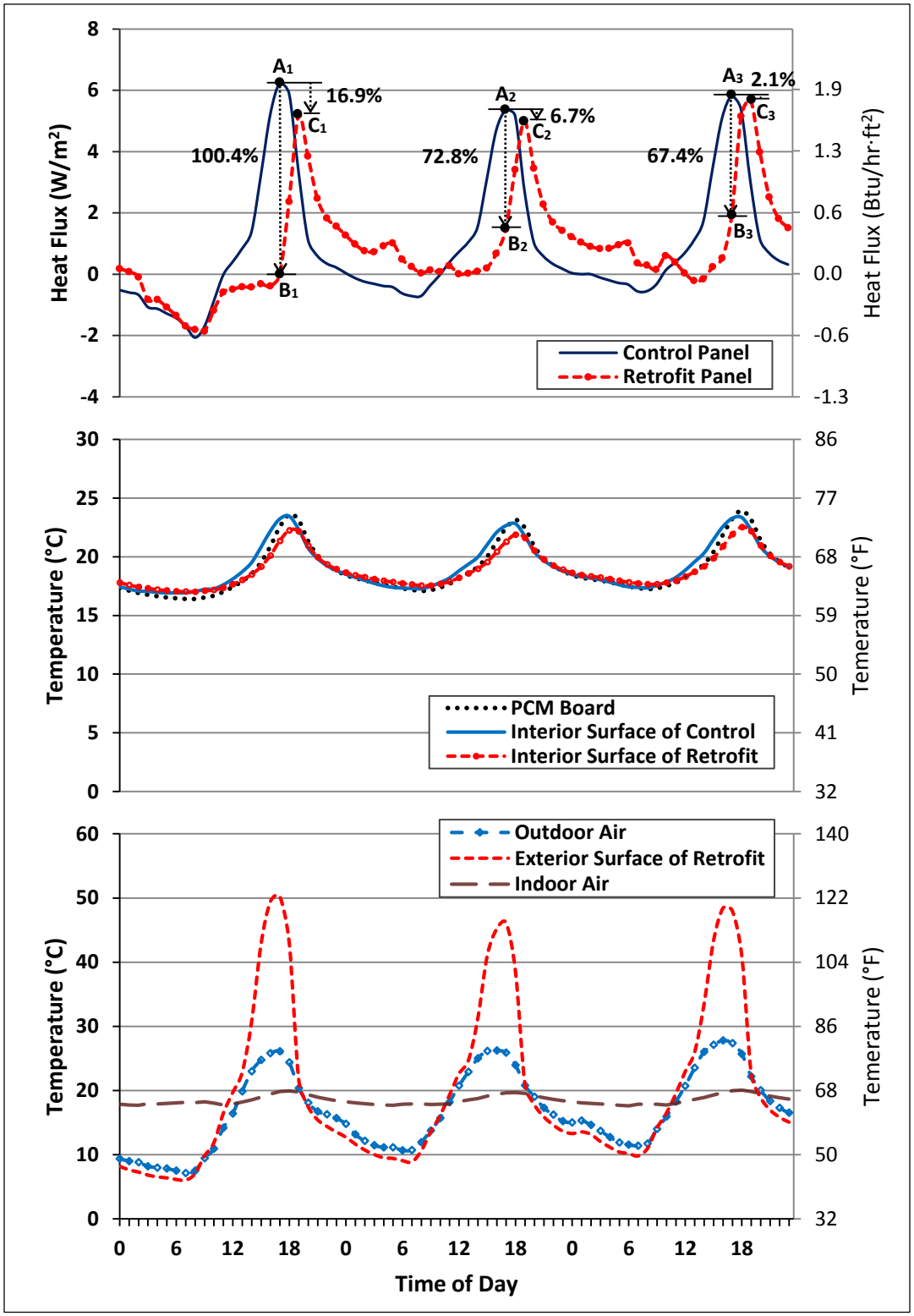

Figure 5.2.7. Wall Heat Fluxes (Top) and Temperatures (Middle and Bottom) for the PCM Board Installed in the West Wall

Table 5.2.3 summarizes the heat flux reductions between the cases when the PCM boards were installed in the south and west wall panels.

Table 5.2.3. Heat Flux Reduction Comparisons Between the South and West Wall Panels Produced by the PCM Board

	South	West
Daily Heat Transfer Reduction (%)	27.4	10.5
Peak Heat Flux Reduction When the Control at Peak (%)	67	80.2
Peak to Peak Heat Flux Reduction (%)	10.7	8.5

CHAPTER VI

DIFFERENTIAL SCANNING CALORIMETER (DSC) ANALYSIS

The in-house differential scanning calorimeter (DSC) experiments were conducted to obtain additional PCM properties. These included specific heats, latent and total heat storage capacities, latent heat of fusions, enthalpies, melting temperatures, and onset of melting temperatures. This information was used to analyze the experimental data in which PCMs were involved and to select the most appropriate input PCM data for the modeling and simulations.

6.1 Differential Scanning Calorimeter (DSC)

A DSC is an instrument used to measure thermal properties of substances associated with their phase transition. These properties include, but are not limited to, melting and solidification points, latent and total heat storage capacities, specific heats, enthalpies, phase transition temperature ranges, including onset of melting and solidification temperatures, and percent crystallinity.

The DSC apparatus used in this research was classified as heat flux DSC, which means that the sample material (PCM) was enclosed in a metallic hermetic pan, which was heated at a linear heating rate during which the heat flows and temperatures were measured. By default, these heat flows and temperatures were compared against previous heat flows and temperatures that were measured using an

empty pan during the initial calibration of the instrument. A sample of a DSC curve provided by the instrument is shown in Figure 6.1.1.

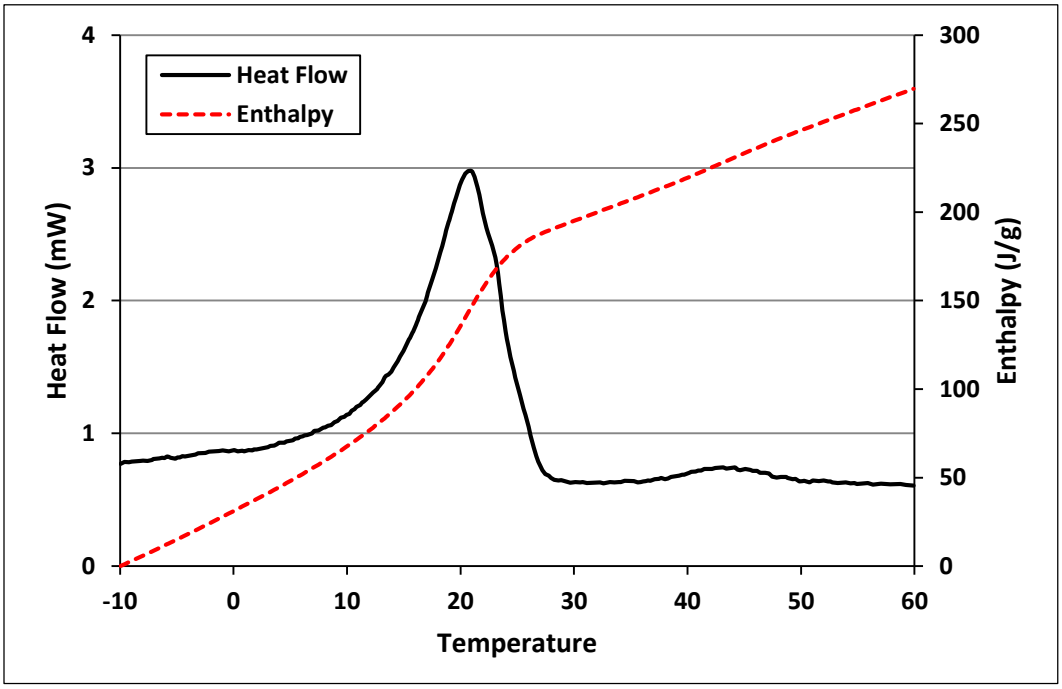

Figure 6.1.1. Sample of a DSC Curve

In Figure 6.1.1, the solid line represents the heat flow in mW as a function of temperature. Each point in the dashed line represents the specific enthalpy of the substance at the corresponding temperature. Both curves were subsequently used to determine the phase transition temperature ranges, the melting temperatures, the onset of melting temperatures, the latent and total heat storage capacities, the specific heats, and enthalpies of the substances.

For the DSC tests, a TA Instrument Model 2920 DSC (see Figure 4.1.10), connected to a dry nitrogen gas cooling system was used. Aluminum hermetic pans

were used to hold the samples during testing. Two samples of the PCM contained in the PCM shield and two samples of the PCM composite contained in the PCM board were tested. All of these were tested at three different heating rates: 0.5, 1.0, and 2.0 °C/min (0.9, 1.8, and 3.6 °F/min). Before each test, the apparatus was calibrated using empty pans. The nitrogen gas was supplied at a rate of 50 ml/min (1.69 fl oz/min) for the all tests.

6.2 Thermal Properties of the PCMs

6.2.1 PCM Contained in the PCM Shield

Two samples of the PCM contained in the PCM shield were tested under various testing conditions. Samples of different masses were prepared, where one sample (Sample A) had a smaller mass and the other sample (Sample B) had a larger mass. The masses of Samples A and B were 13.6 and 24.8 mg (4.8×10^{-4} and 8.7×10^{-4} oz), respectively. Both samples were tested at heating rates of 0.5, 1.0, and 2.0 °C/min (0.9, 1.8, and 3.6 °F/min).

Graphs (a), (b), and (c) of Figure 6.2.1 show the specific heat curves of Sample A, at heating rates of 0.5, 1.0, and 2.0 °C/min (0.9, 1.8, and 3.6 °F/min), respectively. The graphs of Figure 6.2.1 were produced based on DSC data similar to the one presented in Figure 6.1.1 with the modifications that the values of the ordinate axes were normalized based on sample mass and heating rate, which produced the values of specific heats.

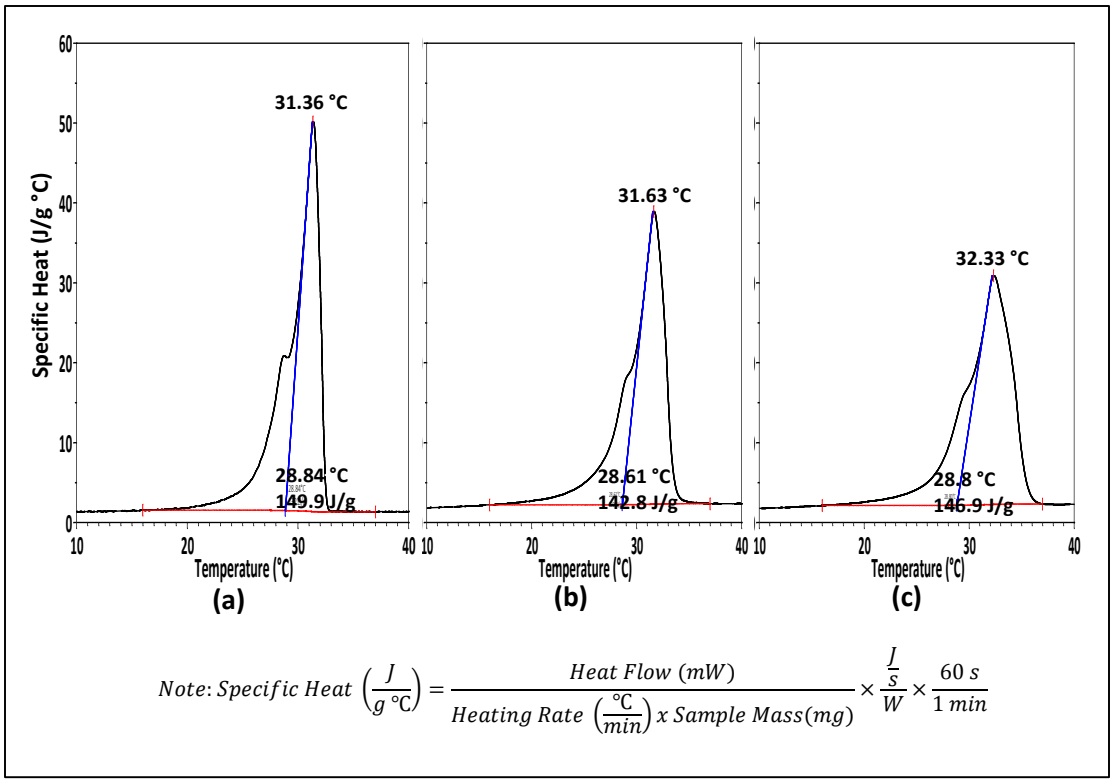

Figure 6.2.1. Specific Heat Curves of Sample A at Various Heating Rates (a) 0.5 °C/min, (b) 1 °C/min, and (c) 2 °C/min

When conducting DSC experiments, the user selects an appropriate phase transition temperature range based on heat flow scans produced by the DSC. Consequently, upon selection of these ranges, required data are produced by the DSC equipment accompanying software. For example, in graphs (a), (b), and (c) of Figure 6.2.1, the phase transition temperature range of 16.0 to 37.0 °C (60.8 to 98.6 °F) was selected. This selection was based on the fact that at 16.0 °C (60.8 °F) the heat flow curve started to separate from a constant heat flow line. The 37.0 °C (98.6 °F) endpoint was selected based on the fact that at this point the heat flow curve joined a second constant heat flow line. The difference in values between these two constant

heat flow lines can be explained by the fact that up to the 16.0 °C (60.8 °F) the PCM was completely solid and from 37.0 °C (98.6 °F) onward it was completely liquid.

Based on these selections, the melting temperatures of 31.36, 31.63, and 32.33 °C (88.4, 88.9, and 90.2 °F) were produced for the heating rates of 0.5, 1.0, and 2.0 °C/min (0.9, 1.8, and 3.6 °F/min), respectively. In addition, the onsets of melting temperatures were 28.84, 28.61, and 28.80 °C (83.9, 83.5, and 83.8 °F) for the same heating rates, respectively. By convention, the determination of these last temperatures is made by drawing a tangent line along the melting curve from its peak, which in the field is referred to as melting temperature, to an intermediate line that joins the heat flow lines during phase transition from solid to liquid.

Furthermore, upon selection of these end points, the 16.0 and 37.0 °C (60.8 and 98.6 °F), the accompanying software carries out an integration of the area of the phase transition curve and produces the latent heat storage capacities, which in this research were 149.9, 142.8, and 146.9 J/g (64.4, 61.4, and 63.2 Btu/lb_m) for the same heating rates, respectively. The total heat storage capacity is obtained by adding the sensible heat portion of the curve to the latent heat. The sensible heat portion is the area under the intermediate line that joins the constant the heat flow lines during phase transition from solid to liquid. For the graphs of Figure 6.2.1 (a), (b), and (c) the total heat storage capacities were 181.4, 189.4, and 192.4 J/g (80.0, 81.3, and 82.7 Btu/lb_m) for the three heating rates, respectively.

Although all the temperatures were relatively close, they were still different. Furthermore, compared to the temperatures the heat storage capacities were

significantly different. The reason for this is that there are inherent flaws related to the apparatus. For example, the apparatus does not measure the temperature of the substance directly but rather it measures the temperature of the bottom of the metallic pan. Consequently, at varying heating rates these temperatures would tend to differ. For the same reason, if a sample with larger mass were used, these temperatures would also tend to be different as will be shown in the following section. At this point, it was imperative to select the appropriate data for the modeling and simulations.

Graphs (a), (b), and (c) of Figure 6.2.2 show similar data to the one of Figure 6.2.1 but for a larger mass, Sample B.

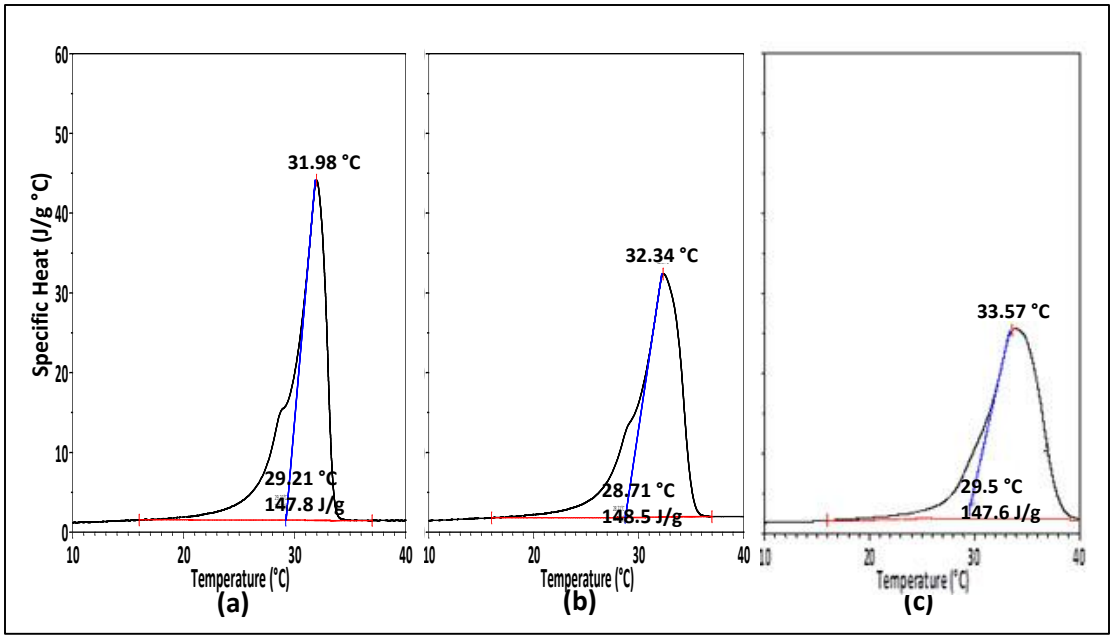

Figure 6.2.2. Specific Heat Curves of Sample B at Various Heating Rates (a) 0.5 °C/min, (b) 1 °C/min, and (c) 2 °C/min

The explanation of Figure 6.2.2 is similar to that of Figure 6.2.1. Based on these results, Table 6.2.1 was constructed to summarize the results.

Table 6.2.1. DSC Test Results Comparisons of the PCM Contained in the PCM Shield

		0.5 °C/min (0.9 °F/min)	**1.0 °C/min (1.8 °F/min)**	**2.0 °C/min (3.6 °F/min)**
Sample A (13.6 mg (4.8×10^{-4} oz))	Melting Temperature (°C (°F))	31.36 (88.4)	31.63 (88.9)	32.33 (90.2)
	Onset of Melting Temperature (°C (°F))	28.84 (83.9)	28.61 (83.5)	28.80 (83.8)
	Latent Heat Storage Capacity (J/g (Btu/lb_m))	149.9 (64.4)	142.8 (61.4)	146.9 (63.2)
	Total Heat Storage Capacity (J/g (Btu/ lb_m))	181.4 (80.0)	189.1 (81.3)	192.4 (82.7)
Sample B (24.8 mg (8.7×10^{-4} oz))	Melting Temperature (°C (°F))	31.98 (89.6)	32.34 (90.2)	33.57 (92.4)
	Onset of Melting Temperature (°C (°F))	29.21 (84.6)	28.71 (90.2)	29.5 (92.4)
	Latent Heat Storage Capacity (J/g (Btu/ lb_m))	147.8 (63.5)	148.5 (63.8)	147.6 (63.5)
	Total Heat Storage Capacity (J/g (Btu/ lb_m))	179.7 (77.3)	186.8 (80.3)	184.0 (79.1)

At this point the question was which data were the most adequate for input into the modeling and simulation program. This question was answered by analyzing

the values of Table 6.2.1. Based on these values it was observed that in general, the melting temperatures had the tendency to increase with higher heating rates as well as with larger sample mass size. The reason for this was explained above, and which inherent flaws are present in the apparatus, in which at higher heating rates and larger masses the instrument is slower to respond (Poel and Mathot, 2006). This generalization was not made based on the data alone, since the observed phenomena did not occur for all values, but together with results presented in the literature (Braga et al., 2011).

Based on this information, it was concluded that those values related to the heating rate of 0.5 °C/min (0.9 °F/min) as well as those produced by Sample A would be used as inputs for the modeling and simulation program. This decision was made because it was most likely that once the PCM was integrated into the PCM shields and into the wall, it would undergo a heating rate closer to 0.5 °C/min (0.9 °F/min). Furthermore, the values obtained from using Sample A were selected because at lower masses, especially in the case of a substance (PCM) with a relatively low thermal conductivity, the thermal inertia effects were less, which would yield a faster apparatus response.

Upon the selection of DSC test result of Sample A at the heating rate of 0.5 °C/min (0.9 °F/min), the graph in Figure 6.2.3, which is the enthalpy as a function of temperature was produced based on the DSC test data. The values of this curve were used as the input data for the simulations of the wall and ceiling containing the PCM shields.

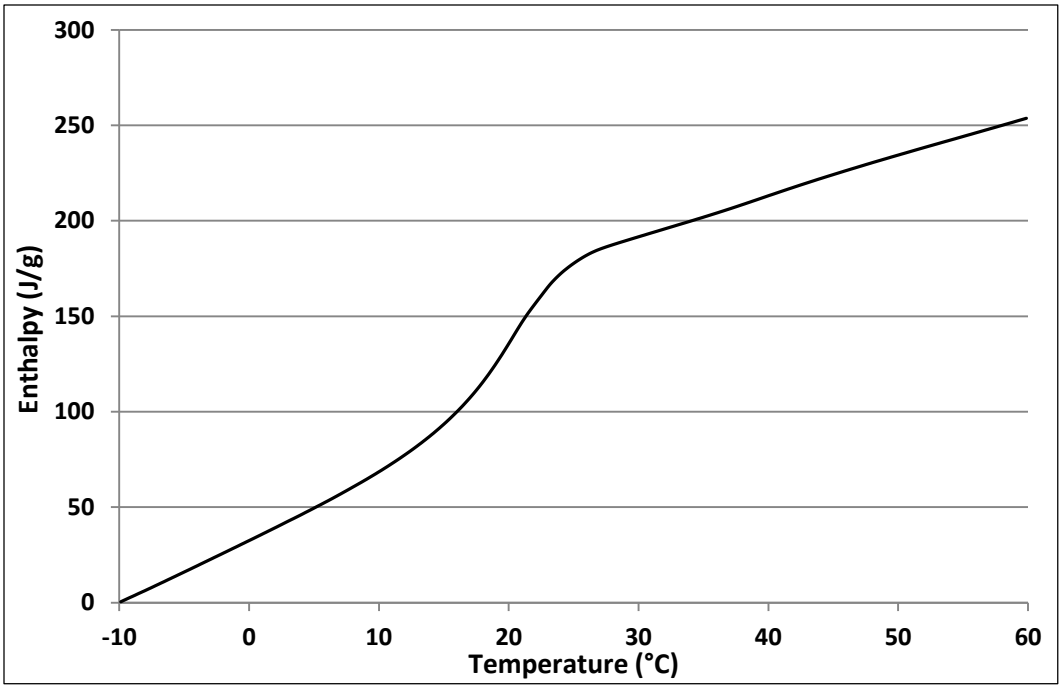

Figure 6.2.3. Enthalpy Curve of Sample A at Heating Rate of 0.5 °C/min As a Function of Temperature

6.2.2 PCM Composite Contained in the PCM Board

Two samples of the PCM composite contained in the PCM board were tested under various testing conditions. Samples of different masses were prepared, where one sample (Sample C) had a smaller mass and the other sample (Sample D) had a larger mass. The masses of Samples C and D were 8.5 and 15.8 mg (3.0×10^{-4} and 5.6×10^{-4} oz), respectively. Both samples were tested at heating rates of 0.5, 1.0, and 2.0 °C/min (0.9, 1.8, and 3.6 °F/min).

Graphs (a), (b), and (c) of Figure 6.2.4 show the specific heat curves of Sample C, at heating rates of 0.5, 1.0, and 2.0 °C/min (0.9, 1.8, and 3.6 °F/min), respectively. These graphs were also produced by the same methods as explained in the previous section. For the graphs in Figure 6.2.4 (a), (b), and (c), the phase

transition temperature range of 0 to 30.0 °C (32.0 to 86.0 °F) was selected. Based on these selections, the melting temperatures of 20.6, 20.99, and 21.34 °C (69.1, 69.8, and 70.4 °F) were produced for the heating rates of 0.5, 1.0, and 2.0 °C/min (0.9, 1.8, and 3.6 °F/min), respectively. In addition, the onsets of melting temperatures were 13.38, 13.63, and 13.62 °C (56.1, 56.5, and 56.5 °F) for the same heating rates, respectively. The latent heat storage capacities were 73.39, 74.43, and 72.45 J/g (31.6, 32.0, and 31.2 Btu/lb_m) for the same heating rates, respectively. The total heat storage capacities were 158.29, 190.54, and 146.20 J/g (68.0, 81.9, and 62.9 Btu/lb_m) for the three heating rates, respectively.

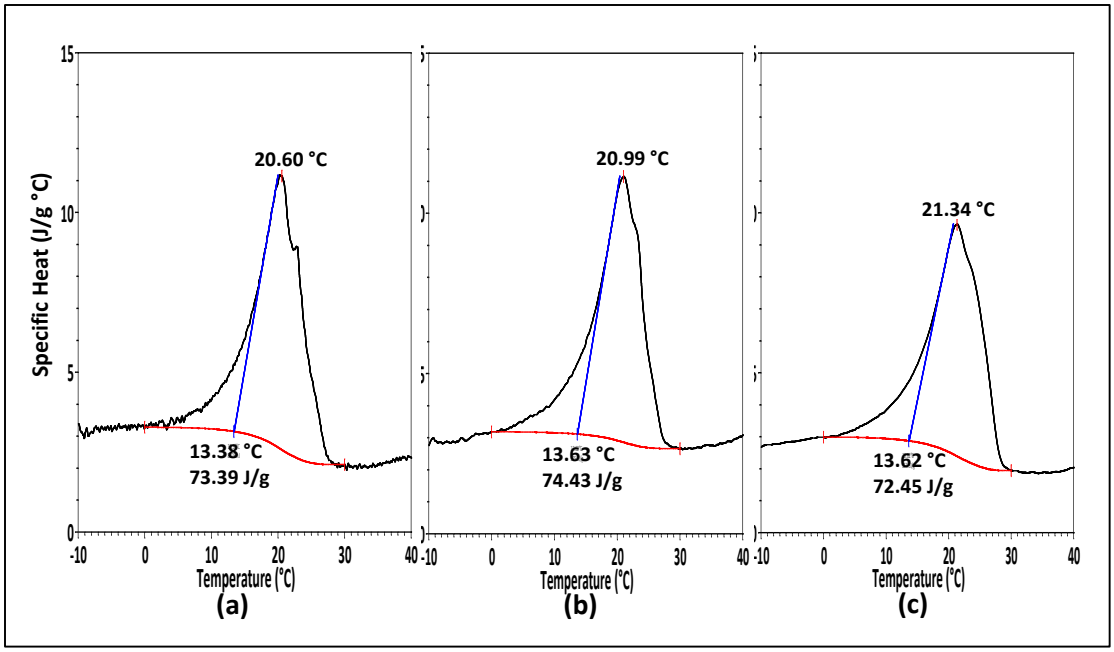

Figure 6.2.4. Specific Heat Curves of Sample C at Various Heating Rates (a) 0.5 °C/min, (b) 1 °C/min, and (c) 2 °C/min

Graphs (a), (b), and (c) of Figure 6.2.5 show the specific heat curves of Sample D, at the same heating rates of 0.5, 1.0, and 2.0 °C/min (0.9, 1.8, and 3.6 °F/min).

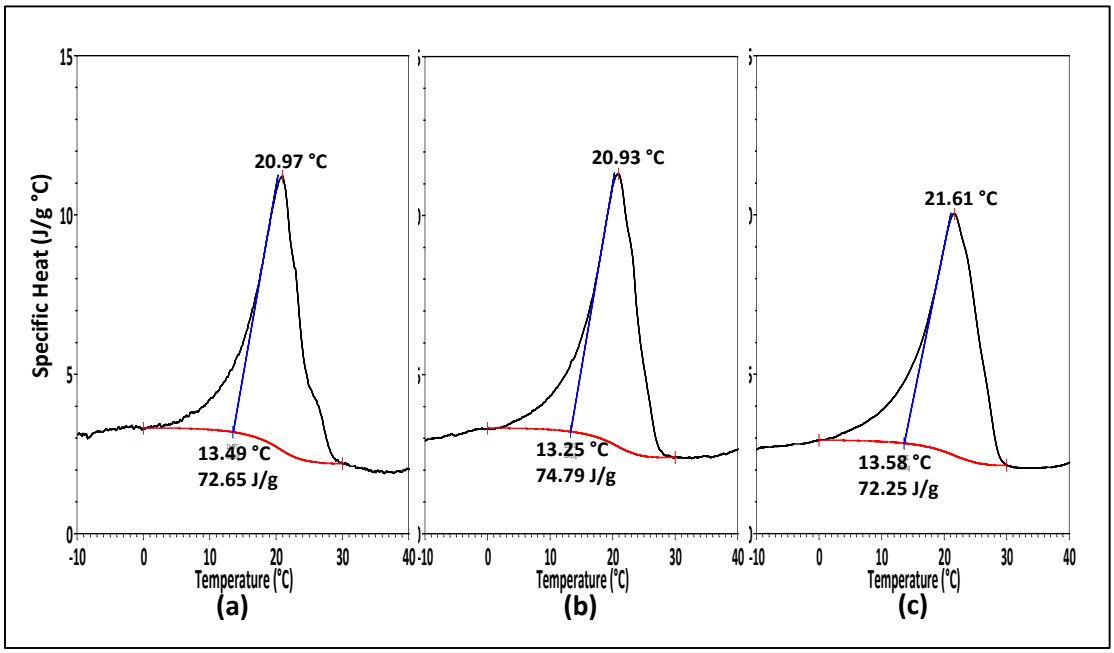

Figure 6.2.5. Specific Heat Curves of Sample D at Various Heating Rates (a) 0.5 °C/min, (b) 1 °C/min, and (c) 2 °C/min

Based on these results, Table 6.2.2 was constructed to summarize the results.

Table 6.2.2. DSC Test Results Comparisons of the PCM Composite Contained in the PCM Board

		0.5 °C/min (0.9 °F/min)	1.0 °C/min (1.8 °F/min)	2.0 °C/min (3.6 °F/min)
Sample C (8.5 mg (3.0×10^{-4} oz))	Melting Temperature (°C (°F))	20.60 (69.1)	20.99 (69.8)	21.34 (70.4)
	Onset of Melting Temperature (°C (°F))	13.38 (56.1)	13.63 (56.5)	13.62 (56.5)
	Latent Heat Storage Capacity (J/g (Btu/lb_m))	73.39 (31.6)	74.43 (32.0)	72.45 (31.2)
	Total Heat Storage Capacity (J/g (Btu/lb_m))	158.29 (68.0)	190.54 (81.9)	146.20 (62.9)
Sample D (15.8 mg (5.6×10^{-4} oz))	Melting Temperature (°C (°F))	20.97 (69.7)	20.93 (69.7)	21.61 (70.9)
	Onset of Melting Temperature (°C (°F))	13.49 (56.3)	13.25 (55.9)	13.58 (56.4)
	Latent Heat Storage Capacity (J/g (Btu/lb_m))	72.65 (31.2)	74.79 (32.2)	75.25 (32.4)
	Total Heat Storage Capacity (J/g (Btu/lb_m))	159.65 (68.6)	162.90 (70.0)	154.86 (66.6)

Based on the analysis, the DSC test results of Sample C at the heating rate of 0.5 °C/min (0.9 °F/min) were selected for the same reasons as stated before. The curve of enthalpy as a function of temperature is shown in Figure 6.2.6. The values of this curve were used as the input for the modeling and simulations of the wall panel containing the PCM boards.

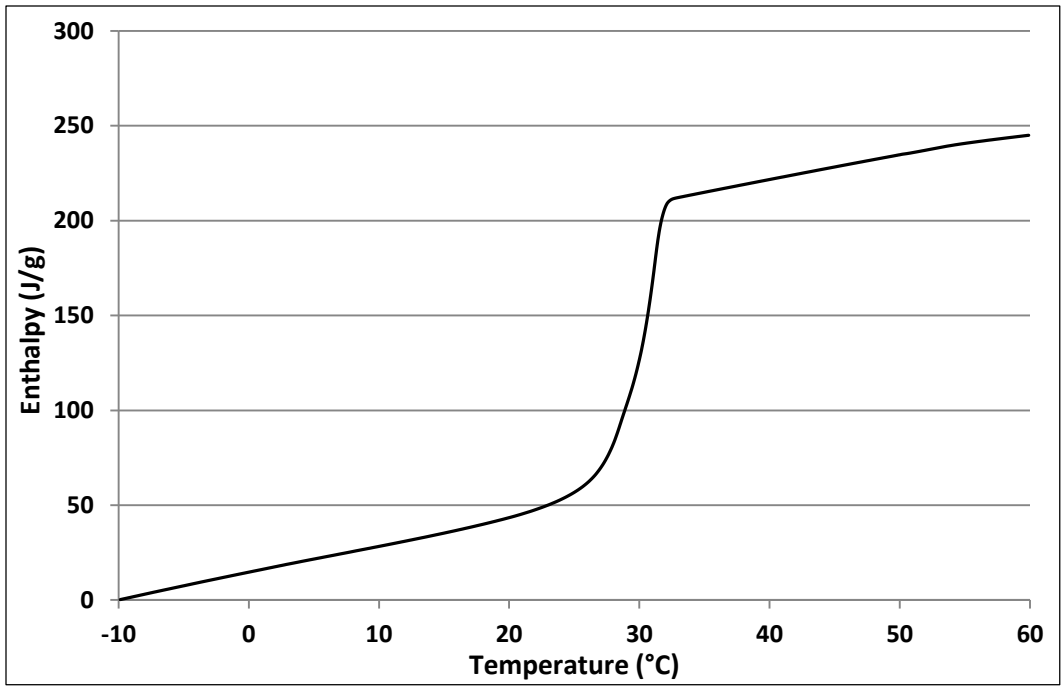

Figure 6.2.6. Enthalpy Curve of Sample C at Heating Rate of 0.5 °C/min As a Function of Temperature

CHAPTER VII

MODEL DEVELOPMENT AND VERIFICATION

7.1 EnergyPlus

EnergyPlus is a building energy analysis and thermal energy simulation program (DOE, 2013). EnergyPlus was developed in 2001 to combine the best features and capabilities of two existing building energy simulation programs: BLAST (Building Energy Analysis and System Thermodynamics) and DOE-2. BLAST was developed in the early 1970's, sponsored by the US Department of Defense (DOD), and DOE-2 was developed in the late 1960's, sponsored by the US Department of Energy (DOE). EnergyPlus was developed with the intention of making the development of the programming tool less expensive with faster periodic update releases and to allow users to make modifications and extensions. As a result, EnergyPlus consists of modular structures for adding new features and integrating it with other programs (Crawley et al., 2000). EnergyPlus was tested and validated using industry-accepted standard methods (DOE, 2013).

In this research, EnergyPlus was used to simulate the energy dynamics across the walls and ceilings of the test houses with and without PCM, including overall house energy consumption. EnergyPlus was also used to simulate the thermal performance of the panels in the M2SEC building walls with and without PCM. Before the simulations, EnergyPlus was validated against experimental data.

7.1.1 PCM Model in EnergyPlus

Phase change materials are simulated in EnergyPlus using a conduction finite difference (CondFD) solution algorithm. EnergyPlus includes two schemes used for the finite difference model. One is the Crank-Nicholson and the other is referred to as fully implicit. The Crank-Nicholson and the fully implicit schemes are finite difference methods used to solve partial differential equations (e.g., heat conduction equation) numerically. Both schemes approximate the solution of the heat conduction equation on finite grids with discretization in space and time (Ames, 1992). The Crank-Nicholson scheme has advantages when dealing with time-accurate solutions because its truncation error is significantly smaller than the truncation error of other schemes. The fully implicit scheme happens to be very stable when dealing with relatively large time steps (Hoffman, 1992).

For this research, the Crank-Nicholson scheme was selected because it offered a higher accuracy (Ames, 1992). The Crank-Nicholson scheme was coupled with an enthalpy-temperature function to model the heat conduction across the PCM-integrated enclosure components. The formulation for the Crank-Nicholson scheme is shown in Equation (7-1) (EnergyPlus, 2013a).

$$C_p \rho \Delta x \frac{T_i^{j+1} - T_i^j}{\Delta t} = \frac{1}{2}\left[\left(k_W \frac{\left(T_{i+1}^{j+1} - T_i^{j+1}\right)}{\Delta x} + k_E \frac{\left(T_{i-1}^{j+1} - T_i^{j+1}\right)}{\Delta x}\right) + \left(k_W \frac{\left(T_{i+1}^{j} - T_i^{j}\right)}{\Delta x} + k_E \frac{\left(T_{i-1}^{j} - T_i^{j}\right)}{\Delta x}\right)\right] \quad (7\text{-}1)$$

where:

T = temperature node, °C (K) (°F (°R))

i = node being modeled

i+1 = adjacent node to interior of construction

i-1 = adjacent node to exterior of construction

j+1 = new time step, seconds

j = previous time step, seconds

Δt = calculation time step, seconds

Δx = finite difference layer thickness, m (ft)

C_p = specific heat of material, J/kg°C (Btu/lb_m°F)

$k_W = \frac{\left(k_{i+1}^{j+1} + k_i^{j+1}\right)}{2}$, thermal conductivity for interface between i node and i+1 node, W/m°C (Btu·in/hr·ft^2°F)

$k_E = \frac{\left(k_{i-1}^{j+1} + k_i^{j+1}\right)}{2}$, thermal conductivity for interface between i node and i-1 node, W/m°C (Btu·in/hr·ft^2°F)

ρ = density of material, kg/m^3 (lb_m/ft^3)

Four types of nodes were used by the CondFD model. These are shown in Figure 7.1.1. These were the internal surface nodes, interior nodes, material interface nodes, and exterior surface nodes. Grids were established by specifying a half node for each edge of each material and equal size nodes for the rest of the materials.

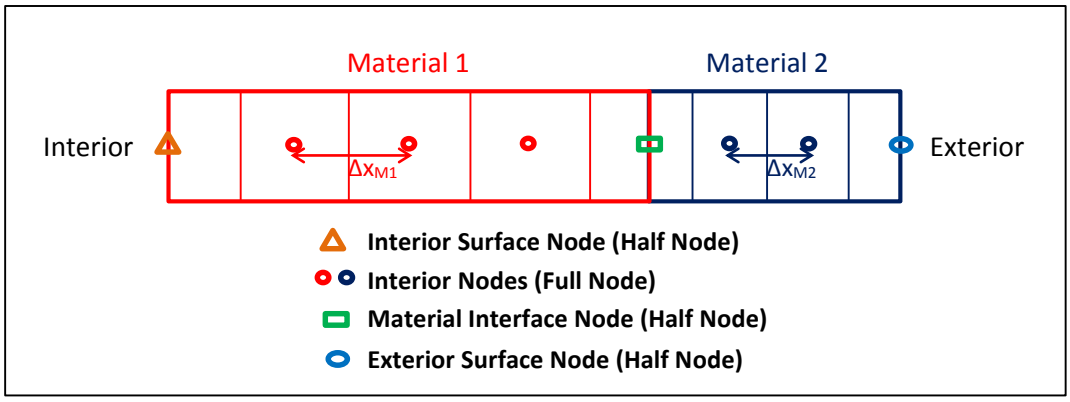

Figure 7.1.1. Node Types for CondFD Model in EnergyPlus (Source: EnergyPlus, 2013a)

Equation (7-1) was coupled with the enthalpy-temperature function (HTF) which is shown in Equation (7-2).

$$h_i(T_i) = HTF(T_i) \tag{7-2}$$

where:

h(T) = enthalpy node as a function of temperature, kJ/kg (Btu/lb_m)

i = node being modeled

T= temperature node, °C (K) (°F (°R))

The enthalpy-temperature function (HTF) was specified from the in-house DSC experimental data shown in Figures 6.2.3 and 6.2.6 for the PCM contained in the PCM shield and the PCM composite in the PCM board, respectively. The HTF was then used to develop an equivalent specific heat (C_p) for each time step.

7.1.2 Inputs for PCM in EnergyPlus

In addition to the standard data required by EnergyPlus (e.g., weather data, indoor conditions, enclosure materials geometry and dimensions, operating schedules, etc.) for the case of simulating PCMs, PCM enthalpy and thermal conductivity as functions of temperature were also required be CondFD.

7.1.2.1 Enthalpy of PCM as a Function of Temperature

Because the enthalpy of the PCM varies as a function of temperature, several values of enthalpy were input based on PCM temperature. A two column table of temperature with its corresponding enthalpy was constructed based on the in-house DSC experiments (see Figures 6.2.3 and 6.2.6). This is shown in Tables 7.1.1 and 7.1.2 for the PCM contained in the PCM shield and the PCM composite in the PCM board, respectively. The values of Tables 7.1.1 and 7.1.2 covered the entire temperature range that the PCM would experience during the simulations. Once the enthalpy-temperature inputs were set, EnergyPlus calculated the enthalpy in a linear fashion based on any two temperature points from the given enthalpy-temperature curve shown in Figures 7.1.2 and 7.1.3.

Table 7.1.1. Experimental Temperature and Corresponding Enthalpy for the PCM Contained in the PCM Shield

Temperature (°C (°F))	Enthalpy (J/kg (Btu/lb_m))
-10.0 (14)	0.001 (7.7)
0.1 (32.2)	14,796 (14.0)
11.6 (52.9)	30,373 (20.7)
18.0 (64.4)	39,861 (24.8)
23.6 (74.5)	51,706 (29.9)
26.0 (78.8)	61,552 (34.1)
26.9 (80.4)	68,379 (37.1)
29.0 (84.2)	101,473 (51.3)
30.4 (86.7)	142,059 (68.8)
31.4 (88.5)	189,017 (88.9)
31.7 (89.1)	201,190 (94.2)
32.1 (89.8)	208,304 (97.2)
33.2 (91.8)	212,515 (99.0)
35.7 (96.3)	215,925 (100.5)
40.7 (105.3)	222,639 (103.4)
60.0 (140.0)	244,963 (113.0)

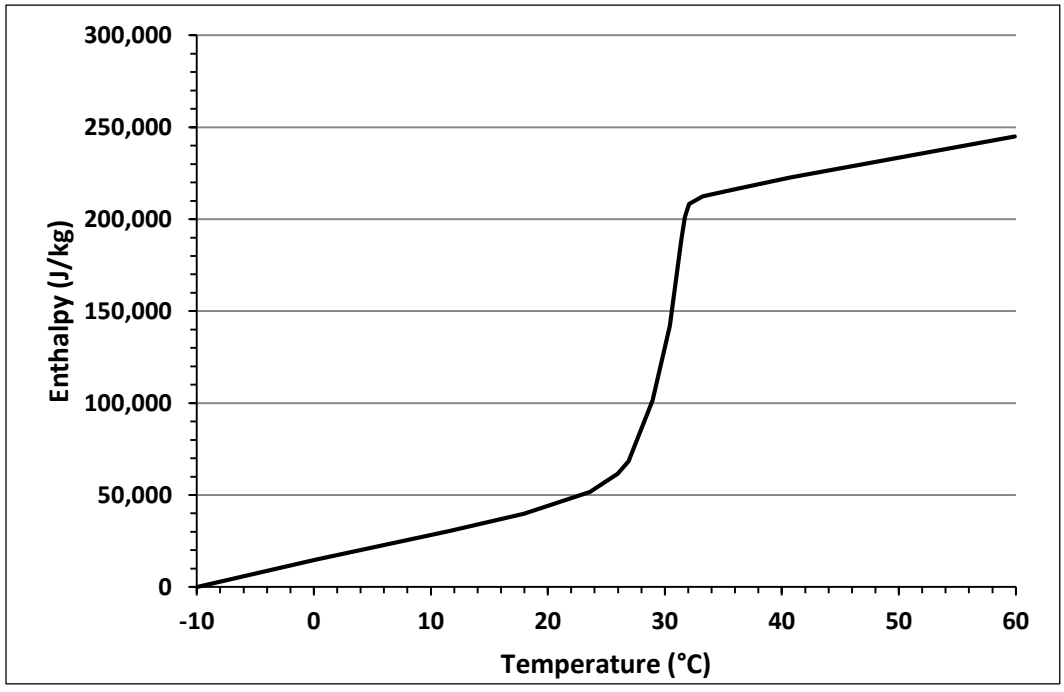

Figure 7.1.2. Calculated Input of Enthalpy as a Function of Temperature for the PCM Contained in the PCM Shield and Used by CondFD from Table 7.1.1

Table 7.1.2. Experimental Temperature and Corresponding Enthalpy for the PCM Composite in the PCM Board

Temperature (°C (°F))	Enthalpy (J/kg (Btu/lb_m))
-10.0 (14.0)	0.001 (7.7)
1.5 (34.7)	37,481 (23.8)
5.1 (41.2)	49,938 (29.2)
8.9 (48.0)	64,125 (35.3)
13.6 (56.5)	85,371 (44.4)
16.2 (61.2)	101,430 (51.3)
18.0 (64.4)	115,417 (57.3)
20.5 (68.9)	141,331 (68.4)
22.3 (72.1)	158,851 (76.0)
23.6 (74.5)	169,682 (80.6)
24.8 (76.6)	176,360 (83.5)
26.5 (79.7)	183,550 (86.6)
29.6 (85.3)	190,827 (89.7)
34.0 (93.2)	199,855 (93.6)
42.9 (109.2)	219,724 (102.1)
60.0 (140.0)	253,687 (116.7)

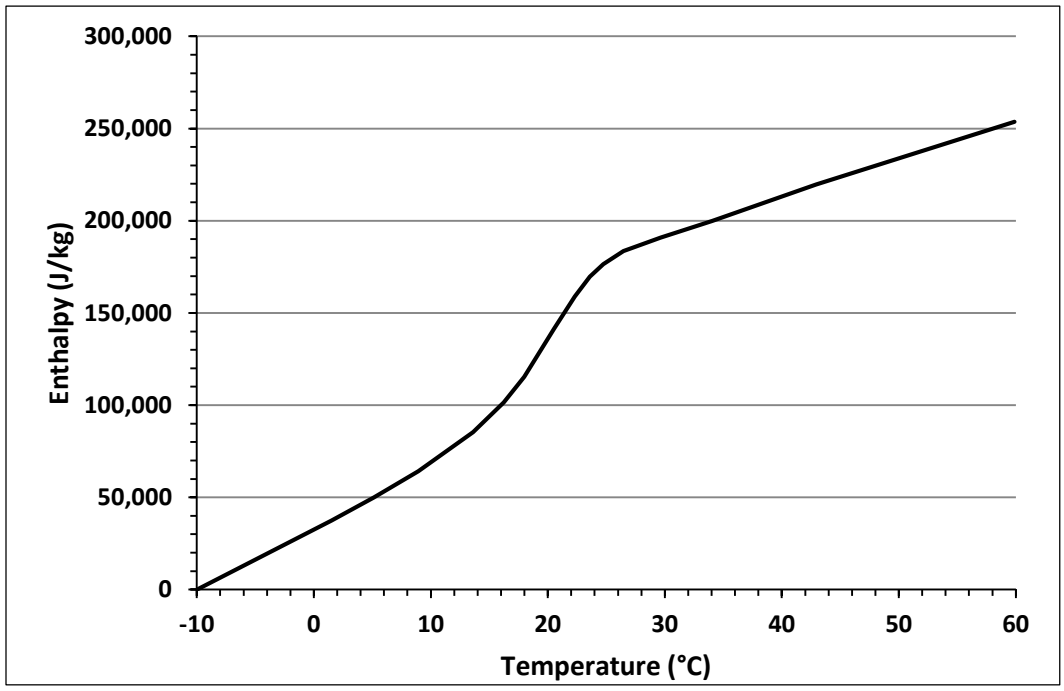

Figure 7.1.3. Calculated Input of Enthalpy as a Function of Temperature for the PCM Composite Contained in the PCM Board and Used by CondFD from Table 7.1.2

An equivalent specific heat as a function of temperature, $C_p(T)$, at each time step was developed by the enthalpy-temperature function of Figures 7.1.2 and 7.1.3 for the PCM contained in the PCM shield and the PCM composite in the PCM board, respectively. The $C_p(T)$ was formulated as shown in Equation (7-3).

$$C_p(T) = \frac{h_i^j - h_i^{j-1}}{T_i^j - T_i^{j-1}} \quad (7\text{-}3)$$

where:

$C_p(T)$ = specific heat as a function of temperature, kJ/kg°C (Btu/lb_m°F)

h(T)= enthalpy node as a function of temperature, kJ/kg (Btu/lb_m)

i = node being modeled

j = new time step, seconds

j-1 = previous time step, seconds

T = temperature node, °C (K) (°F (°R))

7.1.2.2 Thermal Conductivity of PCM as a Function of Temperature

The thermal conductivities of PCMs vary with their phase (e.g., solid and liquid). In other words, the thermal conductivity of a PCM is dependent on its temperature. In EnergyPlus, one of two input fields was required to provide variable thermal conductivities: Variable Thermal Conductivity (VTC) or Temperature Coefficient for Thermal Conductivity (TCTC).

In this research, the VTC was specified by entering the thermal conductivities that corresponded to the temperatures as indicated in Tables 7.1.3 and 7.1.4. Tables

7.1.3 and 7.1.4 show the conductivities for the PCM contained in the PCM shield and the PCM composite in the PCM board, respectively. The temperature range of phase transition of Table 7.1.3 and Figure 7.1.4 were derived from Figure 6.2.1 (a). Similarly, the temperature range of phase transition of Table 7.1.4 and Figure 7.1.5 were derived from Figure 6.2.4 (a). Based on Tables 7.1.3 and 7.1.4 and Figures 7.1.4 and 7.1.5, CondFD calculated the thermal conductivity of the PCM as a function of temperature. According to Figure 7.1.4, the value of the conductivity of the PCM contained in the PCM shield in its solid state was 1.088 W/m°C (7.545 Btu·in/hr·ft^2°F, 0.629 Btu/hr·ft°F) Similarly, the value of the conductivity in its liquid state was 0.540 W/m°C (3.740 Btu·in/hr·ft^2°F, 0.312 Btu/hr·ft°F). When the PCM was undergoing phase transition its conductivity was calculated based on the linear function between its solid and liquid states. The conductivity of the PCM composite in the PCM board was calculated according to Figure 7.1.5 in the same manner as explained before.

Table 7.1.3. Conductivity of the PCM Contained in the PCM Shield (Source: Mehling and Cabeza, 2008)

Temperature (°C (°F))	Conductivity (W/m°C (Btu·in/hr·ft^2°F))
< 18 (64.4) (Solid)	1.088 (7.545)
> 33 (91.4) (Liquid)	0.540 (3.740)

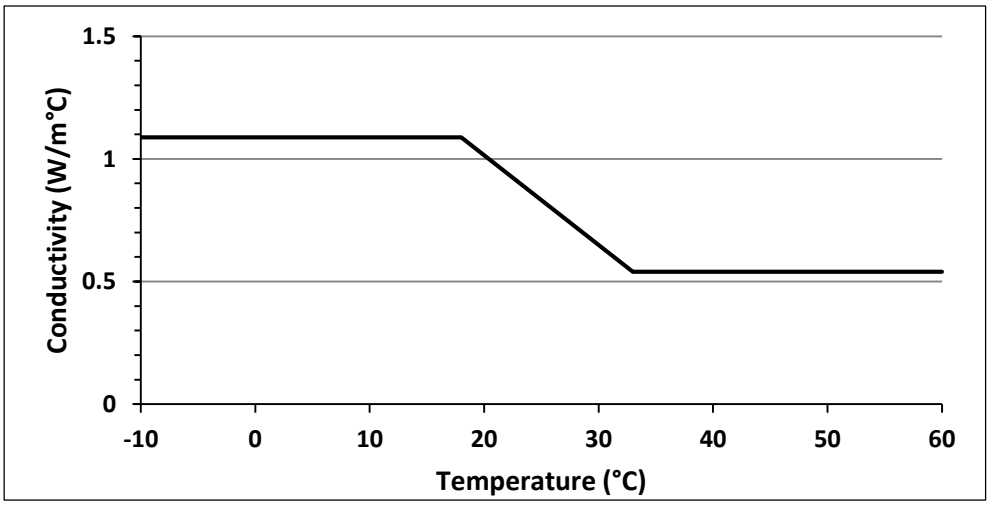

Figure 7.1.4. Calculated Input of Conductivity as a Function of Temperature for the PCM Contained in the PCM Shield and Used by CondFD from Table 7.1.3

Table 7.1.4. Conductivity of the PCM Composite Contained in the PCM Board (Source: Dupont™ Energain® Datasheet)

Temperature (°C (°F))	Conductivity (W/m°C (Btu·in/hr·ft^2°F))
< 0 (32.0) (Solid)	0.18 (1.248)
> 30 (86.0) (Liquid)	0.14 (0.971)

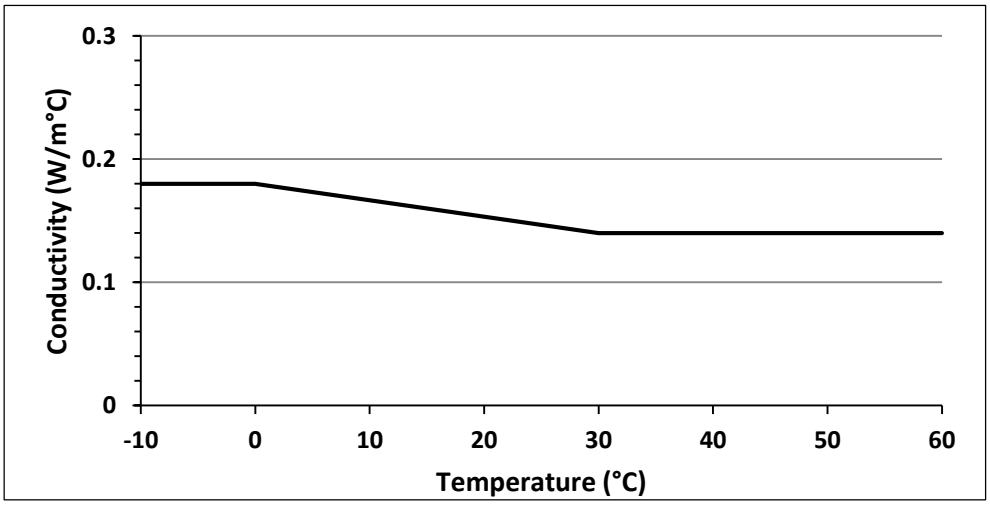

Figure 7.1.5. Calculated Input of Conductivity as a Function of Temperature for the PCM Composite Contained in the PCM Board and Used by CondFD from Table 7.1.4

7.2 Model Verification for the Control Case

7.2.1 Test House Model

The test house (see Figure 4.1.1) was modeled using the same materials and dimensions as described in Chapter 4 (see Figure 4.1.2). A modeling schematic of the test house is shown in Figure 7.2.1. Model predictions without the PCM shield were obtained to verify the accuracy of the inputs of the enclosure components. Model predictions were then compared against the experimental data of the control house to verify the accuracy of the model. The weather data that were collected during the experiments were used for this modeling.

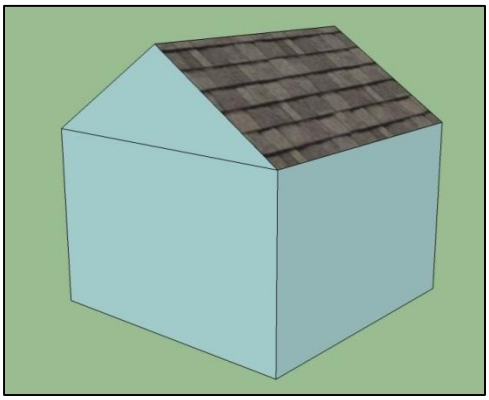

Figure 7.2.1. Modeling Schematic of the Test House

Figures 7.2.2, 7.2.3, and 7.2.4 show heat flux and temperature comparisons of the model predictions against experimental data for the south wall, west wall, and ceiling, respectively.

The model predictions of the heat fluxes across the south wall as well as exterior surface temperatures, shown in Figure 7.2.2, were relatively close to the

experimental values including peaks and valleys. The small discrepancies in the comparison of these values was the result of several factors, which were (1) the differences in indoor air temperatures between the experimental data and the simulation data, (2) measurement errors, and (3) the use of published values for the thermal properties of the materials. For example, the model assumed that the indoor air temperature values were constant; however, keeping these values constant during the experiments proved impossible because the summer in which these experiments were carried out was unusually hot. Experimental errors described in Chapter 5 (e.g., heat flux and contact conductance) played a significant role in the discrepancies between the predicted and experimental values.

The sudden and short duration peaks observed in the heat flux data at the beginning of the peak periods were the result of a blast of cold air blowing over the heat flux sensors when the fan coil units initially started. As expected, sudden experimental events were not modeled. Therefore, when comparing peaks, only those values that were sustained for longer periods of time were used. The average difference between predicted and experimental peaks of the heat fluxes was -4.5%. The difference between predicted and experimental total heat transfer was -10.9%. The difference in exterior surface temperature peaks was -1.04 °C (-1.9 °F) and the average temperature difference between predicted and experimental values was -0.40 °C (-0.7 °F), respectively.

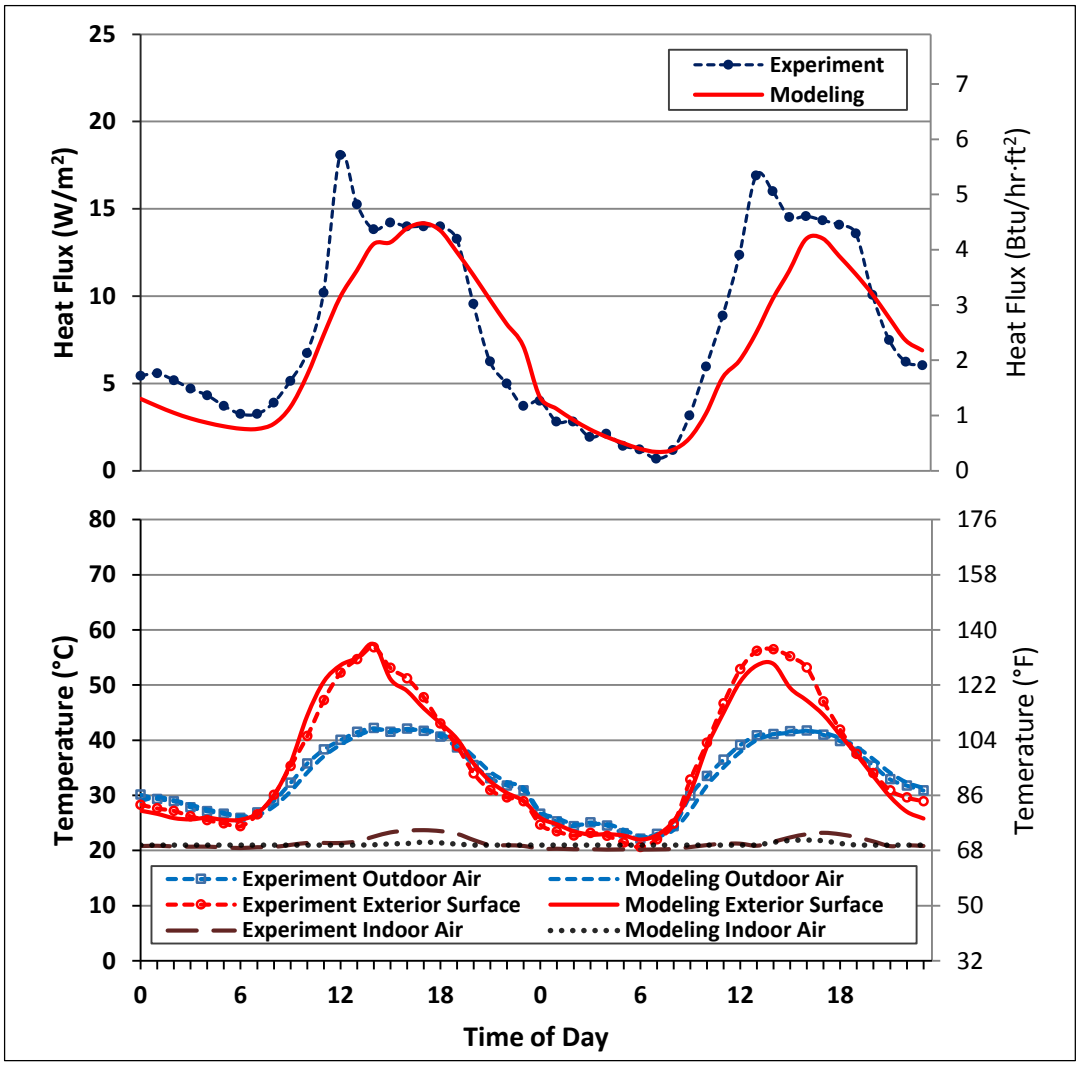

Figure 7.2.2. Model Prediction and Experimental Heat Fluxes Across the South Wall (Top) and Temperatures (Bottom)

Figure 7.2.3 shows the comparisons between the predicted and experimental values for the west wall. Similar to Figure 7.2.2, as explained in the case of the south wall, the heat flux curves of the model predictions show highly comparable trends. The average difference between predicted and experimental peaks of the heat fluxes was -4.4%. The difference between predicted and experimental total heat transfer was

11.9%. The difference in exterior surface temperature peaks was -3.19 °C (-5.7 °F) and the average temperature difference between predicted and experimental values was -0.20 °C (-0.4 °F). The sudden, short-duration peaks were also observed in the west wall data. Again these were the results of cold air flowing over the heat flux sensors once the fan coil unit started.

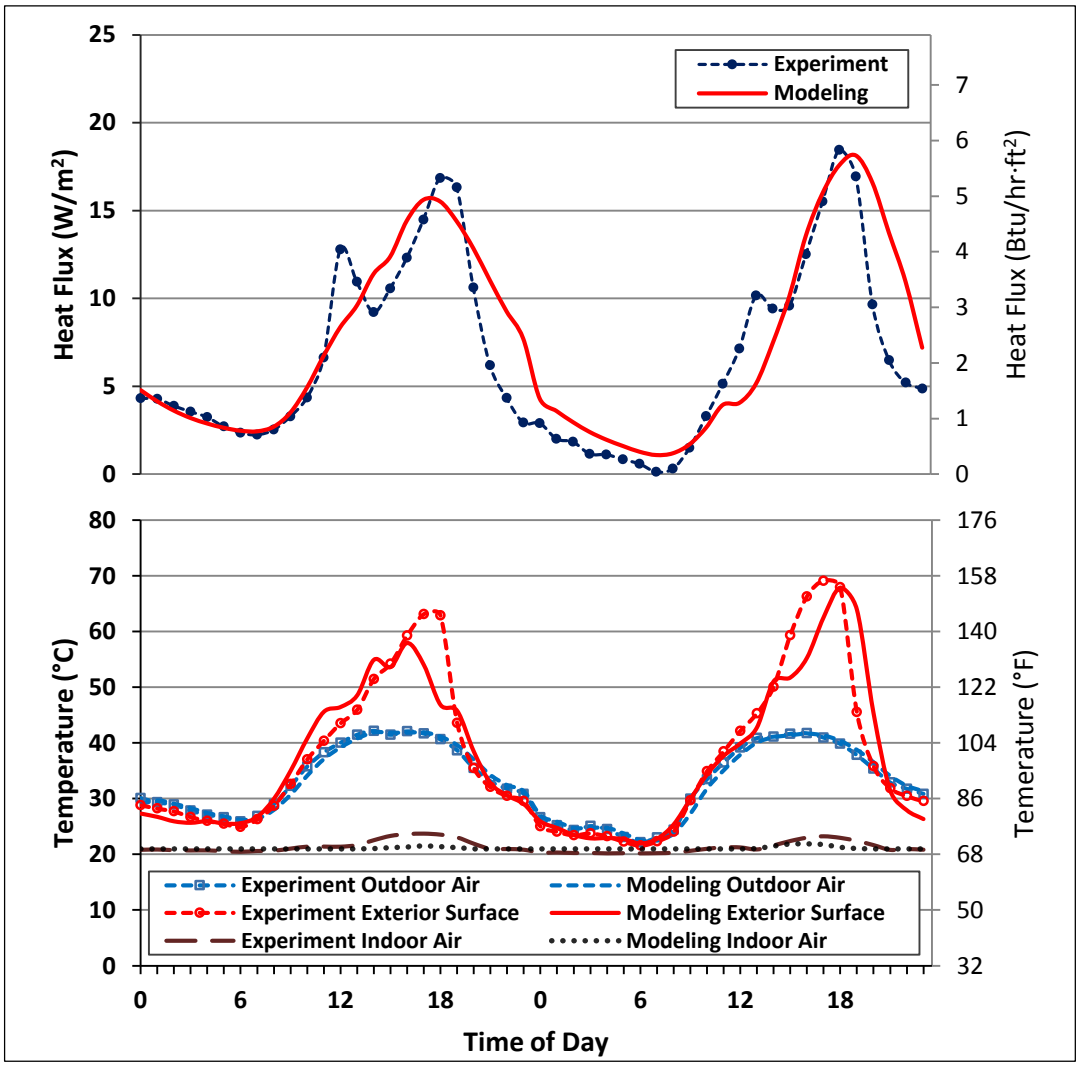

Figure 7.2.3. Model Prediction and Experimental Heat Fluxes Across the West Wall (Top) and Temperatures (Bottom)

Figure 7.2.4 shows the comparisons between the predicted and experimental values for the ceiling component of the house enclosure. The average difference between predicted and experimental peaks of the heat fluxes was 29.4%. The difference between predicted and experimental total heat transfer was 12.1%. The difference in attic air temperature peaks was -0.11 °C (-0.2 °F) and the average temperature difference between predicted and experimental values was 0.23 °C (0.4 °F).

The differences between predicted and measured values of the heat fluxes for the ceiling components, particularly during the peak periods, were larger than the same difference for the heat transfer across the south and west walls. One explanation for this is that attics are complex systems to simulate. In the present case, the attic was a triangular component bound by two roof sections and two end gables in which air flowed naturally. This brought several unknown parameters into the modeling, including attic air flow rate, attic air flow pattern, which were both functions of wind speed and direction. In addition, there were issues related to not only forced and natural convection and radiation, including view factors, but humidity parameters as well. For example in hot and humid summers, such as the one experienced by the test houses, condensation and evaporation processes on attic surfaces are not uncommon. CondFD used default values for most of the above mentioned parameters. This, in turn, may have contributed to the larger discrepancies.

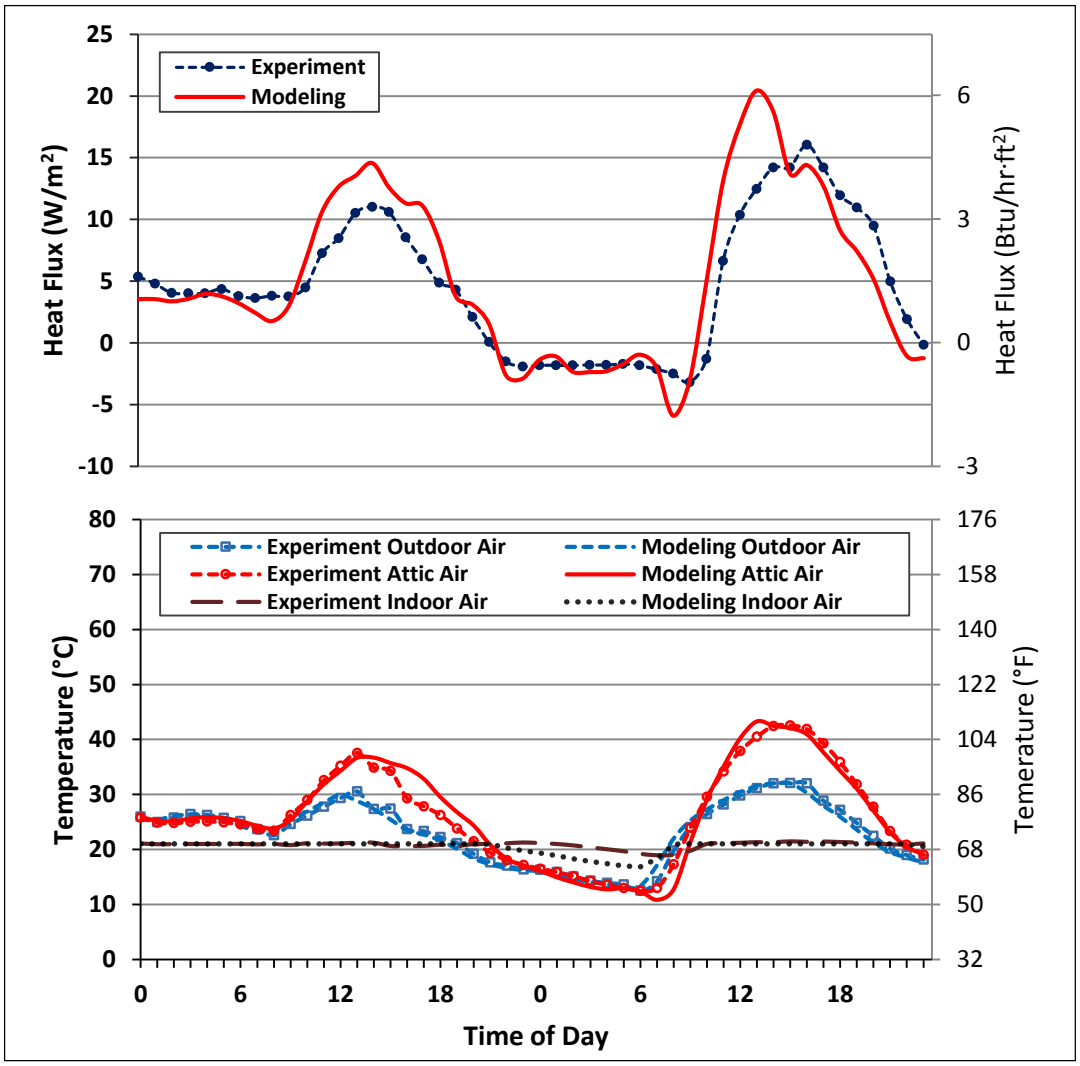

Figure 7.2.4. Model Prediction and Experimental Heat Fluxes Across the Ceiling (Top) and Temperatures (Bottom)

From the model predictions of the control cases for the south and west walls, it was observed that the peak heat fluxes and the average exterior surface temperatures were similar to the experimental values. The predicted total heat transfer for the south wall were slightly underestimated, while the predicted total heat transfer for the west wall were slightly overestimated. For the case of the ceiling, the

predicted average attic air temperatures were closer to the experimental values than the heat fluxes. The predicted total heat transfer for the ceiling was overestimated. The reason why the attic air temperatures were close between predicted and experimental values was because CondFD used a procedure that included several infiltration rates that could have produced a closer to actual attic air flow.

7.2.2 M2SEC Wall Panel Model

The thermal performance of the wall panels in the south and west walls of the M2SEC were also modeled. Model predictions without the PCM board were performed to verify the accuracy of the inputs prior to adding the PCM board. A schematic of the modeled wall panel is shown in Figure 7.2.5.

For these model predictions, local weather data gathered for the same time periods of the experiments were used. The weather data were retrieved from the Natural Resources Conservation Service (NRCS) website. These weather data were collected by The University of Kansas Field Station at the Nelson Environmental Study Area (NESA) in Lawrence, Kansas.

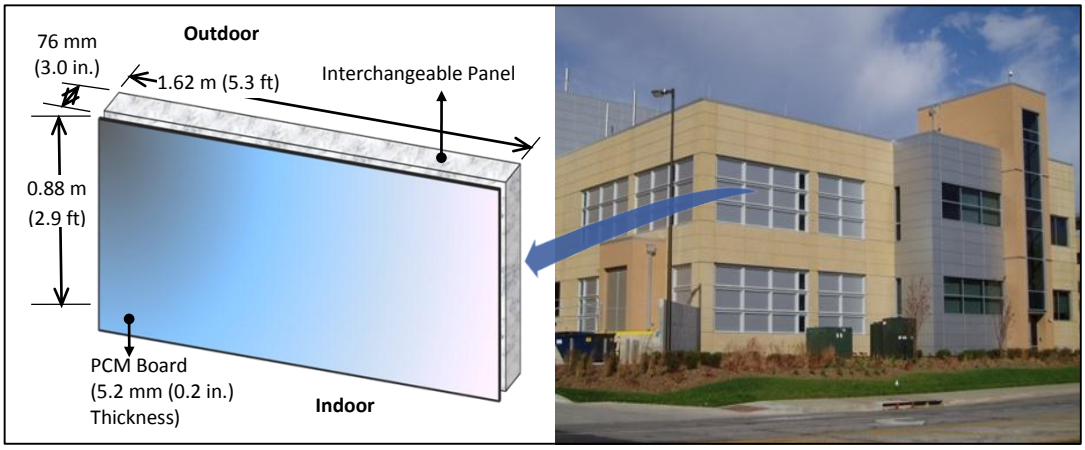

Figure 7.2.5. Modeling Schematic of the Wall Panels in the South and West Walls of M2SEC

Figure 7.2.6 shows the comparisons between the predicted and experimental values for the south wall panel in M2SEC. The average difference between simulated and experimental peaks of the heat fluxes was -13.4%. The difference between predicted and experimental total heat transfer was -61.1%. The difference in exterior surface temperature peaks was -3.39 °C (-6.1 °F) and the average temperature difference between predicted and experimental values was -0.66 °C (-1.2 °F).

The differences between predicted and measured values of the heat fluxes for this wall were larger than the same difference for the heat fluxes across the south wall of the test house. There are several reasons for this. One reason was the lack of weather data from a closer location to the building. A second reason was that the CondFD algorithm was not able to model the highly conductive and very thin (≤ 0.5 mm (0.02 in.) layer of material, such as the aluminum siding on both sides of the M2SEC panels. However, the fact that the trend of the predicted heat flux curve was similar to the experimental trend even in light of the reasons stated above, make these

predictions acceptable. The same is true for the discrepancies in temperatures between measured and predicted values.

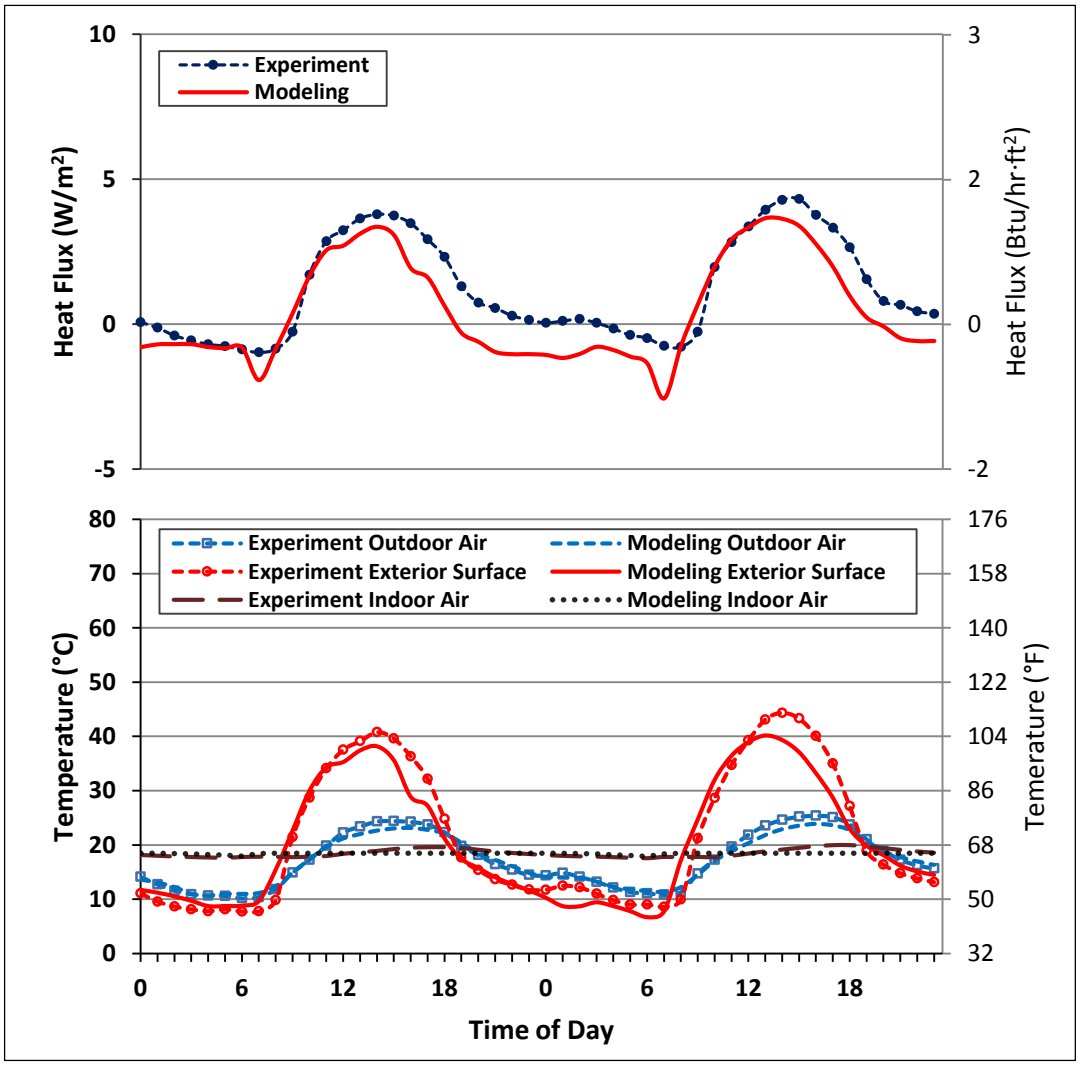

Figure 7.2.6. Model Prediction and Experimental Heat Fluxes Across the South Wall Panel (Top) and Temperatures (Bottom)

Figure 7.2.7 shows the comparisons between the predicted and experimental values for the west wall panel in M2SEC. The reasons for the difference in values

between predictions and actual data are the same as described for the previous figure. The average difference between predicted and experimental peaks of the heat fluxes was -45.0%. The difference between predicted and experimental total heat transfer was -98.0%. The difference in exterior surface temperature peaks was -10.4 °C (-18.7 °F) and the average temperature difference between predicted and experimental values was 3.16 °C (5.7 °F).

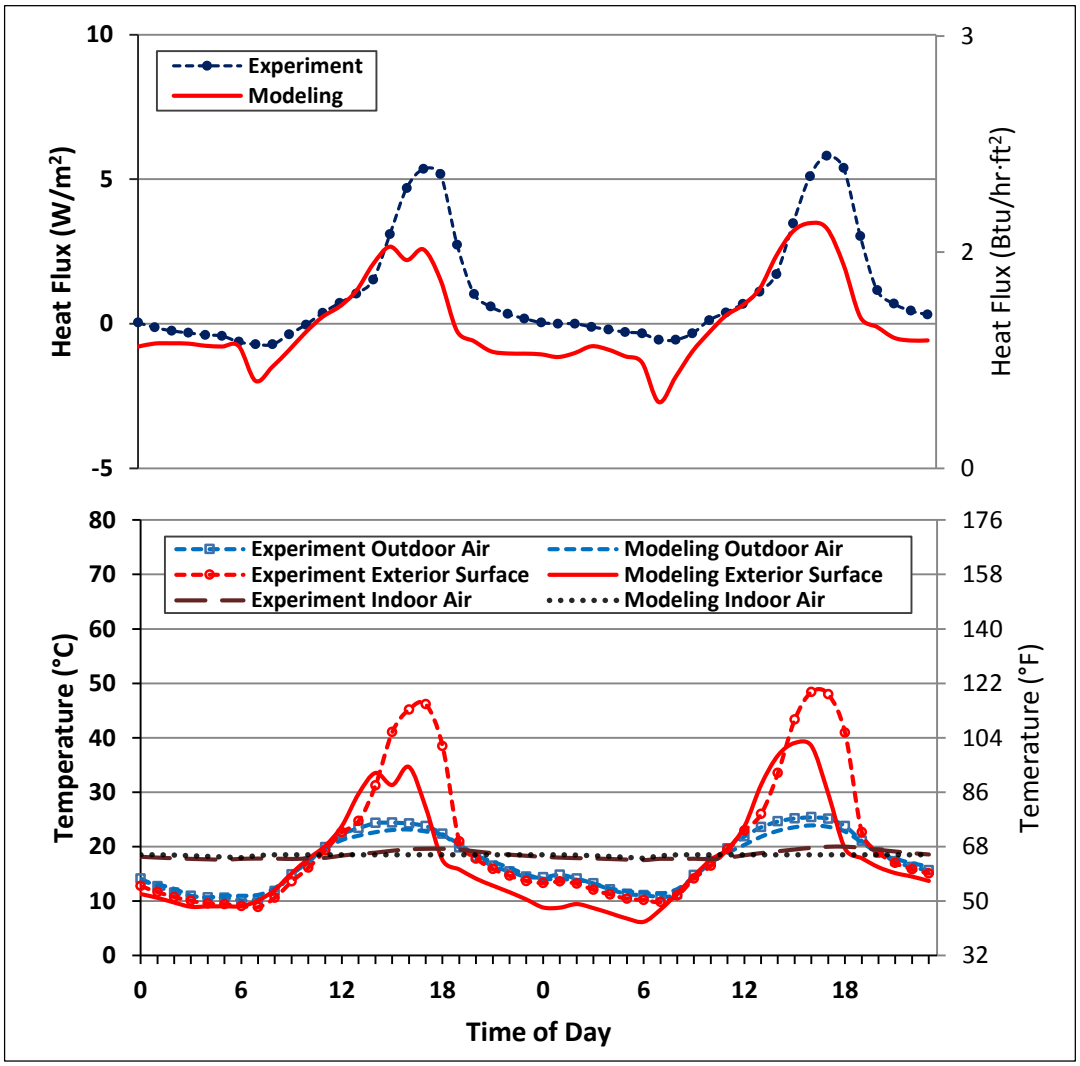

Figure 7.2.7. Model Prediction and Experimental Heat Fluxes Across the West Wall Panel (Top) and Temperatures (Bottom)

7.3 Model Verification for the Retrofit Case

7.3.1 Test House Model with the PCM Shields

The test house walls and ceiling with the PCM shields were modeled and the results were compared against the experimental data to verify the accuracy of both the PCM inputs obtained in Chapter 6 and the ability of CondFD to model the phase transition aspects of the PCM. For the phase transition aspects of the PCM, the enthalpy as a function of temperature in Table 7.1.1 and the thermal conductivity as a function of temperature in Table 7.1.3 were used. In addition, other necessary inputs related to the PCM had to be provided and are shown in Table 7.3.1.

Table 7.3.1. Additional Inputs for the PCM Contained in the PCM Shield

	Input Value
PCM Shield Thickness	0.001 m (0.04 in.)
PCM Density	3,266 kg/m^3 (203.9 lb$_m$/ft^3)*

*ConFD used a single density value.

Figures 7.3.1, 7.3.2, and 7.3.3 show the comparisons between the predicted and experimental values for the south wall, west wall, and ceiling of the retrofit test house.

The average difference between predicted and experimental peaks of the heat fluxes was 9.2% for the retrofit south wall. This is shown in Figure 7.3.1. The difference between predicted and experimental total heat transfer was -6.6%.

When the PCM shields were added to the wall and modeled. The model predictions when compared against the experimental data show that the model was

able to follow the trend of heat fluxes relatively well including peaks and valleys. But, as expected the comparisons were not as close as these were for the control case. This was expected because of the following reasons: (1) although the PCM layer was at the same location for both, model and experiments, the shield created extra air spaces between the shield and the insulation, which were not modeled, (2) the shield was constructed of aluminum foil, which created a reduction in radiation heat transfer between the shield and the insulation, which was also not modeled, (3) the model assumed that the PCM was evenly and symmetrically distributed within the PCM layer, which was not the case in the actual experiments, (4) CondFD assumed a constant PCM density regardless of whether the PCM state was solid or liquid. In other words, although CondFD is the latest and state of the art algorithm for modeling PCMs in enclosure components, there are still several shortcomings within the existing algorithm. Nevertheless, comparisons of heat flux reductions between predicted control and retrofit cases were within 5.0% (Figure 7.3.2) of actual comparisons of control and retrofit cases. This would allow the predictions to be accurate to within an acceptable margin. That is, the predicted heat transfer reductions of the retrofit south wall would be close to the experimental heat transfer reductions.

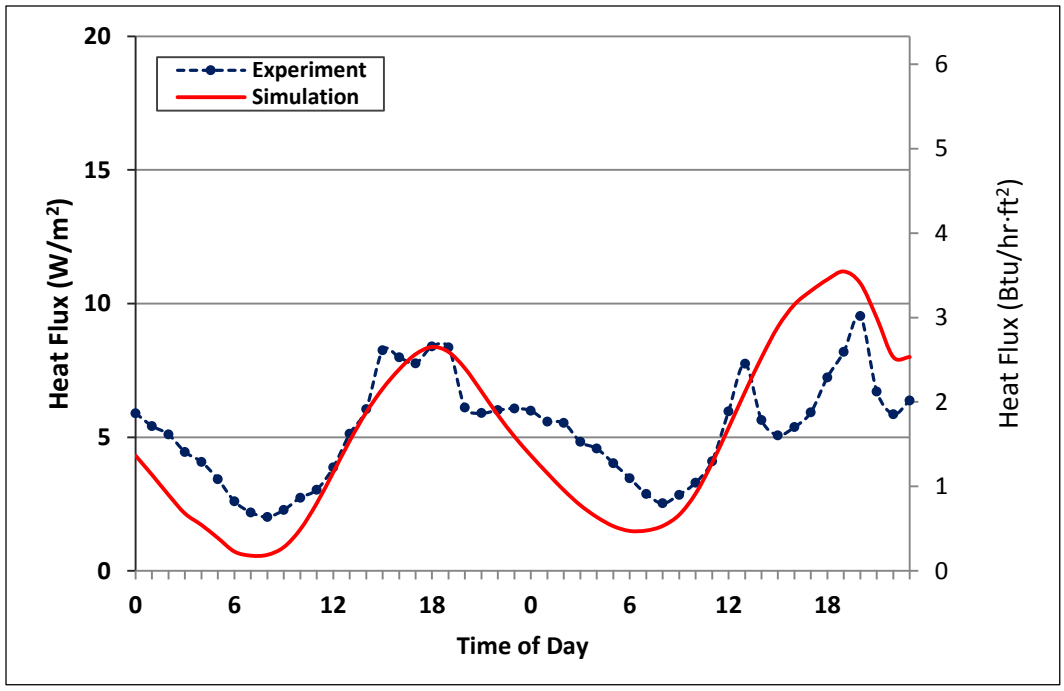

Figure 7.3.1. Predicted Heat Fluxes Across the Retrofit South Wall Compared with the Experimental Data

Figure 7.3.2 shows the comparisons between the experimental and predicted heat fluxes for the control and retrofit south walls.

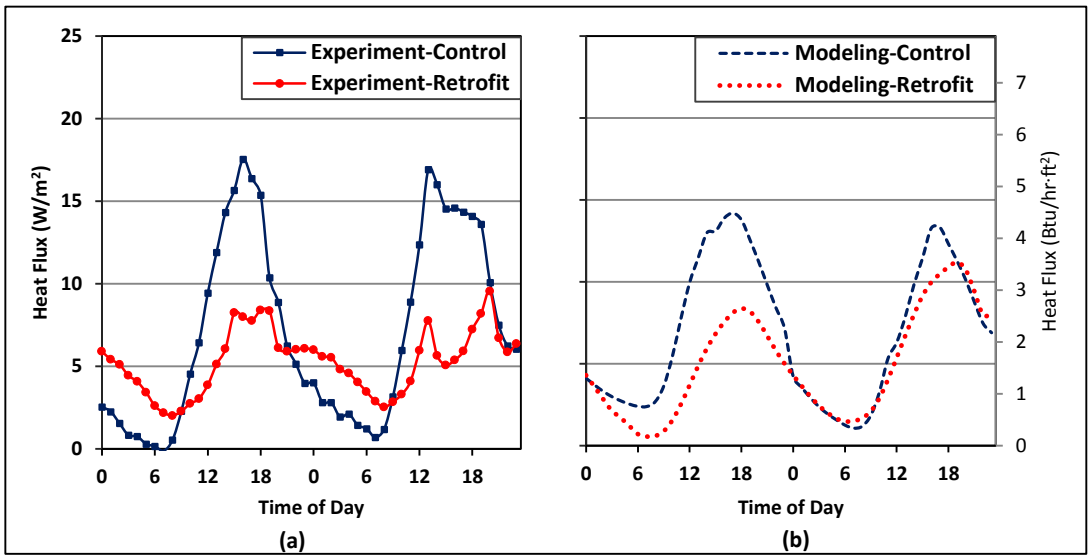

Figure 7.3.2. Heat Flux Comparisons for the South Wall
(a) Experiment and (b) Model Prediction

For the west wall, the average difference between predicted and experimental retrofit peaks of the heat fluxes was 7.9%. This is shown in Figure 7.3.3. The difference between predicted and experimental total heat transfer was 12.0%. For the case of the control west wall in Figure 7.2.3, the difference between predicted and experimental total heat transfer was 11.9%. This implied that the predicted total heat transfer reductions of the retrofit west wall will be within 1% of the experimental results. In other words, with all of its shortcomings, the total heat transfer reductions produced by a PCM shield could be predicted accurately using CondFD. This is in line with the conclusion of Tabares-Valasco et al. (2012) who were members of CondFD development team. The PCM model also did not predict the time delay for the case of retrofit west wall.

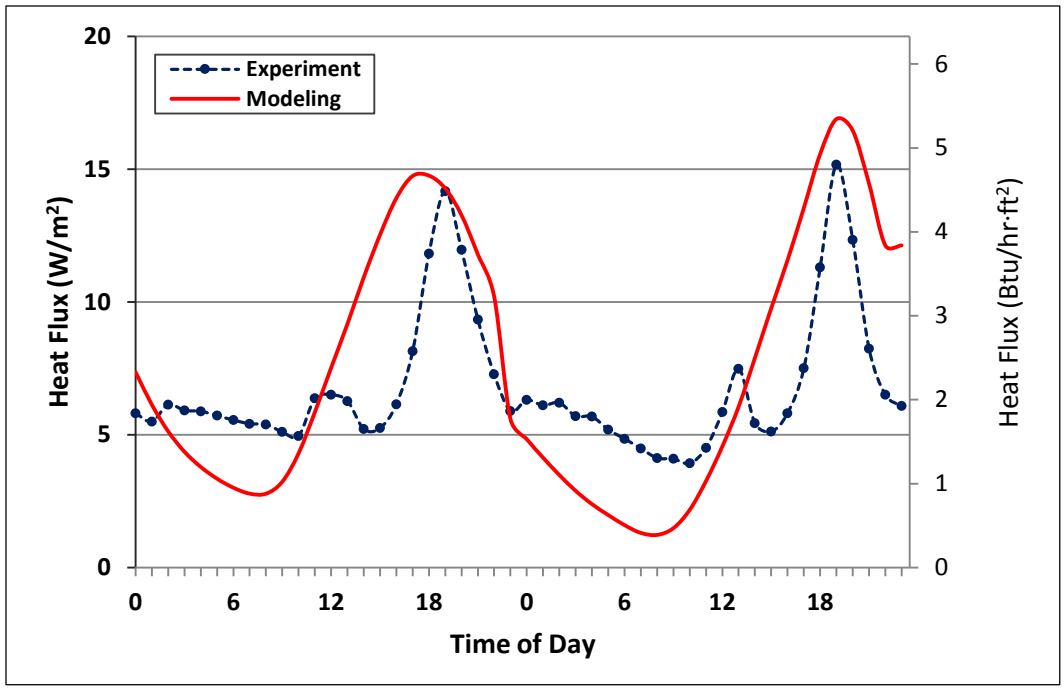

Figure 7.3.3. Predicted Heat Fluxes Across the Retrofit West Wall Compared with the Experimental Data

Figure 7.3.4 shows the comparisons between the experimental and predicted heat fluxes for the control and retrofit west walls.

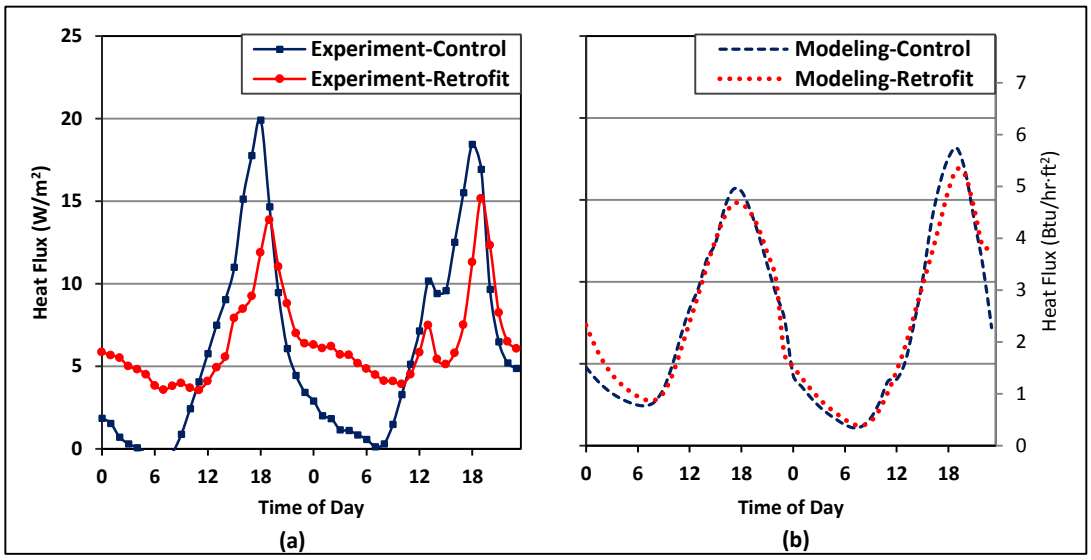

Figure 7.3.4. Heat Flux Comparisons for the West Wall
(a) Experiment and (b) Model Prediction

For the ceiling component, the average difference between predicted and experimental retrofit peaks of the heat fluxes was 18.9%. This is shown in Figure 7.3.5. The difference between predicted and experimental total heat transfer was 7.7%. For the case of the control ceiling in Figure 7.2.4, the difference between predicted and experimental total heat transfer was 12.1%. Similar to the wall cases, the predicted total heat transfer reductions of the retrofit ceiling will be within less than 5.0% of the experimental results as explained before.

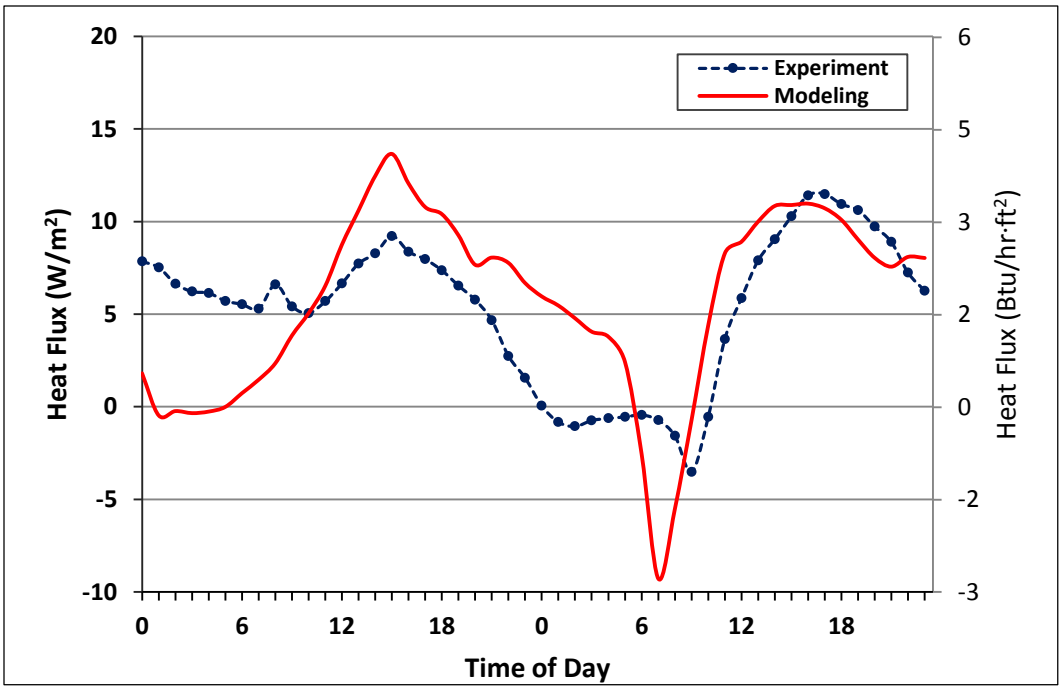

Figure 7.3.5. Predicted Heat Fluxes Across the Retrofit Ceiling Compared with the Experimental Data

Based on the model predictions with the PCM contained in the PCM shield, the predicted heat flux curves were not as similar to the experimental results as in the control cases. In addition to the reasons given above for the differences between model prediction and experimental values, the following reasons also contributed to the discrepancy. The average melting speeds of the PCM during test periods were 0.009 and 0.017 °C/min (0.016 and 0.031 °F/min), for the cases of the south and west walls, respectively. The average solidification speeds of the PCM during the same periods were 0.006 and 0.015 °C/min (0.011 and 0.027 °F/min). These were much lower than the minimum time discretization of 1 minute allowed by the PCM model in CondFD. Another reason for the discrepancy between model prediction and experimental data was the fact that the produced PCM enthalpy as a function of

temperature curve of Tables 7.1.1 and 7.1.2 and Figures 7.1.2 and 7.1.3 resulted from DSC heating rate of 0.5 °C/min (0.9 °F/min), while in actuality the heating and cooling rates were much lower than these values. Therefore, the PCM model could not predict the delays in heat transfer when the PCM was melting or solidifying. This implied that the predicted hourly heat fluxes would not compare favorably to the experimental data. However, the model predictions would be comparable to the experimental results on a basis of the total heat transfer reduction comparisons between of the retrofit and control south wall, west wall, and ceiling.

7.3.2 M2SEC Wall Panel Model with the PCM Boards

The wall panels with the PCM boards were also modeled and the results were compared against the experimental data to verify the accuracy of both the PCM inputs obtained in Chapter 6 and the ability of CondFD to model the phase transition aspects of the PCM composite contained in the PCM board. For the phase transition aspects of the PCM composite, the enthalpy as a function of temperature in Table 7.1.2 and the thermal conductivity as a function of temperature in Table 7.1.4, were used. In addition, other necessary inputs related to the PCM had to be provided are shown in Table 7.3.2.

Table 7.3.2. Additional Inputs for the PCM Composite Contained in the PCM Board (Source: Dupont Energain® Datasheet)

	Input Value
PCM Board Thickness	0.0052 m (0.205 in.)
PCM Composite Density	865 kg/m^3 (54.0 lb$_m$/ft^3)*

*ConFD used a single density values.

Figures 7.3.6 and 7.3.7 show the comparisons between the predicted and experimental values for the retrofit south wall panel and retrofit west wall panel in M2SEC, respectively.

For the retrofit south wall panel, the average difference between predicted and experimental peaks of the heat fluxes was 2.8%. This is shown in Figure 7.3.6. The difference between predicted and experimental total heat transfer was 125.6%.

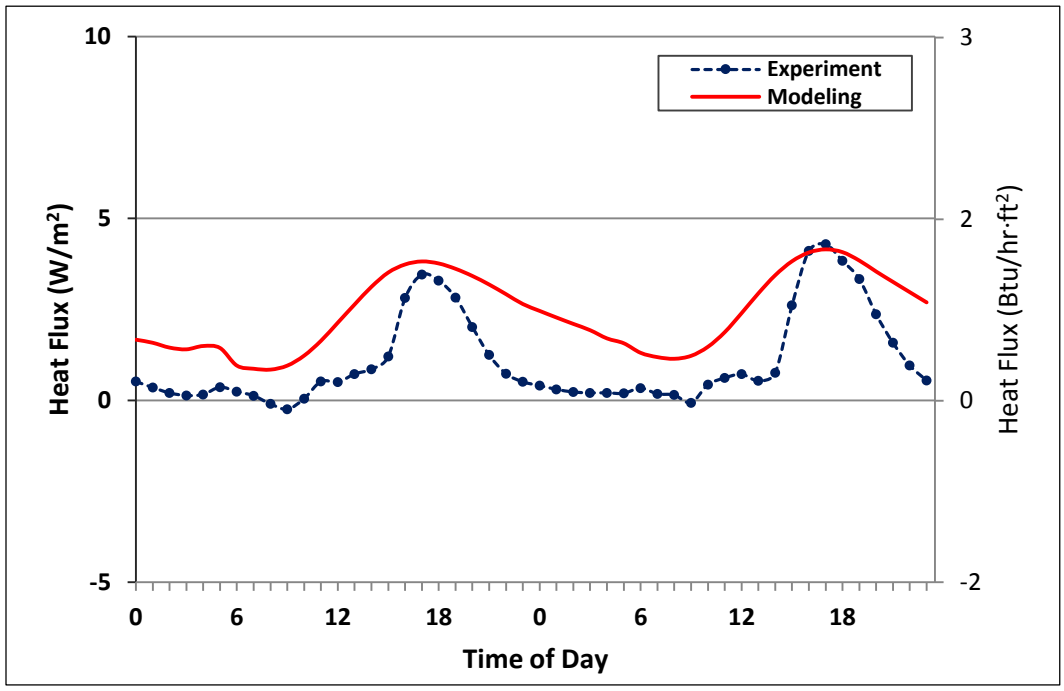

Figure 7.3.6. Predicted Heat Fluxes Across the Retrofit South Wall Panel in M2SEC Compared with the Experimental Data

For the retrofit west wall panel, the average difference between predicted and experimental peaks of the heat fluxes was -33.5%. This is shown in Figure 7.3.7. The difference between predicted and experimental total heat transfer was 65.5%.

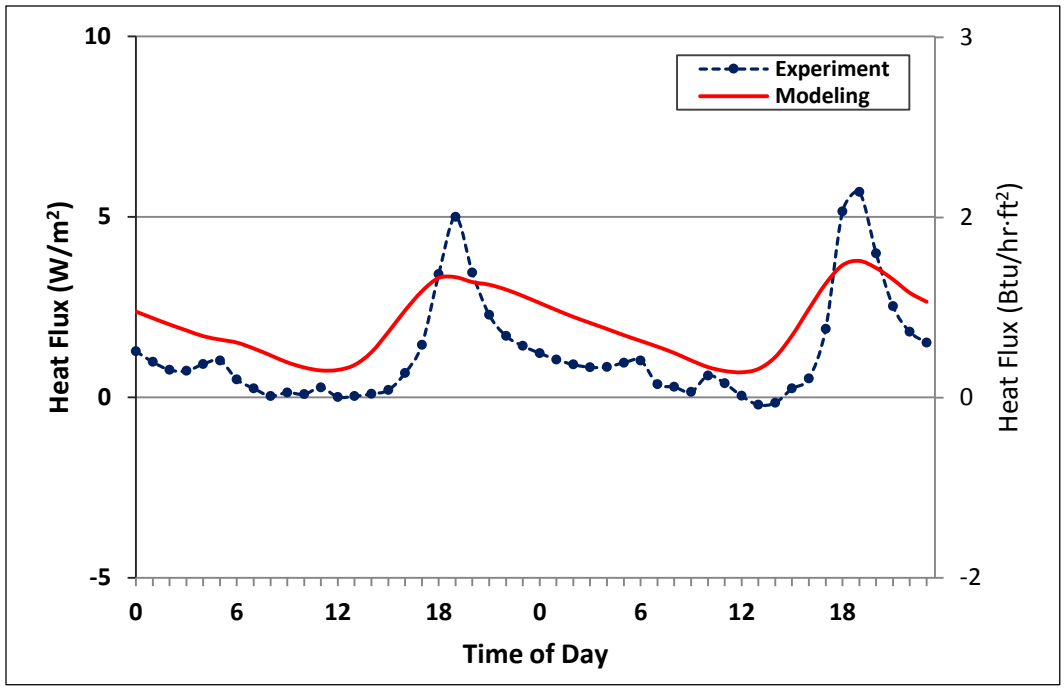

Figure 7.3.7. Predicted Heat Fluxes Across the Retrofit West Wall Panel in M2SEC Compared with the Experimental Data

It was obvious from the graphs of Figures 7.3.6 and 7.3.7 that CondFD was not able to model the integration of the PCM board into the M2SEC wall panels. The explanations set forth for similar discrepancies when modeling the PCM shield are true for the PCM board; however, other reasons exist. These were: (1) the weather data used in the simulations were not from a nearby location, (2) CondFD modeled an evenly distributed PCM within the polymer matrix of the board; however, from in-house microscopic images it was found that the PCM was not evenly distributed, and (3) the boards were lined with aluminum foil sheets on all sides, which CondFD could not take into account because of the foil thickness of less than 0.5 mm (0.02 in.). Given the severity of the discrepancies produced by the modeling of the integration of the PCM boards, no further effort was made at this time to continue with simulations

of commercial or institutional building walls outfitted with PCM boards as was done with residential walls with PCM shields (Chapter 8). This is because as stated previously the PCM shield modeling results were closer during both control and retrofit cases and the total heat transfer reductions produced by the PCM shield in both modeling and experiments were within a difference of 5.0% or less. This was not the case with the PCM boards.

CHAPTER VIII

COMPUTER SIMULATIONS

8.1 Representative Cities

EnergyPlus simulations related to the performance of walls and ceilings outfitted with PCM shields were carried out for four major cities, which were Miami, FL, Phoenix, AZ, Las Vegas, NV, and Kansas City, MO. These cities were superimposed on the DOE Climate Zone map which is shown in Figure 8.1.1.

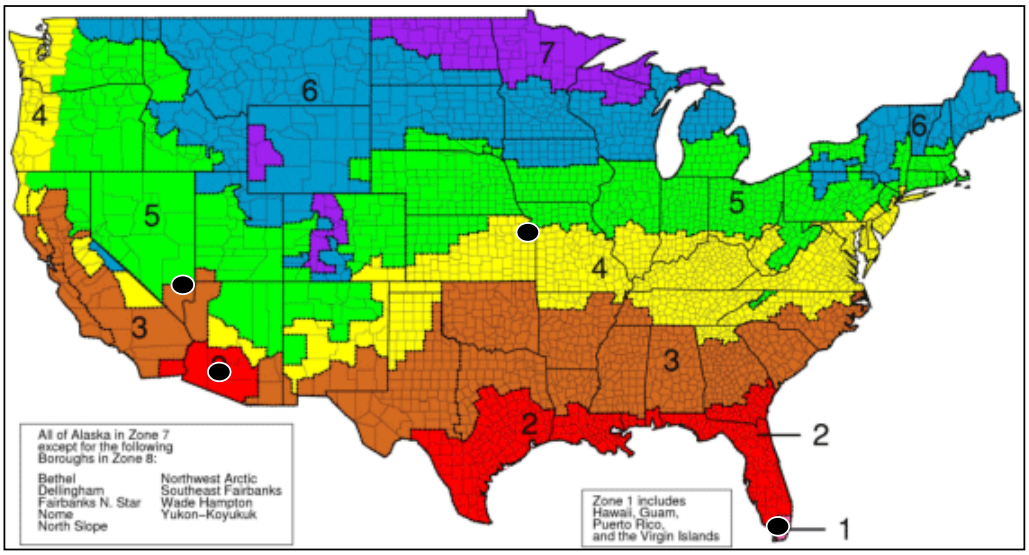

Figure 8.1.1. DOE Climate Zone Map Showing the Cities Included in the Simulation (Map Source: DOE, 2010)

These cities, which by their locations facilitated the inclusion of Climate Zones 1 - 4 in the DOE Climate Zone Map, were selected because their locations enabled a wide range of climatic conditions to be simulated, including climates such

as hot and humid (Zone 1 - Miami), hot and dry (Zone 2 - Phoenix), mixed dry (Zone 3 - Las Vegas), and mixed humid (Zone 4 - Kansas City) (DOE, 2010). Once the cities had been selected, TMY3 weather files for each of the cities were downloaded and linked to EnergyPlus. These weather files were downloaded from the Energy Efficiency & Renewable Energy (EERE) Office, of the US Department of Energy (DOE) website. The 'TMY' refers to typical meteorological year and the files provide typical weather conditions for a time span of 30 years. TMY data sets are composed of hourly values for one year (8,760 hours), which include solar irradiation, ambient air dry bulb, wet bulb, and dew point temperatures, wind speed and direction, cloud cover index, and many more. The TMY3 weather data sets used in this research represent the latest update and include values from 1976 through 2005 (Wilcox and Marion, 2008).

8.2 Model House

The model house used to carry out the simulations was a residential building of conventional construction. This house was a 228.0 m^2 (2,454 ft^2), one-story, slab-on-grade residence. The conditioned area was a 185.8 m^2 (2,000 ft^2). The garage area was unconditioned. Typical residence operating schedules of occupancy, lighting, and electric equipment were used in the simulation assuming three occupants. Table 8.2.1 shows the basic information of the model house and Figure 8.2.1 depicts its simple schematic of the model house used in the simulations.

Table 8.2.1. Model House Basic Information

Total Building Area	228.0 m^2 (2,454 ft^2)
Conditioned Area	185.8 m^2 (2,000 ft^2)
Construction Type	New
Front Orientation	North
Number of Stories	One
Floor Construction Type	Slab on Grade
Number of Conditioned Zones	One
Conditioned Volume	453.1m^3 (16,000 ft^3)
Conditioned Slab on Grade Area	185.8 m^2 (2,000 ft^2)
Conditioned Gross Wall Area	119.8 m^2 (1,289 ft^2)
Conditioned Gross South Wall Area	42.04 m^2 (452.5 ft^2)
Conditioned Gross West Wall Area	26.28 m^2 (282.9 ft^2)
Conditioned Gross Ceiling Area	185.8 m^2 (1999.9 $ft^{2)}$
Glazing Percentage	23.3 percent of Conditioned Gross Wall Area
Average Glazing U-Value	3.159 W/m^2°C (0.556 Btu/hr·ft^2°F)
Average Glazing SHGC*	0.762
Average Ceiling Height	2.44 m (8 ft)

*SHGC: Solar Heat Gain Coefficient

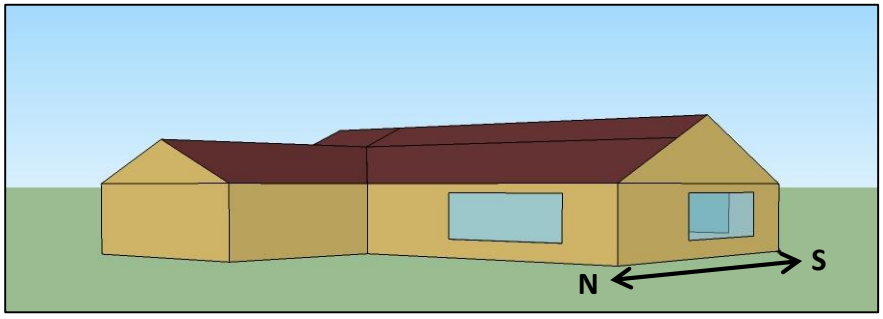

Figure 8.2.1. Schematic of the Model House Used in the Simulation

The wall construction was identical to the walls of the experimental test house described in Section 4.1.1. That is, the walls included the following layers: wood siding, insulation, and wallboard. In the simulations, it was assumed that only the south wall, the west wall, and the ceiling were outfitted with PCM shields. The reason for this was that there were no experimental data to validate either the north or east facing walls as these walls were compromised in the experimental set-up. That is, the east-facing wall was the main structural support for the fan coil unit and the north wall was the access door to the test house interior. Thus, in the simulation these walls were assumed to be of standard construction as the other two, but were not retrofitted with PCM shields.

Although not retrofitting all the walls is not a widespread practice, in the case of PCM retrofits it would make sense to not retrofit all the walls. The reason for this is that the main mode of operation of PCMs is to absorb heat during the warm period of the day and release this heat during the colder period of the day. With the case of retrofitting the east wall, the situation could arise that a part of the heat absorbed in the morning by the PCM could be released to the interior space during the afternoon. This has been observed in previous research (Fang, 2009a). The same reference indicated that care must be exercised when retrofitting the north wall for the same reasons indicated above.

From the experiments, it was observed that the peak heat fluxes and total heat transfer were reduced as a result of the retrofit of the building enclosure components (i.e., the south wall, the west wall, and the ceiling) compared to their control

counterparts. Also, the peak heat fluxes were delayed by a few hours once the components were retrofitted. In addition to these results, the reductions on peak heat fluxes and total heat transfer were different when the PCM shields were installed at different locations within the cavities of the south wall, the west wall, and the ceiling.

Although improvements in the thermal performance of the retrofit component were observed during the cooling season, their thermal performances during the heating season were not tested. However, buildings operate on a year-round basis; therefore, their thermal performance must be evaluated during the entire year. Accordingly, annual simulations were carried out to extrapolate the experimental results to estimate annual total heat transfer during the cooling and heating seasons for a conventional house. Four geographical locations were selected and their weather files used in the simulations because the thermal performance of the retrofit walls and ceiling would differ under various climates. In addition, the optimal location of the PCM shield for the most favorable thermal performance of the enclosure components would also differ depending on climate. From the experimental results, the optimal locations for the PCM shield varied for the south wall, west wall, and ceiling. These locations were location 3 for the south wall, location 2 or 3 for the west wall, and location 4 for the ceiling. This implied that the shield location had to be found for these enclosure components once the climates where the house was located changed. For example, the optimal location of the shield in the south wall may be different in the hot and humid climate, than in the mixed dry climate.

For this reason, a total of 17 simulation runs were performed: one run for a case of no PCM shield; five runs for each location of the PCM shield in the south wall, five runs for each location of the PCM shield in the west wall, and five runs for the ceiling; and one run for a combination of optimized locations of the PCM shield in all three enclosure components. All 17 simulations runs were carried out for a model house located in each of the cities. The indoor air temperatures were set at 26.6 and 22.0 °C (80.0 and 71.6 °F) for space cooling and space heating, respectively (ASHRAE, 2010).

8.3 EnergyPlus Simulations by Climate Type

8.3.1 Climate Zone 1 - Miami, FL

8.3.1.1 Climate Conditions for Miami, FL

The city of Miami, FL is located in DOE Climate Zone 1. Miami's climate is considered hot and humid, which means that summers are hot and humid while winters are dry. This climate is characterized by plenty of sunshine all year round. The summer temperatures range between the mid 20's to low 30's (low 80's to high 80's in degrees F). Average summer humidity levels are in the high 60's percent. Winter temperatures range from the mid 10's and high 10's (high 50's and mid 60's in degrees F) to the mid 20's (mid and high 70's in degrees F) (Sperling, 2013). A summary of Miami's climatic conditions is shown in Table 8.3.1.

Table 8.3.1. Climate Summary for the City of Miami, FL (Source: Sperling, 2013)

Miami, FL	Jan	Feb	Mar	Apr	May	June	July	Aug	Sep	Oct	Nov	Dec	Year
Avg. High Temperature (°C)	23.9	25.0	26.1	27.8	29.4	31.1	31.7	32.2	31.1	29.4	26.7	25.0	28.3
Avg. Low Temperature (°C)	15.0	15.6	17.8	20.0	22.2	23.9	24.4	24.4	24.4	22.2	18.9	16.1	20.6
Number of Days Warmer than 32.2 °C	0	0	Tr	1	3	9	14	16	10	2	0	0	55
Number of Days Cooler than 0 °C	Tr	0	Tr	0	0	0	0	0	0	0	0	Tr	Tr
Relative Humidity at 4-5 PM (%)	59	57	57	57	62	68	66	67	69	65	63	60	63
Avg. Wind Speed (knots)	8	10	10	10	9	9	8	8	9	10	11	8	9
Skycover (clear, scattered, broken, overcast)	Sct	Sct	Sct	Sct	Sct	Sct	Sct	Sct	Sct	Sct	Sct	Sct	Sct

8.3.1.2 Simulation Results for Miami, FL

From the simulation results, for the control case, the annual total heat transfer across the entire enclosure (i.e., walls, ceiling, floor, and windows) during the cooling and heating seasons were 36.6 GJ (34.69 MMBtu), and 2.2 GJ (2.09 MMBtu), respectively. Table 8.3.2 shows the summary of annual total heat transfer percent reductions per each enclosure component's area of the retrofit house as a result of installing the PCM shield during the cooling and heating seasons compared to the control house. The area of each enclosure component (i.e., south wall, west wall, and ceiling) is described in Table 8.2.1. The order of the PCM shield locations corresponded to the same locations as in the experiments (see Figures 5.1.6 and

5.1.28) from the interior side to the exterior side of the enclosure components. The 'heat in' in Table 8.3.2 refers to the amount of heat that entered into the conditioned space during the cooling season and 'heat out' refers to the amount of heat that went out from the conditioned space during the heating season. Figures 8.3.1, 8.3.2, and 8.3.3 show the total heat transfer percent reductions when the PCM shield was installed in the entire south wall, west wall, and ceiling, respectively.

The total heat transfer percent reductions during the cooling season were from 0.0022%/m^2 at location 5 in the ceiling to 0.0049%/m^2 at location 2 in the south wall. The total heat transfer percent reductions during the heating season were from 0.0542%/m^2 at location 5 in the west wall to 0.1553%/m^2 at location 2 in the south wall. From Figures 8.3.1, 8.3.2, and 8.3.3, the results showed that the total heat transfer reductions during the cooling season were not as much as the total heat transfer reductions during the heating season.

One noticeable result was that the PCM shield installation at location 1 in all three enclosure components should be avoided. The total heat transfer across the three components during both the cooling and heating seasons for PCM shield location 1 increased in all cases. The reason for this was that during the cooling season, the PCM absorbed the heat during the daytime while it melted and released it during the nighttime when it solidified. Furthermore, when the PCM shield was installed at location 1, which was closer to the indoor, the PCM released the heat right back into the conditioned space. This resulted in the increase of total heat transfer into the conditioned space. During the heating season, the PCM shield prevented heat from

going in; however, during this season such heat into the conditioned space was desired yet the shield blocked it in a similar manner as it did during the cooling season case when it was placed at location 1.

Based on Table 8.3.2, locations 2 were chosen for all cases because they showed the largest total heat transfer reductions of all. In Figure 8.3.4, which was generated from simulations when the PCM shields were installed at locations 2 in all three components, the total heat transfer percent reductions were 1.0% and 25.7% for the cooling and heating seasons, respectively.

Table 8.3.2. Annual Total Heat Transfer Reductions per Unit Area for Various Locations of the PCM Shield for Miami, FL

		PCM Shield Location				
		1	2	3	4	5
Reduction of Heat in (%/m^2)	South Wall	-0.0515	0.0049	0.0039	0.0033	0.0026
	West Wall	-0.0814	0.0046	0.0037	0.0030	0.0023
	Ceiling	-0.0655	0.0045	0.0037	0.0031	0.0022
Reduction of Heat out (%/m^2)	South Wall	-0.3832	0.1553	0.1262	0.1171	0.1102
	West Wall	-0.3775	0.0887	0.0628	0.0544	0.0542
	Ceiling	-0.4066	0.0974	0.0675	0.0571	0.0559

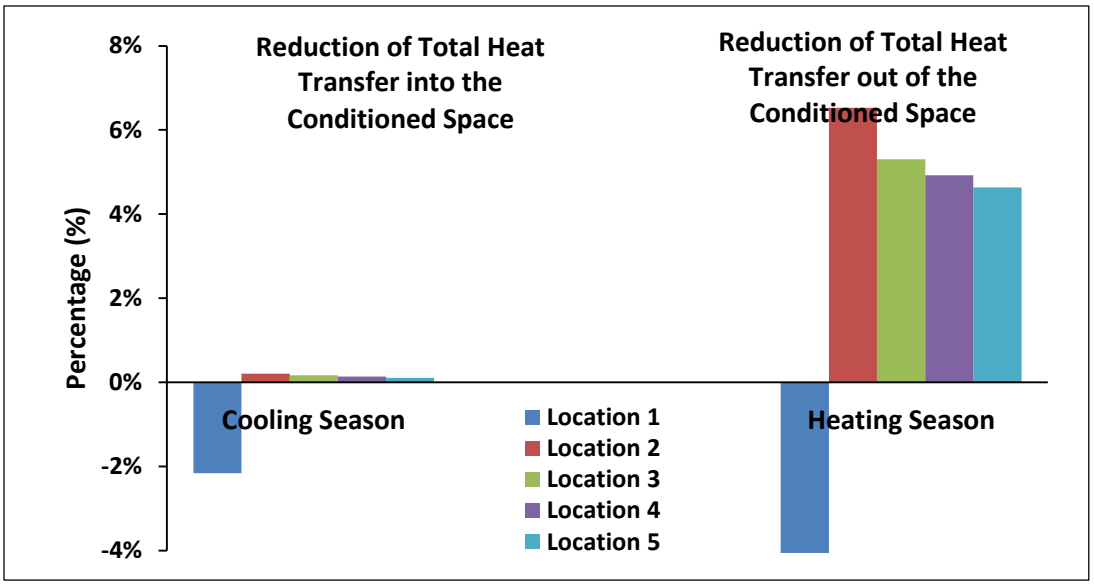

Figure 8.3.1. Reductions in Total Heat Transfer at Various Locations of the PCM Shield in the South Wall for Miami, FL

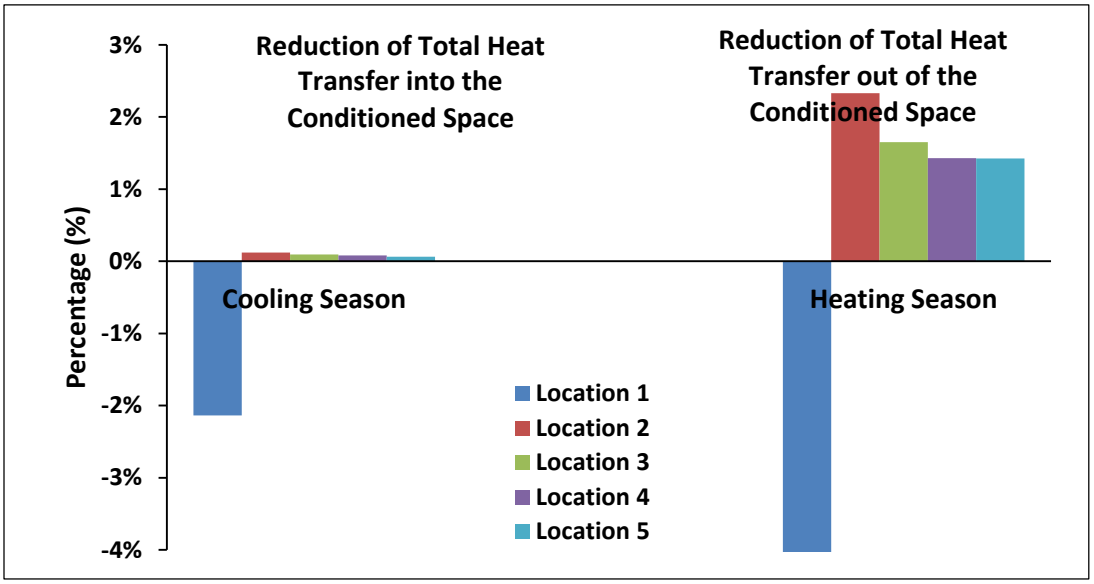

Figure 8.3.2. Reductions in Total Heat Transfer at Various Locations of the PCM Shield in the West Wall for Miami, FL

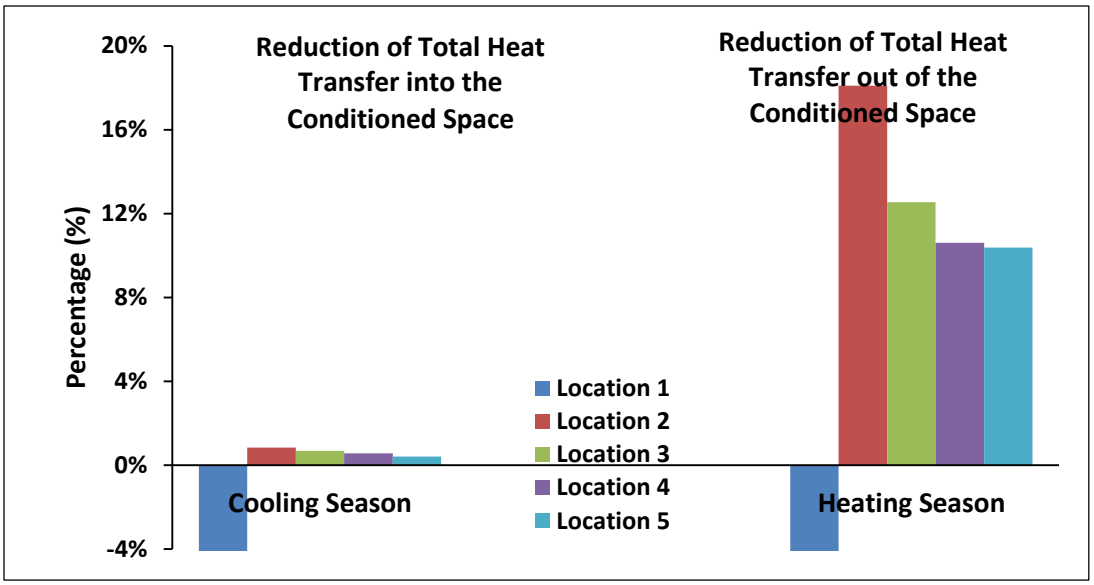

Figure 8.3.3. Reductions in Total Heat Transfer at Various Locations of the PCM Shield in the Ceiling for Miami, FL

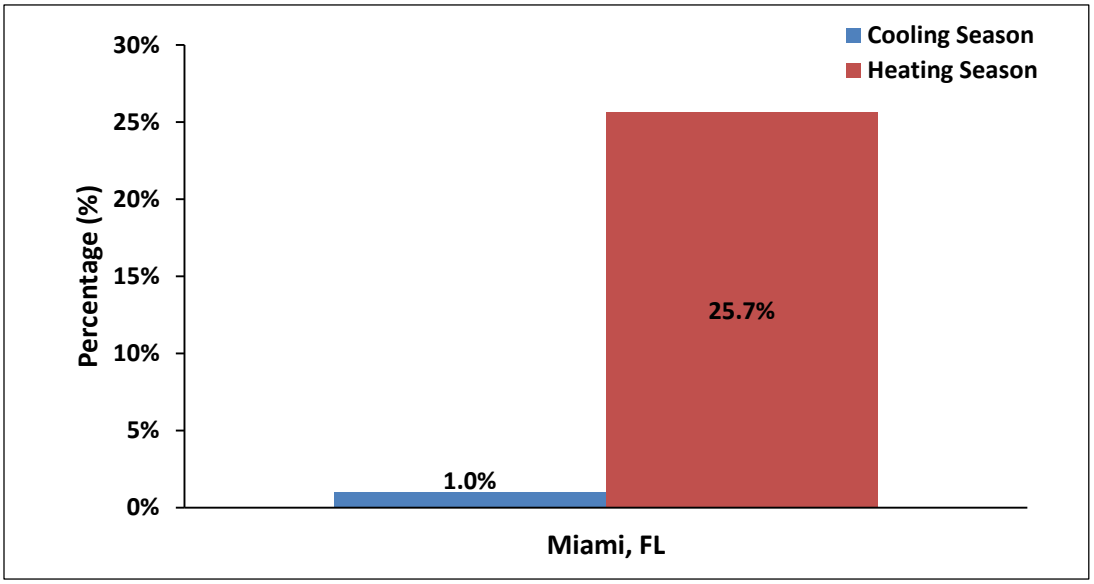

Figure 8.3.4. Total Heat Transfer Reduction at Combined Optimum Locations of the PCM Shield in the South Wall, West Wall and Ceiling for Miami, FL (the north and east walls were not retrofitted)

8.3.2 Climate Zone 2 - Phoenix, AZ

8.3.2.1 Climate Conditions for Phoenix, AZ

The city of Phoenix, AZ is located in DOE Climate Zone 2. This climate is a hot and dry climate. Phoenix is one of the hottest cities in the United States. The temperature in this city registers greater than 32.2 °C (90.0 °F) an average of 167 days out of the year, mostly between May and September. Most days are clear and sunny. Winters are mild, with sunny days, with an occasional fog. Frost is frequent in winter months (Sperling, 2013). A summary of Phoenix's climatic conditions is shown in Table 8.3.3.

Table 8.3.3. Climate Summary for the City of Phoenix, AZ (Source: Sperling, 2013)

Phoenix, AZ	Jan	Feb	Mar	Apr	May	June	July	Aug	Sep	Oct	Nov	Dec	Year
Avg. High Temperature (°C)	18.9	21.1	23.9	28.9	33.9	39.4	40.6	39.4	37.2	31.1	23.9	19.4	30.0
Avg. Low Temperature (°C)	4.4	6.7	8.9	12.8	17.2	22.2	26.7	25.6	22.2	15.6	8.9	5.0	15.0
Number of Days Warmer than 32.2 °C	0	Tr	2	9	22	29	31	31	28	15	Tr	0	167
Number of Days Cooler than 0 °C	4	2	Tr	0	0	0	0	0	0	0	1	3	10
Relative Humidity at 4-5 PM (%)	34	28	24	17	14	12	21	24	23	24	28	34	24
Avg. Wind Speed (knots)	5	6	6	6	6	8	7	6	6	6	6	5	6
Skycover (clear, scattered, broken, overcast)	Clr	Clr	Clr	Clr	Clr	Clr	Clr	Clr	Clr	Clr	Clr	Clr	Clr

8.3.2.2 Simulation Results for Phoenix, AZ

From the simulation results, for the control case, the annual total heat transfer across the entire enclosure during the cooling and heating seasons were 60.2 GJ (57.06 MMBtu) and 6.9 GJ (6.54 MMBtu), respectively. Table 8.3.4 shows the summary of annual total heat transfer percent reductions per each enclosure component's area of the retrofit house as a result of installing PCM shields during the cooling and heating seasons compared to the control house. Figures 8.3.5, 8.3.6, and 8.3.7 show the total heat transfer percent reductions when the PCM shield was installed in the entire south wall, west wall, and ceiling, respectively.

The total heat transfer reductions during the cooling season were from 0.0008%/m^2 at locations 5 in the west wall and the ceiling to 0.0025%/m^2 at location 2 in the south wall. The total heat transfer percent reductions during the heating season were from 0.0357%/m^2 at location 5 in the west wall to 0.1187%/m^2 at location 2 in the south wall. From Figures 8.3.5, 8.3.6, and 8.3.7, similar to Zone 1, the results showed that the total heat transfer reductions during the cooling season were not as much as the total heat transfer reductions during the heating season.

The same noticeable results found in the simulations for Zone 1, the PCM shield installation at location 1 in all three enclosure component should be avoided. The total heat transfer across the three components during both the cooling and heating seasons for PCM shield location 1 increased in all cases. The reason for this is the same as explained in the previous section.

Based on Table 8.3.4, locations 2 were chosen for all cases because they showed the largest total heat transfer percent reductions of all. In Figure 8.3.8, which was generated from simulations when the PCM shields were installed at locations 2 in all three components, the total heat transfer reductions were 0.5% and 16.6% for the cooling and heating seasons, respectively.

Table 8.3.4. Annual Total Heat Transfer Reductions per Unit Area for Various Locations of the PCM Shield for Phoenix, AZ

		PCM Shield Location				
		1	2	3	4	5
Reduction of Heat in (%/m^2)	South Wall	-0.1133	0.0025	0.0017	0.0013	0.0010
	West Wall	-0.1280	0.0022	0.0015	0.0011	0.0008
	Ceiling	-0.1014	0.0022	0.0016	0.0012	0.0008
Reduction of Heat out (%/m^2)	South Wall	-0.5034	0.1187	0.1022	0.0974	0.0866
	West Wall	-0.4915	0.0559	0.0414	0.0362	0.0357
	Ceiling	-0.5020	0.0612	0.0449	0.0385	0.0364

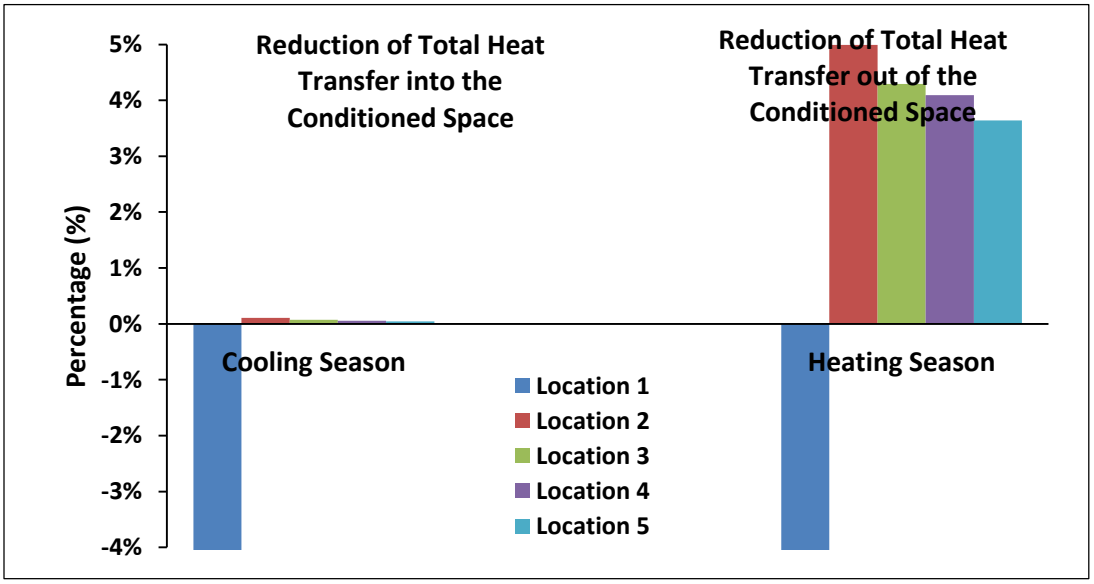

Figure 8.3.5. Reductions of Total Heat Transfer at Various Locations of the PCM Shield in the South Wall for Phoenix, AZ

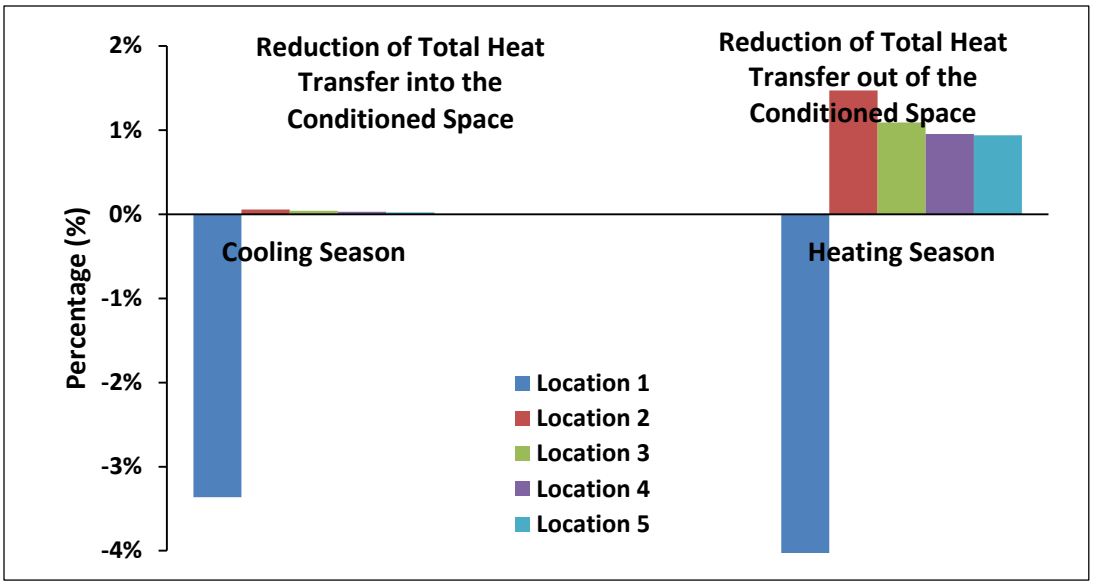

Figure 8.3.6. Reductions of Total Heat Transfer at Various Locations of the PCM Shield in the West Wall for Phoenix, AZ

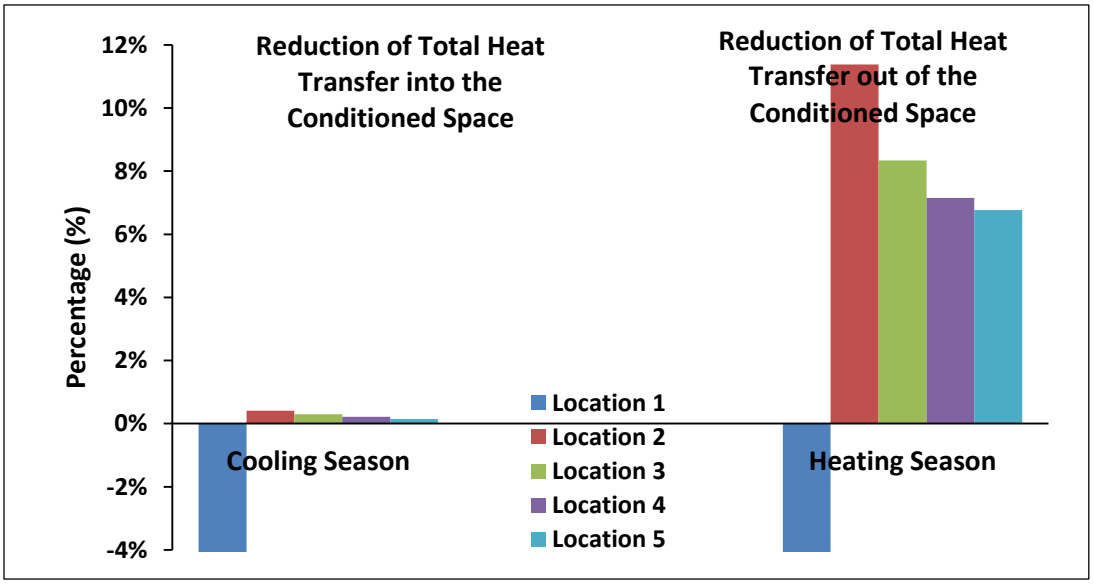

Figure 8.3.7. Reductions of Total Heat Transfer at Various Locations of the PCM Shield in the Ceiling for Phoenix, AZ

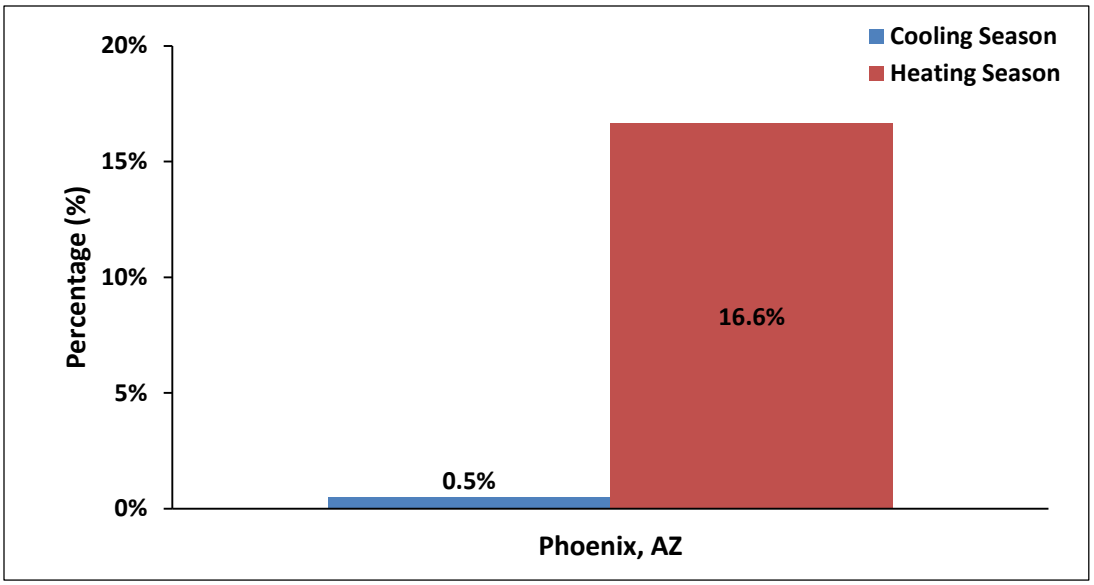

Figure 8.3.8. Total Heat Transfer Reduction at Combined Optimum Locations of the PCM Shield in the South Wall, West Wall and Ceiling for Phoenix, AZ (the north and east walls were not retrofitted)

8.3.3 Climate Zone 3 - Las Vegas, NV

8.3.3.1 Climate Conditions for Las Vegas, NV

The city of Las Vegas, NV is located in DOE Climate Zone 3. The climate in Las Vegas is considered a mixed dry climate with desert-liked characteristics. The city enjoys plenty of sunshine all year round. In the hottest part of the summer, July and August, the temperatures reach above 38.0 °C (100.0 °F). Winters are cooler with daytime highs in the mid 10's (60's in degrees F) and chilly nights in the low 1's (40's in degrees F). Las Vegas sees little rain, most of it in winter. There are some occasional thunderstorms in summers, most of them in late afternoons that come from the south (Sperling, 2013). A summary of Las Vegas' climatic conditions is shown in Table 8.3.5.

Table 8.3.5. Climate Summary for the City of Las Vegas, NV (Source: Sperling, 2013)

Las Vegas, NV	Jan	Feb	Mar	Apr	May	June	July	Aug	Sep	Oct	Nov	Dec	Year
Avg. High Temperature (°C)	13.3	16.7	20.6	25.6	31.1	37.2	40.0	38.9	34.4	27.2	18.9	13.9	26.7
Avg. Low Temperature (°C)	0.6	3.3	6.1	10.6	15.6	20.6	24.4	23.3	18.9	12.2	5.0	1.1	11.7
Number of Days Warmer than 32.2 °C	0	0	Tr	3	15	26	31	30	23	6	0	0	134
Number of Days Cooler than 0 °C	14	6	2	Tr	0	0	0	0	0	Tr	3	12	37
Relative Humidity at 4-5 PM (%)	32	25	20	15	13	10	14	16	16	18	26	31	20
Avg. Wind Speed (knots)	7	7	12	13	13	13	11	11	11	7	7	7	10
Skycover (clear, scattered, broken, overcast)	Clr	Clr	Clr	Clr	Clr	Clr	Clr	Clr	Clr	Clr	Clr	Clr	Clr

8.3.3.2 Simulation Results for Las Vegas, NV

From the simulation results, for the control case, the annual total heat transfer across the entire enclosure during the cooling and heating seasons were 52.2 GJ (49.44 MMBtu) and 14.46 GJ (13.69 MMBtu), respectively. Table 8.3.6 shows the summary of annual total heat transfer percent reductions per each enclosure component's area of the retrofit house as a result of installing PCM shields during the cooling and heating seasons compared to the control house. Figures 8.3.9, 8.3.10, and 8.3.11 show the total heat transfer percent reductions when the PCM shield was installed in the entire south wall, west wall, and ceiling, respectively.

The total heat transfer reductions during the cooling season were from 0.0022%/m^2 at locations 5 in the west wall to 0.0054%/m^2 at location 2 in the south wall. The total heat transfer percent reductions during the heating season were from 0.0147%/m^2 at location 5 in the west wall to 0.0579%/m^2 at location 2 in the south wall. From Figures 8.3.9, 8.3.10, and 8.3.11, similar to Zones 1 and 2, the results showed that the total heat transfer reductions during the cooling season were not as much as the total heat transfer reductions during the heating season. The same noticeable results found in the simulations for Zones 1 and 2, the PCM shield installation at location 1 in all three enclosure component should be avoided. The reason for this is also explained in the previous section for Zone 1.

Based on Table 8.3.6, locations 2 were chosen for all cases because they showed the largest total heat transfer percent reductions of all. In Figure 8.3.12, which was generated from simulations when the PCM shields were installed at locations 2 in all three components, the total heat transfer reductions were 1.10% and 8.15% for the cooling and heating seasons, respectively.

Table 8.3.6. Annual Total Heat Transfer Reductions per Unit Area for Various Locations of the PCM Shield for Las Vegas, NV

		PCM Shield Location				
		1	2	3	4	5
Reduction of Heat in (%/m^2)	South Wall	-0.0935	0.0054	0.0040	0.0032	0.0027
	West Wall	-0.1050	0.0044	0.0031	0.0025	0.0022
	Ceiling	-0.0829	0.0047	0.0035	0.0028	0.0024
Reduction of Heat out (%/m^2)	South Wall	-0.4234	0.0579	0.0501	0.0477	0.0446
	West Wall	-0.4345	0.0252	0.0185	0.0157	0.0147
	Ceiling	-0.3940	0.0291	0.0211	0.0179	0.0167

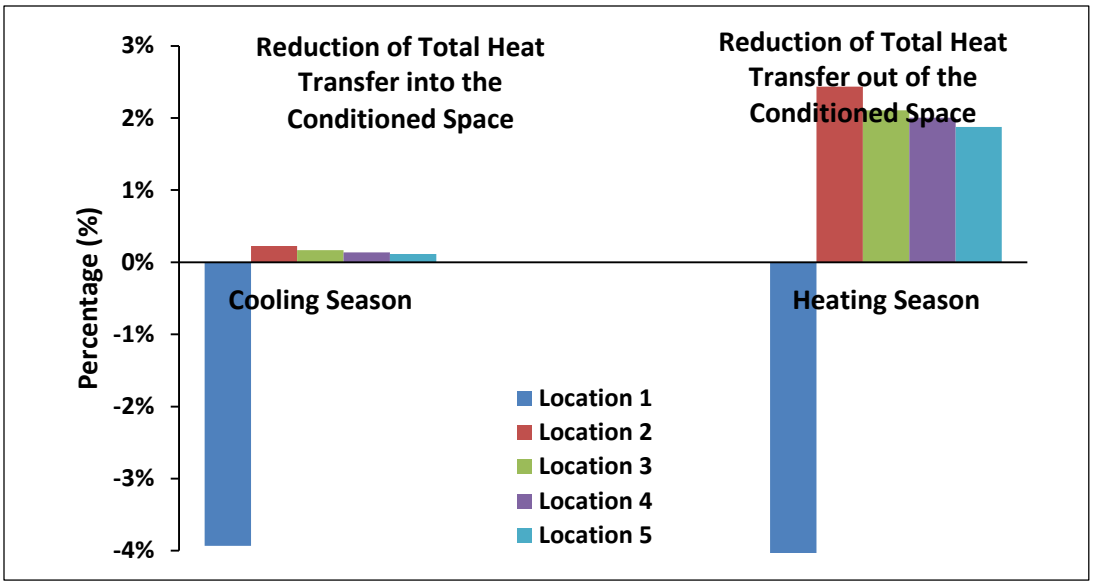

Figure 8.3.9. Reductions of Total Heat Transfer at Various Locations of the PCM Shield in the South Wall for Las Vegas, NV

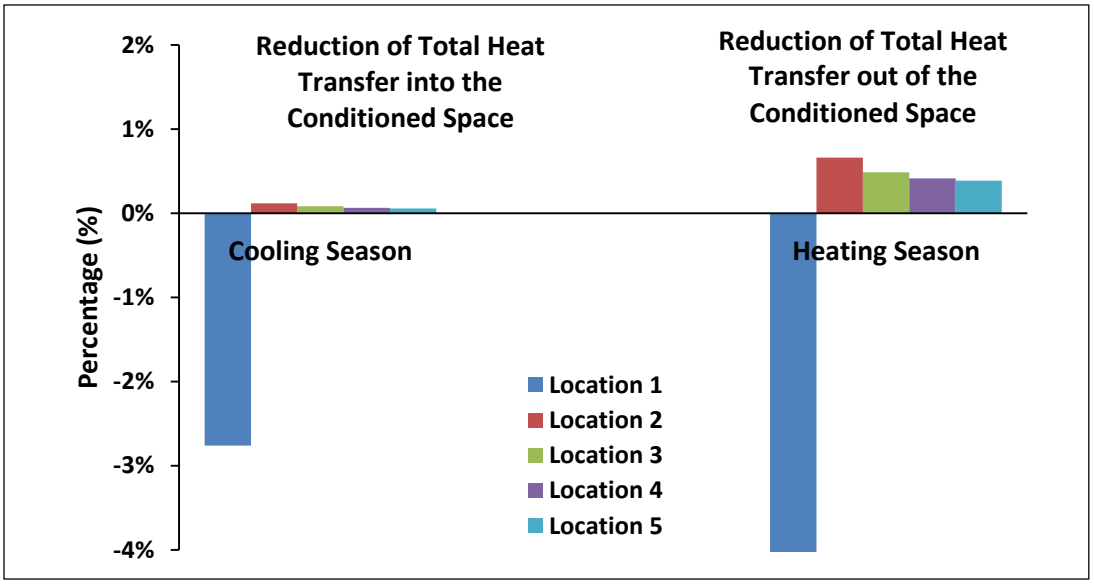

Figure 8.3.10. Reductions of Total Heat Transfer at Various Locations of the PCM Shield in the West Wall for Las Vegas, NV

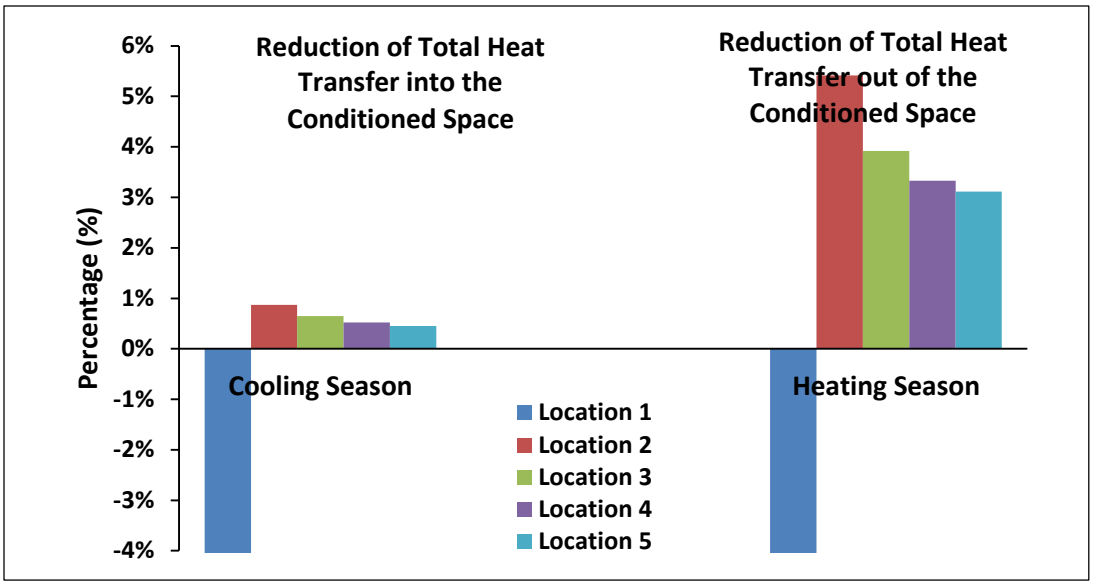

Figure 8.3.11. Reductions of Total Heat Transfer at Various Locations of the PCM Shield in the Ceiling for Las Vegas, NV

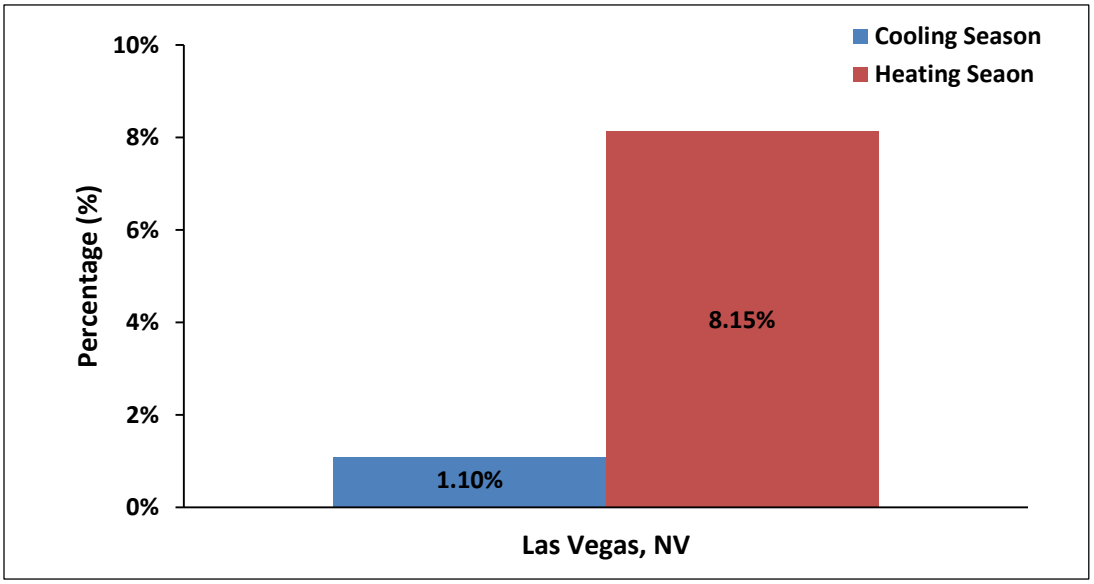

Figure 8.3.12. Total Heat Transfer Reduction at Combined Optimum Locations of the PCM Shield in the South Wall, West Wall and Ceiling for Las Vegas, NV (the north and east walls were not retrofitted)

8.4.4 Climate Zone 4 - Kansas City, MO

8.4.4.1 Climate Conditions for Kansas City, MO

The city of Kansas City, MO is located in DOE Climate Zone 4. Kansas City's climate is considered mixed humid, experiencing extreme hot and cold temperatures. Summers in Kansas City are very humid, with moist air riding up from the Gulf of Mexico. July and August are the hottest months where temperatures surpass 37.8 °C (100.0 °F). During the winter months, from November through February, the weather conditions range from mild to very cold (Sperling, 2013). A summary of Kansas City's climatic conditions is shown in Table 8.3.7.

Table 8.3.7. Climate Summary for the City of Kansas City, MO (Source: Sperling, 2013)

Kansas City, MO	Jan	Feb	Mar	Apr	May	June	July	Aug	Sep	Oct	Nov	Dec	Year
Avg. High Temperature (°C)	1.7	4.4	12.2	18.3	23.3	28.9	32.2	30.6	26.1	18.9	11.1	3.9	17.8
Avg. Low Temperature (°C)	-8.3	-5.6	1.1	6.7	12.2	17.2	20.6	18.9	14.4	7.2	1.1	-6.1	6.7
Number of Days Warmer than 32.2 °C	0	0	0	Tr	Tr	6	16	12	4	Tr	0	0	39
Number of Days Cooler than 0 °C	28	22	14	4	Tr	0	0	0	0	2	13	26	110
Relative Humidity at 4-5 PM (%)	58	59	54	50	54	54	51	53	53	51	57	60	54
Avg. Wind Speed (knots)	12	11	13	13	12	11	10	10	11	11	12	11	11
Skycover (clear, scattered, broken, overcast)	Ovr	Ovr	Ovr	Ovr	Ovr	Clr	Clr	Clr	Clr	Clr	Ovr	Ovr	Ovr

8.4.4.2 Simulation Results for Kansas City, MO

From the simulation results, for the control case, the annual total heat transfer across the entire enclosure during the cooling and heating seasons were 28.6 GJ (27.09 MMBtu) and 42.0 GJ (39.78 MMBtu), respectively. Table 8.3.8 shows the summary of annual total heat transfer percent reductions per each enclosure component's area of the retrofit house as a result of installing PCM shields during the cooling and heating seasons compared to the control house. Figures 8.3.13, 8.3.14, and 8.3.15 show the total heat transfer percent reductions when the PCM shield was installed in the entire south wall, west wall, and ceiling, respectively.

The total heat transfer reductions during the cooling season were from 0.0081%/m^2 at locations 5 in the west wall to 0.0173%/m^2 at location 2 in the south wall. The total heat transfer percent reductions during the heating season were from 0.0017%/m^2 at location 5 in the west wall to 0.0059%/m^2 at location 2 in the south wall. From Figures 8.3.13, 8.3.14, and 8.3.15, the results showed that the total heat transfer reductions during the heating season were not as much as the total heat transfer reductions during the cooling season.

Similar to Zones 1, 2, and 3, the PCM shield installation at location 1 in all three enclosure component should be avoided. The total heat transfer across the three components during both the cooling and heating seasons for PCM shield location 1 increased in all cases. The reason for this is the same as explained in the section for Zone 1.

Based on Table 8.3.8, locations 2 were chosen for all cases because they showed the largest total heat transfer percent reductions of all. In Figure 8.3.16, which was generated from simulations when the PCM shields were installed at locations 2 in all three components, the total heat transfer reductions were 0.88% and 3.83% for the cooling and heating seasons, respectively.

Table 8.3.8. Annual Total Heat Transfer Reductions per Unit Area for Various Locations of the PCM Shield for Kansas City, MO

		PCM Shield Location				
		1	2	3	4	5
Reduction of Heat in (%/m^2)	South Wall	-0.0453	0.0173	0.0137	0.0121	0.0108
	West Wall	-0.0612	0.0142	0.0106	0.0090	0.0081
	Ceiling	-0.0400	0.0160	0.0123	0.0108	0.0103
Reduction of Heat out (%/m^2)	South Wall	-0.2999	0.0059	0.0051	0.0047	0.0045
	West Wall	-0.3143	0.0027	0.0021	0.0018	0.0017
	Ceiling	-0.2497	0.0031	0.0024	0.0020	0.0018

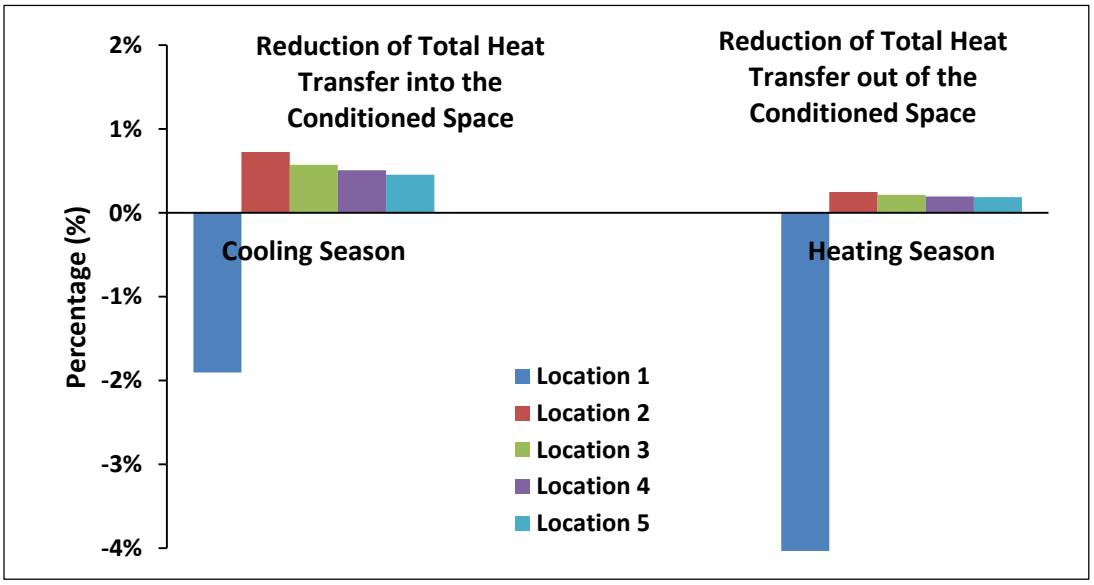

Figure 8.3.13. Reductions of Total Heat Transfer at Various Locations of the PCM Shield in the South Wall for Kansas City, MO

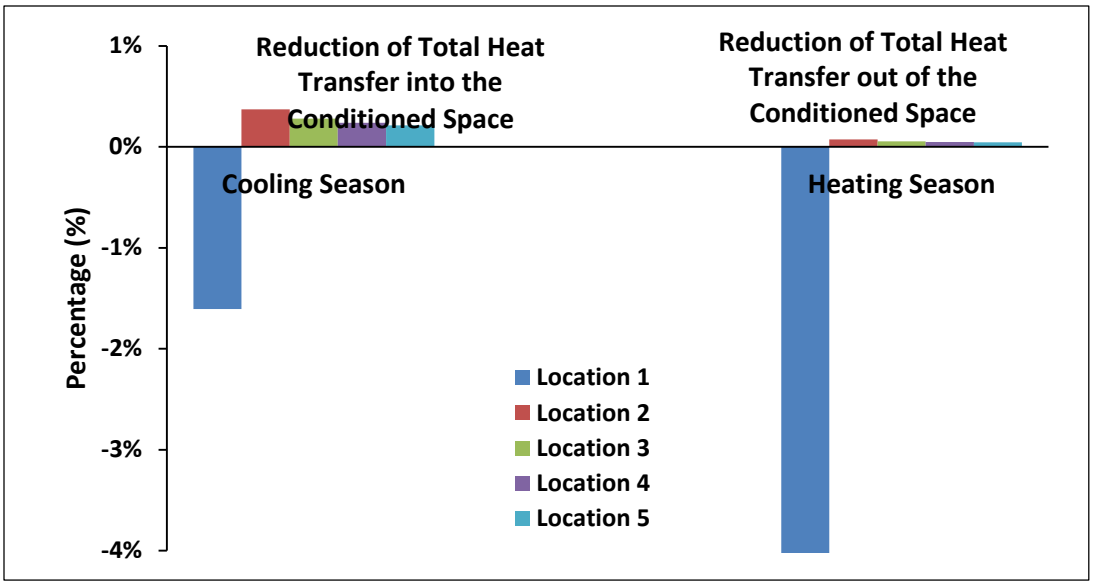

Figure 8.3.14. Reductions of Total Heat Transfer at Various Locations of the PCM Shield in the West Wall for Kansas City, MO

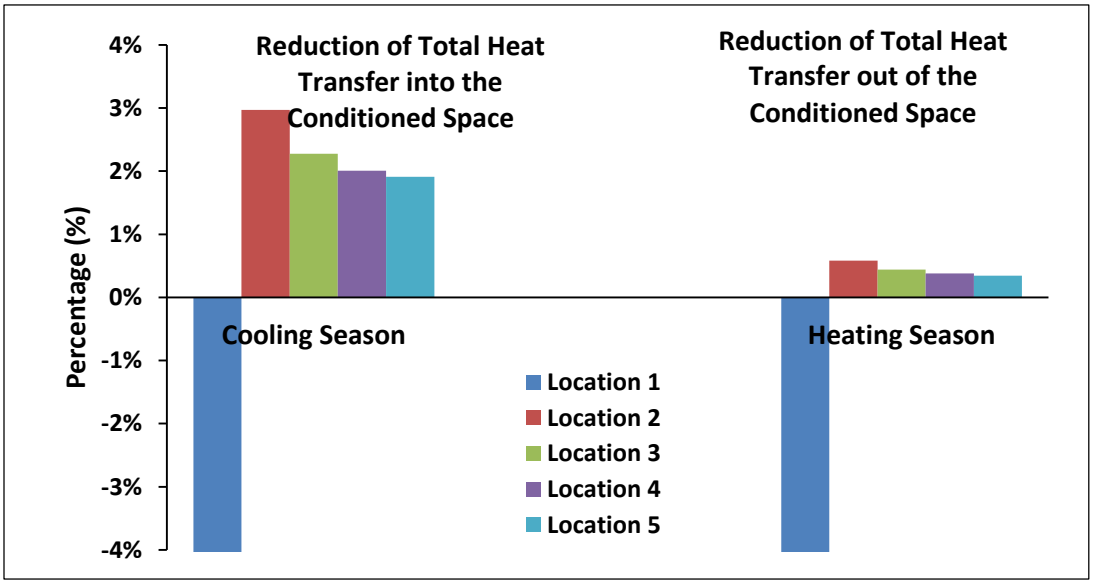

Figure 8.3.15. Reductions of Total Heat Transfer at Various Locations of the PCM Shield in the Ceiling for Kansas City, MO

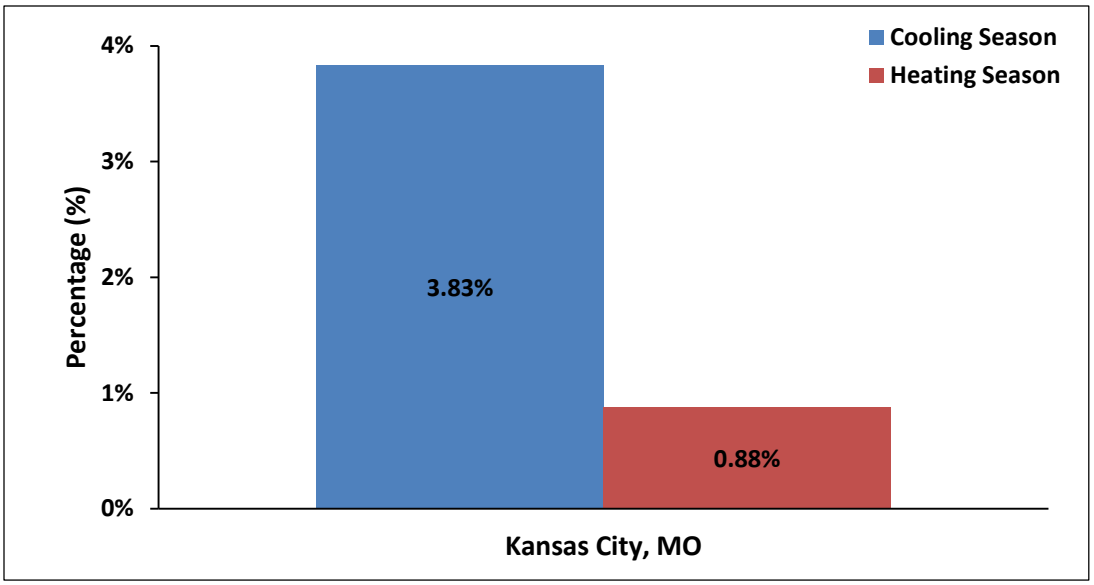

Figure 8.3.16. Total Heat Transfer Reduction at Combined Optimum Locations of the PCM Shield in the South Wall, West Wall and Ceiling for Kansas City, MO (the north and east walls were not retrofitted)

8.4 Computer Simulation Discussion

Figure 8.4.1 depicts the results generated from simulations when the PCM shield was installed at optimum locations (location 2 for all cases). The average percent reduction in total heat transfer into the conditioned space during the cooling season was 1.6%. The trend implied that this reduction increased as the location of the house moved from a hot and humid to a mixed humid climate. The opposite was true with the reduction of total heat transfer out of the conditioned space during the heating season, which the trend showed that the colder regions would see a lower percentage of this reduction. The explanation for these trends is more related to the calculation of the percent difference, which yields larger reductions in the cases where the values are smaller. For example, there is little heating in a climate like the

one where Miami is located; therefore, smaller differences in total heat transfer produce larger percent reduction values.

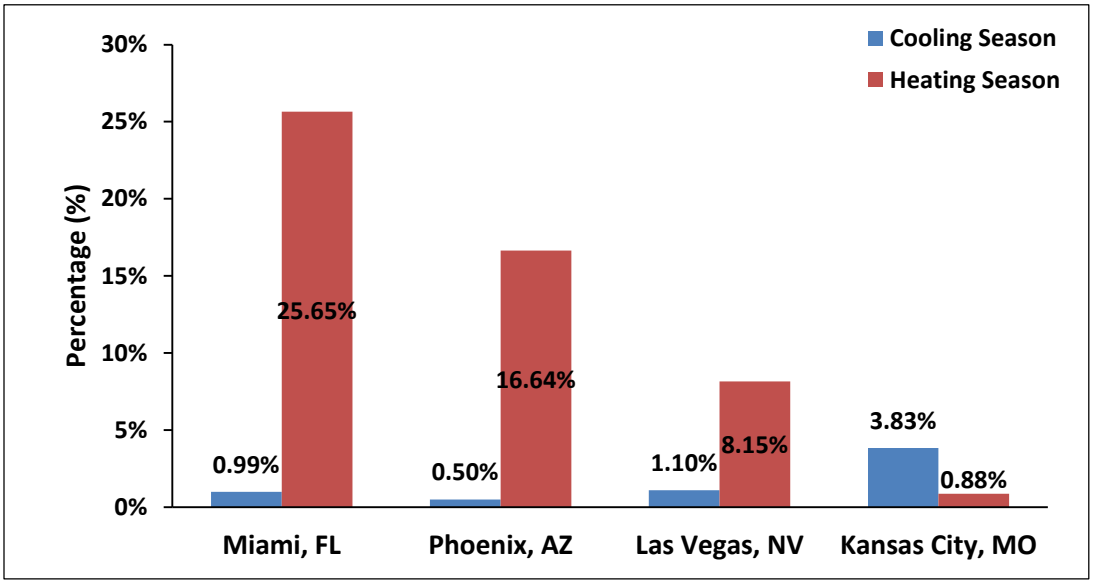

Figure 8.4.1. Comparison of Total Heat Transfer Reductions at Combined Optimal Locations of the PCM Shield in the South Wall, West Wall, and Ceiling for the Various Cities.

8.5 Overall Space Cooling and Space Heating Energy Reductions

The overall space cooling and space heating energy that would be required to keep the conditioned space of the model house under comfortable conditions were simulated. The results in space cooling energy percent reductions, space cooling energy demand percent reductions, and space heating energy percent reductions are summarized in Figure 8.5.1 for the model house located in all four climate zones.

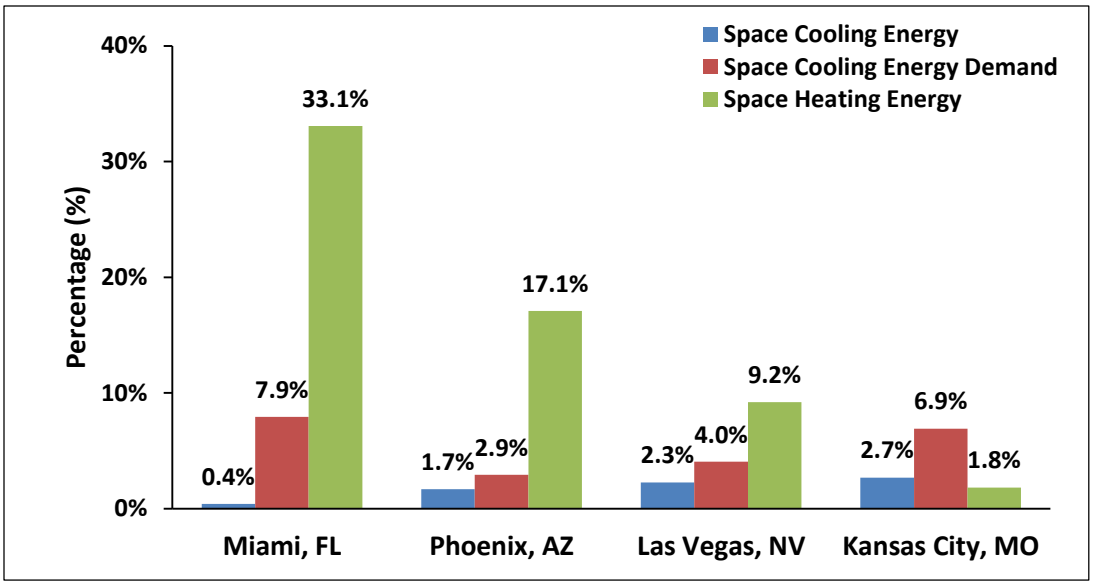

Figure 8.5.1. Reductions of Space Cooling Energy, Space Cooling Energy Demand, and Space Heating Energy at Combined Optimal Locations of the PCM Shield in the South Wall, West Wall, and Ceiling for the Various Cities

For the control house located in Zone 1 (Miami, FL), the space cooling energy use was estimated at 40.26 GJ (38.13 MMBtu). The overall electric energy consumption, which included space cooling, lighting, appliances and equipment, and HVAC fans for the summer months, was estimated at 77.29 GJ (73.20 MMBtu). Once the PCM shield was installed in the south wall, west wall, and ceiling, in all cases in location 2, the space cooling energy was reduced by 0.16 GJ (0.15 MMBtu) or 0.4% of the total space cooling energy use. In other words, the retrofit space cooling energy was 40.10 GJ (37.98 MMBtu). The result is shown in Figure 8.5.1.

The space cooling energy demand for the control house was estimated at 4.90 kW (16.73 MBtu/hr). The overall electric energy demand, which included space cooling, lighting, appliances and equipment, and HVAC fans for the summer months, was estimated at 7.08 kW (24.16 MBtu/hr). Once the PCM shield was installed in the

south wall, west wall, and ceiling, in all cases in location 2, the space cooling energy demand was reduced by 0.39 kW (1.33 MBtu/hr) or 7.9% of the total space cooling energy demand. The reason for this is related to total heat transfer rate peak reduction.

The space heating energy use for the control house was estimated at 1.33 GJ (1.26 MMBtu). In this case, the overall natural gas consumption was the same as the space heating energy use since no hot water system was simulated. Once the PCM shield was installed in the south wall, west wall, and ceiling, in all cases in location 2, the space heating energy use was reduced by 0.44 GJ (0.42 MMBtu) or 33.1% of the total space heating energy consumption.

For the control house located in Zone 2 (Phoenix, AZ), the space cooling energy use was estimated at 47.45 GJ (44.94 MMBtu). The overall electric energy consumption was estimated at 84.48 GJ (80.01 MMBtu). Once the PCM shield was installed in the south wall, west wall, and ceiling, in all cases in location 2, the space cooling energy was reduced by 0.8 GJ (0.76 MMBtu) or 1.7% of the total space cooling energy use.

The space cooling energy demand for the control house was estimated at 8.96 kW (30.57 MBtu/hr). The overall electric energy demand was estimated at 6.79 kW (23.17 MBtu/hr). Once the PCM shield was installed in the south wall, west wall, and ceiling, in all cases in location 2, the space cooling energy demand was reduced by 0.20 kW (0.68 MBtu/hr) or 2.9% of the total space cooling energy demand.

The space heating energy use for the control house was estimated at 10.0 GJ (9.47 MMBtu). Once the PCM shield was installed in the south wall, west wall, and

ceiling, in all cases in location 2, the space heating energy use was reduced by 1.71 GJ (1.62 MMBtu) or 17.1% of the total space heating energy consumption.

For the control house located in Zone 3 (Las Vegas, NV), the space cooling energy use was estimated at 35.51 GJ (33.63 MMBtu). The overall electric energy consumption was estimated at 72.54 GJ (68.70 MMBtu). Once the PCM shield was installed in the south wall, west wall, and ceiling, in all cases in location 2, the space cooling energy was reduced by 0.8 GJ (0.76 MMBtu) or 2.3% of the total space cooling energy use.

The space cooling energy demand for the control house was estimated at 6.82 kW (23.27 MBtu/hr). The overall electric energy demand was estimated at 9.0 kW (30.71 MBtu/hr). Once the PCM shield was installed in the south wall, west wall, and ceiling, in all cases in location 2, the space cooling energy demand was reduced by 0.30 kW (1.02 MBtu/hr) or 4.0% of the total space cooling energy demand.

The space heating energy use for the control house was estimated at 23.61 GJ (22.36 MMBtu). Once the PCM shield was installed in the south wall, west wall, and ceiling, in all cases in location 2, the space heating energy use was reduced by 2.17 GJ (2.06 MMBtu) or 9.2% of the total space heating energy consumption.

For the control house located in Zone 4 (Kansas City, MO), the space cooling energy use was estimated at 17.85 GJ (16.91 MMBtu). The overall electric energy consumption was estimated at 54.88 GJ (51.98 MMBtu). Once the PCM shield was installed in the south wall, west wall, and ceiling, in all cases in location 2, the space

cooling energy was reduced by 0.48 GJ (0.45 MMBtu) or 2.7% of the total space cooling energy use.

The space cooling energy demand for the control house was estimated at 5.20 kW (17.74 MBtu/hr). The overall electric energy demand was estimated at 7.37 kW (25.15 MBtu/hr). Once the PCM shield was installed in the south wall, west wall, and ceiling, in all cases in location 2, the space cooling energy demand was reduced by 0.36 kW (1.23 MBtu/hr) or 6.9% of the total space cooling energy demand.

The space heating energy use for the control house was estimated at 78.86 GJ (74.69 MMBtu). Once the PCM shield was installed in the south wall, west wall, and ceiling, in all cases in location 2, the space heating energy use was reduced by 1.44 GJ (1.36 MMBtu) or 1.8% of the total space heating energy consumption.

Similar to the results of total heat transfer percent reductions, the trend also implied that space cooling energy reductions increased as the location of the house moved from a hot and humid to a mixed humid climate. A maximum space cooling energy reduction of 2.7% was predicted for a house in Kansas City, MO (Zone 4). The space heating energy reductions increased as the location of the house moved from a mixed humid to hot and humid climate. A maximum space heating energy reduction of 33.1% was predicted for a house in Miami, FL (Zone 1).

CHAPTER IX

CONCLUSIONS AND RECOMMENDATIONS

9.1 Summary of Research Work

With the research presented in this dissertation, it was intended to evaluate the latest generation of PCM integration in buildings. This PCM integration consisted of bringing the PCM into the building enclosure via the use of thin PCM layers. For this, a PCM shield and a PCM board were used. The PCM shields were thin sheets containing polymer pouches laminated with aluminum foil on both sides. The PCM was contained in the sealed polymer pouches. The type of PCM contained in the PCM shields was a hydrated salt-based PCM. The PCM boards were thin boards of polymeric compounds saturated with PCMs and laminated with aluminum foil on both sides and around the edges. The type of PCM contained in the PCM boards was a paraffin-based PCM.

For the intended evaluation, two experimental set-ups were used. One consisted of two test houses of typical residential construction and the other consisted of an institutional building (known as M2SEC) that was constructed so that its enclosure could be used to perform heat and mass transfer experiments. Interchangeable wall panels allowed for this testing. The PCM shields were tested in the test houses and the PCM boards were tested in the institutional building. In addition to the experimental research, building modeling and simulations were carried out. For the modeling, which had to include the phase transition aspects of the PCMs,

a public domain algorithm known as CondFD was used. To be able to use the CondFD algorithm, actual values of the enthalpy as a function of temperature and thermal conductivity as a function of temperature had to be determined. This was done by conducting differential scanning calorimeter (DSC) tests. With this information, together with standard modeling information (e.g., building material properties, building dimensions, and climates), the thermal performance of the walls and ceiling, both for the control and retrofit cases were evaluated. A critical part of this research was to find the optimal location of the thin PCM layer. For this, experiments, modeling, and simulations were carried out.

In the test houses only the south wall, the west wall, and the ceiling were outfitted with the PCM shield. The reason for this was that the east-facing wall was the main structural support for the fan coil unit and the north wall was the access door to the test house interior. Similarly, only the south and west walls of the M2SEC building were available for testing. The reason for this was that this building was designed to allow this type of testing only in the south and west walls.

For the experimental evaluation of the PCM shield, it was necessary to perform calibration tests before any retrofit. For this, the thermal performance of the two houses were compared and recorded as reference. Average indoor air temperatures, average exterior and interior wall surface temperatures, average attic air temperatures, average interior ceiling surface temperatures, and average wall and ceiling heat fluxes were measured and compared to verify their similarity. The calibration tests provided very accurate baseline of the thermal performance of the

houses. Average wall and ceiling surface temperature differences between the surfaces of the control house and the soon-to-be retrofit house were in the order of 0.30 °C (0.54 °F). In terms of wall and ceiling heat fluxes, the average difference was 4.6%. During all of the experiments, the indoor air temperatures of the houses were well controlled to a difference value of 0.34 °C (0.61 °F). This level of control guaranteed that once the retrofit took place any of the observed changes in wall temperature and heat fluxes would be the results of the retrofit only.

For the experimental evaluation of the PCM boards, calibration tests were also carried out before any retrofit. Average exterior and interior surface temperatures and average heat fluxes of the wall panels were measured and compared to verify their thermal similarity. For this case, indoor air temperatures were not compared since all wall panels were under the same indoor conditions. Similar to the test houses, these calibration tests provided a very accurate baseline of the thermal performance of the test panels.

Average wall panel surface temperature differences between the surfaces of the control panel and the soon-to-be retrofit panel were in the order of 0.13 °C (0.23 °F). In terms of wall panel heat fluxes, the average difference was 3.4%. This level of the control also guaranteed that once the retrofit took place any of the observed changes in wall temperature and heat fluxes would be the results of the retrofit only.

9.2 Conclusions

The results indicated that the addition of the PCM shield to a standard wall would produce the average heat flux reductions of 39.1% for a south facing wall, 23.3% for a west facing wall, and 22.7% for a ceiling. The percent peak heat flux reductions in the walls and ceiling as a result of using PCM shields varied with the location of the shield. In the south facing wall, the maximum peak heat flux reduction of 57.4% was observed when the shield was placed at location 3, which was near the middle of the wall cavity. For the west facing wall, the maximum peak heat flux reduction of 37.3% was observed in location 2 which was between the mid-section of the wall cavity and the interior face of the wallboard. For the ceiling the maximum peak heat flux reduction of 41.1% was observed when the shield was located close to the attic air space (location 4).

In terms of total heat transfer, the integration of the PCM shield produced average daytime reductions of 34.9, 28.0, and 25.1%, for the south wall, west wall, and ceiling, respectively. The maximum daytime heat transfer reduction in the south wall was 47.9%, which corresponded to location 3. The maximum daytime heat transfer reduction in the west wall was 34.1%, which corresponded also to location 3. The maximum daytime heat transfer reduction in the ceiling was 27.5%, which corresponded to location 4.

The results indicated that the addition of the PCM boards to a standard wall panel would produce reductions in peak heat flux of 67.0% for a south wall panel and 80.2% for a west wall panel. In terms of total heat transfer, the integration of the

PCM boards produced average daily reductions of 27.4% in the south wall and 10.5% in the west wall.

Comparisons between predicted and experimental heat fluxes and temperatures were carried out for both the test house walls and ceiling and the M2SEC building's wall panels. The model prediction differences related to the walls and ceilings of the test house were relatively less than those of the wall panels for the control cases. The model prediction differences once the PCM shields and the PCM boards were integrated into the modeling were relatively larger than those for the control cases. However, even for the retrofit case the model predictions for the test house walls and ceiling were closer to the experimental data than those for the wall panels. Therefore, it was concluded that the CondFD algorithm was not able to model the phase transition process of PCMs accurately. Subsequently, the decision was made to only simulate a house with the PCM shields and not an institutional wall panel outfitted with PCM boards.

For the simulation of a typical residential building outfitted with PCM shields, four cities were selected according to the DOE Climate Zone Map in which such cities covered Climate Zones 1 through 4. These cities, which by their location facilitated the inclusion of a wide range of climatic conditions, included Miami, FL (Zone 1 - hot and humid), Phoenix, AZ (Zone 2 - hot and dry), Las Vegas, NV (Zone 3 - mixed dry), and Kansas City, MO (Zone 4 - mixed humid). TMY3 weather files for each of the cities were used.

The simulated house was a 228 m^2 (2,454 ft^2), one-story, slab-on-grade residence. From the result, the simulation indicated that the optimal location of the PCM shield would be location 2 for the walls and ceiling in all climates. The results also indicated that PCM installation at location 1 in all three enclosure components should be avoided. This was because the heat transfer during the cooling and heating seasons for location 1 were increased in all cases. The simulation program predicted lower heat transfer percent reductions than the experimental data. The average percent reduction in total heat transfer into the conditioned space during the cooling season was 1.6%. The trend implied that this reduction increased as the location of the house moved from a hot and humid to a mixed humid climate. The opposite was true with the reduction of the total heat transfer out of the conditioned space during the heating season in which the trend showed that the colder regions would see a lower percentage of this reduction.

The overall space cooling and space heating energy that would be required to keep the conditioned space of the model house under comfortable conditions were simulated together with the energy reduction produced by the PCM shield. The PCM shield produced overall space cooling energy percent reductions of 0.4, 1.7, 2.3, and 2.7% for Miami, FL (Zone 1), Phoenix, AZ (Zone 2), Las Vegas, NV (Zone 3), and Kansas City, MO (Zone 4), respectively. The PCM shield produced space cooling energy demand percent reductions of 7.9, 2.9, 4.0, and 6.9% for the same cities, respectively. The PCM shield produced overall space heating energy percent reductions of 33.1, 17.1, 9.2, and 1.8% for the same cities, respectively.

9.3 Recommendations for Future Research

Future research should include a "local" calibration of CondFD and EnergyPlus. For example, during such a calibration it could be determined which discretization values and time steps would produce better results. Furthermore, for the local calibration and validation of CondFD and EnergyPlus weather data from on-site weather stations should be used. At the time of this research, the smallest time step that CondFD was able to handle for the modeling of PCM was one minute. In addition, CondFD had the limitation that it could not accommodate thin layers of highly conductive materials (e.g., aluminum layers of less than 0.5 mm (0.02 in.)). CondFD should be updated to include smaller time steps and to accommodate these types of layers because it is believed that such changes would produce more accurate heat transfer and temperature predictions.

It is recommend that experimental testing be conducted that includes winter and swing seasons in addition to summer seasons. This will help in the validation of heat transfer models. All testing should also include ways to monitor building space cooling and heating energy consumption in addition to the heat transfer and temperature data.

The integration of PCM in various types of walls (e.g., concrete, steel frame, brick, prefabricated walls, etc.) should be investigated as well as various types of PCMs, with more emphasis placed on those PCMs that are manufactured from renewable sources.

It is important that DSC measurement standard be proposed for PCMs. For example, there are ASTM standards on how to use the DSC for measuring properties of polymers, but no standards exist for measuring properties of PCMs. Similarly, new standards for evaluating the performance of PCMs should be produced. This is important because the building industry evaluates most insulation-like products based on R-values. However, R-values are estimated using steady state heat transfer methods, which are not compatible with energy storage.

REFERENCES

Ahmad M, Bontemps A, Sallée H, Quenard D. 2006. Thermal testing and numerical simulation of a prototype cell using light wallboards coupling vacuum isolation panels and phase change material. Energ Buildings. 38(6):673-681; [retrieved 2010 Jul 19]. Available from: http://dx.doi.org/10.1016/j.enbuild.2005.11.002

Alkan C. 2006. Enthalpy of melting and solidification of sulfonated paraffins as phase change materials for thermal energy storage. Thermochim Acta. 451(1-2):126-130; [retrieved 2010 Jul 19]. Available from: http://dx.doi.org/10.1016/j.tca.2006.09.010

Al-Saadi SN, Zhai Z. 2013. Modeling phase change materials embedded in building enclosure: A review. Renew Sust Energ Rev. 21:659-673; [retrieved 2013 Aug 21]. Available from: http://dx.doi.org/10.1016/j.rser.2013.01.024

American Society of Heating, Refrigerating and Air-Conditioning Engineers, Inc. 2010.Thermal environmental conditions for human occupancy. Atlanta, GA. ANSI/ASHRAE Standard 55-2010.

Ames WF. Numerical methods for partial differential equations. 1992. Academic Press, Inc., Boston, MA. 3rd ed.

Baraga CI, Rezende MC, Costa ML. 2011. Methodology for DSC calibration in high heating rates. J Aerosp Technol Manag. 3(2):179-192; [retrieved 2013 Sep 6]. Available from: http://www.jatm.com.br/ojs/index.php/jatm/article/viewFile/98/173

Bauer M, Mosle P, Schwarz M. 2009. Green building: Guidebook for sustainable architecture.

Barbour JP, Hittle DC. 2006. Modeling phase change materials with conduction transfer functions for passive solar applications. J Sol Energ-T ASME. 128(1):58-68; [retrieved 2013 Sep 6]. Available from: http://solarenergyengineering.asmedigitalcollection.asme.org/article.aspx?articleid=1457632

Callister WD, Rethwisch DG. Materials science and engineering: an introduction. John Wiley & Sons, Inc., New York, NY. 8th ed.

Castell A, Martorell I, Medrano M, Pérez G, Cabeza LF. 2010. Experimental study of using PCM in brick constructive solutions for passive cooling. Energ Buildings. 42(4):534-540; [retrieved 2011 Jan 17]. Available from: http://dx.doi.org/10.1016/j.enbuild.2009.10.022

Castellón C, Günther E, Mehling H, Hiebler S, Cabeza LF. 2008. Determination of the enthalpy of PCM as a function of temperature using a heat-flux DSC-A study of different measurement procedures and their accuracy. Int J Energ Res. 32(13):1258-1265; [retrieved 2013 Sep 6]. Available from: http://onlinelibrary.wiley.com/doi/10.1002/er.1443/pdf

Chazhengina SY, Kotelnikova EN, Filippova IV, Filatov SK. 2003. Phase transitions of n-alkanes as rotator crystals. J Mol Struct. 647(3):243-257.

Cooper MG, Mikict BB, Yovanovich MM. 1969.Thermal contact conductance. Int J Heat Mass Tran. 12:279-300.

Delcroix B, Kummert M, Daoud A, Hiller M. 2012. Conduction transfer functions in TRNSYS multizone building model: Current implementation, limitations and possible improvements. In: Proceedings of the Fifth National Conference of IBPSA-USA; 2012 Aug 1-3; Madison (WI). p. 219-226; [retrieved 2013 Sep 6]. Available from: http://www.ibpsa.us/simbuild2012/Papers/SB12_TS04a_3_Delcroix.pdf

Department of Energy. 2013. Energy Efficiency & Renewable Energy website. [retrieved 2013 Sep 2]. Available from: http://apps1.eere.energy.gov/buildings/energyplus/energyplus_testing.cfm

Department of Energy (DOE). 2010. Guide to determining climate regions by county. Washington DC. Pub. No.: Report PNNL 17211; [retrieved 2013 Sep 2]. Available from: http://apps1.eere.energy.gov/buildings/publications/pdfs/building_america/ba_climateguide_7_1.pdf

Diaconu BM, Cruceru M. 2010. Novel concept of composite phase change material wall system for year-round thermal energy savings. Energ Buildings. 42(10):1759-1772; [retrieved 2011 Jan 17]. Available from: http://dx.doi.org/10.1016/j.enbuild.2010.05.012

Denholm P, Ong S, Booten C. 2012. Using utility load data to estimate demand for space. Denver, CO: Pub. No.: NREL/TP-6A20-5450.9; [retrieved 2013 Sep 2]. Available from: http://www.nrel.gov/docs/fy12osti/54509.pdf

DuPont™ Energain® Datasheet. [retrieved 2013 Mar 5]. Available from: http://energain.co.uk/Energain/en_GB/tech_info/technical_data.html

Energy Information Administration. 2011 Mar. Emissions of greenhouse gases in the United States 2009. Washington, DC: Pub. No.: DOE/EIA-0573(2009)); [retrieved 2013 Jun 17]. Available from: http://www.eia.gov/environment/emissions/ghg_report

Energy Information Administration. 2012 Sep. Annual energy review 2011. Washington, DC: Pub. No.: DOE/EIA-0384(2011); [retrieved 2013 Jun 17]. Available from: http://www.eia.gov/totalenergy/data/annual

Energy Information Administration. 2013 Apr. Annual energy outlook 2013 with Projections to 2040. Washington, DC: Pub. No.: DOE/EIA-0383(2013); [retrieved 2013 Jun 17]. Available from: http://www.eia.gov/forecasts/aeo

EnergyPlus. 2013a. EnergyPlus engineering reference: the reference to EnergyPlus calculations. Ernest Orlando Lawrence Berkeley National Laboratory; [retrieved 2013 May 6]. Available from: http://apps1.eere.energy.gov/buildings/energyplus/energyplus_documentation.cfm

EnergyPlus. 2013b. Input output reference: The encyclopedic reference to EnergyPlus input and output. Ernest Orlando Lawrence Berkeley National Laboratory; [retrieved 2013 May 6]. Available from: http://apps1.eere.energy.gov/buildings/energyplus/energyplus_documentation.cfm

Evers AC. 2008. Development of a quantitative measure of the functionality of frame walls enhanced with phase change materials using a dynamic wall simulator [master's thesis]. [Lawrence (KS)]: University of Kansas; [retrieved 2010 May 11]. Available from: http://hdl.handle.net/1808/4164

Evers AC, Medina MA, Fang Y. 2010. Thermal performance of frame walls enhanced with paraffin and hydrated salt phase change materials using a dynamic wall simulator. Build Environ.45(8):1762-1768; [retrieved 2011 Jan 17]. Available from: http://dx.doi.org/10.1016/j.buildenv.2010.02.002

Evola G, Marletta L, Sicurella F. 2013. A methodology for investigating the effectiveness of PCM wallboards for summer thermal comfort in buildings. Build Environ. 59:517-527; [retrieved 2013 May 6]. Available from: http://dx.doi.org/10.1016/j.buildenv.2012.09.021

Eyres NR, Hartree DR, Ingham J, Jackson R, Sarjant RJ, Wagstaff JB. 1946. The calculation of variable heat flow in solids. Phil. Trans. R. Soc. Lond. 240:1-57.

Fang Y. 2009a. A comprehensive study of phase change materials (PCMs) for building walls applications [dissertation]. [Lawrence (KS)]: University of Kansas; [retrieved 2010 May 11]. Available from: http://hdl.handle.net/1808/5537

Fang Y, Medina MA. 2009. Proposed modifications for models of heat transfer problems involving partially-melted phase change processes. J ASTM Int. 6(9); [retrieved 2010 May 11]. Available from: http://enterprise.astm.org/SUBSCRIPTION/DIGITAL_LIBRARY/JOURNALS/JAI/PAGES/JAI102059.htm

Feilchenfeld H, Fuchs J, Kahana F, Sarig S. 1985. The melting point adjustment of calcium chloride hexahydrate by addition of potassium chloride or calcium bromide hexahydrate. Sol Energy. 34(2):199-201.

Fletcher LS. 1972. A review of thermal control materials for metallic junctions, J Spacecraft Rockets. 9(12): 849-850.

Ghoneim AA, Klein SA, Duffie JA. 1991. Analysis of collector-storage building walls using phase-change materials. Sol Energy. 47:237-242.

Günther E, Hiebler S, Mehling H, Redlich R. 2009. Enthalpy of phase change materials as a function of temperature: required accuracy and suitable measurement methods. Int J Thermophys. 30(4):1257-1269; [retrieved 2010 Jul 19]. Available from: http://dx.doi.org/10.1007/s10765-009-0641-z

Halford CK, Boehm RF. 2007. Modeling of phase change material peak load shifting. Energ Buildings. 39(3):298-305; [retrieved 2010 May 11]. Available from: http://dx.doi.org/10.1016/j.enbuild.2006.07.005

Hashemi HT, Sliepcevich CM. 1967. A numerical method for solving two-dimensional problems of heat conduction with change of phase. Chem Eng Prog S Ser. 63:34-41.

Hawes DW, Feldman D, Banu D. 1993. Latent heat storage in building materials. Energ Buildings. 20(1):77-86.

He B, Martin V, Setterwall F. 2001. Phase transition temperature ranges and storage density of paraffin wax phase change materials. Energy. 29(11):1785-1804.

Heim D, Clarke JA. 2004. Numerical modeling and thermal simulation of PCM–gypsum composites with ESP-r. Energ Buildings. 36(8):795-805.

Hoffman JD. 1992. Numerical methods for engineers and scientists. McGraw-Hill, New York, NY.

Ibáñez M, Lázaro A, Zalba B, Cabeza LF. 2005. An approach to the simulation of PCMs in building applications using TRNSYS. Appl Therm Eng. 25:1796-1807; [retrieved 2010 May 11]. Available from: http://dx.doi.org/10.1016/j.applthermaleng.2004.11.001

Institute of Electrical and Electronics. IEEE Recommended Practice for Electric Power Systems in Commercial Buildings. 1990. IEEE Gray Book.

International Energy Agency. 2012. CO2 Emissions from fuel combustion: Highlights (2012 ed.). Paris, France; [retrieved 2013 Jun 17]. Available from: http://www.iea.org/publications/freepublications

Jin X, Medina MA, Zhang X. 2013. On the importance of the location of PCMs in building walls for enhanced thermal performance. Appl Energ. 106:72-78.

King J. 2004. Preliminary evaluation of the thermal performance of Phase Change Material - Structural Insulated Panels (PCM-SIPs) [master's thesis]. [Lawrence (KS)]: University of Kansas.

Kissock JK. 2000. Thermal load reduction from phase-change building components in temperature controlled buildings. In: Proceedings of the International Solar Energy Conference; 2000 Jun 16-21; Madison (WI).

Kissock JK, Hanning JM, Whitney TI, Drake ML. 1998. Testing and simulation of phase change wallboard for thermal storage in buildings. In: Proceedings of the International Solar Energy Conference; 1998 Jun 14-17; New York (NY). p. 45-52.

Koo J, So H., Hong SW, Hong H. 2011. Effects of wallboard design parameters on the thermal storage in buildings. Energ Buildings. 43(8):1947-1951; [retrieved 2013 May 6]. Available from: http://dx.doi.org/10.1016/j.enbuild.2011.03.038

Kosny J, Kossecka E. 2013. Understanding a potential for application of Phase Change Materials (PCMs) in building envelopes. ASHRAE Tran. 119(1):3-13.

Kosny J, Kossecka E, Brzezinski A, Tleoubaev A, Yarbrough D. 2012. Dynamic thermal performance analysis of fiber insulations containing bio-based phase change materials (PCMs). Energ Buildings. 52:122–131; [retrieved 2013 Feb 5]. Available from: http://dx.doi.org/10.1016/j.enbuild.2012.05.021

Kosny J, Stovall T, Shrestha S, Yarbrough D. 2010. Theoretical and experimental thermal performance analysis of complex thermal storage membrane containing bio-based phase-change material (PCM). In: Thermal Performance of the Exterior Envelopes of Whole Buildings XI International Conference; 2010; Clearwater Beach (FL); [retrieved 2011 Jan 18]. Available from: http://web.ornl.gov/sci/buildings/2012/B11%20papers/197_Kosny.pdf

Kosny J, Yarbrough DW, Wilkes KE, Leuthold D, Syad A. 2006. PCM-enhanced cellulose insulation: thermal mass in light-weight fibers, In: Proceedings of IEA and DOE Ecostock 2006 Conference; 2006 May 31; Stockton University; [retrieved 2011 Jan 18]. Available from: http://intraweb.stockton.edu/eyos/energy_studies/content/docs/FINAL_PAPERS/8B-5.pdf

Kuznik F, Virgone J, Noel J. 2008a. Energetic efficiency of room wall containing PCM wallboard: A full-scale experimental investigation. Energ Buildings. 40 (2):148-156; [retrieved 2010 Aug 27]. Available from: http://dx.doi.org/10.1016/j.apenergy.2009.01.004

Kuznik F, Virgone J, Noel J. 2008b. Optimization of a phase change material wallboard for building use. Appl Therm Eng. 28(11-12):1291-1298Kuznik F, David D, Johannes K, Roux J. 2011. A review on phase change materials integrated in building walls. Renew Sust Energ Rev. 15(1):379-391.

Kuznik F, Virgone J. 2009a. Experimental assessment of a phase change material for wall building use. Appl Energ. 86(10): 2038-2046; [retrieved 2010 Aug 27]. Available from: http://dx.doi.org/10.1016/j.apenergy.2009.01.004

Kuznik F, Virgone J. 2009b. Experimental investigation of wallboard containing phase change material: Data for validation of numerical modeling. Energ Buildings. 41(5):561-570; ; [retrieved 2010 Aug 27]. Available from: http://dx.doi.org/10.1016/j.enbuild.2008.11.022

Lazaro A, Peñalosa C, Solé A, Diarce G, Haussmann T, Fois M, Zalba B, Gshwander S, Cabeza LF. 2013. Intercomparative tests on phase change materials characterisation with differential scanning calorimeter. Appl Energ. 109:415-420.

Lee KO. 2013. Using hydrated salt phase change materials for residential air conditioning peak demand reduction and energy conservation in coastal and transitional climates in the state of california [master's thesis]. [Lawrence (KS)]: University of Kansas.

Lin K, Zhang Y, Xu X, Di H, Yang R, Qin P. 2005. Experimental study of under-floor electric heating system with shape-stabilized PCM plates. Energ Buildings 37(3):215-220; [retrieved 2010 Jul 20]. Available from: http://dx.doi.org/10.1016/j.enbuild.2004.06.017

Madhusudana CV, Ling FF. 1995. Thermal Contact Conductance. Springer. New York, NY.

Mazo J, Delgado M, Marin JM, Zalba B. 2012. Modeling a radiant floor system with Phase Change Material (PCM) integrated into a building simulation tool: Analysis of a case study of a floor heating system coupled to a heat pump. Energ Buildings. 47:458-466; [retrieved 2013 Feb 5]. Available from: http://dx.doi.org/10.1016/j.enbuild.2011.12.022

Medina MA, King JB, Zhang M. 2008. On the heat transfer rate reduction of structural insulated panels outfitted with phase-change materials. Energy. 33(4):667-678.

Medina MA, Zhu, D. 2008. A comparative heat transfer examination of Structural Insulated Panels (SIPs) with and without Phase Change Materials (PCMs) using a dynamic wall simulator. In: Proceedings of the 16th Symposium on Improving Building Systems in Hot and Humid Climates, 2008 Dec 15-17; Plano (TX).

Mehling H, Cabeza LF. 2008. Heat and cold storage with PCM: an up to date introduction into basics and applications. Springer. Berlin, Germany.

Mirzaei PA, Haghighat F. 2012. Modeling of phase change materials for applications in whole building simulation. Renew Sust Energ Rev. 16(7):5355-5362; [retrieved 2013 Feb 5]. Available from: http://dx.doi.org/10.1016/j.rser.2012.04.053

Morgan K, Lewis RW, Zienkiewicz OC. 1978. An improved algorithm for heat conduction problems with phase change. Int J Numer Meth Eng. 12:1191-1195.

Natural Resources Conservation Service (NRCS) website. ; [retrieved 2013 Oct 10]. Available from: http://www.wcc.nrcs.usda.gov/nwcc/site?sitenum=2147&state=ks

Ozdenefe M, Dewsbury J. 2012. Dynamic thermal simulation of a PCM lined building with Energy Plus. In: Proceedings of the 5th WSEAS International Conference on Environmental and Geological Science and Engineering; 2012 Nov 10-12; Vienna, Australia. p. 359-364.

Pedersen CO. 2007. Advanced zone simulation in EnergyPlus: Incorporation of variable properties and Phase Change Material (PCM) capability. In: Proceedings of the 10th International Building Simulation Conference; 2007 Sep 3-6; Beijing, China. p. 1341-1345; [retrieved 2013 Feb 5]. Available from: http://www.phasechange.com/Research%20Library/phasechangevaribles.pdf

Poel GV, Mathot VBF. 2006. High-speed/high performance differential scanning calorimetry (HPer DSC): Temperature calibration in the heating and cooling mode and minimization of thermal lag. Thermochim Acta. 446(1-2):41-54.

Qureshi WA, Nair NC, Farid MM. 2011. Impact of energy storage in buildings on electricity demand side management. Energ Convers Manage. 52(5): 2110-2120; [retrieved 2013 Feb 5]. Available from: http://dx.doi.org/10.1016/j.enconman.2010.12.008

Reshmeen S. 2009. Determining the optimum placement of a phase change materials (PCM) thermal shield inside frame walls using a dynamic wall simulator [master's thesis]. [Lawrence (KS)]: University of Kansas; [retrieved 2010 May 11]. Available from: http://hdl.handle.net/1808/5659

Salunkhe PB, Shembekar PS. 2012. A review on effect of phase change material encapsulation on the thermal performance of a system. Renew Sust Energ Rev. 16(8):5603-5616; [retrieved 2013 Feb 5]. Available from: http://dx.doi.org/10.1016/j.rser.2012.05.037

Salyer IO, Sircar AK. 1990. Phase change materials for heating and cooling of residential buildings and other applications. In: Proceedings of 25th Intersociety Energy Conversion Engineering Conference; 1990 Aug 12-17; Reno (NV). p. 236-243.

Salyer IO, Sircar AK.1997. Review of phase change materials research for thermal energy storage in heating and cooling applications at the University of Dayton from 1982 to 1996. Int J Global Energy.9(3):183-198.

Schossig P, Henning HM, Gschwander S, Haussmann T. 2005. Micro-encapsulated phase-change materials integrated into construction materials. Sol Energ Mat Sol C. 89:297-306.

Schranzhofer H, Puschnig P, Heinz A, Streicher W. 2006. Validation of a TRNSYS simulation model for PCM energy storage and PCM wall construction element. Ecostock conference.

Sperling B. Sperling's Best Places. [retrieved 2013 Sep 2]. Available from: http://www.bestplaces.net/

Stein B. 1996. Building technology: mechanical and electrical systems. John Wiley & Sons, Inc.New York, NY. 2nd ed.

Stritih U, Novak P. 1996. Solar heat storage wall for building ventilation. Renew Energ. 8:268-271.

Swaminathan CR, Voller R. 1993. On the enthalpy method. Int J Numer Meth Fl. 3:233-244.

Tabares-Velasco PC. 2012. Energy impact of nonlinear behavior of PCM when applied into building envelope. In: Proceedings of the ASME 2012 6th International Conference on Energy Sustainability & 10th Fuel Cell Science, Engineering and Technology Conference; 2012 July 23-26; San Diego (CA): Pub. No.:NREL/CP-5500-54245; [retrieved 2012 Aug 27]. Available from: http://www.nrel.gov/docs/fy12osti/54245.pdf

Tabares-Velasco PC, Christensen C, Bianchi MVA, Booten C. 2012. Verification and validation of EnergyPlus conduction finite difference and phase change material models for opaque wall assemblies. Golden (CO): Pub. No.:NREL/TP-5500-55792; [retrieved 2012 Aug 27]. Available from: http://www.nrel.gov/docs/fy12osti/55792.pdf

Tomlinson JJ, Heberle DD. 1990. Analysis of wallboard containing a phase change material. In: Proceedings of the 25th Intersociety Energy Conversion Engineering Conference; 1990 Aug 12-17; Reno (NV). p. 230-235.

Ukrainczyk N, Kurajica S, Šipušić. 2010. Thermophysical comparison of five commercial paraffin waxes as latent heat storage materials. Chem Biochem Eng Q. 24(2):129-137.

Voller VR. 1997. An overview of numerical methods for solving phase change problems. Advances In Numerical Heat Transfer. p. 341–380.

Wilcox S. Marion W. 2008. User's manual for TMY3 data sets. Golden, Colorado: National Renewable Energy Laboratory. Pub. No.:NREL/TP-581-43156; [retrieved 2013 Feb 5]. Available from: http://www.nrel.gov/docs/fy08osti/43156.pdf

Yinping Z, Yi J, Yi J. 1999. A simple method, the T-history method, of determining the heat of fusion, specific heat and thermal conductivity of phase-change materials. Meas Sci Technol. 10(3):201-205; [retrieved 2013 May 12]. Available from: http://iopscience.iop.org/0957-0233/10/3/015

Zhang M. 2004. Performance evaluation of a phase change frame wall [master's thesis]. [Lawrence (KS)]: University of Kansas.

Zhang M, Medina MA, King J. 2005. Development of a thermally enhanced frame wall with phase-change materials for on-peak air conditioning demand reduction and energy savings in residential buildings. Int J Energ Res. 29(9):795-809.

Zhang YP, Lin KP, Yang R, Di HF, Jiang Y. 2006. Preparation, thermal performance, and application of shape-stabilized PCM in energy efficient buildings. Energ Buildings. 38(10):1262-1269; [retrieved 2010 Jul 19]. Available from: http://dx.doi.org/10.1016/j.enbuild.2006.02.009

Zhong H., Lei B, Feng Y. 2010. Research on the phase change materials for the passive solar house in Tibet. In: Proceedings of the International Conference on Mechanic Automation and Control Engineering; 2010 June 26-28; Wuhan, China. p. 4070-4073; [retrieved 2013 Feb 5]. Available from: http://ieeexplore.ieee.org/xpls/abs_all.jsp?arnumber=5535437&tag=1

Zhou D, Zhao CY, Tian Y. 2012. Review on thermal energy storage with phase change materials (PCMs) in building applications. Appl Energ. 92: 593-605; [retrieved 2013 Feb 5]. Available from: http://dx.doi.org/10.1016/j.apenergy.2011.08.025

Zhu D. 2005. A Comparative heat transfer examination of Structural Insulated Panels (SIPs) with and without Phase Change Materials (PCMs) using a dynamic wall Simulator [master's thesis]. [Lawrence (KS)]: University of Kansas.

Zhu N, Ma Z, Wang S. 2009. Dynamic characteristics and energy performance of buildings using phase change materials: A review. Energ Convers Manage. 50(12): 3169-3181; [retrieved 2010 Jul 19]. Available from: http://dx.doi.org/10.1016/j.enconman.2009.08.019

Zhu N, Wang S, Ma X, Sun Y. 2011. Energy performance and optimal control of air-conditioned buildings with envelopes enhanced by phase change materials. Energ Convers Manage. 52(10): 3197-3205; [retrieved 2012 Aug 27]. Available from: http://dx.doi.org/10.1016/j.enconman.2011.05.011